Synthesis and Self-assembly of DNA-β turn Conjugates.

Thesis submitted to the University of Kent for the degree of Doctor of Philosophy (Ph.D.) in Chemistry.

By

Emerald Rhiannon Taylor

University of Kent

Division of Natural Sciences

2023

Declaration

I declare that all the work presented in this thesis submission was my own work and written in my own words. It has not been submitted to any other institution for a qualification or for any other degree.

Signed: Emerald Rhiannon Taylor 

Acknowledgements

I dedicate this thesis to my father, Vernon Taylor who lost his life during 2020. He would have been so proud to see this work completed, and how far I have come because of it.

Firstly, I wish to thank my supervisors Dr Christopher J. Serpell and Dr Michael R. Reithofer, for all of their belief in and support of me. Without their continued guidance this work would not have been possible. I am especially grateful to Chris, for his belief in me from my master's through to today. Akiko Sato was my partner in crime throughout this process, without her this work would not be what it is. So, thank you Akiko, for all your support and help, and for making wonderful peptides. I would like to thank the Leverhulme trust for the funding to support this work, and the University of Kent for hosting me during my postgraduate studies.

I would like to acknowledge my friends and research group for all their love, laughs, and trials that we have been through during this journey. Saeed, you were my friend from day one, and I appreciate all the guidance and joy you have given and brought to my life. Nadeema, you could always make me smile and taught me so much, I will always be grateful. Alix and Bini, thank you so much for being my unwavering friends during this PhD. It was an understatement to say it was difficult at times. Thank you for getting me through it, and to this day being two of my closest friends. Dave Beal, thank you for being my mentor. The invaluable advice you have given me, still

guides me today. I will always be truly grateful for your friendship and guidance, in academia and in life.

To the love of my life, James, thank you for believing in me every step of the way, even when I could not and did not believe in myself. Your support throughout this process has helped me get to where I am today, words will never fully express what you mean to me. My family, my mother Karen, and my sister Faith, thank you for all your unending love and belief in me. I owe so much to you both.

Abstract

This thesis discusses the synthesis and self-assembly of several DNA-peptide conjugates, through different bi-orthogonal conjugating methods. Chapter 1 explores the current literature and perspective for which this work is based. Chapter 2 discusses the synthesis of DNA by solid phase synthesis, before being modified with a maleimide based phosphoramidite. The chapter goes on to discuss the development of these methods. Commercially bought DNA was modified with two bi-functional crosslinkers, before being further modified with different peptides. The chapter discusses the full scale of method development to obtain DNA-peptide conjugates, including the first known example of DNA β turn conjugates in the literature.

Chapters 3-5 discusses the self-assembly of DNA-peptide conjugates, with peptide directed, DNA and peptide directed, and DNA directed self-assembly respectively. Chapter 3, peptide driven assembly is explored through the doping of the parent peptide ILVAGK with varying amounts of DNA-ILVAGK. These experiments were observed over 28 days, and the resultant structures analysed by atomic force microscopy. In Chapter 4, both peptide and DNA driven self-assembly of DNA-ILVAGK is studied through DNA hybridisation with complementary sequences of 1, 2, and 3 lengths. As in Chapter 3, these studies were supported by atomic force microscopy, dynamic light scattering and circular dichroism. The structures observed in Chapter 4 differed in timeline and type

to those seen in Chapter 3. Chapter 5 investigates DNA driven self-assembly with the peptide assembly disabled using sodium dodecyl sulphate. The structures observed during 28 days of aging showed little change in morphology over the period. This is indicative of the presence of hierarchy within this system.

Chapter 6 consists of an overall conclusion, to draw together the individual conclusions drawn in each chapter.

Covid-19

Covid-19 had a significant effect on the progress of this work. Access was lost to laboratories during 2020 for a period of four months, between March and July 2020. In the months after the initial lockdown, laboratory access was greatly reduced, due to social distancing and the number of people in our shared laboratory. We were on a half-day schedule, meaning we only had access to the laboratories for four hours a day, this was maintained into 2021. Even with a Covid extension agreed by the Leverhulme Trust, and the University of Kent for six months, this time was still reduced access to laboratory facilities. Further isolated events occurred, resulting in total lab closure for two periods of ten-day closures due to Covid enforced isolation.

Publications

Tuning dynamic DNA- and peptide-driven self-assembly in DNA–peptide conjugates†

Emerald R. Taylor, Akiko Sato, Isobel Jones, Prashant G. Gudeangadi, David M. Beal, James A. Hopper, Wei-Feng Xue, Michael R. Reithofer * and Christopher J. Serpell * Chem. Sci., 2023,14, 196-202

Presentations

MASC 2018, Lancaster 17-18th December 2018. Poster presentation.

5th London Polymer Group Symposium 25th March 2019 (Kent). Poster presentation.

Young Researchers Meeting 1st and 2nd July 2019 (Kent). Poster presentation.

RSC Macrocyclic and Supramolecular Chemistry conference (MASC) 16-17th Dec 2019. Poster presentation.

2021 RSC CBBG (Chemical Biology and Bio Organic Group) Forum 7-8th January 2021. Flash oral and poster presentation (virtual).

List of Abbreviations

AFM: Atomic Force Microscopy
APS: Ammonium Persulfate
BME: β-mercaptoethanol
CD: Circular Dichroism
$CDCl_3$: Deuterated Chloroform
CPG: Control Pore Glass Beads
CO: Cyclooctyne
DLS: Dynamic Light Scattering
DCM: Dichloromethane
DMSO: Dimethylsulfoxide
DMAP: Dimethylaminopyridine
DIPEA: *N*, *N*-diisopropylethylamine
EDTA: Ethylenediaminetetra acetic acid
EDC.HCl: *N*-(3-Dimethylaminopropyl)-*N* -ethylcarbodiimide hydrochloride
Eqv: Equivalents
ESMS: Electrospary Mass Spectrometry
ESI^-: Electrospray Ionisation, negative mode
ESI^+: Electrospray Ionisation, positive mode
FITC: Fluorescein Isothiocyanate
g: Gravity
HCl: Hydrochloric Acid
HPLC: High Performance Liquid Chromatography
K_2CO_3: Potassium Carbonate
kV: Kilovolts
LC-MS: Liquid Chromatography Mass Spectrometry
NMR: Nuclear Magnetic Resonance
mAmps: Milliamperes
M: Mass or Molar
m/z: Mass to Charge Ratio
MeOH: Methanol
mL: Millilitres
mM: Millimolar
mmol: Millimoles
MHz: Megahertz
NaB: Sodium Borate
NaCl: Sodium Chloride
nm: Nanometres
PAGE: Polyacrylamide Gel Electrophoresis
RBF: Round Bottom Flask
R_f: Retention Factor
SDS: Sodium Dodecyl Sulfate
SPAAC: Strain Promoted Alkyne Azide Click Chemistry
TAMg: Tris Magnesium Acetate Buffer
TBE: Tris Borate EDTA Buffer
TEA: Triethylamine
TEMED: *N*, *N, N'*, *N'*-tetramethylethylenediamine
TLC: Thin Layer Chromatography
UV-Visible: Ultraviolet Visible

V: Voltage
µL: Microlitre
µM: Micromolar
µm: Micrometres/ microns
˚**C:** Degrees Celsius

Table of Contents

Contents

Chapter 1.0: Introduction

This thesis discusses the synthesis, characterisation, and analysis of the self-assembly of DNA-peptide conjugates prepared via covalent bioconjugation through bio-orthogonal linkers. With the first known example of DNA β turn conjugates (DNA-ILVAGK) within the literature at the time of publication, being explored.

1.1. Biomolecules

There are four main categories of biomolecules: lipids, carbohydrates, nucleic acids (Fig.1), and proteins.[1] Proteins are generally considered as the fourth category over peptides; however, peptides are the building blocks upon which proteins are formed, and for the purpose of this work peptides are discussed and studied in the self-assembly of these DNA conjugates.[1] Nucleic acids and peptides are the focus of this work, nucleotides because of their reliable self-assembly motif, and peptides because they also exhibit interesting self-assembly without the challenges of working with large proteins, both will be discussed in detail throughout this chapter. These building blocks are the foundations upon which biological processes are based. Nucleic acids can be split into two categories: RNA and DNA, RNA has a ribose sugar in its sugar phosphate backbone whereas DNA has a deoxyribose sugar in its backbone (Fig.1a-b).[2,3] DNA and RNA are responsible for coding genetic information within nature. Unlike RNA, which is generally single stranded in nature, DNA can be double stranded.[3] This ability to assemble in a sequence-programmable fashion through hydrogen bonding between base pairs (adenine (A), and thymine (T), cytosine (C), and guanine (G)) has led to a host of new areas of exploration and nanoscale control by synthetic chemists to mimic nature.[4,5]

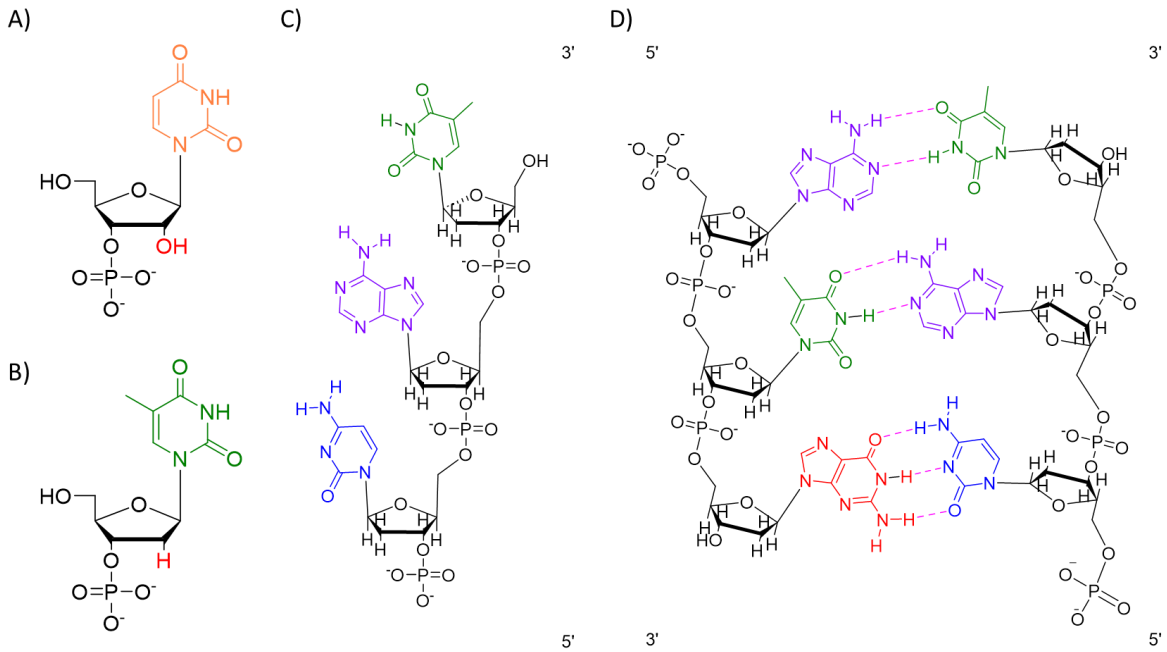

Figure 1: Structural drawings illustrating A) an RNA Uracil (orange) nucleotide highlighting the OH in red, on the 2 carbon on the pentose sugar B) a DNA Thymine (green)nucleotide highlighting the H in red, on the 2 carbon of the pentose sugar, **C**) a single stranded DNA molecule (trimer), and **D**) a double stranded DNA molecule (trimer), hydrogen bonds coloured in pink and represented as a dashed bond. Base colour coding, Adenine: purple, Thymine: green, Guanine: red, Cytosine: blue, and Uracil: orange.

Transfer and messenger RNA are predominately responsible for the transference and transportation of information from the nucleus to organelles.[6] DNA is transcribed into messenger RNA (mRNA) by the protein, RNA polymerase, mRNA is then translated by a ribosome to give a polypeptide chain which goes on to fold into a protein molecule, this important as these biomolecules code for all key biological functions.[3,6,7]

Amino acids (Fig.2a) are small organic molecules which act as the monomer units for the formation of large peptides (Fig.2b). Peptides are short chains of amino acids which vary in length between 2 and 50 amino acids (longer chains typically being referred to as polypeptides).[8] Polypeptides can then self-assemble to form proteins. Amino acids have a carboxylic acid at one terminal (C-terminal) and a primary amine at the other (N-terminal) (Fig.2a), these termini react together through a condensation reaction to form amide bonds (Fig.2).[9] Depending on the sequence of the amino acids, and their respective R-groups used, peptides have a rich and diverse assembly array. These include the structures parallel and anti-parallel β sheets, α-helices, and triple helices (collagen mimetic peptides).[9]

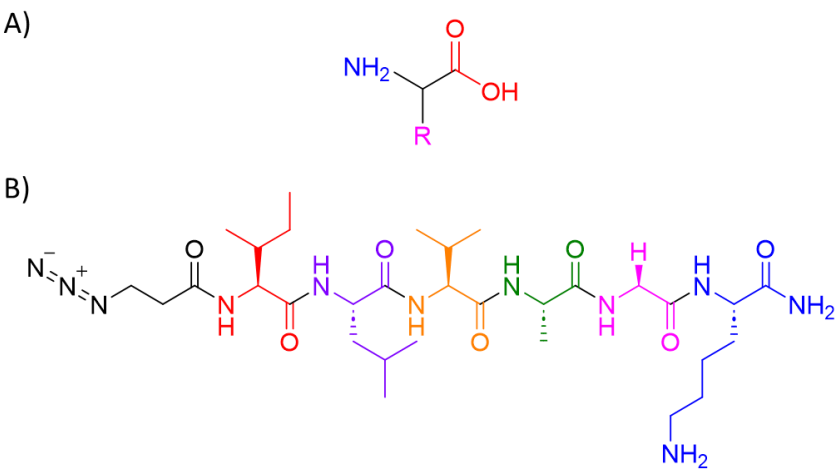

Figure 2: Structural illustrations of A) a general amino acid, with, R-group (pink), N-terminal (blue), and C-terminal (red), B) azide modified (black) β-turn hexa-peptide, ILVAGK, (isoleucine (red), leucine (purple), valine (orange), alanine (green), glycine (pink), and lysine (blue)), with colours to identify the individual amino acid units.

Peptides are useful in the synthesis of biomimetic materials because they can self-assemble into complex structures like proteins but are much smaller, which makes them beneficial to multi-assembly systems.[10] Peptides have a number of useful properties, such as their ease with which they can be synthesised through solid phase synthesis which also means that their naturally diverse library of amino acids can be extended with synthetically modified versions.[10–12] There are also a number of natural peptides which have great biological relevance as neurotransmitters, ion channel ligands, and as hormones such as hydroxy-dopamine.[13,14] This chapter will discuss the advancements made in both DNA and peptide nanotechnology before moving onto discussing current literature on the synthesis and applications of DNA-peptide conjugates.

1.2. Self-assembly

Self-assembly is the process by which a systems individual components organise into an ordered and/or functional structure because of local interactions between molecules, without external direction (Fig.3).[15] Self-assembly occurs at all scales from small molecule interactions to large weather system events, for the purpose of this work this section will focus on the micro and nanoscales.[16,17] Self-assembly is an effective bottom-up method for preparing functional materials through the organisation of molecules into structures and patterns.[17,18]

Self-assembly is ubiquitous within biology and underpins the formation of a wide variety of complex biological structures with properties extending over different length scales.[19] However, the ability to produce synthetic systems with the same complexity as found in biology is yet to be achieved, the current state of the art in what has been achieved to date is discussed further in this section, and this chapter.[20–22] There are multiple levels to biological complexity, if we consider nucleotides and amino acids, as the building blocks, these are the lowest level of complexity in a cell for example.[20] The next layer of complexity would to be to assemble these building blocks into genes, and proteins, these layers of complexity continue to develop through, circuits, pathways and then finally into cells.[20] Each level builds new challenges for the supramolecular chemist. The synthesis of supramolecular organic materials attempts to mimic the lower levels of biological complexity by developing relatively simple molecules which utilise different intermolecular interactions which drive self-assembly to the final state, such as π – π stacking, hydrogen bonding, electrostatic interactions, and hydrophobic behaviour (Fig.3).[23,24] Self-assembly can be characterised by two forms: static and dynamic. It is thought that the introduction of external stimuli into a self-assembling system could drive the formation of hierarchical structures (final state) like those seen in biology (Fig.3).[25,26]

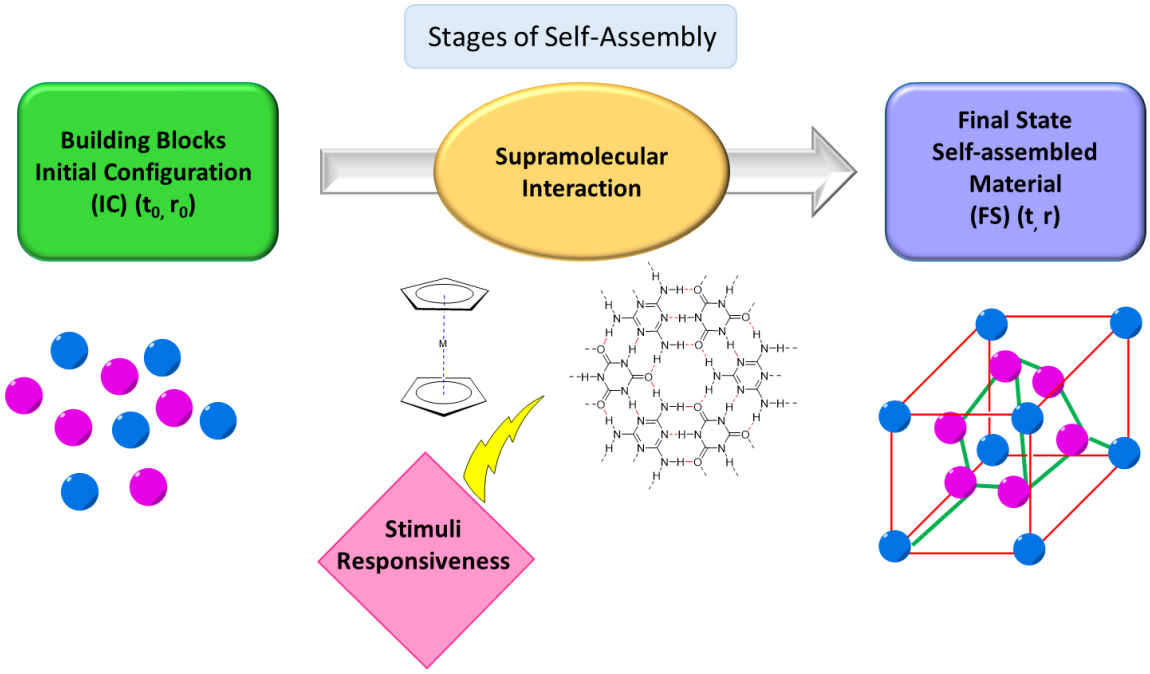

Figure 3: Conceptual scheme indicating the main stages of the self-assembly process in nanoscience, and the role of stimuli responsiveness. IC: initial configuration, t_0: time 0, r_0: reaction time, FS: final state. Reproduced with permission.[24]

Supramolecular chemistry attempts to mimic these properties by utilising biological and synthetic building blocks such as DNA, peptides, polymers, and metal-organic frameworks to build functional materials. A vast majority of studies on non-natural self-assembly focuses on molecule-molecule interactions, whereas biological complexity comes from the assembly of larger biological units, such as peptides and nucleic acids which build in hierarchy, leading to emergence. Emergence occurs when systems with different properties combine to form a final system which exhibits properties which is different to its substituent parts.[27] This is important as it drives the formation of systems which are more complex than the individual components. To confirm emergence, the system will not exhibit the same behaviour if one of the substituents is removed.[27] By using biological building blocks, it is possible to achieve complexity and precision when placing specific groups into materials as well as building in nanoscale control.

One of the challenges of producing biomaterials is controlling the assembly of substituents into desired structures.[18,25] Literature studies have discussed that this can be achieved through internal and external stimuli.[18] Internal stimuli refers to effecting interactions based upon but not limited to

hydrogen bonding, hydrophobicity and hydrophilicity, DNA hybridisation and electrostatics.[18,25] Internal stimuli are considered the initial driving force of self-assembly. External stimuli focus on adjusting system properties such as pH, temperature, ionic strength, and the addition of organic molecules. The reversibility of these noncovalent internal interactions in conjunction with external stimuli lead to dynamic switching of morphology and structure of self-assembled materials.[28] Peptides and DNA are well known for self-assembling through hydrogen bonding. DNA often self-assembles through Watson-Crick base pairing to form the classical B-form double helix, other examples of DNA self-assembly will be discussed later in this chapter. Peptides can form alpha helices, beta sheets and beta turns, through hydrogen bonding between amides and carbonyl groups, as well as aromaticity, charge and amphiphilicity.[28] However interesting structure can be built into peptides by controlling the amino acid sequence, and side groups. Hydrogen bonding is an inter- and intramolecular noncovalent interaction which can often be affected by the solvent in which the system is self-assembling. This can be especially important in nonbiological self-assembling systems where aqueous media can be a hydrogen bond competitor. Diphenylalanine (FF) is a good example of a peptide-based system which utilises hydrogen bonding, hydrophobicity and π - π stacking to assemble into different structures (Fig.4).

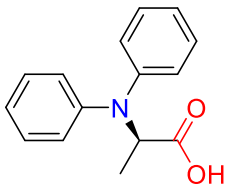

Figure 4: Structural illustration of Diphenylalanine (FF), showing amide in blue, and carboxyl group in red.

Li *et al.* showed FF to self-assemble through hydrogen bonding and hydrophobicity to form three different architectures; nanofibers, microtubes and microrods,[29] while Yang *et al.* showed that FF can self-assemble via both hydrogen bonding and π – π stacking with graphene to form peptide nanowires.[30] A good example of self-assembly control by pH, is Hoogsteen base pairing, an alternate form of DNA self-assembly to Watson-Crick pairing,.[31,32]. Hoogsteen hydrogen bonding allows a

base to bond with two other bases, which opens up the possibility of triplex formation.[31] A change in pH, generally to a lower pH, causes the bases to undergo a morphological shift from the *anti* to *syn* conformation causing complementary DNA strands to form bonds between three bases, enabling the formation of the DNA triplex.[31] Hoogsteen base pairing has been used in the design of pH activated DNA cargo delivery devices, as pH has been used to reversibly open and close a DNA device by shortening and or lengthening the device, as the Hoogsteen base pairing changes the length of the helix.[33,34] Other examples of Hoogsteen base pairing will be discussed in the next section, with relation to G-quadruplexes, which are not pH sensitive.[35]

1.3. DNA Self-Assembly and Applications

Nucleotide based nanotechnology is built upon the coercion of single stranded DNA/RNA to self-assemble into multi-dimensional structures through base pairing, the shape can be tuned by using appropriately selected sequences with different lengths.[18] DNA is favourable over RNA in this sense due to its lower susceptibility to degradation and increased stability of the phosphate backbone by the deoxyribose sugar, enabling longer DNA strands to be used. RNA however is more catalytically active than DNA.[36] Seeman, proposed the first use of DNA outside of biology, to achieve self-assembly of DNA into 2D crystals via 'sticky' ends (Fig.5).[37] The sticky end assembly motif comprises DNA double helices, with overhanging, unbound, single stranded ends, which are complementary to other double helices with the same motif. These complementary 'sticky' ends come together to form extended helices and joints, which lead to the formation of new structures.[37]

Figure 5: Schematic illustration showing 'sticky' end binding between two double stranded DNA units, 'sticky' ends are shown in pink, complementary strands are shown in yellow, and blue.

Seeman's work launched the field of DNA nanotechnology, with Rothemund demonstrating the assembly of 2D DNA origami structures in 2006.[38–40] DNA origami was achieved by the detailed folding of a scaffold strand, interwoven between double helices, with staple strands to secure and

reinforce the assembly.[38] DNA nanotechnology soon grew, and 3D origami structures were developed with more complex architectures than seen previously including curved, and interlocked structures.[41,42] Longfei Liu *et al*, demonstrated the use of DNA in the formation of quasicrystals, yielding great control over structural assembly to yield crystalline 2D structures.[43] Wei *et al.* took the assembly of DNA tiles further than previously seen by designing a four domain single stranded DNA which self-assembles to give distinct tiles (Fig.6).[44] These tiles were then self-assembled into diverse and complex 2D structures, demonstrating high nanoscale control over the bricks, yielding structures such as an eagle's head and triangle to name two of the designs achieved within their work.[44] With the success of the 2D tile architectures, Yin *et al.* went on to develop single stranded DNA bricks which were wholly synthetic in origin unlike the M13 single strand commonly used in DNA origami (which is partially synthetic).[39,40,45] They achieved 102 unique structures, with single brick nanoscale control, opening greater avenues into the field. The examples outlined above, are predominantly for the purpose of structural, programmable structures with pattern specificity.[31,39,46]

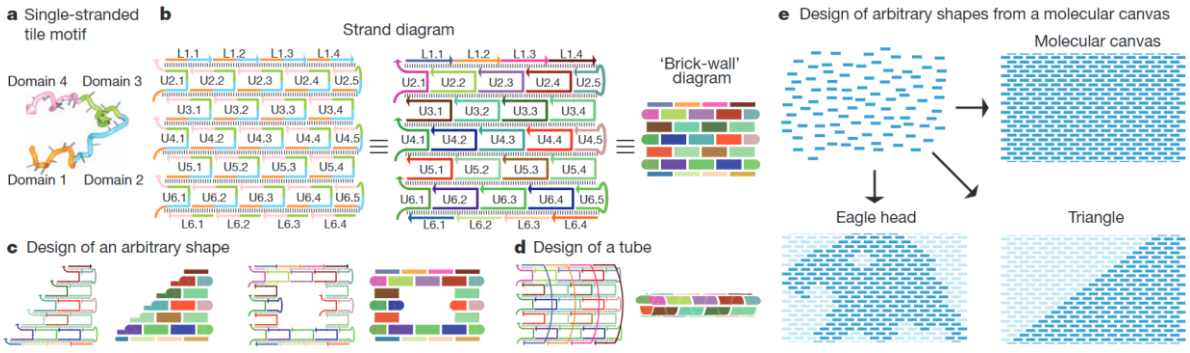

Figure 6: Illustration showing the work designed by Wei *et al.* a) The canonical SST motif. b) Design of an SST rectangle structure. Left and middle: two different views of the same secondary structure diagram. Each standard (full) tile has 42 bases (labelled U), and each top and bottom boundary (half) tile has 21 bases (labelled L). Right: a simplified 'brick-wall' diagram. Standard tiles are depicted as thick rectangles, boundary tiles are depicted as thin rectangles, and the unstructured single-stranded portions of the boundary tiles are depicted as rounded corners. Each strand has a unique sequence. Colours distinguish domains in the left panel and distinguish strands in the middle and right panels. c) Selecting an appropriate subset of SST species from the common pool in b makes it possible to design a desired target shape, for example a triangle (left) or a rectangular ring (right). d) Design of a tube with prescribed width and length. e) Arbitrary shapes can be designed by selecting an appropriate set of monomers from a pre-synthesized pool that corresponds to a molecular canvas (top right). To make a shape, the SST strands corresponding to its constituent pixels (dark blue) will be included in the strand mixture and the remainder (light blue) will be excluded. Adapted with permission.[44]

The field of DNA nanotechnology has continued to expand into dynamic system control, with the goal of investigating or mimicking biology more closely. The goal of mechanising DNA structures has yielded several different avenues of exploration, molecular devices, nanoscale robots, cell surface probes and sensors.[4,47–50] Douglas *et al.* designed a nanorobot which could deliver a payload through cell surface activation by DNA aptamers.[47] They showed they could synthesise a DNA origami robot and tune payload delivery based on the aptamer selection, showing promise as a drug delivery mechanism.

1.3.1. DNA Interactions with Small Molecules and their Applications

So far, DNA-only systems have been discussed, however nature is more complex than one kind of self-assembling molecule. The field has expanded to more complex systems by the incorporation of other molecules, with different intentions for the final application. Some of these modifications include the addition of polymers, small molecules, drugs, and metal organic frameworks.[51–55] DNA small molecule interactions have shown promise in several fields, such as therapeutics, structural control, and sensors.[50,56–58] The two main classes of DNA interaction with small molecules are either through non-covalent interactions, such as hydrogen bonding, intercalation and electrostatic interactions; or through covalent modification of a DNA strand.[59] Both types of interaction have their benefits in the fields mentioned above. This section will first discuss the interactions centred around non-covalent interactions.

DNA metal co-ordination has been used in therapeutics. Cisplatin is a platinum-based cancer therapy drug, which when activated in the cell environment can bind to double stranded DNA through interaction with the purine residues as well as other interactions with sulfhydryl groups and nitrogen donor atoms in other biomolecules.[60–62] Cisplatin is activated in cancer cell environments due to the exchange of its chloride ions with water, which makes it highly potent electrophile. Cisplatin can then form an adduct to purine bases (Fig.7) in DNA causing damage to the double helix, which blocks cell division, and leads to cell death.[60] Platinum is not the only metal

to bind with DNA to give useful interactions, other metals with anti-cancer activities include ruthenium and rhodium.[61,63]

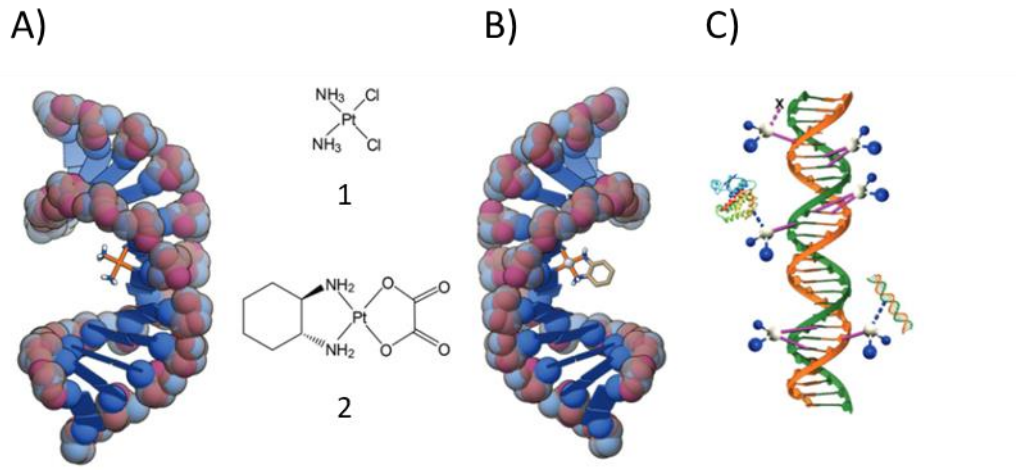

Figure 7: Examples of 1,2-intrastrand adducts formed between DNA, A) cisplatin (1), and B) oxaliplatin (2), and C) an illustration of the numerous types of possible adduct formations. Structures sourced from PDB files 2NPW, 1PG9 and 1BNA, respectively. Adapted with permission.[61]

Given the success of drugs such a Cisplatin and actinomycin D, which form adducts with DNA, it is unsurprising that this mode of action is of interest in the design of targeted drugs.[64,65] DNA exotic architectures like G-quadruplex and triplexes, require other small molecules or cations to stabilise them, similarly to B-form DNA requiring cations to stabilise the double helix. An example of small molecule stabilisation, is the use of cyanuric acid, with three thymine like faces, which has been shown to modulate the formation of unmodified poly(A) DNA strands into long fibres.[55] These fibres have an internal structure of a hexameric rosette, and were shown to be consistent across RNA and peptide nucleic acids as well (Fig.8).[55] This leads to potential in diversifying the assembly and function of nucleic acids and their derivatives.

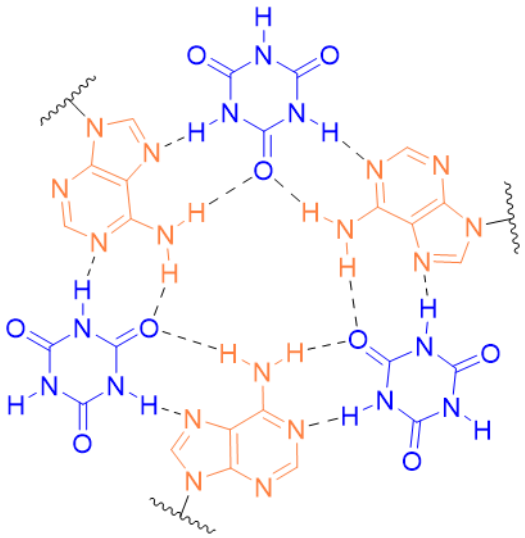

Figure 8: Schematic illustration showing the proposed hexameric rosette structure from reference 44. Cyanuric acid with three Thymine like faces is depicted in blue, with the Adenine bases represented in orange. Hydrogen bonding between the molecules and Adenine are shown with black dashed bonds.

Intercalation is the process by which a planar polycyclic molecule, which can be charged, inserts itself between base pairs, in either the major or minor grove of the DNA helix. This can cause the helix to become more rigid, lengthen, stiffen, and unwind.[61,66] Intercalators of DNA have shown use as stains in electrophoresis, as well anti-cancer activity, such as Doxorubicin. The ability to modify the intercalator can increase its affinity not only for DNA, but other molecules within the cell environment such as glutathione, which can increase cellular uptake and therefore increase the amount reaching the target cells.[61,66] G-quadruplex DNA is formed through Hoogsteen base pairing, however due to the large central pore of the quadruplex, this structure requires stabilising with cations, such as sodium, lithium, magnesium, and potassium (Fig.8) as they counter the electronegativity from the phosphate backbone, just as B-form DNA requires cations, like magnesium cations, to stabilise the double helix.[32,35,61]

G-quadruplexes have been shown to be key in cancer development, due to their presence at telomeres and oncogenic promoters.[35,67] This makes G-quadruplexes ideal targets for drug therapy, and the use of small molecules to achieve this is therefore valuable. Small molecules used to target

G-quadruplexes are generally different to those traditionally used as drug molecules. They generally have an aromatic surface to make use of π – π stacking in the quadruplex, positive charge, or basic groups, which improve binding within the grooves and loops of G4 quadruplexes.

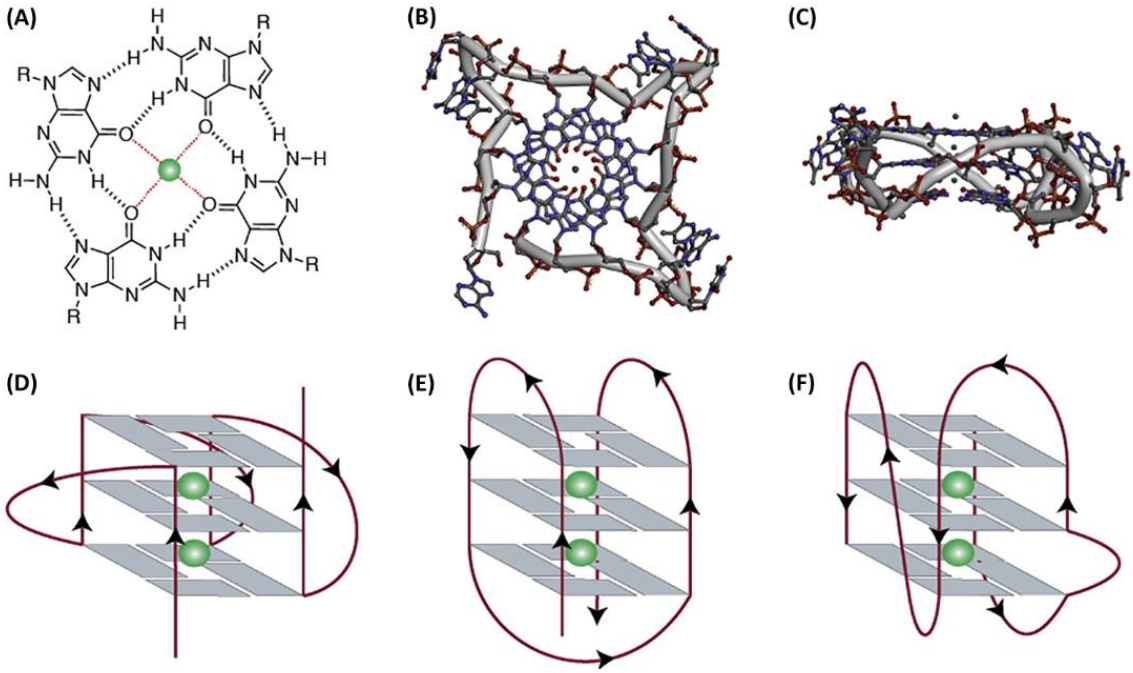

Figure 8: (A) Structure of a G-quartet formed by the Hoogsteen hydrogen-bonded guanines and central cation (coloured green) coordinated to oxygen atoms. Crystal structure of human telomeric G4s (Protein Data Bank: 1KF1): (B) top view and (C) side view; backbone is represented by grey tube and the structures are colour-coded by atoms. Schematic representation of unimolecular G4s based on the strand direction: (D) parallel, (E) anti-parallel, and (F) hybrid with a bulge. Adapted with permission.[35]

They also incorporate steric bulk, designed at preventing intercalation with double stranded DNA helices.[35,58,67,68] These extended interactions drive cellular uptake and could lead to the destabilisation of these quadruplexes leading to further therapeutic applications in cancer treatment.[64,67,68] Small molecule interactions with DNA leads to unique architectures, the incorporation of DNA with other moieties such as polymers opens further avenues of exploration, control, and assembly.

1.3.2: DNA-polymer Conjugates and Applications

DNA is inherently hydrophilic with a high negative charge density; when coupled with a hydrophobic polymer, this can lead to interesting phenomena due to the resulting amphiphilic

character.[69,70] DNA-conjugates are covalently bound, and generally lead to 1D, 2D and 3D nanostructures.[71] Non-covalent interactions can drive, patterning, templating, and architecture formation.[71] In the polymer focused literature there are a number of examples of polymer conjugation with other materials. These include supramolecular polymers which form through host-guest interactions, polymer-graphene oxide conjugates for the unzipping of DNA and binding of proteins, and polymeric sensing probe for α-amino acids to name a few.[72–74] However, for the purpose of this thesis, this section will explore DNA-polymer conjugates.

There are three main ways in which DNA-polymer conjugates may be synthesised, “graft from”, “graft to”, and “graft through” (Fig.9). Each have their positive and negative attributes, but all of these are hindered by both the hydrophilicity and charge density of DNA. These issues are especially noticeable in the merging of hydrophobic polymers with DNA. However, these amphiphilic molecules do show great promise in fields, such as nanoscale control, medicine, and data storage.[53,69,71] “Graft from” synthesis requires a DNA molecule modified with a polymeric active terminal, a unit which can act as the first point in a growing polymer chain. “Graft to” requires the pre-synthesis of both halves of the conjugate before combining them into one molecule. “Graft through” is predominantly used to synthesis polymeric-DNA brushes. This is achieved by assembling DNA chains which are modified with a polymeric unit at one end, the assembly is achieved through the polymerisation of the polymeric units on the DNA conjugates.[75]

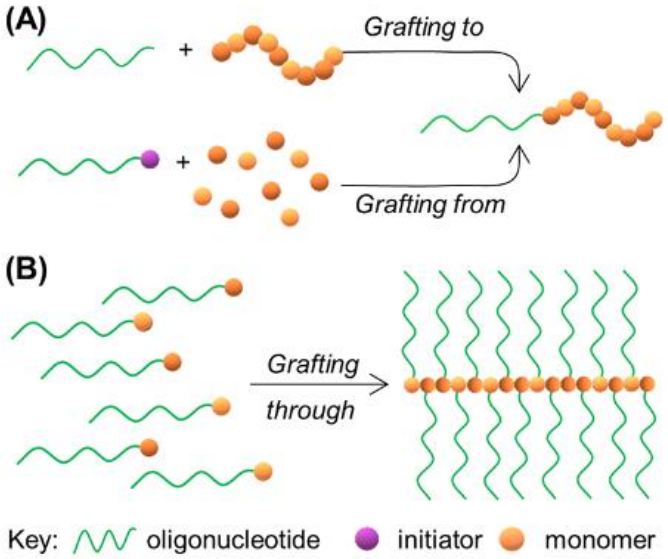

Figure 9: Common approaches to synthesise DNA−polymer conjugates. (A) Grafting to, i.e., polymerization in isolation from DNA, prior to covalent attachment and grafting from, i.e. polymerising from an initiator covalently attached to the DNA. (B) Grafting through polymerization of monomers either with the ODN already conjugated or with a functional group for post polymerization conjugation. Reproduced with permission.[71]

"Grafting to" could be seen as the route of least resistance when forming DNA-polymer conjugates, as each moiety is pre-characterised and controlled before combining them. Whereas the 'through' and 'from' methods must overcome more DNA effects on the system, such as high flexibility, and low reaction volumes, as well as the mixing of different types of assembly chemistry.[71,75] Some of these effects can be overcome by re-designing common polymerisation techniques, such as ROMP to be carried out in aqueous conditions. [75] Photoinduced RAFT polymerisation of DNA-polymer conjugates by the 'graft from' method was demonstrated by Lückerath *et al*., this method was used to design polymer conjugates to overcome the steric hinderance seen in the 'graft to' method. [76] The 'graft to' method was chosen as the preferred method in producing DNA conjugates in this thesis, because of the ability to overcome different reaction chemistries in the preparation of DNA and peptides.

Vyborna *et al.* showed the synthesis of DNA-grafted supramolecular polymers formed through aromatic stacking and hydrophobic interactions, which exhibited model cargo loading and release of DNA-functionalised gold nanoparticles. These structures went on to show chirality and the self-assembly of networks when annealed, through blunt-end DNA self-assembly.[69,77,78] This

self-assembly and control over DNA-polymer conjugates has also shown promise in the understanding of telomerase behaviour in cancer cells, which can be further used in identification and targeted delivery to tumours.[79] Zhu *et al.* showed the synthesis of DNA-polymer conjugates with multiple ligands, increasing the likelihood of successful targeted delivery.[79] They found that live imaging was possible within living cells, with potential in telomerase-based drug screening and cancer cell identification.[79] DNA-polymer conjugates have a wide breadth of use within science, as discussed above, but DNA can also be used to manipulate polymers through patterning and templating.[80] The synthesis of DNA origami-polymer moieties has given rise to precision control and expression of polymer chains on the surface of large architectures.[81] With applications in nanoscale-controlled coatings, and biomedicine to name two, this opens many avenues of exploration.[81] As well as the use of DNA to control polymer assembly like that seen in the encoding of protein templated assembly.[80] With these developments the field moves ever closer to the goal of successfully mimicking biology.

1.4: Peptide Self-Assembly and Applications

As discussed previously in sections 1.1 and 1.2; peptides form several assembly motifs, β-sheet, α-helices, triple helices, and random coils.[9] These assemblies form a variety of complex higher order structures, and can be used to advance a number of fields, such as; drug delivery, nanotechnology, biomaterials, and therapeutics.[82–86] Peptide self-assembly is predominantly driven through non-covalent interactions, encouraged by the utilisation of hydrophilic and hydrophobic residues, leading to amphiphilic properties (Fig.10).[9] This amphiphilicity gives rise to assembly, yielding faces of different amphiphilic character. These assemblies can then further assemble with other assemblies, giving rise to larger structures. Alternating positive and negative residues give rise to alternating charge distributions on the hydrophilic face of β-sheet assemblies, they have four main moduli they can exhibit; - + - + - + is type 1, - - + + - - + + is type 2, - - - + + + - - - + + + is type 3, and - - - - + + + + is type 4.[87]

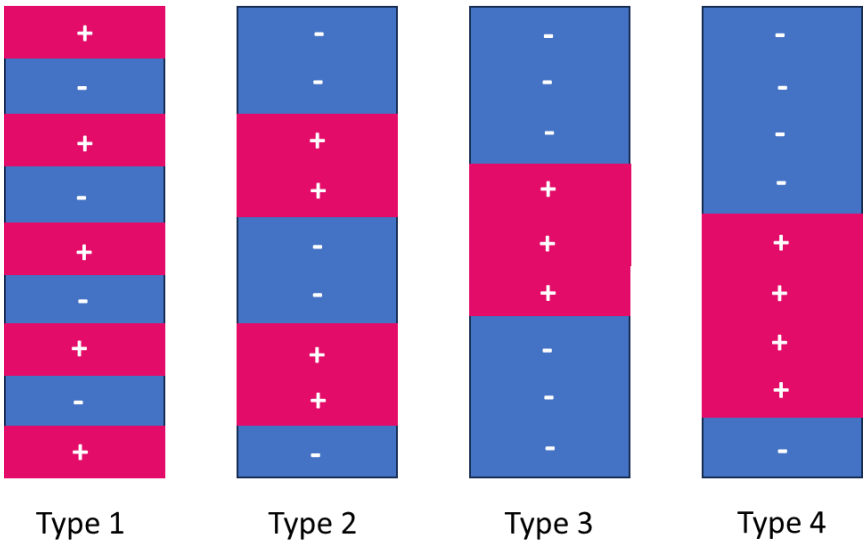

Figure 10: Illustration depicting the different types of charge distribution on the hydrophilic face of β-sheet assemblies. There are four main types, Type 1: alternating singular positive and negative residues, Type 2: alternating dual blocks of positive and negative residues, Type 3: alternating blocks of triplicate positive and negative residues, and Type 4: alternating quadruplet positive and negative residue blocks. Positive blocks are represented in pink, with plus symbols, negative blocks represented in blue with minus symbols.

β-sheet forming peptides can form several higher-level motifs including, tapes, ribbons, fibres, fibrils, and sheets, all facilitated through the complex hydrophilic/phobic and charge relationships along the faces of these assemblies (Fig.11). Shao, Wong and Seroski, showed the complementary co-assembly of two oppositely charged β-sheet forming peptides in to amyloid forming structures.[88] These peptides showed little propensity to assembly when separate, but when co-assembled showed an ABAB motif, with some AABB structures found.[88] Controlling the self-assembly of such materials allows further investigation and understanding into the study of diseases such as Alzheimer's disease and Dementia.

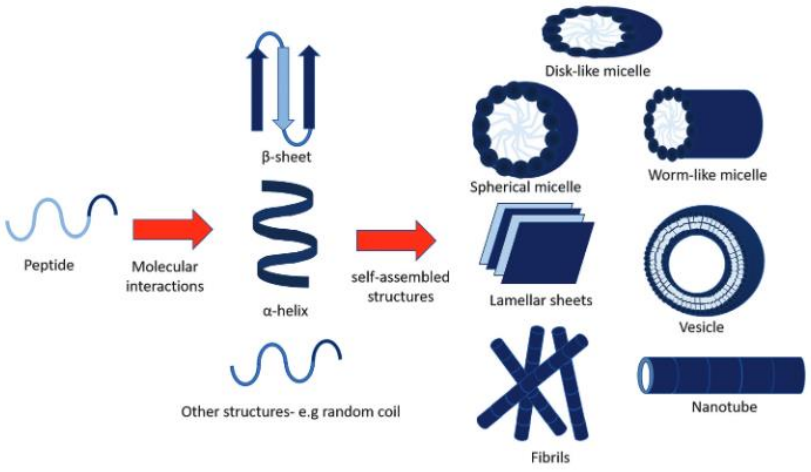

Figure 11*:* Possible self-assembled structures of peptide amphiphiles. Amphiphilic peptides may assemble into different secondary structures through inter and intra molecular interactions (e.g. electrostatic interactions and hydrogen bonding), and continue to aggregate into larger self-assembled structures. Reproduced with permissions from The Royal Society of Chemistry.[9]

An example of β-turn self-assembly is the work by Loo et al., where they use short hexameric peptides, such as ILVAGK to form a strong peptide bioink.[82] Bioprinting is a technique to produce multicellular 3D constructs for use in biomedicine This fields growth has been stunted due to a lack of suitable bioinks. Bioinks should have several properties, including but not limited to, mechanical strength, tuneable gelation, and biocompatibIlity.[82] Loo et al. were able to demonstrate that their hydrogel was highly biocompatible and stable in cell culture with fibroblasts without shrinking for 3 weeks. As well as maintaining in-vivo injection into mice for two months with limited immune response.[82] This work shows a broad range of use and application of bioinks with potential to vastly improve the field of bioprinting. Alpha helices are a folding pattern found in proteins they form through a mixture of hydrophobic and hydrophilic residues, with a periodicity of 3.6 amino acids per turn.[84,87] Alpha helices can assemble into coiled coils, however a downside of this assembly is it often requires long chain lengths to stabilise the helix.[84] Woolfson et al. showed the ability to control the lateral association and longitudinal assembly of coiled coil peptide nanotubes from α-helical barrels.[89] They achieved this through modular design and stimuli responsiveness to pH, by controlling acidity, the assembly - through positive and negative residues - is switched on and off.[89] The internal porosity of the materials showed successful internalisation 1,6-diphenyl hexatriene,

which when in hydrophobic conditions behaves as a fluorophore.[89] This modular control and internal hydrophobic cavity, show promise in fields such as storage and drug delivery for peptide nanotubes.

Collagen is a key component of the extracellular matrix of cells within humans, it also has numerous structural and mechanical properties useful within and outside of biology.[90] The collagen family consists of 28 different types, each with a varied architectures and functionalities, however they all remain true to having triple helical bundles.[87] Natural collagen is susceptible to low thermal stability and contamination by pathogens. Collagen mimetic peptides have been developed, using the same sequential structure with proline and hydroxy proline driving the triple helix formation (Fig.11).[90] Collagen mimetic peptides have been used in several fields, such as targeted delivery, collagen healing and extracellular matrix mimicry, because of their structural stability and programmability through residue choice.[90,91]

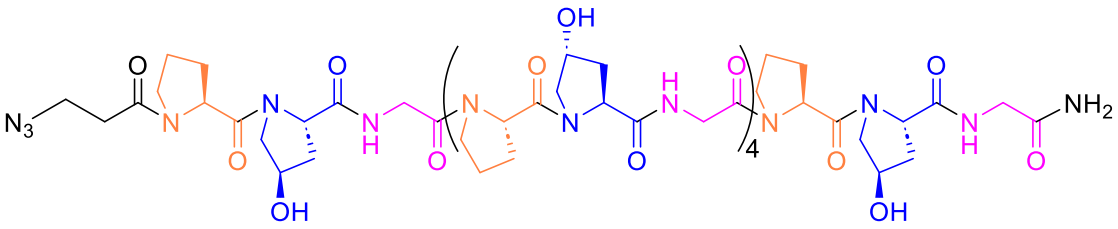

Figure 11: Schematic illustration of azide modified (black) POG_6 (proline (orange), hydroxyproline (blue), and glycine (pink)), a collagen mimetic peptide made of six repeating units of proline, hydroxyproline, and glycine.

Kiik *et al.* demonstrated control over the self-assembly of collagen-like peptide (CLPs) and elastin-like polypeptides (ELPs).[91] By changing the length of the ELP domain, they were able to change the morphology from vesicles in their prior work, to platelets with the ELP sandwiched between two CLP domains.[91] With control over this bilayer-like structure the work shows promise in the encapsulation of hydrophobic and or aromatic drugs, especially when combined with the biocompatibility of the peptide domains chosen.

Peptides have such a broad range of applications, and drug delivery is one of the most promising, with several peptide based drugs on the market today, Enfuvirtide, used in the treatment of HIV-1,

Exenatide, used on the treatment of Type 2 Diabetes, and Ziconotide, used to manage chronic pain.[92,93] These are to treat areas such as cancer, cardiovascular disease and endocrinology.[94,95] The vast majority of these peptide based drugs take their design from antibody drug conjugates (ADC), where instead of a large cumbersome antibody is being attached to the drug, a smaller peptide is being attached instead.[94] These smaller peptides have a number of advantages over antibodies, largely due to their simplicity to synthesise and the loss of steric bulk. However, a drawback of peptide-based drugs, is their, *in vivo* instability and poor membrane permeability.[92] The peptides are attached through well-established bioconjugation, using thiol-maleimide and click chemistry motifs.[94] An interesting example of peptides in drug delivery is through cyclization of peptides. Peptides which have been cyclized have been used as drug delivery vessels.[83,95] Wang *et al*. showed an eight-residue cyclic D,L-α-peptide self-assembled into nanotubes, which was then used to encapsulate doxorubicin, which showed an increased uptake in human breast cancer cells.[95]

In this chapter the diversity of self-assembly and applications achieved in both DNA and peptide chemistry has been summarised. This exploration into the literature and discussion of what can be done with these biomolecules, is broad and can be seen in fields such as, self-assembly, nanotechnology, and medicine. This highlights the benefits which could be achieved by combining DNA and peptides into singularly covalently bound molecules, by bringing together the best properties from both molecules, new knowledge can be gained from the types of structures observed and the control over their formation. This knowledge can advance our understanding of, and ability to produce synthetic biological systems. In the next section a review of the literature with regards to the conjugation of DNA and peptides is explored, with an emphasis on how this supports the work discussed within this thesis.

1.5: DNA-Peptide Self-Assembly and Applications

The self-assembly of DNA-peptide conjugates is driven by the individual properties of DNA and peptides as discussed previously in sections 1.3 and 1.4 respectively. DNA-peptide conjugates

combine the programmability of DNA base pairing with the versatility of peptide assembly.[96] In this section the applications of DNA-peptide conjugates will be discussed with a focus on the areas in which they are relevant. Figure 12 is an overview of DNA-peptide materials, adapted from reference 77 with permission.[96]

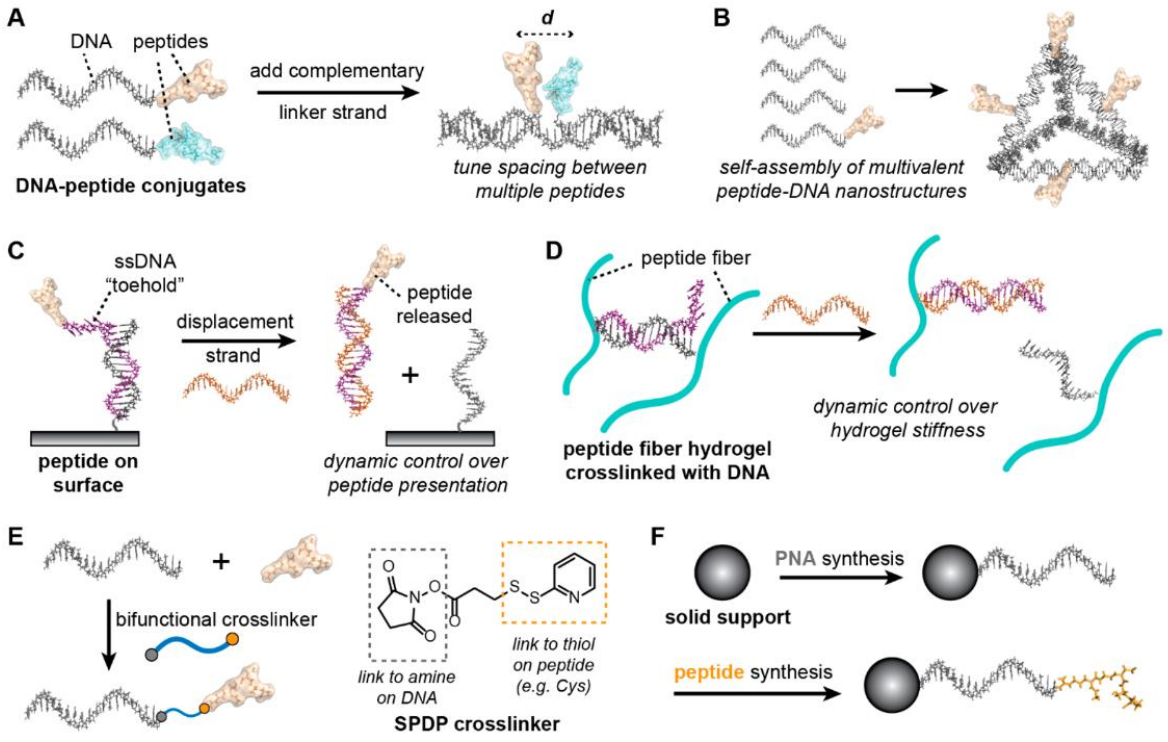

Figure 12: Peptide–DNA nanomaterials. (A) DNA–peptide conjugates can be used to tune the distance between the peptides using a complementary strand linker. (B) Self-assembly of DNA nanostructures (e.g., a tetrahedral cage) from DNA–peptide conjugates and unmodified strands. (C) Toehold-mediated strand displacement to remove a bioactive peptide from a biomaterial surface. (D) Reversible cross-linking of peptide–DNA hydrogels to tune mechanical properties and hierarchical assembly. (E) Synthesis of DNA–peptide conjugates using a bifunctional cross-linker (like the amine- and thiol-reactive linker SPDP). (F) Synthesis of PNA–peptide conjugates through sequential on-resin coupling of PNA monomers followed by amino acid monomers. Reproduced with permission.[96]

1.5.1: Applications of DNA-Peptide Conjugates

DNA-peptide conjugates have been used to demonstrate nanoscale control over self-assembly with various examples in the literature, including the assembly of DNA origami blocks, the formation of DNA nucleoproteins, and tuneable DNA-peptide fibres.[97–99] Jiang *et al.*, showed the assembly of nanowires from the co-assembly of DNA origami sheets and collagen mimetic

peptides.[100] The collagen mimetic peptide once assembled was designed to have positively charged domains at each end. When these domains encountered the negatively charged DNA origami sheets, charge induced self-assembly occurred.[100] This assembly could be tuned using the number of extruding positive residues on the collagen mimetic peptide, when the number was below three on each side, there was disordered assembly observed with the DNA sheets. Changing the dimensions of the DNA tiles into ribbons also changed the assembly, allowing both face to face and edge to edge assembly.[100] An example of controlled assembly of DNA origami blocks using DNA-peptide conjugates is that by Buchberger *et al*. In Buchberger's work they synthesised a coiled-coil heterodimeric pair of DNA-peptide conjugates, with the DNA sequences being complementary to the DNA handles found on the DNA origami blocks (Fig.13).[97] Buchberger explored the effect of number of handles on assembly and found that they were able tune the length of their 1-dimensional linear arrays. Two handles or less, formed mostly monomers and dimers, four and six handles produced short arrays, and eight plus handles produced long arrays.[97]

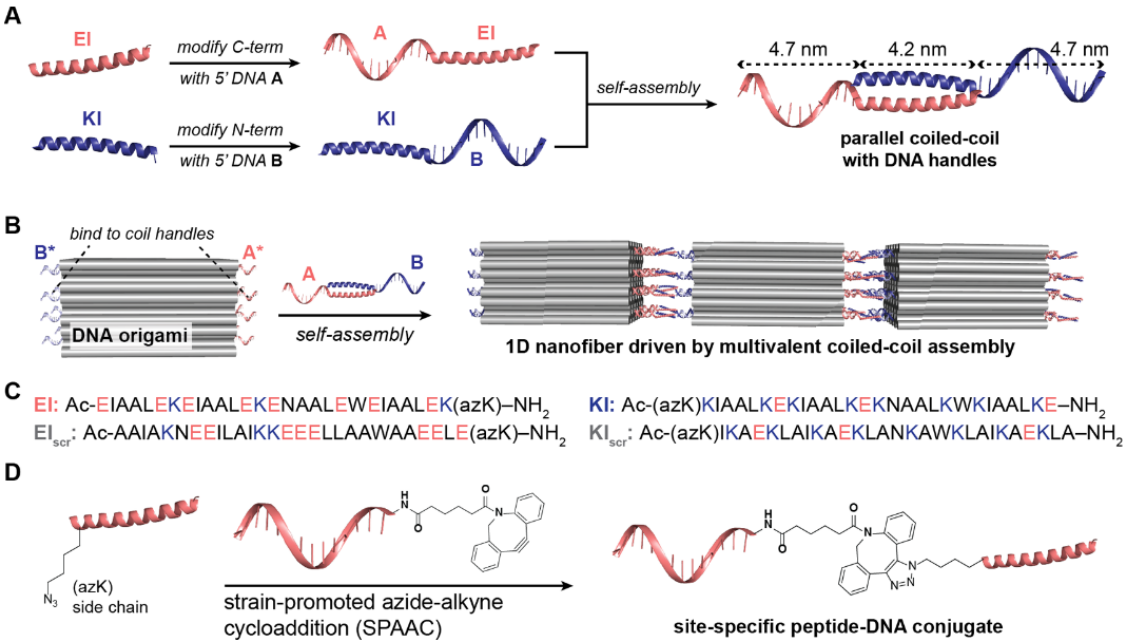

Figure 13: Overview of strategy for assembling DNA origami with coiled-coils. (A) Site-specific functionalization of two peptides comprising a coiled-coil with DNA. Mixing the two peptide–DNA conjugates yields a self-assembling coiled-coil with two orthogonal oligonucleotide handles. (B) Assembling a DNA origami structure (e.g., a cuboid) with multiple ssDNA handles into 1D nanofibers driven by the coiled-coil bearing complementary handles. (C) Amino acid sequences (N→C) of the four peptides used in this study; (azK) indicates azido lysine. (D) Strain-promoted alkyne–azide cycloaddition (SPAAC) conjugation between

the side chain of (azK) and the dibenzocyclooctyne (DBCO) moiety on DNA to yield a peptide−DNA conjugate. Reproduced with permission.[97]

Moving away from DNA-peptide conjugates and pre-assembled architectures, Daly *et al.* demonstrated the self-assembly of DNA-peptide conjugate fibres, with controlled structure using diphenylalanine conjugated to complementary DNA sequences.[99] As already discussed in this chapter, diphenyl alanine is known to assemble into well-defined structures.[29,99,101] Daly *et al*. analysed the peptide assembly first and found that it formed filaments, which when annealed formed twisted fibres, they then went on to explore how the addition of DNA to this system effected the assembly of diphenylalanine.[99] This resulted in controlled helicity of the fibres based on the length of the DNA domain. They demonstrated bundling of these fibres through complementary DNA assembly, as well as showing control over the type of assembly observed by utilising strand displacement, and environmental control.[99] DNA-peptide conjugates can be formed through various routes, an example of this is to join the DNA and peptide portions to an organic core, creating a triblock peptide-oligonucleotide. Merg *et al*., demonstrated the design of a triblock peptide-oligonucleotide, which could assemble into single walled vesicles by controlling salt concentration.[102] The morphologies of these triblock conjugates could be controlled by increasing or decreasing this salt concentration with annealing. At high salt concentrations, bundled fibres were observed whereas at low salt concentrations, indistinct structures were observed which is likely explained by the charge shielding effects of salt on the DNA backbone.[102] The efficacy of this system was tested by reducing the length of the DNA domain, and repeating the same experiments at different salt concentrations, they found that a shorted DNA domain allowed fibres to form at lower salt concentrations confirming that the charge of the DNA backbone played a large role in assembly.[102]

So far, controlled assembly of DNA-peptide conjugates has been discussed. Controlled assembly aids development in fields such as biology and medicine.[5,98,103,104] This precise control over assembling systems is something nature does very well, and if scientists are to achieve the same

level of complexity as seen in nature this control is key. Kye has demonstrated precise control over the assembly of a β-sheet forming peptide and complementary DNA sequences into a deoxyribonucleoprotein (DNP).[98] In this work Kye exhibited the assembly of DNA-peptide conjugates into DNPs via two routes, DNA assembly or peptide assembly first resulting in the same overall structure (Fig.14). By using an antisense DNA strand within the structure, they were able to show uptake into a HeLa cells, with an effect of 50 % on GFP expression.[98] They were also able to show that by tailoring the strength of the DNA duplex, they could reduce non-specific binding of the antisense strand within target cells.[98]

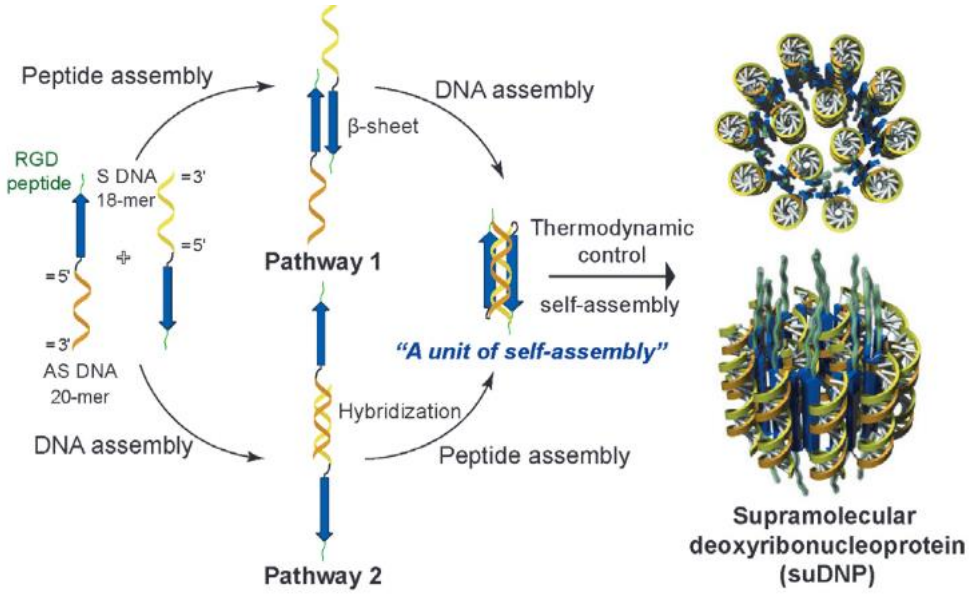

Figure 14: Pathways for the dual-mode self-assembly of complementary peptide–DNA conjugates into a toroidal global minimum state. Reproduced with permission.[98]

DNA-peptide conjugates can also be used in the analysis of single molecule sequencing of proteins.[103] Biswas *et al.* showed the click addition of DNA to peptides aided the translocation of these peptides through solid state nanopores.[103] This method of sequencing peptides and proteins has been largely held back by the variable charge found across the molecules due positive, negative, and neutral side chains. Biswas showed that the addition of a polyT_{20} strand via click chemistry aided the translocation of peptides through the nanopores, where the individual peptides showed no translocation and the single DNA did.[103] They also observed that the end of the DNA in which the peptide was attached, 3 or 5 positioning also effected the amount of translocation through

the nanopore, with modification at the 5 end being favoured.[103] This work shows promise in the potential to improve protein and peptide sequencing in situ and to advance this technology forward.

DNA-peptide conjugates, formed from two biological molecules, lend their use in fields such as *de novo* protein design, an example of this is the work by Lou *et al*.[5] Lou *et al*. began by synthesising three separate DNA-peptide conjugates, two longer DNA domains, and a shorter one in order to achieve a DNA triplex, to each of these a coiled coil forming peptide was attached.[5] It was observed that the DNA triplex without peptide domains was less stable than the triplex with peptide domains, in addition the α-helicity was increased in the peptide domain when attached to the DNA triplex when compared with the native peptide.[5] It was also observed at higher concentration of assembled units dimerization was observed between assemblies opening up the possibility of larger assemblies and de novo protein design.[5]

Already discussed in section 1.4 was the benefit peptides have in the development of networks which mimic the extracellular matrix, it therefore suggests that DNA-peptide conjugates may exhibit the best of both molecules in this regard. The work by Stephanopoulos *et al.*, combines DNA double crossover tiles with sticky ends and DNA-peptide conjugates, with a RDGS protruding peptide, known for its potent cell binding.[104] Firstly they explore the assembly of the DNA nanotubes with and without the presence of the peptide, yielding the same structures in both instances, confirming little structural changes induced by the peptide.[104] The nanotubes were incubated with 3T3 fibroblast cells to demonstrate the presence of RDGS on the surface. The survival and differentiation of neural cells was assessed, with the potential to have an impact in regenerative medicine, such as neurodegenerative conditions like Alzheimer's and Parkinson's diseases.[104] Stephanopoulos *et al.* were able to successfully show the survival and differentiation of neural stem cells into neurons over astrocytes using these DNA-peptide conjugate nanotubes.[104]

In this section the applications of DNA-peptide conjugates have been explored in some detail with a focus on nanoscale control, assembly, and applications within medicine.

1.6: Aims of this PhD Thesis

The aim of this work was to combine DNA with peptides and study their self-assembly, both individually and together. By combining two different building blocks, the integration of hierarchical assembly in these systems was able to be explored. This thesis discusses the synthesis of DNA-peptide conjugates via several methods, before diving into three distinct self-assembly studies designed at understanding the role of both DNA and peptides within our system. Chapter 2 discusses the synthesis of DNA, DNA maleimide and DNA azide monomers, before the final synthesis of DNA-peptide conjugates vis these routes. The characterisation and purification of these structures is also explored, as well as several studies aimed at better understanding the conjugation strategies selected.

Chapters 3, 4, and 5 explore the self-assembly of our DNA-peptide conjugate system. The assemblies were observed over a 28-day aging period, with analysis by circular dichroism (CD), dynamic light scattering (DLS) and atomic force microscopy (AFM) at 0, 7, 14, 21 and 28-days of aging. Chapter 3 focuses on peptide driven self-assembly, with a focus on the effect the addition of DNA-peptide conjugates of different concentrations effects the native peptide. Chapter 4 combines both DNA and peptide driven self-assembly, by hybridising the DNA-peptide conjugate with a single, double, and triple length ssDNA complement. Chapter 5 switches off peptide self-assembly by the addition of denaturant and observes the change in morphology with only DNA driven assembly present. Chapter 6 consists of a brief overall conclusion with a look towards future work and references.

Chapter 2: Synthesis and Characterisation of DNA-Peptide Conjugates for the Study of their Self-assembly

2.1: Introduction

Biological system complexity is built through the self-assembly of biological material building blocks, like DNA and peptides.[105] DNA is well-known for its predictable self-assembly architecture, like double helices, G-quadruplexes, as well as its and Watson-crick [106] , and Hoogsten base pairing. Making it an ideal candidate to be utilised in the chemists' pursuit of complex self-assembling motifs which can mimic the complexity of nature. In an attempt to utilise the natural self-assembly motifs in nature, early DNA nanotechnology utilised unspecific base stacking between DNA strands to form 2D arrays.[105] Sticky ends were originally applied to linear DNA strands but their use in the formation of junctions led to the advancement and formation of more complex architectures such as; DNA crystals, lattices and cages.[106] Sticky ends utilised along non-linear arrays led to the development of 3D DNA crystal structures; formed from DNA 2D triangles by Zhang from the Seeman lab in 2009.[107] Another method used to form DNA architectures used a scaffold strand: a long single strand of DNA often kilobases long.[38,108] These scaffold strands are folded into specific shapes using short single strand 'staples'. These short DNA sequences bind to specific points along the scaffold manipulating its folding into specific shapes.[106]

These two principles began the foundations with which structural DNA nanotechnology took hold; researchers have focused on extending the complexity of these systems. Either by scaling up the synthesis to form megastructures[109] or by finding new binding based motifs such as end-to-end base stacking interactions between tiles or sticky-end adhesion of blocks.[44,45] The translation of DNA information is facilitated in biology by other macromolecules such as proteins.[110] In order to truly mimic biology in its complexity DNA nanotechnology must become dynamic. One of the simpler ways to achieve this is by using phosphoramidite chemistry, either by introducing synthetic monomers into the backbone of the DNA or by first functionalising DNA bases before attachment

onto the backbone.[111] These functionalities are placed with nanometre precision aiding in the ability of this functionalised DNA to interact with surface membranes. An example of this in the literature is the ability to exploit functionalised staples to self-assemble DNA origami on the surface of lipid membranes allowing the formation of nanopores or changing surface layer construction.[112,113]

A way of increasing the dynamic character of DNA structures is by conjugating DNA to other molecules such as polymers and peptides or proteins.[114–116] Peptides are becoming a more common constituent in the formation of DNA conjugates because of their ability to perform the same jobs as large proteins as well as their rich self-assembly motifs.[10] Peptides can also have amphiphilic character meaning they can form similar structures to those seen in DNA – polymer conjugates.[117] Another reason peptides are preferable over proteins is the ease with which they can be synthesised through solid phase synthesis which also means that their naturally diverse library of amino acids can be extended with synthetically modified versions.[10–12] Peptide nucleic acids (PNAs) are synthesised generally by solid phase synthesis which has been modified to accept both peptide and DNA solid phase synthesis methods. However, DNA-peptide conjugates are covalently bonded by a linker molecule using chemistries such as an azide-alkyne or maleimide – thiol.[12,118] The synthesis of peptide – oligonucleotide chimeras in a triblock co-polymer show stimuli responsive self-assembly. In the presence of high salt concentrations micelle like structures are formed but a reduction in salt concentration generates the formation of ribbon like fibres which have been shown to be mediated by the β-sheet forming peptide.[102] As discussed previously in section 1.3, DNA origami is often used as a scaffold upon which more complex structures are built.[109] Recent work by Jiang has shown that complex DNA origami structures can self-assemble with collagen mimetic peptide sheets to form nanowires with high order and structure.[115] The use of an amphiphilic peptide in this case allow both the formation of the collagen mimetic sheet and complexation with DNA sheets through electrostatic interactions. This chapter details the synthesis and characterisation of two bifunctional crosslinkers, as well as the method development to

achieve modification of DNA with these bifunctional crosslinkers. Finally, the synthesis and characterisation of DNA-peptide conjugates will be discussed.

2.2: Results and Discussion

All buffer compositions and details can be found in section 7.1.1.

2.2.1: Synthesis and Characterisation of Compounds 1 to 3, and the Attachment of Compound 3 to DNA

Compounds **1** to **3** are shown in Fig. 2.1, this section will describe their stepwise synthesis, and challenges experienced at each stage. As well as discussion around how these challenges were overcome to yield the next compound. Compounds **1** and **2**, were precursors to the target compound **3**, which was a phosphoramidite based bifunctional linker, it was designed to be attached to DNA oligonucleotides through standard solid phase synthesis via the DNA phosphate backbone.

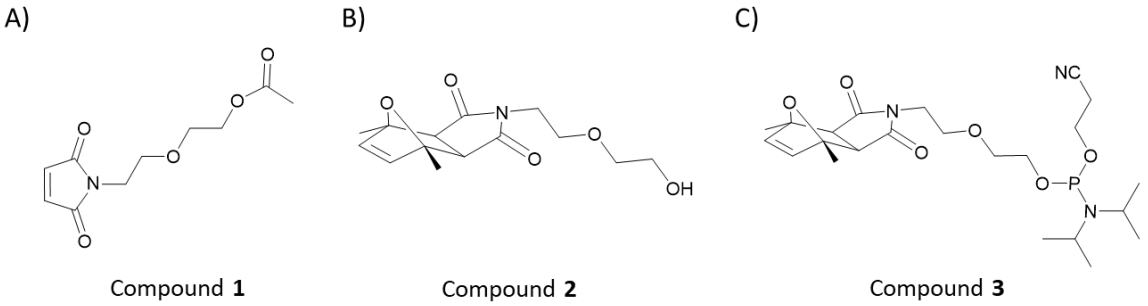

Figure 2.1: Structural illustrations of compounds **1** to **3**. A) an acetal protected maleimide ethoxyethanol (compound **1**), B) maleimide ring protected (furan) with acetyl group removed (compound **2**), C) furan protected maleimide phosphoramidite (compound **3**).

Compound **1** (acetate protected maleimide ethoxyethanol); the synthesis of an acetyl protected maleimide was originally conducted at a molar ratio of 2.36–1 (maleic anhydride – amino-ethoxyethanol) based upon a method used previously in the group. This yielded a mixture with many similarly structured compounds, which included the ring open form (Fig.2.2) and excess starting materials. In an attempt to purify the crude mixture, silica gel chromatography in 3:2 hexane : ethyl acetate was performed, however this yielded no product due to sample loss to the

column. Referring to the literature the molar ratio was adjusted to 1.1 : 1 (maleic anhydride : amine), this yielded a crude product with some ring opened form.[119]

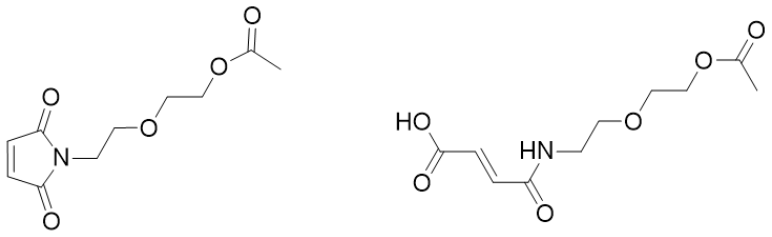

Figure 2.2: Structural illustration of compound **4**, and compound **4** which has ring opened.

When left to sit at room temperature for two days the impurities crystallised out, because compound **1** was a thick oil, the crystallites were removed by aqueous washing with concentrated HCl, K_2CO_3 and brine extracted the impurities more successfully. The original target compound had an alcohol end group however despite purification only compound **1** with an acetyl end group was isolated (Fig.2.3). The primary alcohol on the end of the ethoxy chain attacks the acetic acid. The primary alcohol was then substituted with an acetyl group with the formation of water as a by-product. The acetyl group generated a peak a 2.0 ppm in the ^{1}H spectrum (Fig. 2.3, peak f). Carbon 13 1D NMR can be found in section 7 (Fig. 7.2).

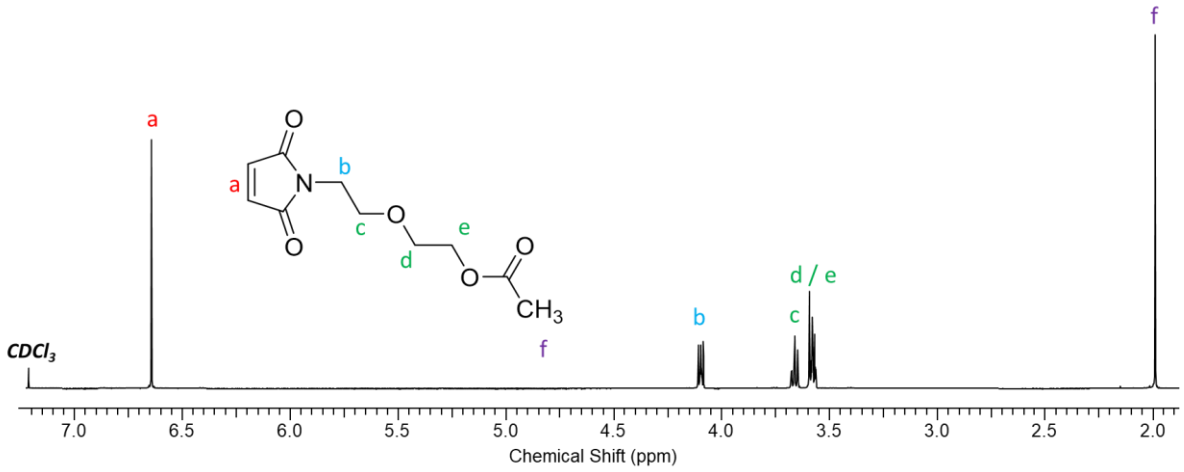

Figure 2.3: ^{1}H 1D NMR spectrum of compound **1** (maleimide ethoxy acetyl) in deuterated chloroform. : ^{1}H 1D NMR (400 MHz, $CDCl_3$) δ H_a 6.64 (2H, s) H_b 4.11-4.08 (2H, t) H_c 3.68-3.65 (2H, t) $H_{d,e}$ 3.60-3.56 (4H, dt) H_f 1.99 (3H, s).

This was easily rectified later in purification of compound **2** because deprotection of an alcohol protected by an acetyl group is readily achieved in basic conditions upwards of pH 9.0, which concentrated ammonia hydroxide solution is. After purification compound **1** was taken onto the synthesis of compound **2**.

Compound **2** was a protected form of compound **1**, the maleimide was protected with dimethyl furan, as the maleimide ring is susceptible to degradation in basic conditions, during cleavage and deprotection in solid phases synthesis of DNA oligomers.[119,120] Protection of compound **1** was achieved via Diels-Alder chemistry and yielded a stereoisomeric mixture of *endo* and *exo* forms as confirmed by 1D proton NMR (Fig.2.4). Unlike standard Diels-Alder chemistry where the *endo* form is usually favoured and forms first, this reaction favours the *exo* form this is in part due to the aromatic character of furan making it unusually stable.[119] The temperature of the reaction (65 ˚C) causes the *endo* product to form and quickly undergo a retro-Diels Alder to the starting materials allowing the *exo* product to form, being less sterically hindered it does not undergo retrosynthesis as readily as the *endo* form.[119] The next step was to isolate the *exo* form of compound **2** this was achieved by treating the mixed product with concentrated aqueous ammonia at room temperature overnight. This degraded the *endo* form alone, producing a brown viscous oil. Compound **2** (*exo*) was extracted by aqueous washing with concentrated HCl, K_2CO_3, and brine yielding a clear yellow oil.

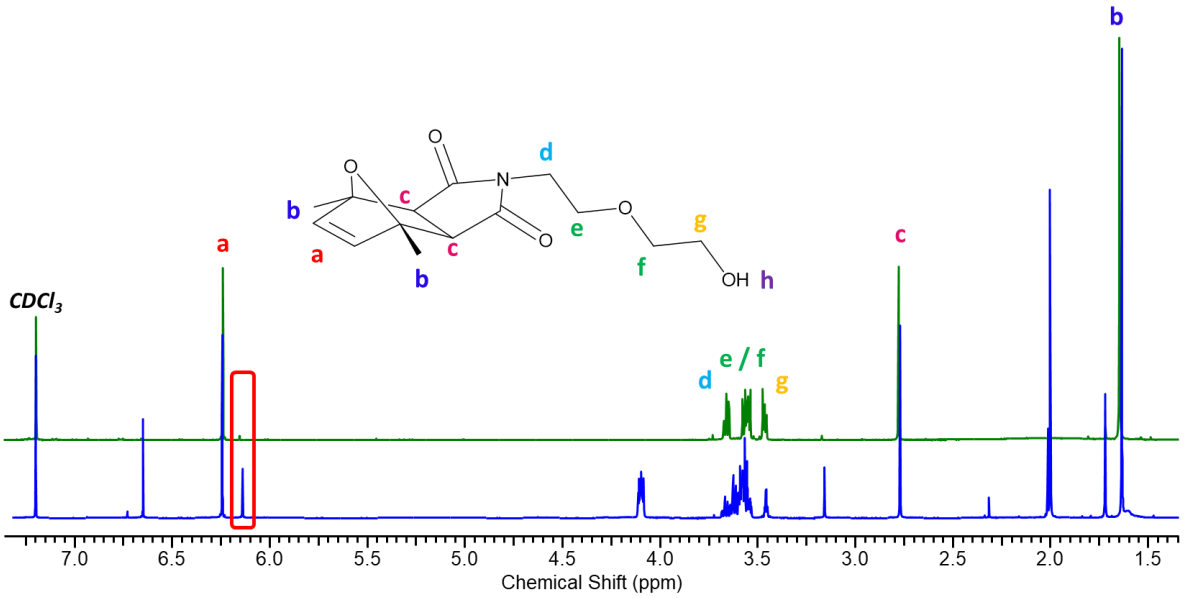

Figure 2.4: Overlaid ^{1}H 1D NMR spectra of compound **2** (*endo*) and (*exo*), crude spectrum is shown in blue. Unreacted compound **1**, can be seen by the triplet at 4.1 ppm, representing the protons situated next to the amine in the maleimide ring. The endo form of compound **2** is shown by the peak at 6.16 ppm. Purified spectrum of compound **2** is shown in green, after treatment with concentrated aqueous ammonia to remove the *endo* form. Carried out in deuterated chloroform. Note the disappearance of the highlighted peak at approximately 6.16 ppm which represents the *endo* form of compound **2**. ^{1}H NMR (400 MHz, $CDCl_3$) δ H_a 6.24 (2H, s) H_d 3.68-3.65 (3H, t), $H_{e,f}$ 3.60-3.55 (6H, dt) H_g 3.49-3.46 (3H, t) H_c 2.78 (2H, s) H_b 1.85 (6H, s).

Phosphoramidites are prone to rapid oxidation during synthesis and purification. The synthesis of the phosphoramidite (compound **3**) version of compound **2** proved to be the most difficult due to oxidation. The first synthesis was based upon a method already established within the group and adapted from the literature. This method used an excess of 2-cyanoethyl N,N-diisopropylchlorophosphoramidite (P–Cl) and DIPEA and purification was carried out by silica gel chromatography in DCM : Hx : TEA (41 : 58 : 1) as this showed good separation by TLC. TEA was used to basify the silica as acidic conditions activate phosphoramidites in preparation for nucleophilic displacement which in turn promotes oxidation of phosphoramidites. However, the product remained stuck on the baseline of the column despite increasing the amount of DCM and TEA in the running buffer. This method was repeated several times with varying solvent ratios, and chloroform in place of DCM, however the product always remained on the column. The product was oxidising on the silica column, alumina chromatography was attempted as an alternative to silica chromatography however the same issue was encountered.

To overcome oxidation and loss of product, the purification method was changed to aqueous extraction with K_2CO_3 and brine. Initial attempts with this method of purification showed extraction of unreacted starting materials but did not remove oxidised compound **3**. Phosphorous NMR showed the presence of only oxidised compound **3** as shown in Figure 2.5.

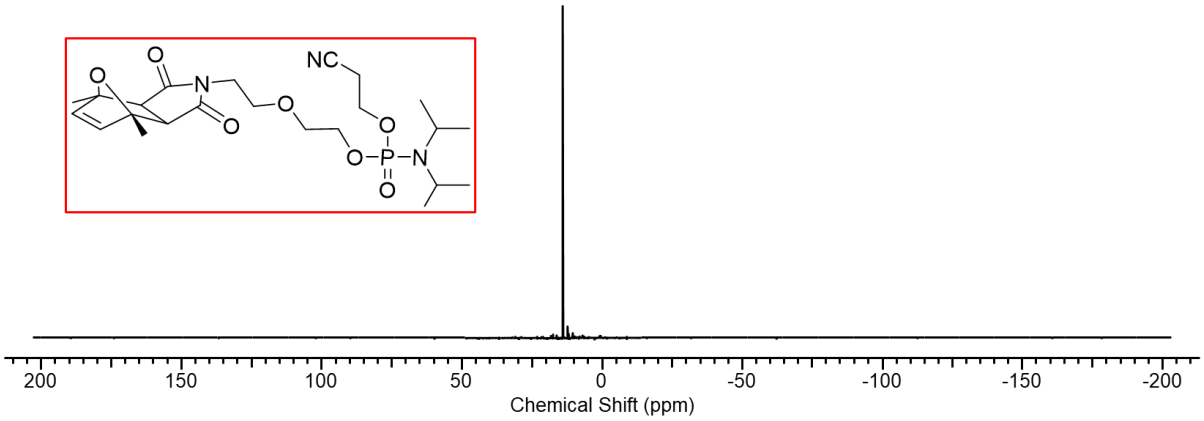

Figure 2.5: Phosphorous NMR of oxidised compound 3 purified by aqueous extraction in dichloromethane with a deuterated DMSO capillary.

To reduce the amount of oxidised compound **3** the reaction solvent (dry tetrahydrofuran, THF) was replaced with dry DCM, as this removed a solvent removal step before aqueous washing, allowing purification to be carried out in the same solvent. Aqueous solvents were also degassed with nitrogen for a minimum of 1 hour. These changes to the method did increase the purity of compound **3** however large peaks of oxidised product were still visible in the ^{31}P NMR (Fig. 2.6). As a large percentage of the product was still being oxidised, it was decided to change the molar ratios of the starting materials from 1 : 3 : 5 (**2** : P-Cl : TEA) to 1 : 1 : 5 (**2** : P-Cl : TEA).

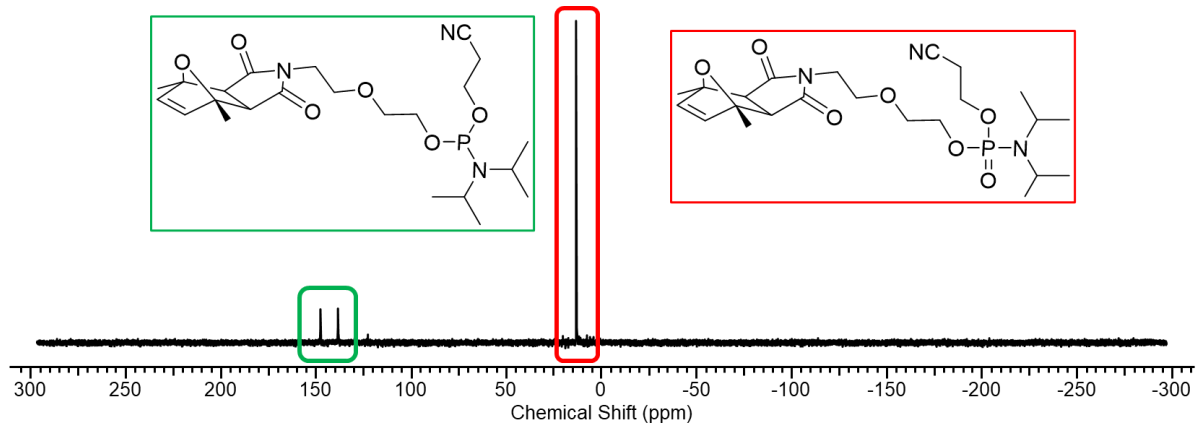

Figure 2.6: Phosphorous NMR of compound **3**: Unoxidised: Phosphorous 3, ≈ 147 ppm (*exo*) and ≈ 137 ppm (*endo*). Oxidised: Phosphorous 5, ≈ 12 ppm. Purified by aqueous extraction in dichloromethane with deuterated DMSO capillary.

It was hypothesised that by removing the excess phosphoramidite chloride, that the amount of oxidised product might be reduced. Purification was further improved by the use of small-scale silica gel column chromatography. As the oxidised product would remain on the baseline of the column a flash purification should have been enough to purify compound **3**. This was achieved in a solvent system of DCM and TEA (95 : 5), by increasing the percentage of TEA the likelihood of oxidation of compound **3** was further reduced. A 5 mL column was prepared, and the compound loaded onto the column. The product eluted at between 3–5 fractions (3–5 mL each) and monitored by TLC. Phosphorous NMR of compound **3** showed a majority of unoxidized compound **3** (147.72 ppm) with two small peaks around 12 ppm which were indicative of oxidised phosphorous 5 species (Fig. 2.7).

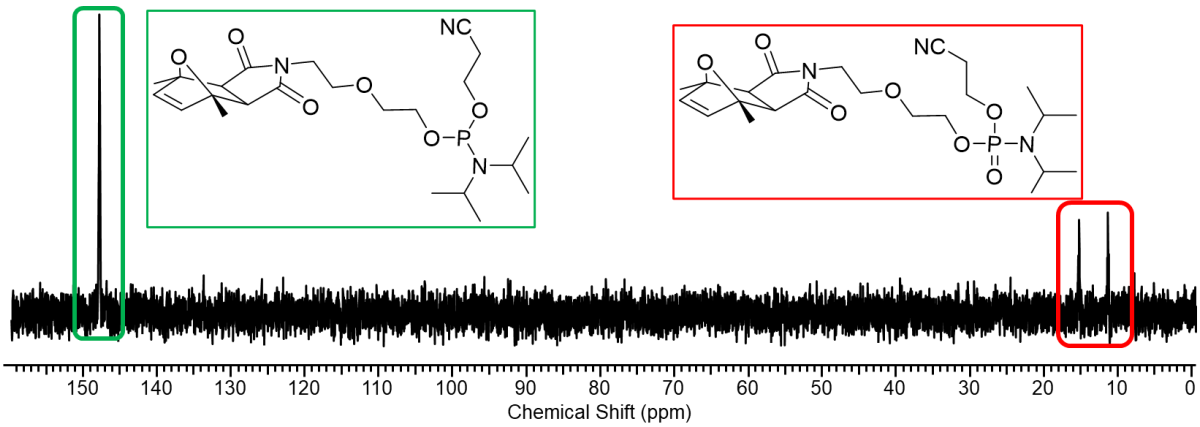

Figure 2.7: Phosphorous NMR of compound **3** in dichloromethane with a deuterated DMSO capillary.

Compound **3** could be attached to pre-synthesised DNA oligomers, T5–**A** and T5–**A'** by automated solid phase synthesis or by hand coupling. Initially, automated synthesis was used as the system is sealed and under nitrogen which maintained a dry and inert atmosphere. However, when looking at the manual, it was discovered that there was a 2 mL loss to solvent lines in the system. When synthesising compound **3** on a 2 mL scale this meant that much of the product was wasted and did not encounter DNA oligomers. Coupling was changed to hand coupling to increase the amount of compound **3** meeting the oligomers. Once attached the modified oligomers were cleaved from the solid support and purified by size exclusion chromatography before being analysed by mass spectrometry. Oligomers were being synthesised in house using an Expedite 8909 automated synthesiser (Fig. 2.8). Initially this instrument produced oligomers of the correct length and sequence however issues began to arise with the running of this system which caused synthesis of DNA oligomers to be unsuccessful. Issues with consumables such as leaking columns and reagent degradation caused many syntheses to not reach completion.

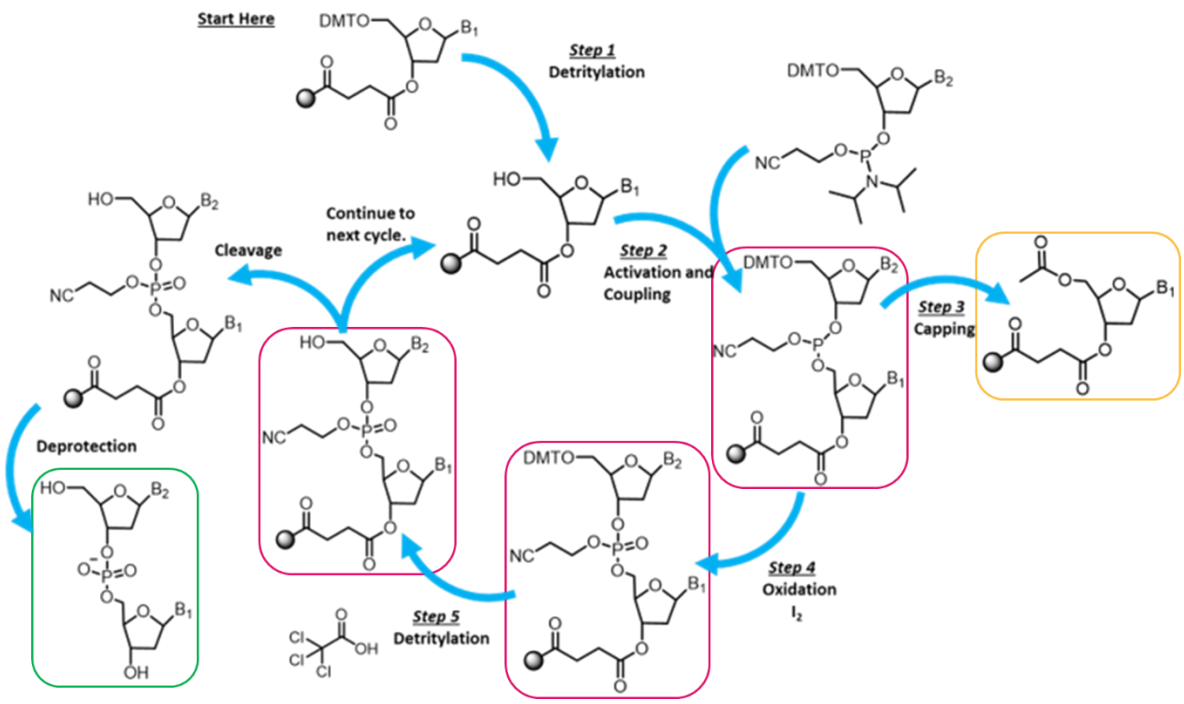

Figure 2.8: Schematic representation of solid phase synthesis of DNA oligomers. Intermediates are highlighted in pink, capped incomplete sequences are highlighted in orange, and the final product is highlighted in green.

These are sequences which did not progress to full extension of the sequence. This was occasionally due to a system error within the trityl detection. The trityl monitor is a UV detector which monitors the intensity of cleaved dimethoxytrityl (DMT) during solid phase synthesis. A strong orange colour would be indicative of many sites being available for attachment to a base, as this colour reduces the number of free coupling sites also reduces. This can occur as coupling sites are capped during synthesis to prevent incorrect sequenced products. Completed sequences were coupled with compound **3** and analysed by mass spectrometry (Fig. 2.9).

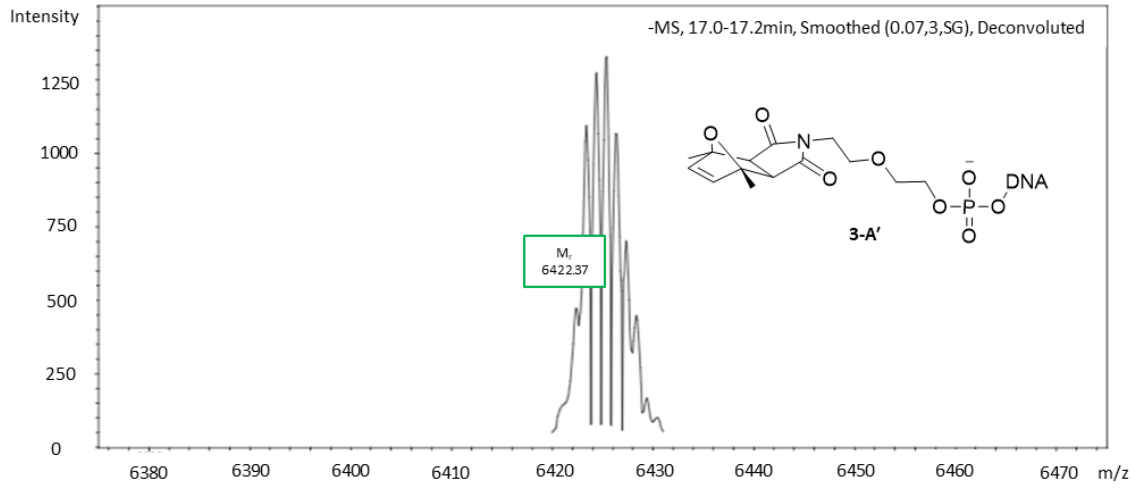

Figure 2.9: Deconvoluted mass spectrum of compound **3** modified oligomer **A'**. ESI (-) at 260 nm, expected: M [6421.12], observed: [M + H] 6422.37.

However, the results of each attempt to obtain the intended product were unsuccessful, either showing the incorrect oligomer mass and no attachment of **3** or showing the correct oligomer mass without the attachment of compound **3**. There was one instance were **3** attached to oligomer **A'** but this accounted for less than 20 % of the overall sample and was not able to be repeated or improved upon. This process was repeated by hand coupling a six-carbon amine terminated linker to synthesised oligomers, with the hope of eliminating oxidation of compound **3** during synthesiser preparation, and to also limit sample loss to the synthesiser lines. The mass spectrometry of these samples showed incomplete oligomer sequences, the proposed fragments were expected mass [6279.09], observed masses: [M – GATCCC + Na] 4503.96, [M – CCCAT + Na] 4835.03 and [M – CCCA] 5161.08 (Fig. 2.10).

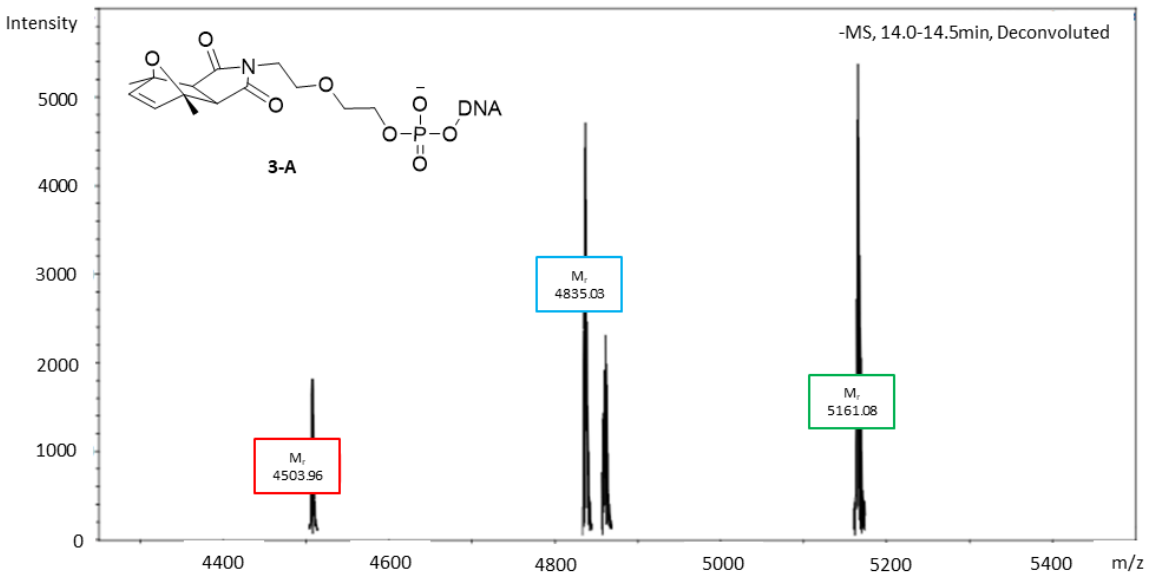

Figure 2.10: Deconvoluted mass spectrum of hand-coupled oligomer **A** with compound **3** showing truncated products. ESI (-), expected: M [6279.09], observed: [M – GATCCC + Na] 4503.96, [M – CCCAT + Na] 4835.03 and [M – CCCA] 5161.08. Proposed missing nucleotides from synthesis due to failed capping step during solid phase synthesis.

Due to the limited success of this method of synthesising and modifying DNA oligomers with compound **3**. It was decided to change the method of modification in favour of a well-established bioconjugation technique, through amide coupling with an activated ester.[121] Oligomers H_2N-**A** and H_2N-**A'** were purchased from IDT, to prevent wastage of expensive automated synthesis reagents as well as research time. This ensured that oligomers of the correct length and sequence were being modified eliminating one of the issues associated with the previous method.

2.2.2: Synthesis and Characterisation of Compound **4** Maleimido Hexanoic Activated NHS Ester, DNA Attachment and Synthesis of DNA-Peptide Conjugates via Michael Addition

Compound **4**, maleimidohexanoic NHS ester, is shown in Figure 2.11a, as well as the general scheme for its attachment to amine terminated DNA (Fig. 2.11b). The synthesis and characterisation of compound **4** will be discussed in this section, as well discussing the modification of DNA sequences **A** and **A'** with compound **4**, and its subsequent reaction with thiol containing peptides by Micheal addition.

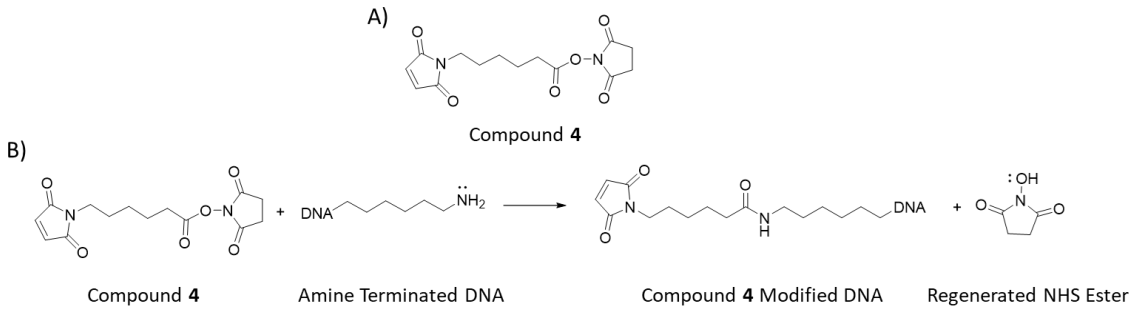

Figure 2.11: A) Structural illustration of compound **4** and B) general synthesis scheme for Maleimide modified DNA, showing compound **4**, amine terminated DNA, and maleimide terminated DNA, with regenerated NHS ester.

Compound **4** was synthesised using 6-maleimidohexanoic acid, *N*-hydroxy succinimide in the presence of EDC.HCl. The first conditions attempted contained DIPEA during reaction overnight however, when analysed by TLC the following day, multiple spots were evident. Omitting DIPEA from the reaction overnight produced a cleaner reaction mixture, with only two spots visible by TLC. It is possible the presence of DIPEA assists in the hydrolysis of the NHS ester, representing the staring material and the product. Gram scale reactions were then achieved with yields between 84-94 %. The successful synthesis of compound **4** was confirmed by 1D proton (Fig. 2.12) and carbon NMR, as well as mass spectrometry (section 7.2.).

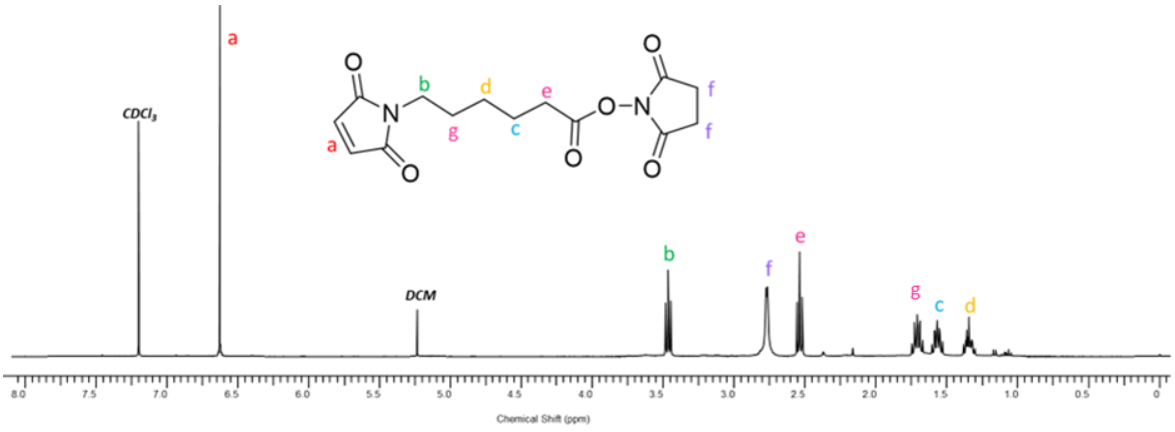

Figure 2.12: ^{1}H 1D NMR of 6-maleimidohexanoic activated NHS ester in $CDCl_3$. ^{1}H 1D NMR (400 MHz, $CDCl_3$) δ H_a 6.62 (2H, s), H_b 3.47 (2H, t), H_f 2.77 (2H, s), H_e 2.54 (2H, t) 1.71 (2H, q), H_g 1.57 (2H, q), H_c 1.34 (2H, q).

With compound **4** successfully synthesised the next stage was to modify amine terminated oligonucleotides allowing the project to move forward in synthesising oligonucleotide-peptide conjugates. Amide coupling between the NHS ester of compound **4** and the amine terminated end of the DNA was carried out. Amide coupling conditions traditionally are extremely harsh when coupling a primary amine and a carboxylic acid, by using an NHS ester the reaction conditions are milder due to the labile nature of the ester bond between the NHS and carboxcylic acid of compound **4**. Which is beneficial when using oligonucleotides in preventing damage to the oligonucleotide, this also eliminates coupling agents improving the cleanliness of the modification. This method is common in biology, however achieving this between compound **4** which was solely soluble in organic solvents and DNA which was soluble in aqueous solvents proved challenging. An aqueous miscible solvent system, such as dimethyl sulfoxide or dimethylformamide and DI autoclaved water, was required to fully dissolve compound **4** and to allow modification of the DNA. The first solvent tested was dimethyl sulfoxide (DMSO), the first attempt with DMSO was to be achieved by using as little organic solvent as possible. This was due to the high boiling point of DMSO, making it difficult to remove from the DNA solution after modification, without causing damage to the DNA or loss of product. Compound **4** was dissolved in 400 µL of DMSO before being added (200 µL) to 1 mL of 10 µM of **H_2N-A** and (200 µL) **H_2N-A'** respectively. Both solutions became cloudy with a white precipitate, indicating that there was too little organic solvent present to prevent compound **4** from precipitating. This was rectified by gradually increasing the amount of DMSO, 100 µL at a time. A total of 1000 µL of DMSO was added to each solution yielding 2 mL solutions for both **H_2N-A** and **H_2N -A'**. The samples were split into aliquots before being incubated at 37 ˚C for 90 minutes. After heating the samples contained a white precipitate; this was likely excess **4** and the by-product of the coupling, NHS, which was regenerated during the amide coupling. Mass spectrometry of this coupling showed the successful attachment on compound **4** however this was achieved in low yield when compared to the unmodified species. This can be observed in Figure 2.13a. The peak at approximately 15 minutes represents unmodified **H_2N-A'** with

a mass of 6258.40 [M + H^+]. The smaller peak observed at around 16 minutes represents the successful modification of **H_2N-A'** with compound **4** with a mass of 6450.45 [M] (Fig. 2.13b).

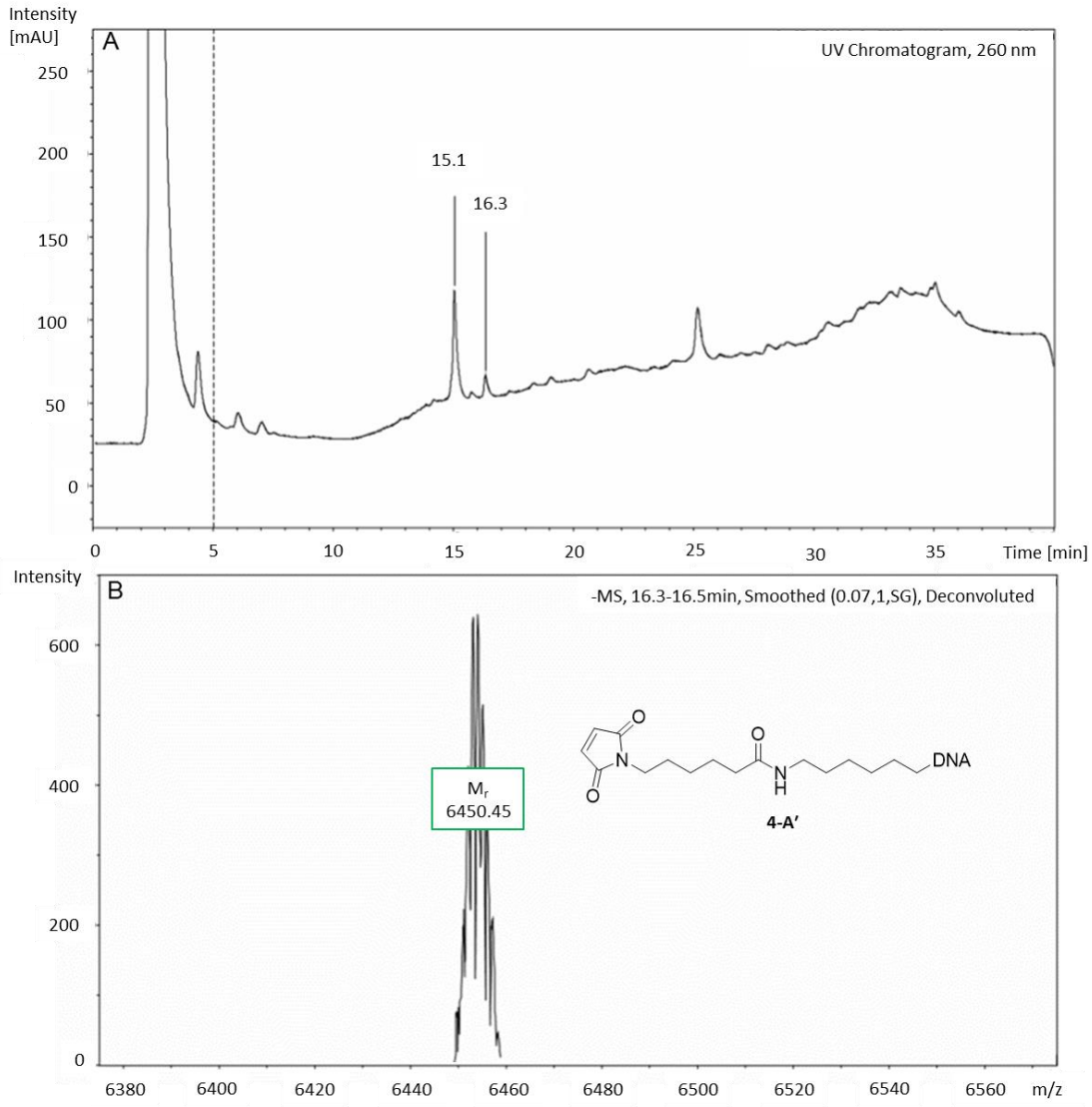

Figure 2.13: A: Ultraviolet Visible HPLC trace of **4-A'**, showing both unmodified (15.1 min) and modified (16.3 min) **A'**. B: Mass spectrum of UV trace peak (16.3 min) showing partially successfully modified **4-A'**. ESI-, expected: 6450.18 and observed: 6450.45 [M].

Compound **4**, used in the above experiment, was stored as aliquots in DMSO and kept in the freezer. Upon further inspection by proton NMR, compound **4** had degraded to NHS and carboxylic acid after 2 weeks of storing, effecting the efficiency of the coupling due to the molar ratios no longer being as calculated. To limit this reoccurring compound **4** was stored as a dry oil in vials at room temperature and dissolved before reaction. This greatly improved the reaction efficiency as demonstrated in Figure 2.14. The UV chromatogram (Fig. 2.14a) shows a strong single DNA peak at

15.3 minutes with a mass of 6473.26 $[M + H]^+$ (Fig. 2.14b). Later peaks observed in the chromatogram are indicative of impurities within the sample.

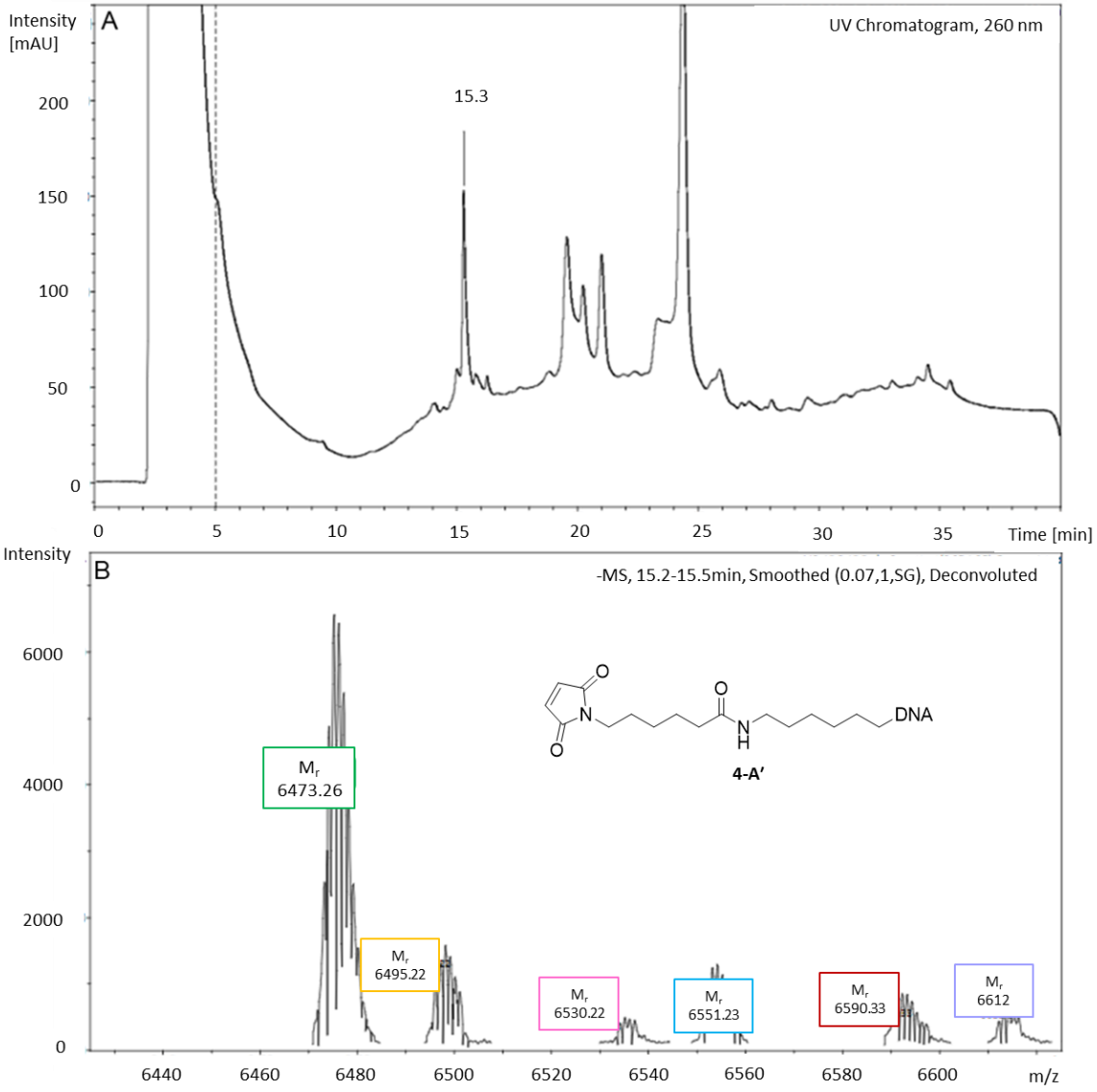

Figure 2.14: A: Ultraviolet Visible HPLC trace of **4-A**, modified (15.3 min). B: Mass spectrum of UV trace peak (15.3 min) showing successfully modified **4-A**. ESI-, expected: 6472.16 and observed: 6473.26 $[M + H]^+$.

Despite purification by size exclusion chromatography the sample still contained residual DMSO and excess compound **4**, freeze drying may have removed excess DMSO but still left residual compound **4** behind, as well as there being limited access to freeze drying at the time. The reaction solvent was changed to dimethyl formamide (DMF), as a smaller volume (500 µL) was required to fully dissolve compound **4** and was still water miscible. Samples were reacted at 37 ˚C for 2 hours in a thermocycler before the DMF was removed size exclusion chromatography. However, a new

issue arose after removing the organic solvent impurity: there was a large excess of unreacted compound **4** which was not being removed by size exclusion chromatography. Analysis by UV-Visible spectroscopy showed a large peak around 240 nm, which is indicative of the maleimide double bond within the ring. Several methods were employed to overcome this issue, including small scale aqueous extraction with volatile organic solvents, centrifugation, and filtration. Small scale aqueous extraction was based on the premise that compound **4** would be more soluble in organic solvent than water and that the organic solvent would be easily removable. UV-Vis spectroscopy was used the analyse the efficacy of purification, **4-A** pre and post washing was analysed by UV-Vis as well as a control of **H_2N-A. 4-A**, post size exclusion chromatography was washed with either dichloromethane or ethyl acetate. Figure 2.15 shows the UV-Visible spectra results of this experiment. From Figure 2.15 there is a large absorbance observed around 240 nm which is indicative of excess maleimide, we also see the absorbance is shifted for DNA from 260 nm to 300 nm. Washing with DCM showed an increase in the absorbance at 260 nm and a reduction in the absorbance around 300 nm, suggesting some excess maleimide was removed during the washing. There was a limited decrease in the absorbance at 240 nm, with this peak shifting towards 230 nm. However, washing with ethyl acetate shifted the peak at 240 nm towards 230 nm and increase the observed absorbance, along with increasing the observed absorbance at 260 nm. Ethyl acetate has an absorbance range between 210-250 nm, which suggests this marked increase in absorbance at 230-250 nm is explained by ethyl acetate remaining within the water despite blowing compressed air over the sample and allowing evaporation at room temperature. This method of preparation would have been greatly improved by employing other drying techniques such as, freeze drying, or in vacuo drying. However, at the time it was simpler to change the purification method entirely than to develop this process further.

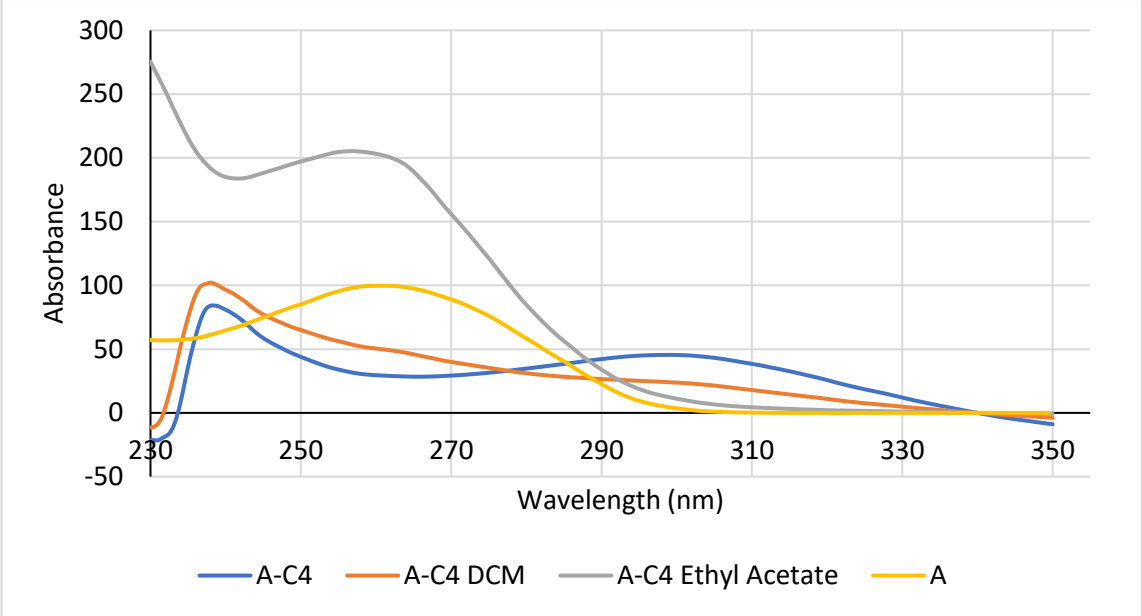

Figure 2.15: Ultraviolet visible spectrum for the aqueous extraction of excess compound **4** from **4-A**. All samples were analysed in autoclaved deionised water, **A** was at a concentration of 10 µM, as it was prepared from a 100 µM stock solution. All other samples were analysed at the concentration of extraction from a solution of 20 µM reaction mixture.

Therefore, this method of purification was abandoned in favour of purification which would be more successful and reduce the presence of organic solvents within the sample. Modified DNA which had only been purified by size exclusion chromatography, was frozen between uses. Upon defrosting a visible off-yellow precipitate was observed, this was believed to be unreacted compound **4**, due to compound **4** being a yellow oil and immiscible with water, when the water frozen Compound **4** precipitated out. The sample was centrifuged at 2000 x g for 5 minutes and the supernatant removed, the supernatant was then filtered through an aqueous syringe filter. This yielded a cleaner UV-visible spectrum for compound **4** modified DNA (Fig. 2.16). It can be seen from Figure 2.17a that there were still impurities within the sample, which may have been due to excess maleimide.

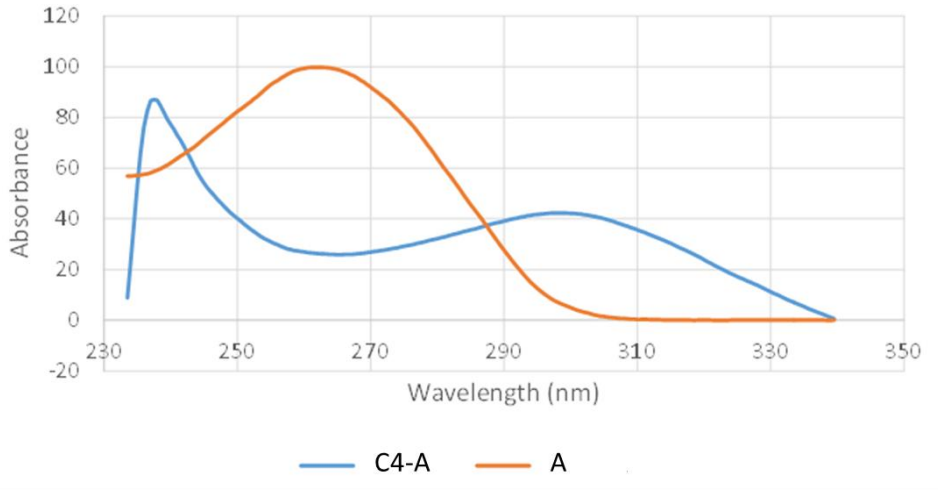

Figure 2.16: Ultraviolet visible spectrum for the extraction of excess compound **4** from **4-A** by syringe filtration. All samples were analysed in autoclaved deionised water, **A** was at a concentration of 10 µM, as it was prepared from a 100 µM stock solution. **C4-A** was analysed at the concentration of extraction from a solution of 20 µM reaction mixture.

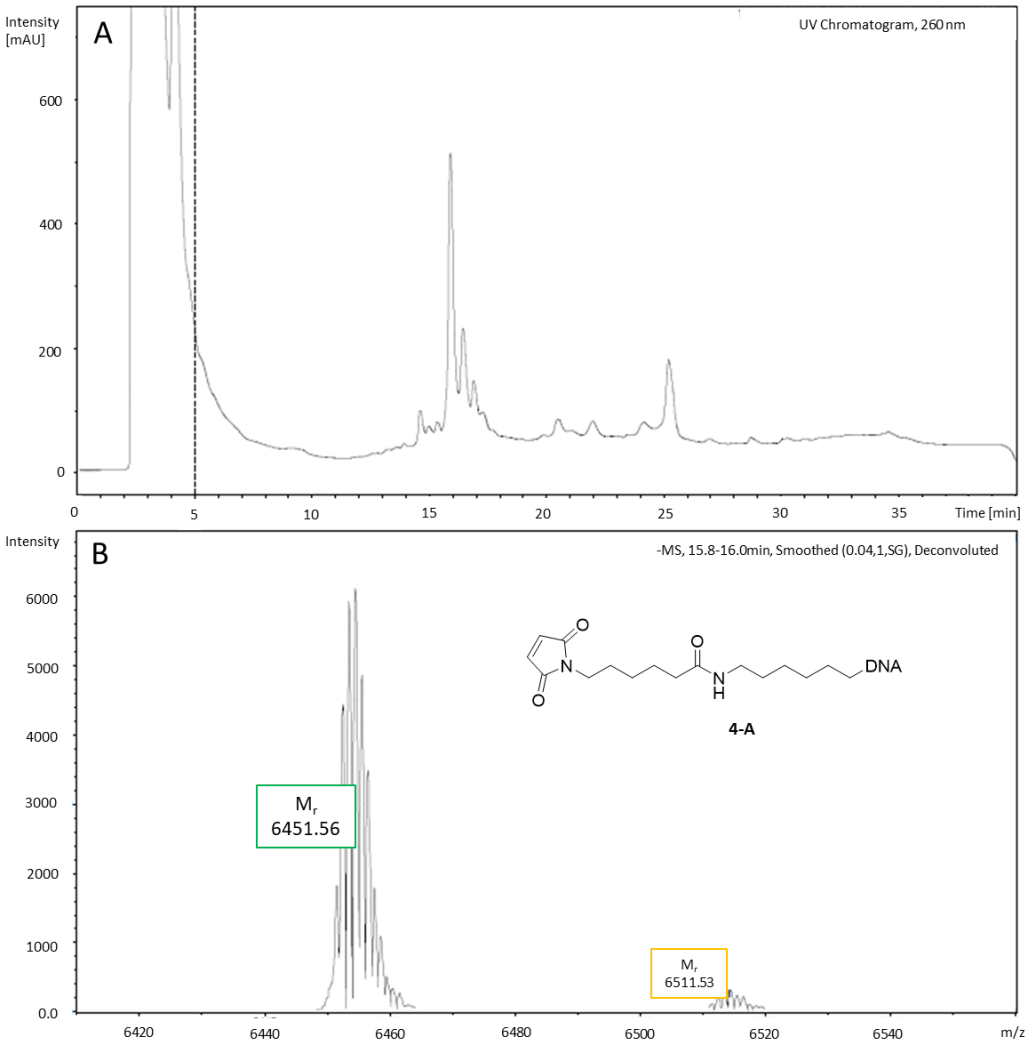

Figure 2.17: A: Ultraviolet Visible HPLC trace of **4-A'**, showing modified (15.9 min) **A'**. B: Mass spectrum of UV trace peak (15.5 min) showing successfully modified **4-A'**. ESI -, expected: 6450.18 and observed: 6451.56 $[M+H]^+$.

Reviewing the calculations of the equivalents of maleimide used to DNA, it was discovered that there was a 1000-fold error in the amount being used. The amount of maleimide NHS ester was reduced, this led to problems in the amide coupling reaction, which resulted in reduced success in modifying DNA with compound **4**. This was due to the amide coupling occurring at very high molar ratios at the previous concentration, by reducing the amount of maleimide NHS ester present in the reaction mixture the efficiency reduced. Optimisation of the reaction conditions were required to achieve successful DNA modification with compound **4** with any consistency and reliability. Figure 2.18 shows the un-successful modification of amine DNA with compound **4** after the corrected molar ratios were used. Exploring the literature led to the discovery that amide couplings mediated through NHS esters were more favourably conducted in basic pH.[122]

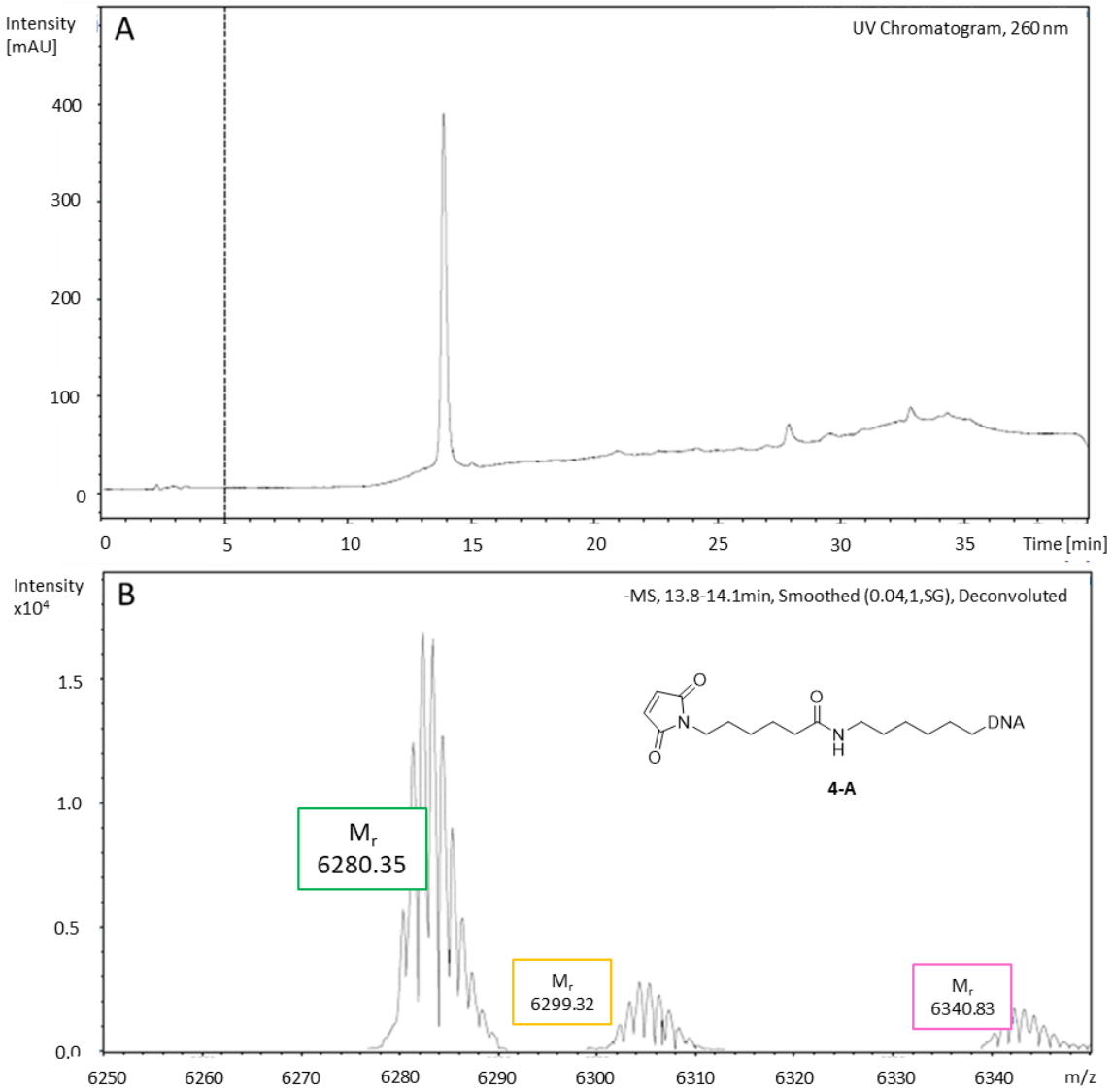

Figure 2.18: A: Ultraviolet Visible HPLC trace of **4-A**, un-modified (14.0 min). B: Mass spectrum of UV trace peak (14.0 min) showing un-successfully modified **4-A**. ESI-, expected: 6472.16 and observed: 6280.35 $[M + H]^+$.

To assess the success of the amide formation with the amine terminated DNA, several small-scale reactions were carried out with molecules of a larger mass. This was so that an appreciable shift could be observed by PAGE to confirm the successful conjugation. **H_2N-A** (50 µM, 200 µL made with phosphate buffer or sodium chloride solution) was reacted with a 5k PEG NHS ester (25 mg, directly dissolved in **H_2N-A**), pH 8.0 phosphate buffer, pH 9.0 phosphate buffer, 100 mM sodium chloride, 250 mM sodium chloride and 500 mM sodium chloride, all samples were heated to 37 ˚C for 1.5 hrs. **H_2N-A** (50 µM, 100 µL made with autoclaved DI water) was also reacted with 1:10 (100 µL, 50 µM:0.135 mg) and 1:20 (100 µL, 50 µM:0.275 mg) equivalents of Traut's reagent at 37 ˚C for 1.5

hrs before being treated with 1 mM of 5k PEG maleimide. All experiments were analysed by Kaiser test and denaturing PAGE (Fig. 2.19).

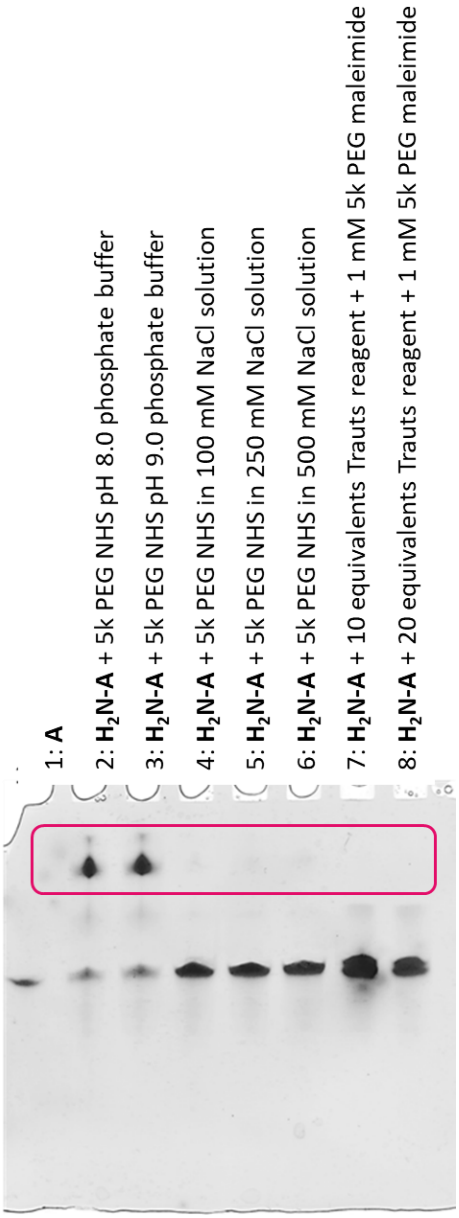

Figure 2.19: Denaturing PAGE (running buffer tris borate EDTA (TBE), pH 8.0, chapter 7) of amine DNA test reactions. All reactions were reacted at 37 ˚C for 90 minutes. 1: **A**, 2: **H_2N-A** + 5k PEG NHS pH 8.0, 3: **H_2N-A** + 5k PEG NHS pH 9.0, 4: **H_2N-A** + 5k PEG NHS 100 mM NaCl, 5: **H_2N-A** + 5k PEG NHS 250 mM NaCl, 6: **H_2N-A** + 5k PEG NHS 500 mM NaCl, 7: **H_2N-A** + Traut's reagent + 5k PEG maleimide (1:10 eqvs), 8: **H_2N-A** + Traut's reagent + 5k PEG maleimide (1:20 eqvs). PEG modified DNA bands are highlighted by the pink box.

From Figure 2.19 the amine DNA successfully reacted with 5k PEG NHS at pH 8 and 9, with a strong secondary band towards the top of the gel. For the reactions carried out in the presence of salt, it can be seen that there were a very faint bands in all concentrations at the same point on the gel as

observed in the reactions, where the pH was changed, it can also be seen there is minimal reaction in the Traut's reagent experiment. This gel shows that these reactions were successful. However, the most successful conjugations were carried out at pH 8 and 9. With this information, the reactions for the maleimide NHS and cyclooctyne NHS ester reactions (Fig.2.20) in pH 8.0 sodium phosphate buffer (0.2M) was chosen, sodium phosphate buffer was also chosen for use in the thiol maleimide reaction between maleimide modified DNA and thiol containing peptides, which will be discussed further in the next section.

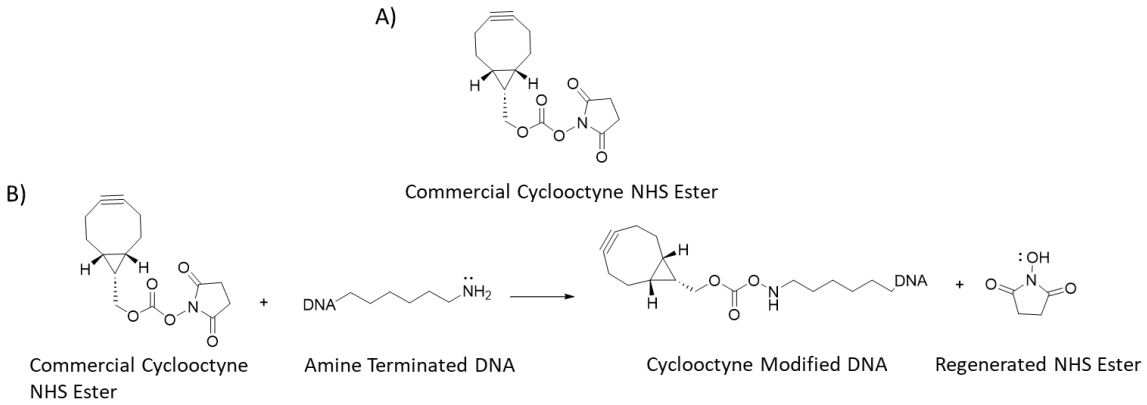

Figure 2.20: A) Structural illustration of the commercially available cyclooctyne NHS ester and B) general synthesis scheme for cyclooctyne modified DNA, showing cyclooctyne, amine terminated DNA, and cyclooctyne terminated DNA, with regenerated NHS ester.

Method development of DNA modification with a bifunctional crosslinker was carried out with the maleimide NHS ester, this meant the expensive cyclooctyne was saved until the linking chemistry had been optimised. There were a few differences in the linking of the cyclooctyne; for example: the cyclooctyne needed to be dissolved in DMF, similarly to the maleimide NHS, but it was also easier to clean after modification. As can be seen from Figure 2.21 the successful linking of cyclooctyne to amine DNA was achieved at a pH of 8.0.

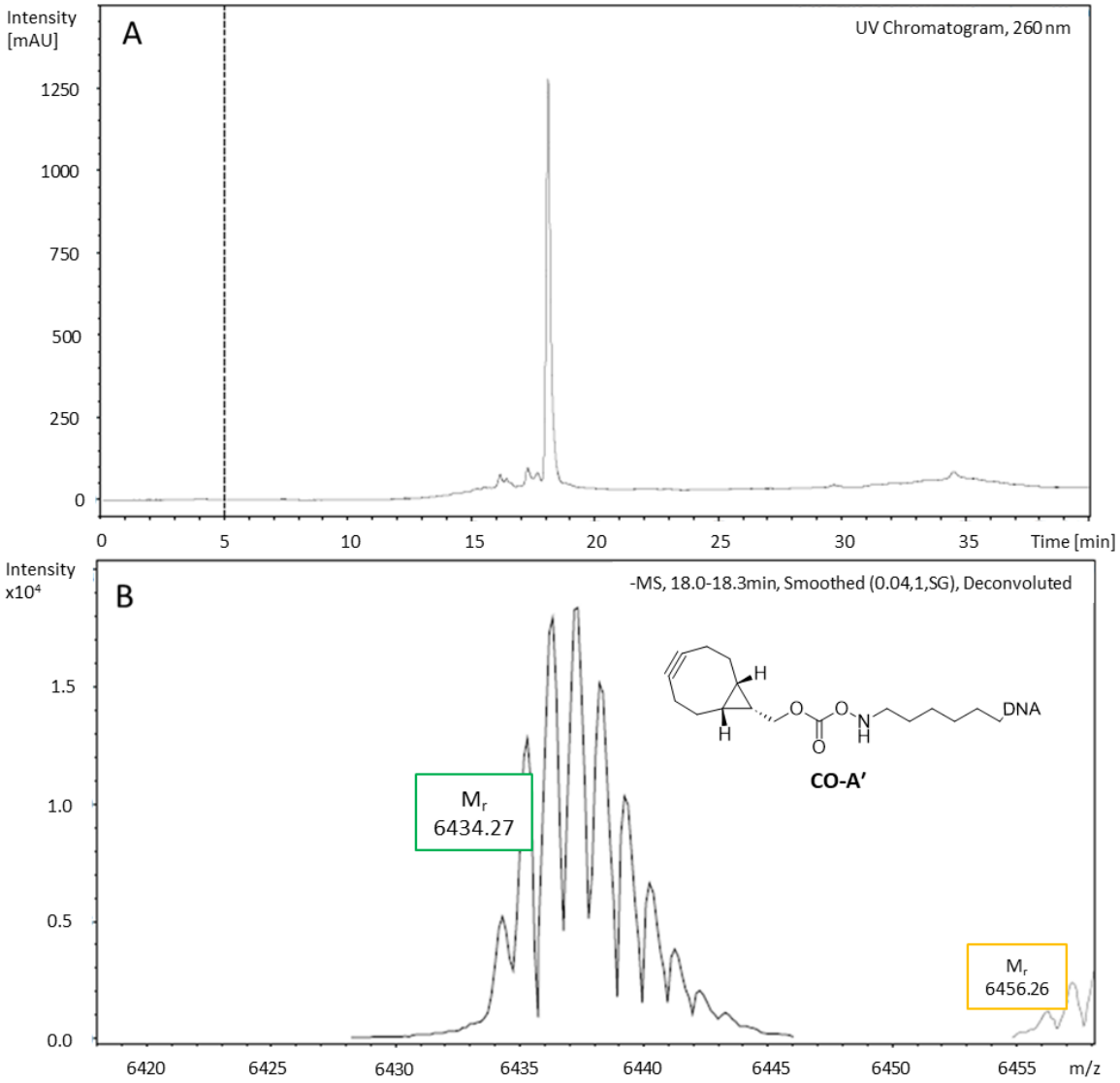

Figure 2.21: A) Ultraviolet Visible HPLC spectrum of **CO-A'**, modified (18.2 min). B) Mass spectrum of UV trace peak (18.2 min) showing successfully modified **CO-A'**. ESI -, expected: 6433.19 and observed: 6434.27 $[M + H]^+$.

This section discussed the method development to successfully form DNA modified with two bifunctional crosslinkers. This gave the optimal reaction conditions of pH 8.0 phosphate buffer at 37 ˚C for 1 hour. These conditions were successful for both the maleimide and cyclooctyne bifunctional crosslinkers. The next section will discuss the synthesis and method development of DNA-peptide conjugates formed through thiol-maleimide chemistry.

2.2.3: Synthesis and Characterisation of DNA-peptide Conjugates Formed by 1,4 Michael Addition

Peptides used in the method development of maleimide-thiol formed conjugates were made and fully characterised by Akiko Sato, another PhD student in the group. We worked as co-equal partners on these investigations into conjugation methods. The results discussed here are my interpretation of the results we obtained throughout our investigations. Conjugation reactions with maleimide DNA were carried out with a number of different peptide sequences. The two we focused on more completely were the parallel β-sheet peptide HYFNIF (Fig. 2.22), and the second was a collagen mimetic peptide POG_6 both with a CGSG spacer. POG_6 has good solubility in water whereas HYFNIF is only partially soluble and requires the addition of HFIP to promote full dissolution in aqueous media. The sequence KLVFFA (Fig. 2.23) with a cysteine residue was also analysed in later experiments. Peptides were conjugated to maleimide modified DNA via the 1,4 Micheal addition; a structural illustration of the proposed reaction mechanism is given in Figure 2.24.

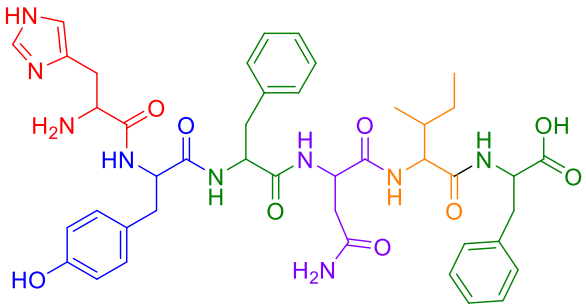

Figure 2.22: Schematic illustration of HYFNIF (histidine (red), tyrosine (blue), phenylalanine (green), asparagine (purple), isoleucine (orange), and phenylalanine (green)), a β-sheet forming peptide.

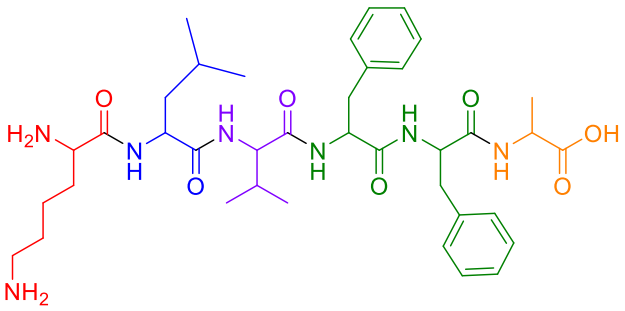

Figure 2.23: Schematic illustration of KLVFFA (lysine (red), leucine (blue), valine (purple), phenylalanine (green), phenylalanine (green), and alanine (orange)), a β-sheet forming peptide.

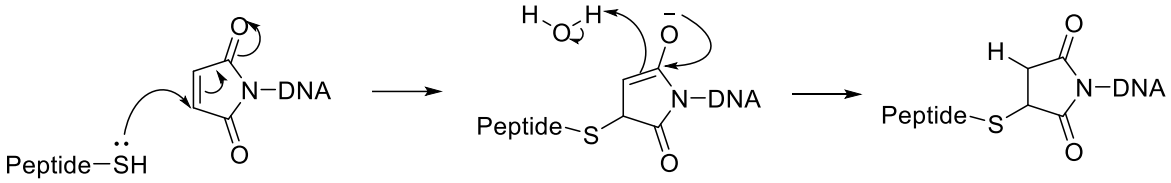

Figure 2.24: Structural illustration showing the proposed 1,4 Michael addition reaction mechanism between maleimide modified DNA and a thiol containing peptide.

The success of conjugate reactions was assessed by polyacrylamide gel electrophoresis (PAGE). There are different buffer systems used in PAGE experiments to investigate different aspects of biomolecules, such as size i.e, length/mass in denaturing PAGE, self-assembly or protein folding in native PAGE, as two examples. The passage of a biomolecule through PAGE is determined by their, mass to charge ratio, and the physical size of the biomolecule. A graphical representation of this can be seen in Figure 2.25.

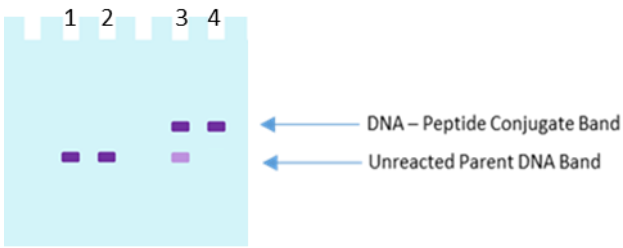

Figure 2.25: Representation of PAGE analysis of DNA–peptide conjugation. 1: A, 2: A , 3: DNA-peptide conjugate with unreacted DNA, and 4: DNA-peptide conjugate.

The first conjugate reaction was carried out in TBE buffer (pH 8.0). DNA maleimide (10 µM) was reacted with ten equivalents of CGSG-HYFNIF peptide (100 µM) one overnight at room

temperature, and one overnight at 37 °C in a water bath. To analyse the success of the reaction a 20 % denaturing gel was ran on the reaction mixtures, the gel did not show the presence of a second band above the control DNA band (Fig. 2.26). A gel concentration of 20 % was chosen as the pore size was sufficient to retain small DNA strands, as well as show a distinct shift between larger peptide modified DNA strands and the unmodified version. Based on this result, it was hypothesised that the conjugation did not occur. There was also no evidence of DNA in the **4-A'** heated sample. This may be due to a lower concentration of DNA in the sample.

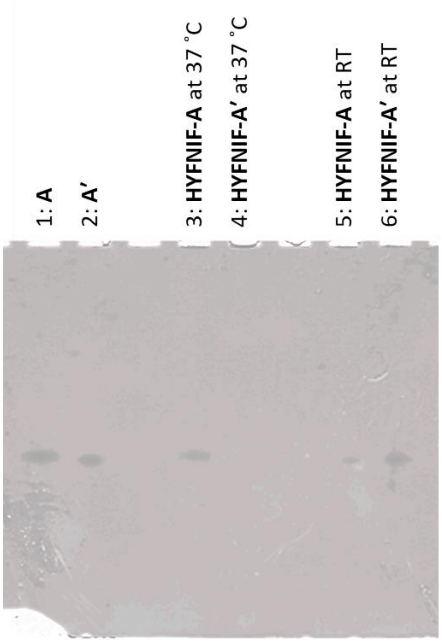

Figure 2.26: 20 % Denaturing polyacrylamide gel ran in TBE buffer at maximum volts (300 V); 15 mAmps for 1 hour. Gel was stained in stains-all DNA stain. 1: **A**, 2: **A'**, 3: **HYFNIF-A**, heated, 4: **HYFNIF-A'**, heated, 5: **HYFNIF-A**, RT, and 5: **HYFNIF-A'**, RT.

A white precipitate was observed in the reaction mixtures of the first conjugation, which was most likely unreacted excess **CGSG-HYFNIF**, this is because **CGSG-HYFNIF** is a white solid when dry, as well as being less readily soluble in waster than other peptides. This reaction was repeated in different buffers (phosphate buffered saline, PBS, pH 7.4) and in the presence of HFIP to aid in the dissolution of **CGSG-HYFNIF**. The volume of the reaction was reduced from 900 µL to 200 µL, to reduce the dilution of DNA maleimide, as it can be hard to visualise low concentrations of DNA by PAGE due to the sensitivity of gel stains, like stains all. Also, by increasing the concentration of DNA within the solution, this may improve reaction kinetics by increasing the interactions between the

DNA and the peptide. The experiments were heated for 2 hours (1 each of **A + HYFNIF**, and **A' + HYFNIF**) and overnight (1 each of **A + HYFNIF**, and **A' + HYFNIF**) respectively at 37 ˚C, when analysed by PAGE there were no new band visible. In an attempt to salvage these experiments, 1 mg of the peptide was directly dissolved in the DNA solution (1 mg in 100 µL, 10 µM DNA), this reaction was heated at 37 °C overnight. When analysed by PAGE, the multiple experiments showed the presence of not one but two secondary bands (Fig. 2.27). This may have been due to double modification of the DNA although is more likely due to self-assembly of the peptide forming a dimer, because the gel conditions were denaturing, containing urea, these bands are unlikely to be due to a DNA dimer. This could have been confirmed by mass spectrometry, or circular dichroism, however this was not possible at the time of this experiment. Circular dichroism can give information on the secondary structure of peptides and DNA. Although crude, this was the first step in moving forward with the synthesis of DNA-peptide conjugates.

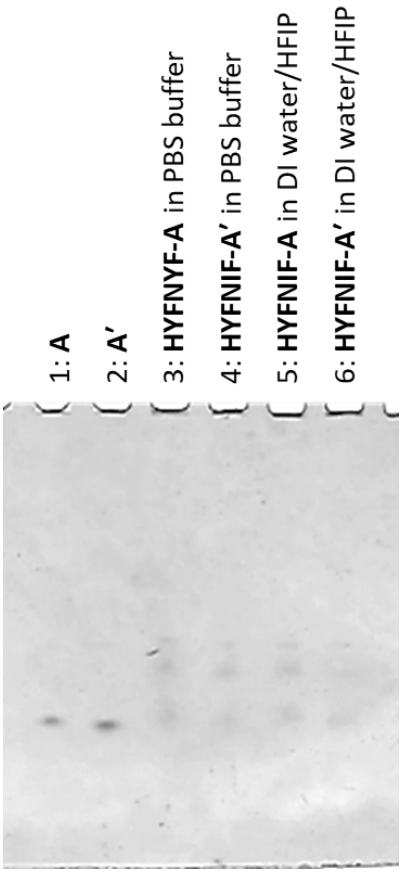

Figure 2.27: 20 % denaturing TBE PAGE of DNA-peptide conjugate reaction 2 biii; maximum volts (300 V), 15 mAmps 1 hour. Stained in stains-all stain. 1: **A**, 2: **A'**, 3: **HYFNIF-A**, PBS, 4: **HYFNIF-A'**, PBS, 5: **HYFNIF-A**, water/HFIP, and 5: **HYFNIF-A'**, water/HFIP.

Following this initial success, the effect of peptide concentration on the formation of DNA peptide conjugates was assessed. Conjugation reactions were conducted with varying peptide concentrations 0.1-0.4 mM and 1-4 mM. The 1 mg addition of peptide was calculated to equate to a concentration of approximately 4 mM. These reactions were not successful despite the addition of HFIP. Next, many small-scale test reactions were carried out with the aim of acquiring more reproducible results. This would allow testing of a number of conditions at one time while reducing wastage of synthesised starting materials. This system was high-throughput in design. Initial reaction conditions focused on buffer system, peptide concentration and the effect of denaturants during synthesis. The reaction temperature (37 °C) and concentration of 2 mM peptide was kept as standard when changing buffer systems. Water was used as the reaction media when investigating peptide concentration. Once the best conjugation conditions were established, improvements could be made to the reaction components. Initial results by PAGE were promising with secondary

bands being visible for peptide concentration 0.5, 1 and 2 mM as well as 2 mM in the presence of 8 M urea (Fig. 2.28).

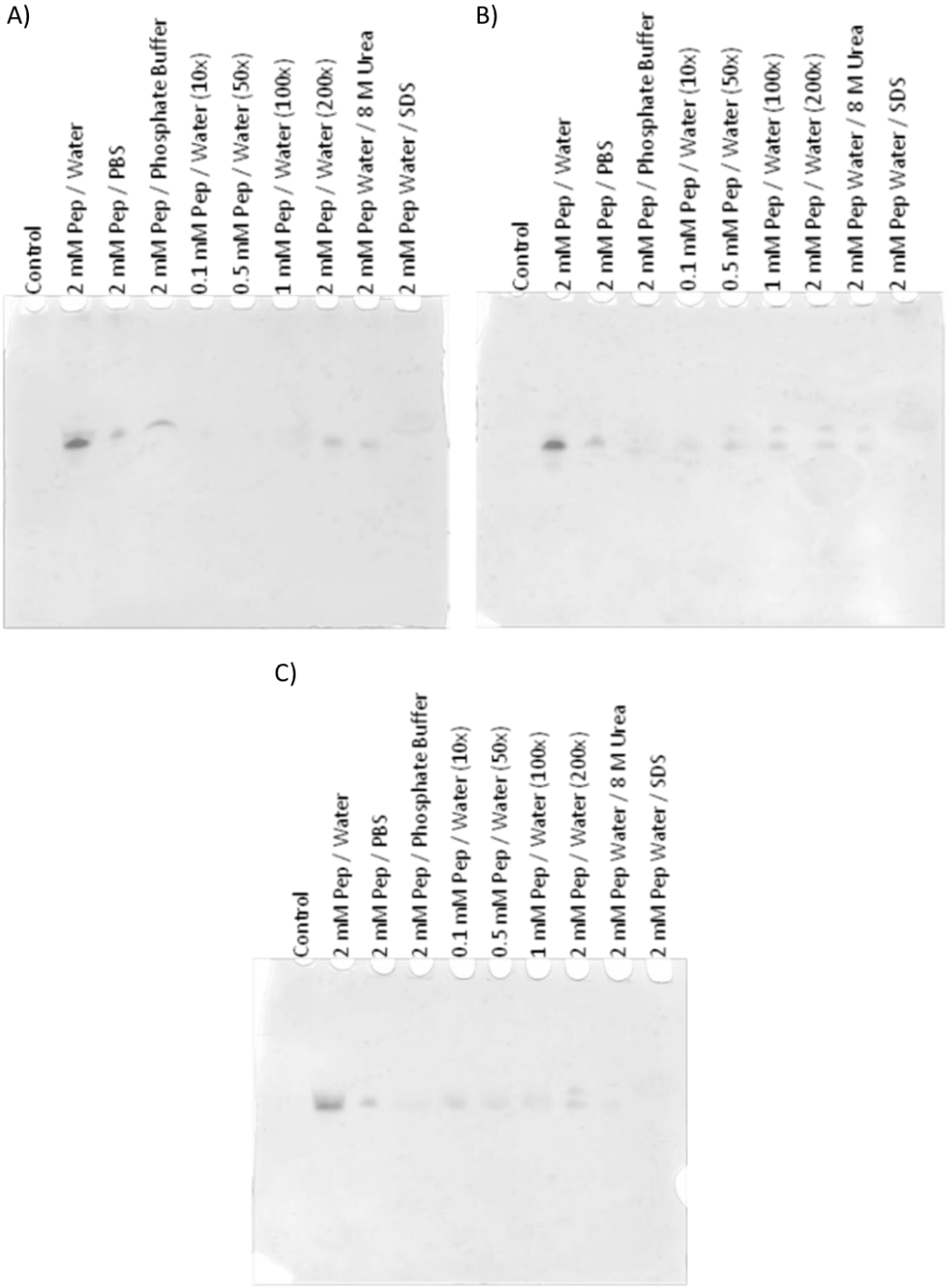

Figure 2.28: 20 % denaturing PAGE in TBE buffer; maximum volts (300 V), 15 mAmps for 45 minutes. Stained in stains all DNA stain. A) gel showing **POG_6** test reactions with different conditions, B) gel showing **CGSGHYFNIF** test reactions with different conditions, and C) gel showing CHYFNIF test reactions with different conditions.

As can be seen from Figure 2.28 there were only new bands visible in the HYFNIF peptide samples. It was hypothesised at the time that **POG_6** may need to be conjugated to DNA at a higher temperature due to its propensity to self-assemble at low concentrations. However, when conducting temperature dependant studies (60 and 90 °C for 1 hour) the gel showed no presence of any bands other than the control, it was hypothesised that the higher temperatures (60 and 90 °C) was degrading the DNA (Fig. 2.29).

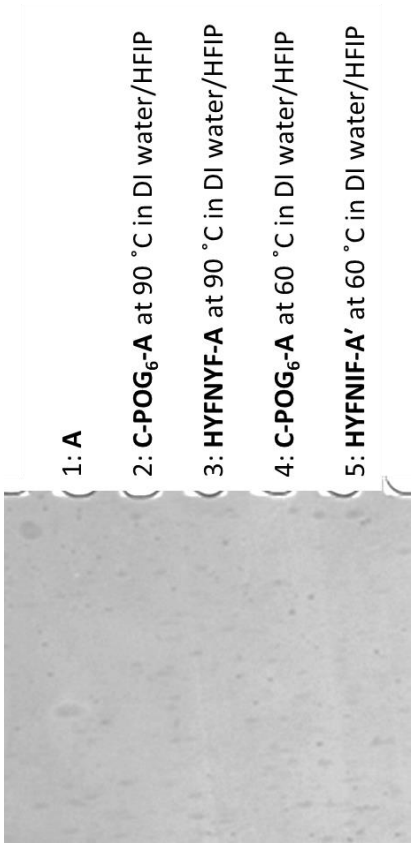

Figure 2.29: 10 % denaturing PAGE ran in TBE; maximum volts (300 V), 15 mAmps for 15 minutes. Stained in stains all stain. Reactions were carried out in DI water/HFIP. 1: **A**, 2: **C-POG$_6$-A,** at 90 ˚C 3: **HYFNIF-A**, at 90 ˚C, 4: **C-POG$_6$-A**, at 60 ˚C, 5: **HYFNIF-A'**, at 60 ˚C.

The original reaction temperature of 37 °C was returned and focus moved to pH adjustments. It believed that the reaction could be pushed towards completion by manipulating the pH within the range of 6.5-8.0, as above this pH amines begin to attack maleimides more favourably over thiols. However, these reactions also proved unsuccessful, because the modified DNA being used was yet to be by mass spectrometry, as described in section 2.2.2. The majority of these reactions were conducted on DNA samples which we were awaiting confirmation by mass spectrometry, due to

delays within the facility and machine malfunctions. This meant that there was uncertainty as to whether the DNA was successfully modified, which may have explained the inability to repeat successful conjugation reactions. Confirmation experiments were developed to assess peptide conjugation. A fluorescein isothiocyante modified thiol was synthesised, if the DNA was modified with a maleimide it would react with the thiol modified fluorescein isotiocyanate (SH-FITC) and give a fluorescent band on a PAGE gel. These gels were successful at showing that the DNA was not modified with the maleimide linker due to the lack of fluorescent band overlaying the blue bands (Fig. 2.30).

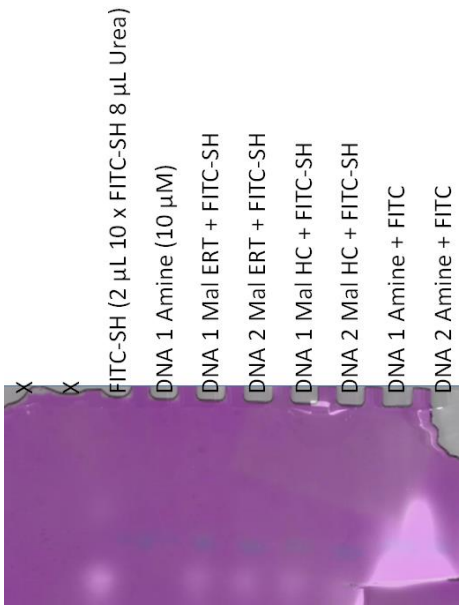

Figure 2.30: 20 % denaturing FITC thiol PAGE ran in TBE buffer. Maximum volts (300 V), 15 mAmps 35 minutes. Imaged on a transilluminator then stained in stains all stain and overlaid.

To further investigate the reaction of maleimide with a thiol a number of NMR studies were conducted. The reaction was monitored by 1D proton NMR for the disappearance of a singlet at 6.7 ppm (Fig.2.29), this singlet represents the double bond of the maleimide ring if the pi portion of this bond is broken the singlet will disappear. Maleimidohexanoic acid (0.5 mol), β-mercaptoethanol (1 mol) and diisopropylamine (DIPEA, 0.5 mol) were combined in an NMR tube with 300 µL of deuterated dichloromethane. A 1D proton NMR was collected at time = 0, and after 48 hours. The maleimide used to synthesise compound **4**, 6-maleimidohexanoic acid was reacted

with β-mercaptoethanol (BME) in varying amounts to assess the viability of the reaction. First the molar ratios were changed however, the singlet at 6.7 ppm remained visible. The conditions in which the disappearance of this peak was in the presence of base (DIPEA) with a molar ratio of 0.5-1-0.5 (maleimide: BME: DIPEA) (Fig. 2.31).

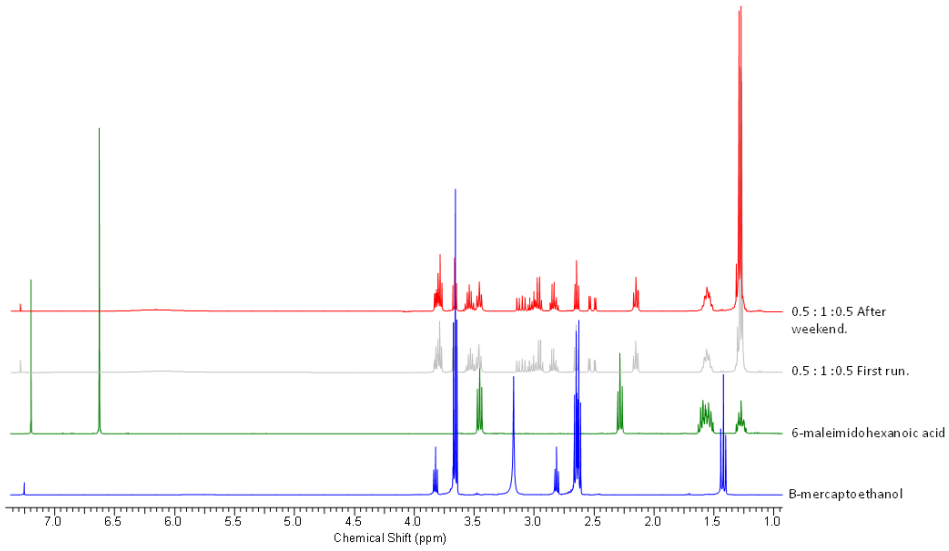

Figure 2.31: Overlaid proton NMR spectra of 6-maleimidohexanoic acid, BME and 0.5-1-0.5 maleimide: BME: DIPEA reaction at beginning of experiment and after reaction over the weekend.

Once the maleimide modification of the DNA was confirmed as discussed in section 2.2.2, the DNA-peptide conjugation reactions could continue. In literature the Michael addition between maleimide and thiols in bio-conjugation reactions occurs best at a pH range of 6.5-7.5.[122,123] A phosphate buffered solution of pH 6.8 was prepared from sodium phosphate buffer components. Both the DNA (50 µM, 100 µL) and peptide (2.5 mM, 100 µL) solutions were prepared in this buffer before reaction at 37 °C overnight. PAGE analysis of this conjugate reaction showed successful production of a second band for both the **CGSG-HYFNIF** and **CGSG-POG$_6$** peptides (Fig. 2.32). There was still the presence of some unreacted maleimide modified DNA this could be overcome by experimenting with reaction conditions, such as, molar equivalents, temperature, and reaction time.

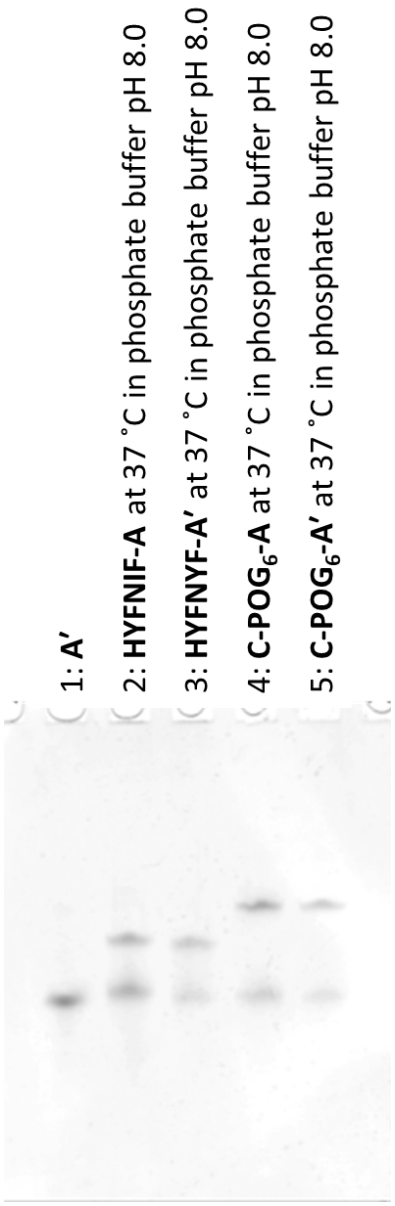

Figure 2.32: 20 % denaturing PAGE showing 1: **A'**, 3: **HYFNIF-A**, 4: **HYFNIF-A'**, 5: **POG_6-A**, 6: **POG_6-A'**, and 7: **HYFNIF-A**, amide coupling, 8: **HYFNIF-A'**, amide coupling. In TBE buffer; maximum volts (300 V), 15 mAmps for one hour. Stained in stains all stain. All samples have a final peptide concentration of 1.25 mM, and a DNA concentration of 25 μM.

The addition of hexafluoroisopropanol (HFIP) to the **CGSG-HYFNIF** peptide improved the coupling efficiency of the DNA peptide conjugate. Mass spectrometry confirmed conjugation by this method of the crude mixture (Fig. 2.33 and 2.34).

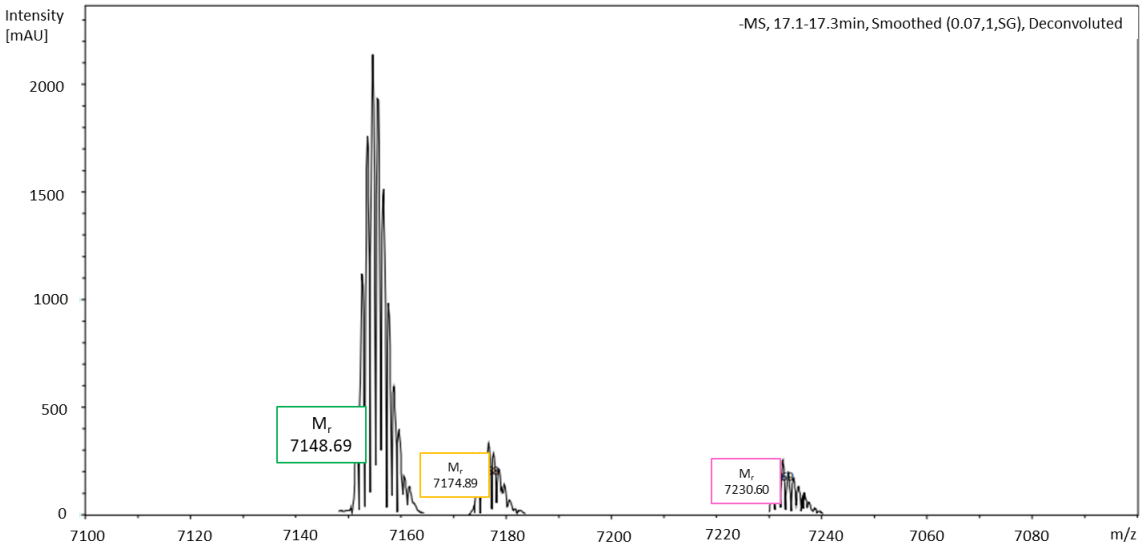

Figure 2.33: Deconvoluted mass spectrum of crude **A-ILVAGK**. Calculated = 7151.61, found 7148.69 m/z $[M - 3H]^{3-}$.

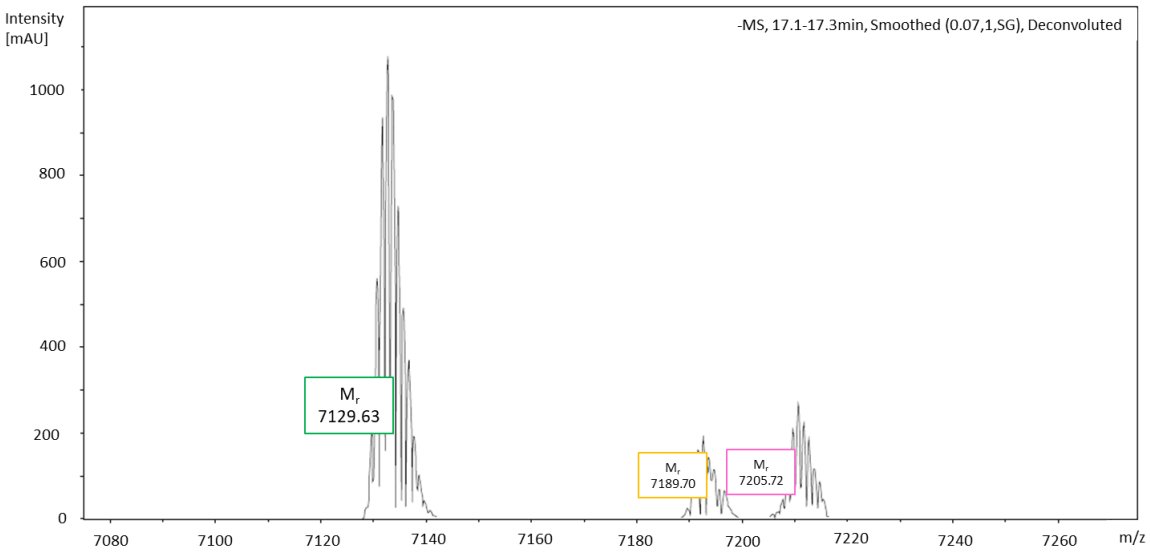

Figure 2.34: Deconvoluted mass spectrum of crude **A'-ILVAGK**. Calculated = 7129.63, found 7129.72 m/z $[M + H^+]^+$.

2.2.4: Synthesis of DNA Peptide Conjugates-Strain Promoted Alkyne Azide Click Chemistry (SPAAC).

A strained cyclic molecule reacts with an azide to form a 1,4 triazole linkage, in our case we are using a strained cyclooctyne (bicyclononyne, BCN) instead of dibenzocyclooctyne (DBCO). Although DBCO is more strained and therefore more reactive it is larger and may have inherently caused interference between the DNA and peptide self-assembly.

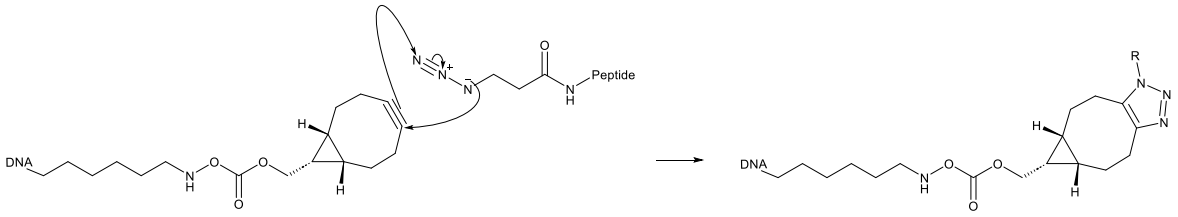

Figure 2.35: Proposed reaction mechanism of DNA-cyclooctyne conjugation to an azido modified peptide.

SPAAC conjugations were carried out at room temperature in water / DMF solvent systems to begin with, to mitigate heating of the azide component, the first experiment was carried out at a molar ration of 1:4 DNA to peptide, and the second at a ratio of 1:1 respectively. These reactions did not show a second conjugation band when analysed by PAGE (Fig. 2.34).

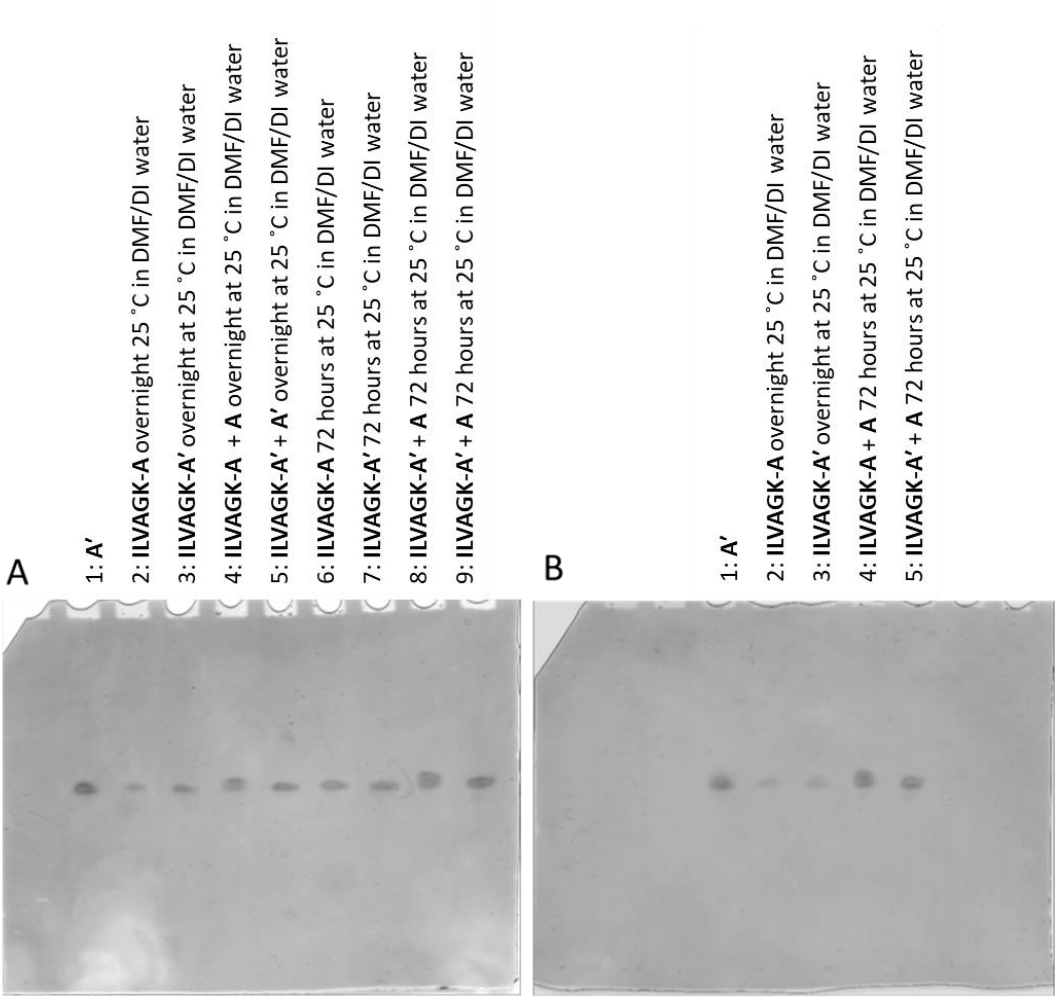

Figure 2.35: 20 % denaturing PAGE of DNA-cycloctyne and N_3-ILVAGK-NH_2 SPAAC conjugations in DMF and DI water. A: molar ratio of 1:4 DNA to peptide 1) **A'**; 2) **ILVAGK-A** reacted overnight, 3) **ILVAGK-A'** reacted overnight, 4) **ILVAGK-A** reacted overnight + **A**, 5) **ILVAGK-A'** reacted overnight + **A'**, 6) **ILVAGK-A** reacted over 72 hours, 7) **ILVAGK-A'** reacted over 72 hours, 8) **ILVAGK-A'** reacted over 72 hours + **A** control, 9) **ILVAGK-A'** + **A** control. B: molar ratio of 1:1 DNA to peptide 1) **A'**; 2) **ILVAGK-A** reacted overnight, 3) **ILVAGK-A'** reacted overnight, 4) **ILVAGK-A** reacted overnight + **A** control, 5) **ILVAGK-A'** reacted overnight + **A** control.

Conjugation in 50 mM triethylammonium acetate buffer, was carried out but did not yield the formation of secondary bands (Fig. 36a), the experiment was repeated, and the reaction mixture treated with fluorescein isothiocyanate (FITC) azide to trap any unreacted DNA-cyclooctyne (Fig. 2.36b). This experiment was devised to assess whether the addition of the peptide was not causing an appreciable band shift.

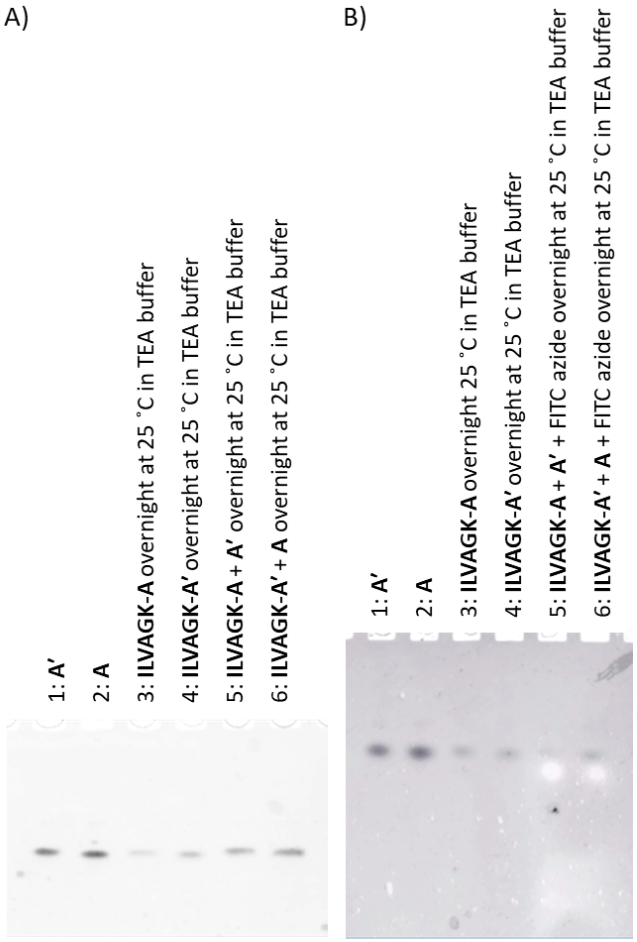

Figure 2.36: 20 % denaturing PAGE of DNA-cyclooctyne and **N_3-ILVAGK-NH_2** SPAAC conjugation in 50 mM TEA buffer. A: 1) **A;** 2) **A'**, 3) **ILVAGK-A** reacted overnight, 4) **ILVAGK-A'** reacted overnight, 5**) ILVAGK-A** reacted overnight + **A'**, 6) **ILVAGK-A'** reacted overnight + **A**. B: 1) **A**, 2) **A'**, 3) **A-ILVAGK** reacted overnight, 4) **ILVAGK-A'** reacted overnight, 5) **ILVAGK-A** reacted overnight + FITC azide, 6) **ILVAGK-A'** reacted overnight + FITC azide.

By increasing the reaction temperature to 50 °C overnight and peptide concentration to 20 equivalents, the reaction yielded nearly full conversion of the cyclooctyne modified DNA to the DNA-peptide conjugate when analysed by PAGE (Fig. 2.37). The conjugate bands were pale on this gel image, this was because the peptide was preventing the stain from intercalating with the DNA fully.

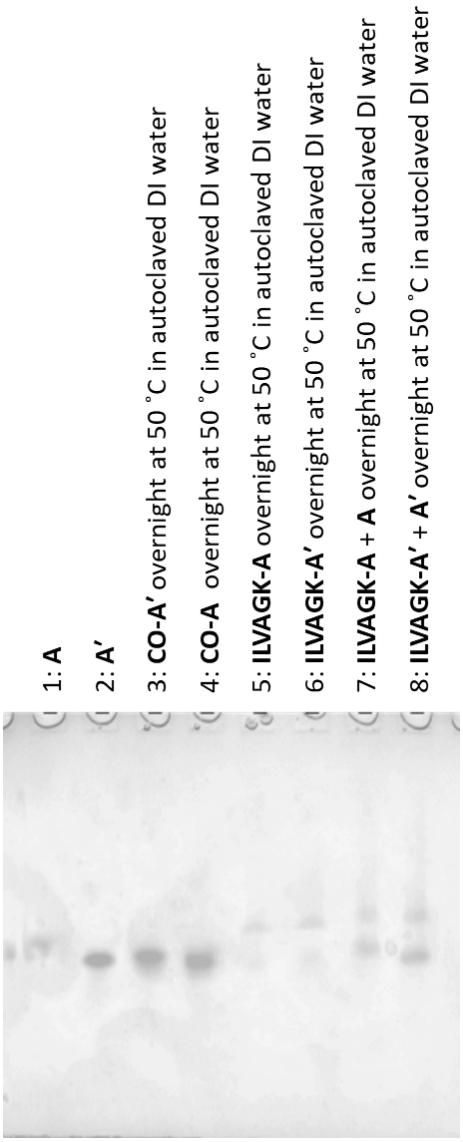

Figure 2.37: 20 % denaturing PAGE of DNA cyclooctyne azide peptide conjugation reaction in DI water, peptide concentration 20 equivalents, at a temperature of 50 ˚C. Ran in TBE buffer; maximum volts (300 V), 15 mAmps and 1 hour. Stained in stains all stain. A: 1) **A;** 2) **A'**, 3) **CO-A**, 4) **CO-A'**, 5**) ILVAGK-A**, 6) **ILVAGK-A'**, 7: **ILVAGK-A** + **A**, and 8: **ILVAGK-A'** + **A'**.

The staining issue was further supported by the issues with purification. When attempting to purify the conjugates by size exclusion chromatography, the peptide was extracted but not the larger DNA-peptide conjugate, which is counter intuitive to the method of purification. The addition of a denaturant (8 M urea) to the column afforded some removal of the DNA conjugate. **ILVAGK-DNA** was treated with 8 M urea before purification by anion exchange resin. **ILVAGK-DNA** was incubated for 30 minutes before addition to the resin, and further incubation. The conjugate was purified as outlined in section 2.3.25, then freeze dried to solid. The solid was resuspended in autoclaved DI

water, then purified by size exclusion chromatography to remove the NaCl from the conjugates, UV-Vis was used to monitor the elution of DNA from the mini column as DNA and NaCl have different absorbances, DNA also comes off quicker than NaCl due to its size difference. The efficiency of the conjugate reaction was improved by reducing the amount of time at 37 ˚C. The conjugation carried out for 2 hours showed an unreacted **CO-DNA**, by reducing the reaction time to 1.5 hours, the visual strength of the unreacted **CO-DNA** band was reduced (Fig. 2.38). Further reduction of the reaction time to 1 hour, continued to improve the reaction efficiency by PAGE (Fig. 2.39). **ILVAGK** is a heat sensitive peptide, it was thought that by carrying out the conjugation for a longer duration increased the self-assembly of **ILVAGK**, this may also be why the conjugates were stained less strongly by stains all. By reducing the reaction time, it limited the amount of time the peptide could assemble leaving the peptide free to react with the DNA, giving a higher efficiency.

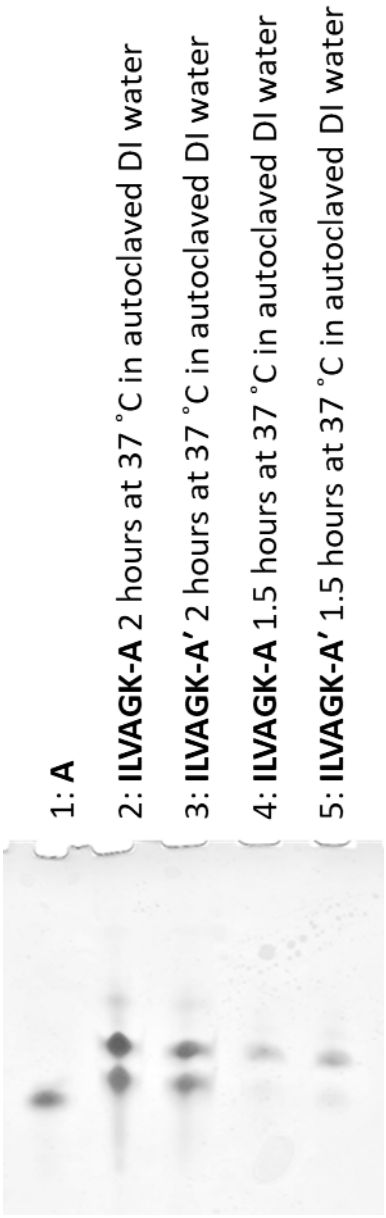

Figure 2.38: 20 % denaturing PAGE of DNA cyclooctyne azide peptide conjugation reaction at 37 ˚C for 1.5 or 2 hours, in DMF. Autoclaved DI water. Ran in TBE buffer; maximum volts (300 V), 15 mAmps and 1 hour. Stained in stains all stain. A: 1) **A;** 2) **ILVAGK-A**, 2 hrs 3) **ILVAGK-A'**, 2 hrs 4) **ILVAGK-A**, 1.5 hrs 5**) ILVAGK-A'**, 1.5 hrs.

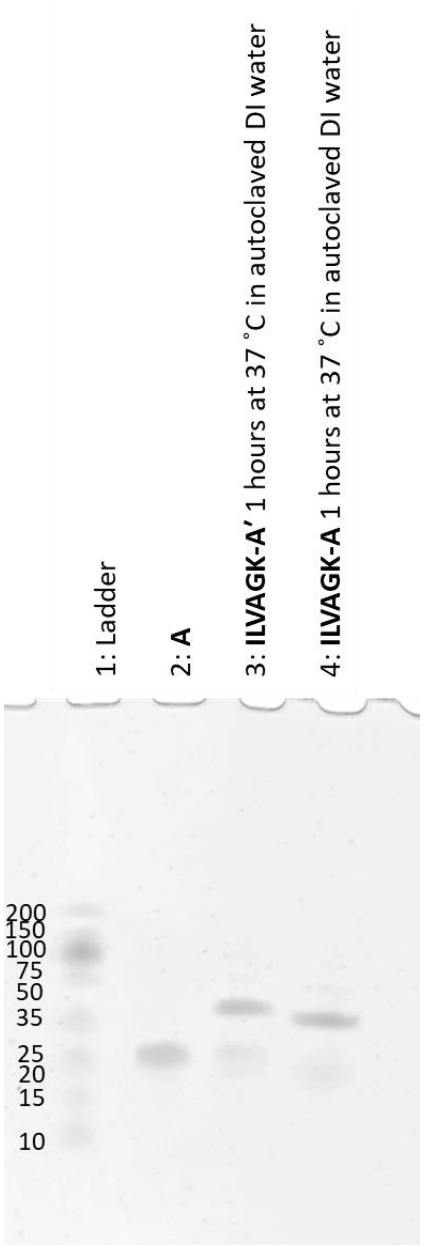

Figure 2.39: 20 % denaturing PAGE of DNA cyclooctyne azide peptide conjugation reaction at 37 ˚C for 1 hour in DMF/autoclaved DI water. Ran in TBE buffer; maximum volts (300 V), 15 mAmps and 1 hour. Stained in stains all stain. A: 1) Ladder, 2) **A;** 3) **ILVAGK-A**, 4) **ILVAGK-A'**.

In this chapter two main types of chemistry have been discussed to achieve DNA modified with a bioconjugate linker, phosphoramidite chemistry, and amide coupling. Zhang *et al*. used solid phase phosphoramidite chemistry to attach ferrocene to DNA molecules, which were then self-assembled to give DNA nanoflowers.[56] These nanoflowers were shown to be cancer targeting, and self-degradable, allowing the release of a drug-based cargo.[56] Staphanopoulos *et al*. attached dibenzylcyclooctyne to DNA through NHS ester mediated amide coupling, similarly, to as discussed

in this chapter.[104] The modified DNA was then attached to a RDGS peptide sequence through copper free click chemistry, like discussed in section 2.2.4.[104] Jin *et al*. also used phosphoramidite chemistry to make DNA modified with a dibenzylcyclooctyne bifunctional crosslinker.[124] Conjugation was achieved between the megadalton DNA structures through strain promoted copper free click chemistry, similarly to Zhang *et al*. and as discussed in this chapter.[124] Alleva *et al*. also used NHS ester mediated amide coupling to make their DNA-polymer conjugates, which they then used to demonstrate surface patterning of DNA origami structures.[81] The frequency of use of these conjugation chemistries within the literature demonstrate their usefulness in achieving biomolecule conjugates, and further support their use within this thesis, some review articles which further discuss the breadth of conjugation chemistry between biomolecules is available at the end of this sentence.[125–127]

2.3: Conclusions

Section 2.1 discussed the synthesis of DNA with bi-conjugate linkers attached. The synthesis of inhouse DNA was plagued by system issues, and phosphoramidite oxidation issues. Although these were overcome to a degree, by modification of the method the yields were low and contained many by-products. This resulted in the purchasing of oligonucleotides from IDT, with consistent purity and yield. The synthesis of the maleimide bi-functional crosslinker was made less complicated by removing the phosphonamidite portion of the molecule. This allowed attachment of **4** to DNA via amide coupling. Amide coupling was used to attach a cyclooctyne NHS to **A** and **A'**, this was achieved in high yield and purity by mass spectrometry (Fig. 2.21). Maleimide and cyclooctyne modified DNA were taken forward for conjugation with peptides. Many conjugation reactions were carried out, to investigate the attachment of peptide to DNA through Michael-thiol addition for **HYFNIF** peptides or strain promoted alkyne azide chemistry for the **POG_6** and **ILVAGK** peptides. Most conjugate reactions were assessed by PAGE, due to lack of availability of the mass spectrometer and processing times for the facility. This also led to delays in confirming the

successful attachment of the bi-functional linker to the DNA. Therefore, it was difficult to discern which conjugation conditions were truly unsuccessful or simply due to the lack of DNA with a maleimide or cyclooctyne attached. Once the reactions conditions were optimised for the **CO-DNA** and **4-DNA** compounds, the correct conclusions could be made about the conjugate reaction conditions. A number of studies concluded that the maleimide-thiol conjugation with **HYFNIF**, was most successful at pH 8.0 in sodium phosphate buffer and a temperature of 50 ˚C. Whereas the more water soluble **ILVAGK** was successful conjugated in pure water, at a temperature of 37 ˚C. It was also found that the **ILVAGK** conjugation improved with shorter reaction times, likely due to reduced energy to the self-assembly of the system.

To further develop the work discussed in this chapter, a reduction in the equivalents of peptide to DNA would be beneficial to reductions in cost, and loss of valuable materials. To achieve this, further studies around the reaction conditions would be required. These included changing the buffer type, but I would not change the pH. One of the biggest learning points from this chapter was the consideration around pH. When undertaking a chemistry PhD, it is very easy to miss the nuances of biochemistry, especially when working with biological materials like DNA and peptides. It is very often neglected when considering wholly organic chemical reactions and should always be given fair consideration. Reducing the amount of material in the reaction, and any excess would also improve the purification process, which would increase time efficiency when studying these materials. More development on the conjugation and purification of the **POG_6** peptide was required. It was found that only around 50 % of the initial peptide was successfully modified with the azide linker. So, improvements to this would improve the overall efficiency and purity of the reaction, by eliminating unreactive peptides. This could be done, by either improving the coupling efficiency, or by purifying the peptide with the azide attached from the peptide without the azide, it would be more cost efficient to improve the azide coupling reaction to the **POG_6** peptide. Optimisation to the visualisation of PAGE gels could be improved by experimenting with other stains, such as gel red, and SYBR green. Where possible it is recommended to have all of your

samples and reactions analysed by mass spectrometry, or the analytical method which is beneficial for your work. Having this data early on allows better understanding of the results gained in subsequent experiments, instead of moving forward with the expectation that the previous reaction was successful, always be sceptical of the result until the facts are collected which confirm the success of the experiment.

Chapter 3 discusses the peptide driven self-assembly of **ILVAGK**, when doped with varying amounts of **ILVAGK-DNA**. The aim of these experiments was to explore the impact DNA-peptide may have on the parent peptide system, as well as to establish a baseline for the types of structures formed by **ILVAGK**.

Chapter 3.0: Peptide Directed Self-assembly of DNA-ILVAGK

3.1: Introduction

ILVAGK (isoleucine (I), leucine (L), valine (V), alanine (A), glycine (G), and lysine (K)) is a hexapeptide with a hydrophobic block (VAGK), preceded by gradually increasing hydrophilic residues (K and L), this character aids the self-assembly (through electrostatic interactions) shown by **ILVAGK**, to form random coil, α-helical and to finally β-turn self-assembly.[128,129] This diversity in self-assembly is further promoted by **ILVAGK'**s salt and pH sensitivity, which has been shown to cause **ILVAGK** to form hydrogels, with interesting potential applications within medicine, such as drug delivery and cell growth matrix.[82,130,131]

In this chapter the role of peptide-driven self-assembly of **DNA-ILVAGK** will be discussed. The self-assembly of **ILVAGK** was analysed for changes in observed morphology as influenced by the addition of differing amounts of **DNA-ILVAGK**. This self-assembly process was observed over the course of 28 days. By observing this system over a prolonged time period, as often performed in amyloid research,[132–134] we studied the dynamic and diverse nature of this system.

3.2: Results and Discussion

The composition of the buffer was important in investigating the self-assembly of **ILVAGK** and **DNA-ILVAGK**. The buffer chosen was tris magnesium acetate (TAMg), because the magnesium acetate aids the assembly of **ILVAGK** due to it being a salt, but also DNA duplex formation due to the magnesium ions shielding the negative charges on the DNA phosphate backbone in base stacking, which will be discussed in chapters 4 and 5.[135] Self-assembly was monitored over 28 days by dynamic light scattering (DLS), circular dichroism (CD) and atomic force microscopy (AFM), to allow better understanding of the stability and dynamic nature of this system. A range of nanostructures were observed, which were classified with the following morphologies: small and large flakes, fractal-like, fibre-like, dot-like, and network-like (Fig. 3.1).[136] Zhang et al, defined their

morphologies based on the most common structures they observed, these included fiber-like structures, and random compacts which were similar to the small and large flakes observed throughout the following chapters.[136]

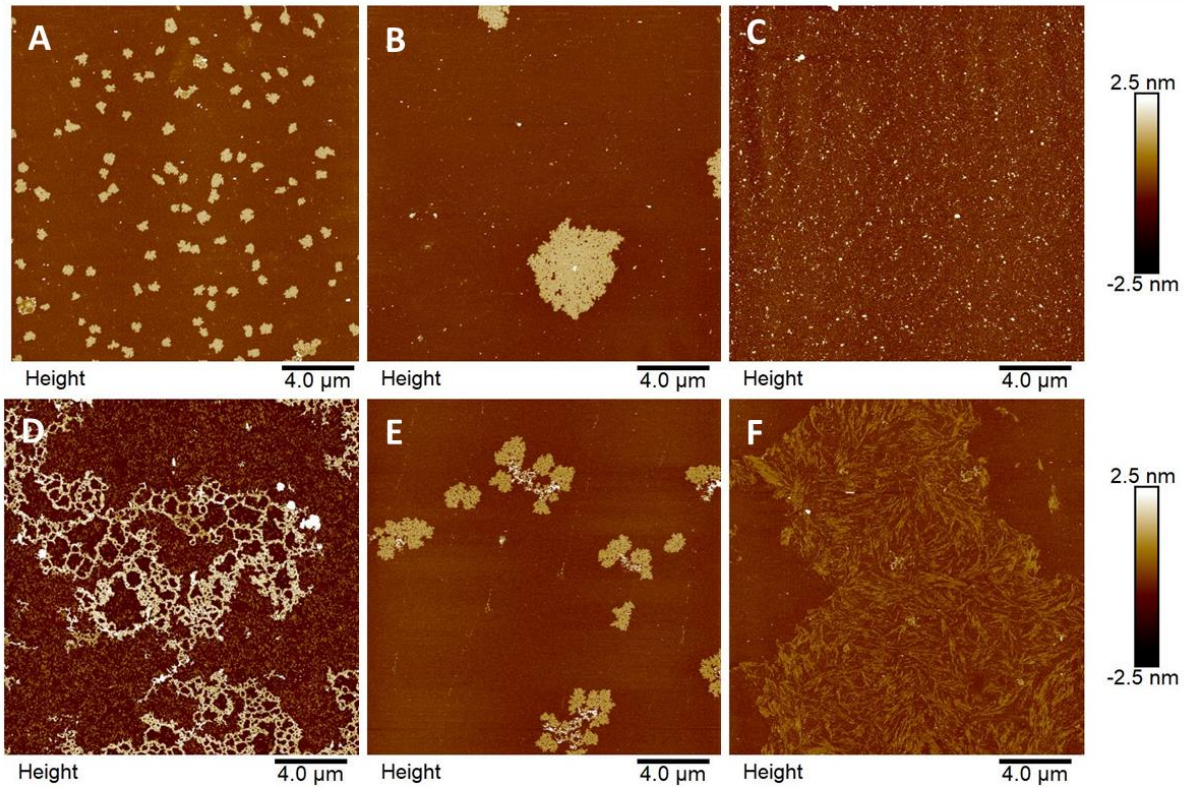

Figure 3.1**:** Morphologies within this paper. A: Small flakes, B: large flakes, C: dot-like, D: network-like, E: fractal-like and F: fibre-like.

ILVAGK, **A**, **A'**, and **A+A'** were analysed as controls at a final concentration of 10 µM. Samples of **ILVAGK** (20 µM) were doped with varying amounts of **A'-ILVAGK** (1, 0.5, 0.1 and 0.01 equivalents) with a final concentration of 10 µM (**ILVAGK** + **A'-ILVAGK**) for all samples. Samples were aged at room temperature, in the dark (to eliminate UV degradation of the DNA component), and aliquots taken at 0, 7, 14, 21 and 28 days. Days 0 was designated to the day on which the samples were prepared.

DLS is an analytical method which is used to assess the hydrodynamic radius of nanoparticles by laser scattering. Although DNA and peptides are not generally spherical, they can form spherical or sphere like objects. It has been found in previous work that DLS can be a useful tool in assessing the structural changes within a DNA/DNA-like system.[137] Full DLS method can be found in the

experimental section 7.2. Figure 3.2 shows the DLS data collected for the controls over 28 days. From Figure. 3.2a and b, we can see that **A** and **A'** have low scattering intensity. This was shown by the lack of overlap of measured data, and apparent change in hydrodynamic diameter given that this was single stranded DNA it was unlikely that it would aggregate in TAMg buffer leading to a change in apparent size especially without the presence of a DNA complement. Also, because the DNA is comparatively small it does not scatter the light in the same way an aggregate might, giving inconsistent data.

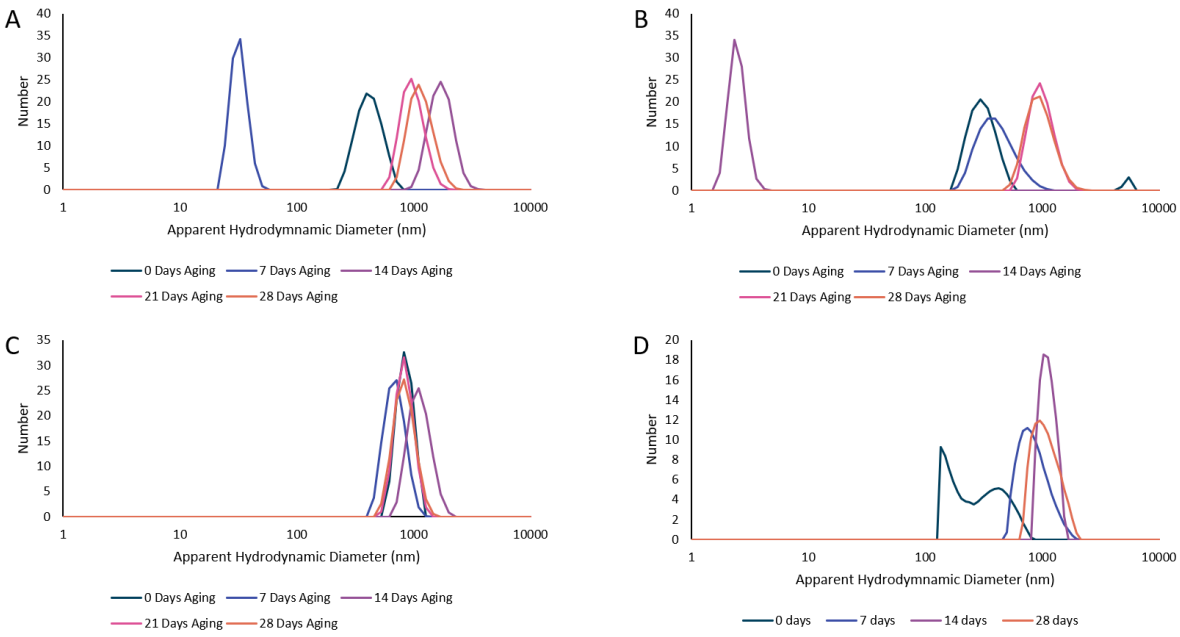

Figure 3.2: DLS control data for studies 1 and 2 over 28 days of aging. All samples at a final concentration of 10 µM and in tris magnesium acetate buffer, at 25 ˚C. A) **A**, B) **A'**, C) **ILVAGK**, and D) **A** + **ILVAGK** (unconjugated). All samples measured in tris magnesium acetate buffer (pH 8.0), at 25 ˚C, with a final DNA/peptide concentration of 10 µM. Measurements taken at 0, 7, and 14, 21, and 28 days of aging.

What is of interest, however, is Figure 3.2 c **ILVAGK** shows consistent hydrodynamic diameter over the 28-day period, centred around 1000 nm. For Figure 3.2d a mixture of unconjugated **A** and **ILVAGK** after 0 days of aging the peaks sit around the same point as Figure 3.2 c, it can also be seen that the number is roughly half that of **ILVAGK** which matches with the concentration of each component. The peak shape at 0 days, may be attributed to the system not being at equilibrium.

Figure 3.3 shows the DLS data collected for the samples of interest in this study. All samples sit around this 1000 nm hydrodynamic diameter mark, and do not change significantly over 28 days. What can be noticed is that there is slight broadening of the peaks at 21 and 28 days, which may be representative of larger structures forming, as this broadening is indicative of a greater dispersity of particles. This possibility will be further discussed within the CD and AFM data.

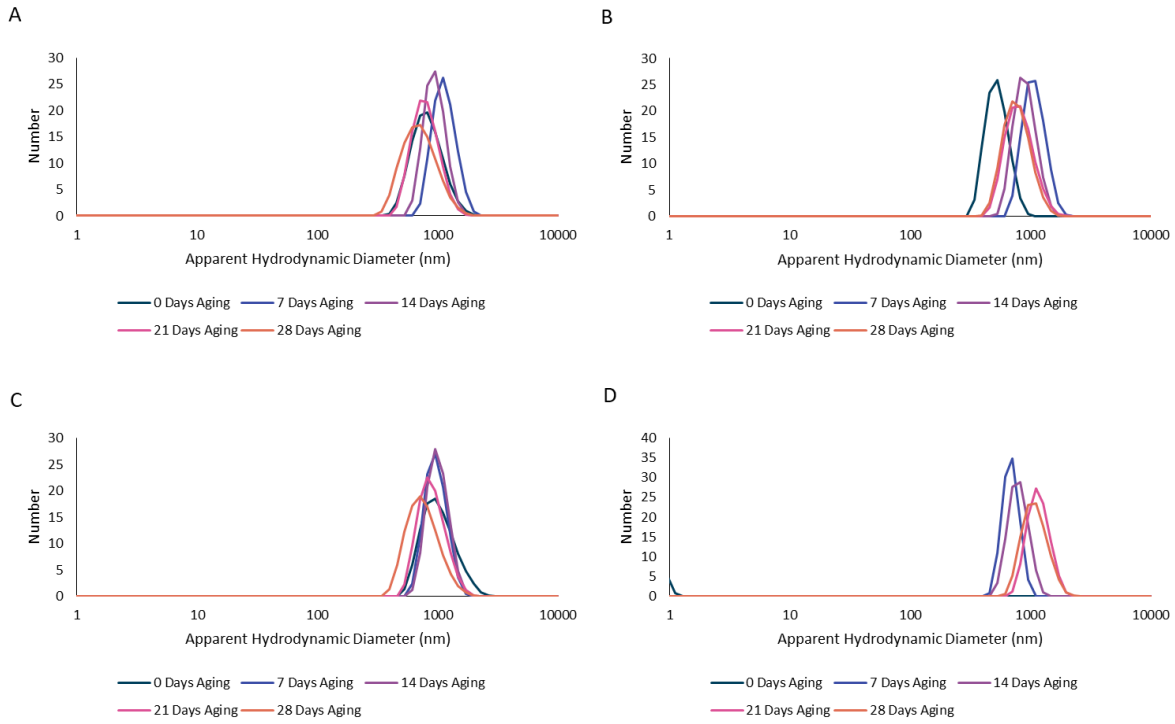

Figure 3.3**:** DLS of Study 1, measured over 28 days of aging. A) 1:1 equivalents of **ILVAGK** to **A'-ILVAGK**, B) 1:0.5 equivalents of **ILVAGK** to **A'-ILVAGK**, C) 1:0.1 equivalents of **ILVAGK** to **A'-ILVAGK**, and D) 1:0.01 equivalents of **ILVAGK** to **A'-ILVAGK**. All samples measured in tris magnesium acetate buffer (pH 8.0), at 25 ˚C, with a final DNA/peptide concentration of 10 µM. Measurements taken at 0, 7, and 14, 21, and 28 days of aging.

Whereas the DLS data shows little change over the 28-day period, the CD data does show changes over the course of the experiment. Figure 3.4 and 3.5 show the recorded CD data from the controls and experiment respectively (data from 21 and 28 days is missing due to a lab closure due to Covid-19; it was not possible to re-run these experiments due to the time remaining for experimental work). For DNA a concentration of 10 µM is usually a substantial amount to gather detailed CD data from DNA self-assemblies, as DNA interacts strongly with UV light giving rise to a stronger CD signal. However, peptides often require higher concentrations to gather detailed

structural information. During the experiment it was found that, general structural characteristics from the peptide portion of the experiment could be seen, and strong DNA signals in the samples where the concentration of the DNA was 5 or 10 µM. Fig 3.4a and b show the CD traces for **A** and **A'**, these spectra show the classical single stranded DNA shape, with two maxima, one around 220 nm and the other around 275 nm.[138] Fig 3.4c shows the spectrum is largely flat, except for a maximum around 192 nm, this maxima is indicative of the β-turn structure.[139,140] Reducing the data interval from 100 nm/min to 20 nm/min would have improved the CD spectre for **ILVAGK**, especially as the concentration of the peptide is lower than would be usually used, reducing the interval may also have improved the over-voltage seen around 190 nm.

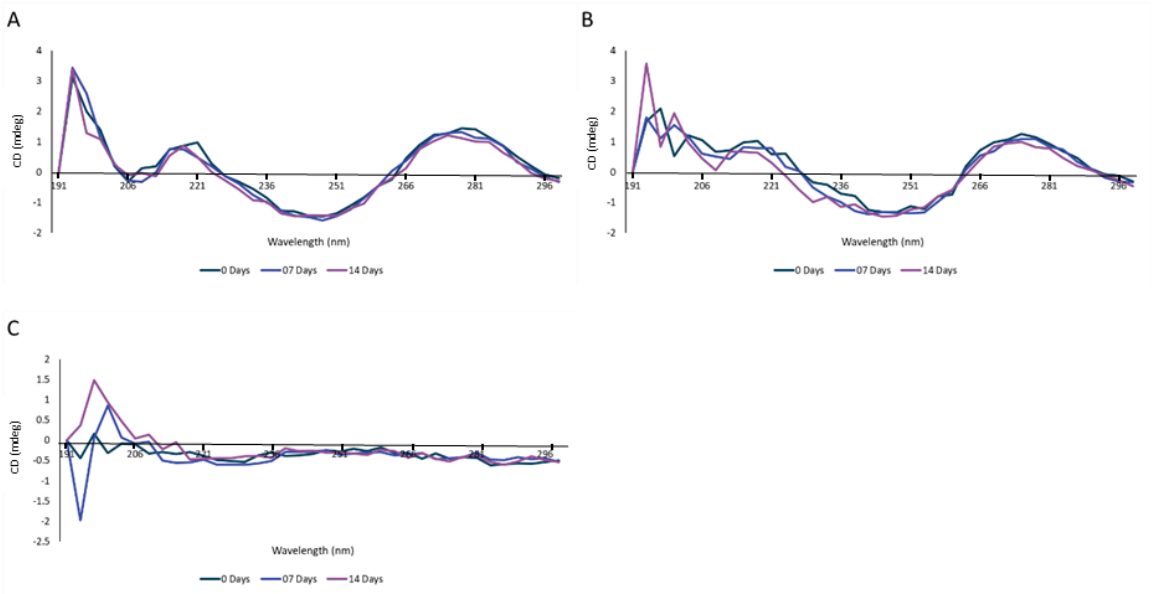

Figure 3.4: CD control data. A: **A**, B: **A'**, C: **ILVAGK**. All samples measured in tris magnesium acetate buffer (pH 8.0), at 25 ˚C, with a final DNA/peptide concentration of 10 µM. Measurements taken at 0, 7, and 14 days of aging.

Figure 3.5 a and b contain the largest percentage of DNA within this experiment, at 1:1 and 1:0.5 respectively. At 0 and 7 days of aging, the canonical DNA CD spectra is visible, with maxima at 220 and 275 nm. What is particularly interesting is, the change in the spectra by 14 days of aging to a spectrum more closely relating to that of the β-turn with a maximum at 197 nm, and a minimum around 223 nm, this minimum is representative of the fibril formation of β-turn. This is suggestive that the self-assembly of the peptide, was changing with time, but also by diminishing the signal of

the DNA component it would suggest that the self-assembly is more strongly chiral than that of the single stranded DNA thus giving a stronger signal. Unfortunately, due to the lower DNA concentration in Figure 3.5c and d, we do not see this diminishing of the DNA signal, however we do see the appearance of the minima around 223 nm, which may support the reduction in DNA signal in all samples.

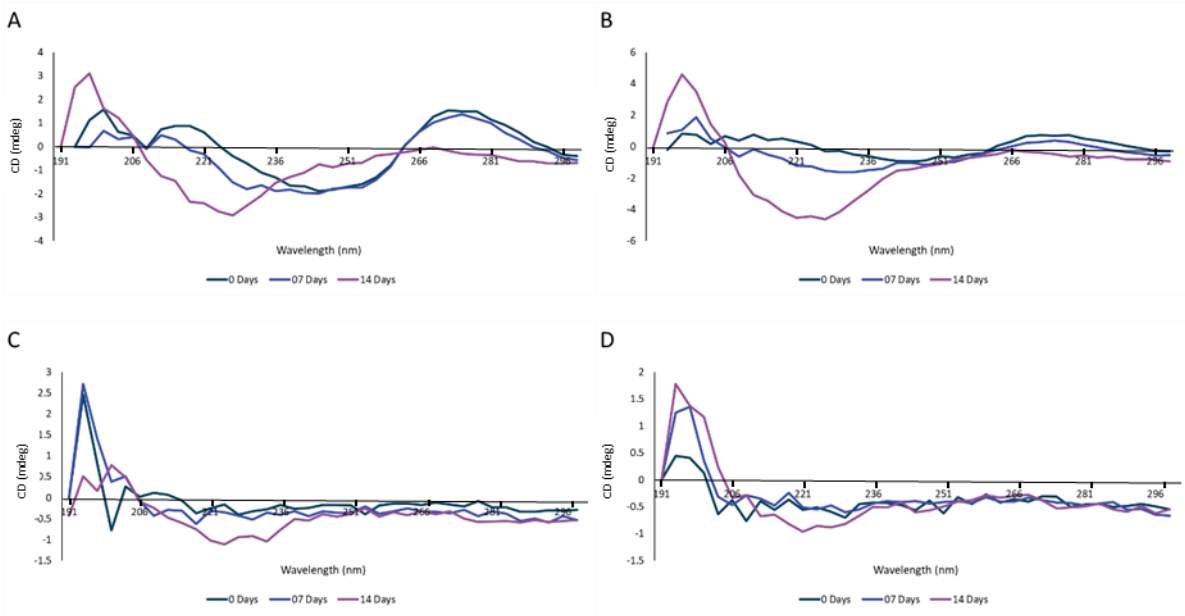

Figure 3.5: CD data for Study 1. A: 1:1, B: 1:0.5, C: 1:0.1 and D: 1:0.01 ratios of **ILVAGK**:**A-ILVAGK**. All samples measured in tris magnesium acetate buffer (pH 8.0), at 25 ˚C, with a final DNA/peptide concentration of 10 µM. Measurements taken at 0, 7, and 14 days of aging.

The use of DLS and CD characterisation is valuable in providing a preliminary idea of the kind of conformation that is occurring within the system, however, to truly understand how these signals translate into nano-structural form, there is a need to explore the self-assembly via microscopy. Atomic force microscopy allows the detailed nanoscale analysis of self-assembling systems, with a full range from sub nanometre to hundreds of nanometres, allowing the investigation and understanding of self-assembly from the miniscule building blocks, up to fully evolved systems. This is where the timescale of 28-days allows the full evolution of the system to be truly explored, allowing further insight to be drawn about the evolution and dynamism of the system.

ILVAGK showed interesting growth over the aging period, Figure 3.6 shows the overall change in self-assembly over the 28-days. This change in nanoscale morphology reflects the observations drawn from the DLS and CD data discussed previously in this chapter. At 0 days of aging **ILVAGK** shows no visible self-assembly, this was consistent across the surface of the mica. At 7 days of aging, we see the formation of small dot like structures with an average height of 7.44 ± 2.03 nm and diameter of 109.88 ± 32.89 nm. These structures were consistent across the surface in multiple locations. In contrast at 14 days of aging, we see the system evolve into a mixture of small flakes and network-like structures. The small flakes had an average diameter of 160.1 ± 40.8 nm, with a height of 1.67 ± 0.35 nm, whereas the network like structure had an average height of 2.3 ± 2.2 nm. Given that both morphologies are observed in the same area, it may suggest that the small flakes act as building blocks for the network-like structures. This is further supported by the shape and surface texture of the networks; they had similar cauliflowery edges as observed with the small flakes.

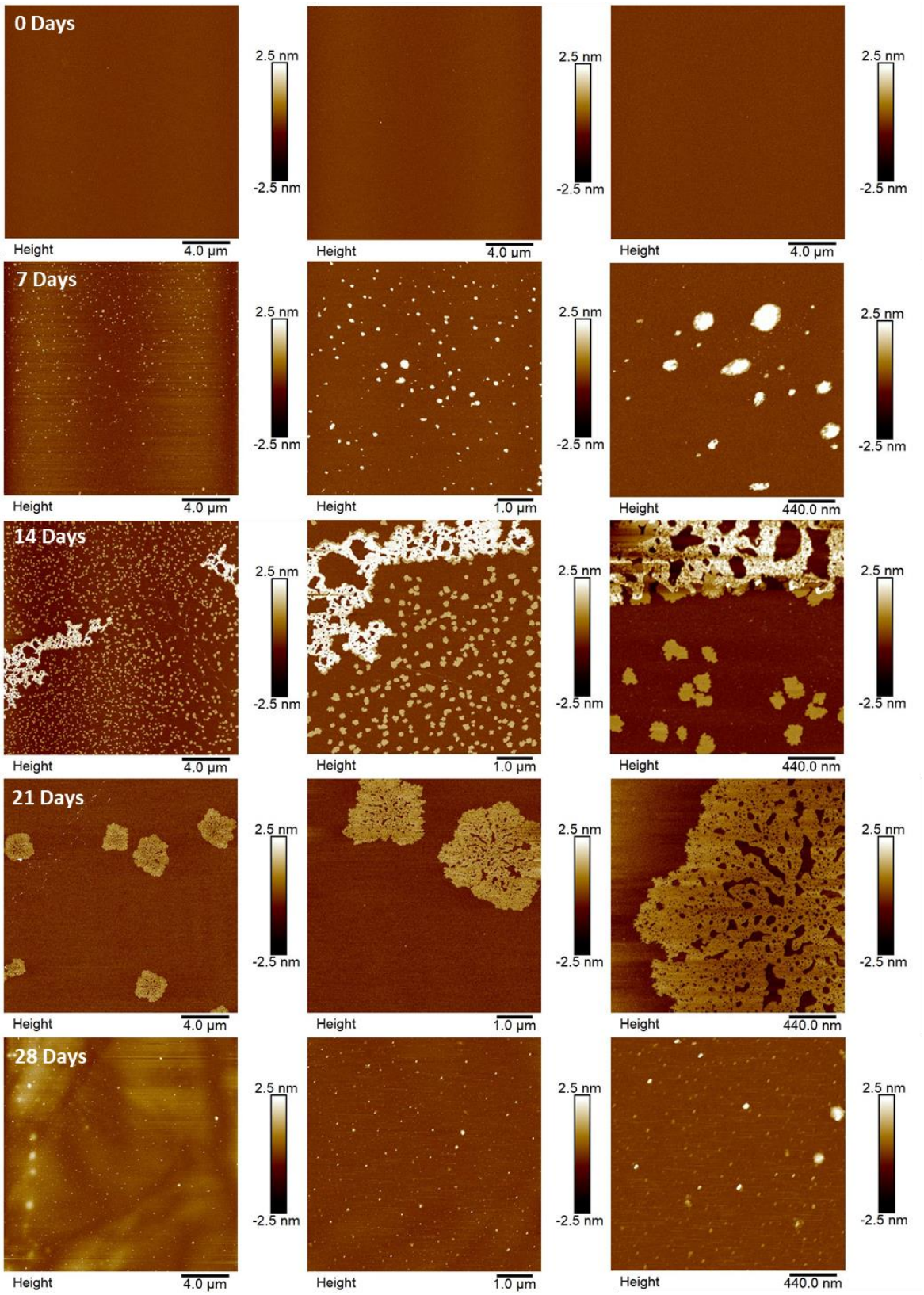

Figure 3.6: AFM images of **N_3-ILVAGK-NH_2** in tris magnesium acetate buffer over 28 days of aging, images from left to right show increased magnification of the same area.

At 21 days of aging (Fig. 3.6) a further change in the self-assembly was observed, the evolution of large flakes from the small flakes and network-like structures observed at 14 days of aging. These

large flakes had and average height of 1.9 ± 1.1 nm and diameter of 1.1 ± 1.0 µm. Making the difference in height and diameter between the small flakes observed at 14 days of aging and the large flakes at 21 days of aging, ≈ 0.3 nm and ≈ 840 nm respectively. Up until this point in the aging of **ILVAGK** the structures observed become gradually larger, however, at 28 days of aging the morphology devolves back to dot-like structures. This may suggest that the **ILVAGK** had reached it thermodynamic equilibrium, and that these dot-like structures were the most stable for **ILVAGK** in the presence of TAMg buffer. These dot-like structures had an average height of 3.9 ± 2.1 nm and diameter of 94.4 ± 16.7 nm. Which are slightly smaller than those observed at 7 days of aging. If this dynamic changing of structural morphology is maintained within the **DNA-β turn** doped **ILVAGK**, conclusions could be drawn about the effect the addition of DNA-peptide conjugates have on the peptide driven self-assembly of this system.

ILVAGK was doped with varying amounts of **A'-ILVAGK**, the first of which was 0.01 equivalents of the DNA-peptide conjugate to the pure peptide. The structures observed during the aging of the 0.01 eqv sample was similar to those observed in Figure 3.6. At 0 days of aging, we see the emergence of small flakes (Fig. 3.7), this is two weeks earlier than was observed in Figure 3.6, where small flake structures were only observed at 14 days of aging. The small flakes observed at 0 days of aging (Fig. 3.7), had an average height of 1.6 ± 0.2 nm and an average diameter of 123.6 ± 32.5 nm. However, at 7 days of aging we see the formation of dot-like structures, which were observed similarly at 7 days of aging in the pure **ILVAGK** sample. These dot-like structures had an average height of 2.6 ± 1.1 nm and diameter of 89.1 ± 18.5 nm, this was similar to the height and diameter observed for these structures at the same time point in the **ILVAGK** sample. At 14 days of aging (Fig. 3.7) little change in morphology is observed, dot-like structures are still visible, but there is the addition of a few larger clusters. The smaller dot-like structures had an average diameter of 297.1 ± 78.9 nm and height of 5.9 ± 2.5 nm, with the larger structures having a diameter of 328.3 ± 73.7 nm and height of 8.3 ± 1.8 nm. When compared with the dot-like structures observed at 7 days of aging, it is seen that the overall diameter and height increase, as well as a greater

variation is size across the structures, as shown by the error associated with the measurements. At 21 days of aging, a departure from the morphologies observed in the **ILVAGK** sample is seen. The formation of fractal-like structures is observed, these structures have dense centres, similar to those seen in the network-like morphology, however it also shows the large plate like morphologies branching out from the centre of the structure. The average height of these fractal-like structures at the bundled centres was 7.5 ± 4.0 nm, and 4.5 ±4.1 nm for the flattened plate-like edges. ILVAGK is a peptide which has been demonstrated to self-assemble into hydrogels.[128,141] Hydrogels generally consist of a fibre-like network which is swollen with liquid media, like buffer.[142] When dried and analysed by AFM, it would not be a surprise to see structures similar to those observed here, especially as the self-assembly is peptide driven and in the presence of magnesium containing buffer.

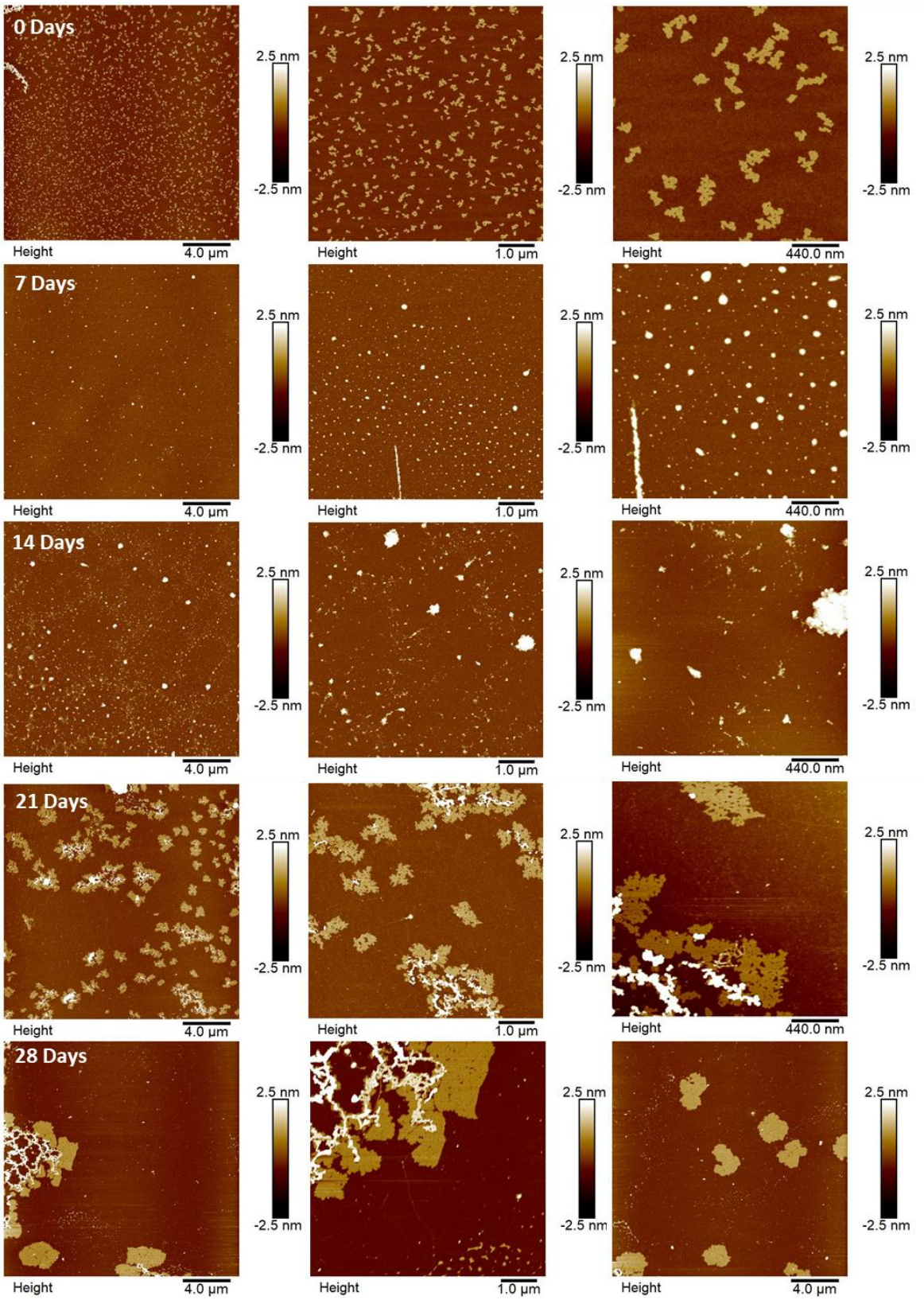

Figure 3.7: AFM images of **N_3-ILVAGK-NH_2** doped with 0.01 equivalents of **A'-ILVAGK** in tris magnesium acetate buffer over 28 days of aging, images from left to right show increased magnification of the same area.

The presence of large flakes (Fig. 3.7, 21 days, H: 6.2 ± 4.9 nm, D: 742.6 ± 235.6 nm) may suggest that these fractal-like structures are building blocks in the formation of network-like structures. At

28 days of aging these fractal-like networks, evolve into much larger assemblies with an average height of 10.9 ± 5.3 nm for the bundled centres and a height of 2.1 ±0.3 nm for the flatter edges. The addition of DNA-peptide conjugate to **ILVAGK**, even at this level, did change the self-assembly observed, but not only did it do this, but it also changed the rate at which different assemblies emerged. Initially self-assembly of the peptide was increased, as we see the formation of small flakes at 0 days of aging unlike at the same time point for **ILVAGK** where, we observe no self-assembly at all. It is then observed that the self-assembly slows, returning to dot-like structures at 7 days of aging in both the 0.01 eqv and **ILVAGK** samples. If it is assumed that the fractal-like structure is a dynamic stage in the further formation of network-like structures, then this may be further proof of the addition of DNA-peptide conjugates slowing the self-assembly of **ILVAGK** into larger structures. To fully understand why this occurs, the addition of 0.1 eqv of DNA-peptide was added to **ILVAGK**, and subsequent increases in concentration of 0.5 and 1 equivalents.

The self-assembly of the 0.1 eqv DNA-peptide doped **ILVAGK** sample is detailed in Figure 3.8. At 0 days of aging, we see disordered structures which were different to those observed at the same time point in the pure **ILVAGK** sample, the height of these structures was 4.0 ± 1.6 nm. However, at 7 days of aging we see the emergence of fractal-like structures, this was quicker than observed (21 days) in the 0.01 eqv doped sample. This may suggest an increase in the speed of self-assembly within the DNA-peptide doped system. The presence of large flakes was also present as observed in Figure 3.7 at 21 days of aging. The height of the fractal-like structures was 3.3 ± 2.0 nm, and the height and diameter of the large flakes was 1.5 ± 0.9 nm and 459.1 ± 434.6 nm respectively. Interestingly, at 14 days of aging the formation of network-like structures was observed, this would suggest that the original argument that the fractal-like structures were building blocks in the formation of network-like structures. These network-like structures appeared at the same point in aging as in the pure **ILVAGK** sample (14 days). It would appear the original slowing down of self-assembly in **ILVAGK** by the addition of 0.01 eqv DNA-peptide is overcome by the further increase to 0.1 eqv. The height of the network-like structures at 14 days of aging was 3.7 ± 4.8 nm.

At 21 days of aging, unlike in the pure **ILVAGK** sample, the network-like structures grow and become more densely interlinked with a height of 4.0 ± 1.8 nm. Small flake structures can also be observed at 21 days of aging, with a height and diameter of 2.4 ± 1.9 nm and 113.0 ± 44.1 nm. It is possible these structures are encouraging further growth within the system. At 28 days of aging, a large structure can be observed. This large structure may be the final evolution of the network-like self-assembly, this is supported by the lack of large structures on the surface and due to its size, with a height of 8.8 ± 7.9 nm.

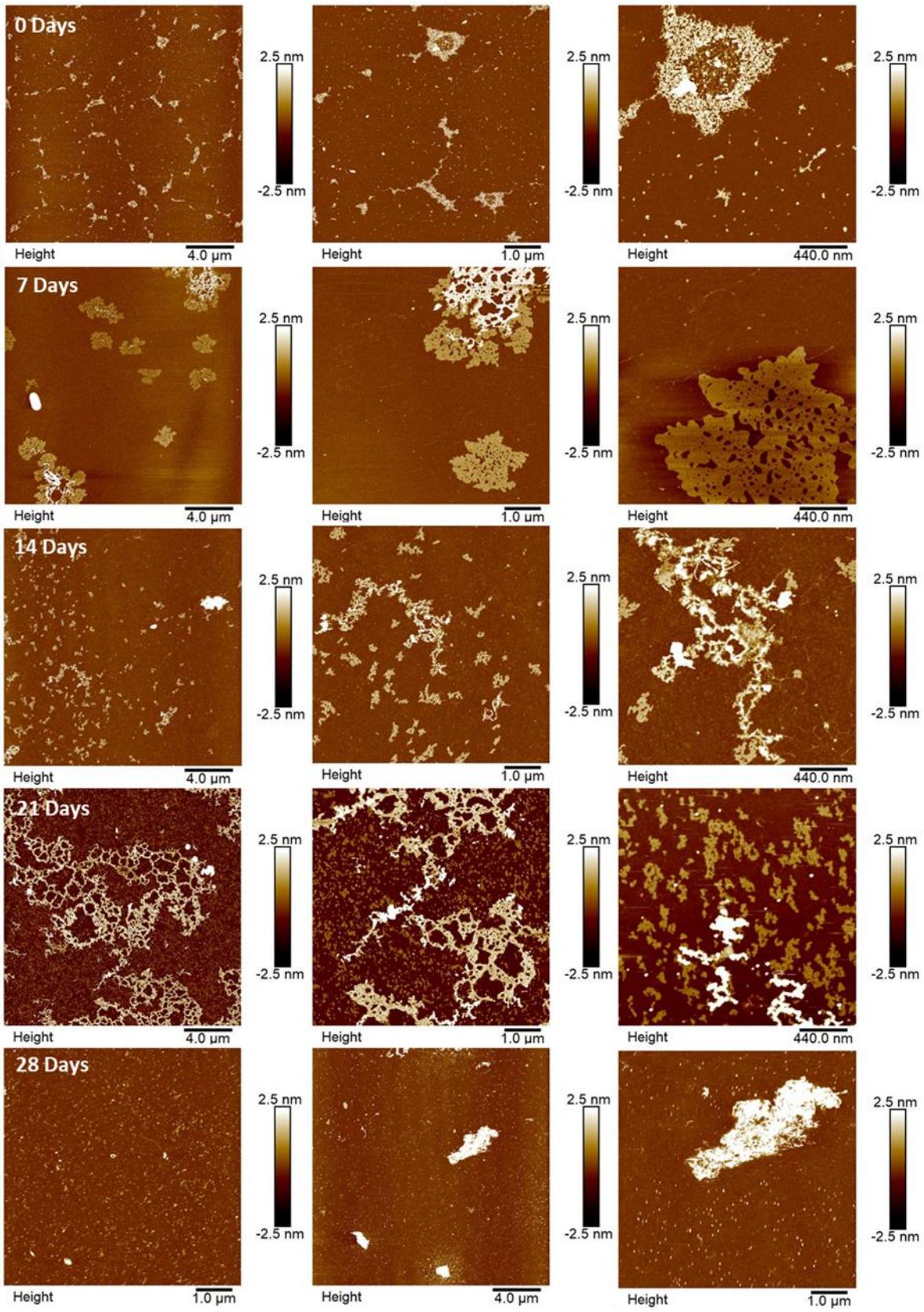

Figure 3.8: AFM images of **N_3-ILVAGK-NH_2** doped with 0.1 equivalents of **A'-ILVAGK** in tris magnesium acetate buffer over 28 days of aging, images from left to right show increased magnification of the same area.

As well as the presence of small flakes with and average height and diameter of 1.4 ± 0.9 nm and 100.3 ± 29.5 nm. Due to the size of the assembly observed at 28 days of aging, more detail could not be obtained without causing damage to the cantilever used to collect these images on the AFM. In summary, with the addition of 0.1 equivalents of DNA-peptide conjugate we see the evolution of self-assembly from fractal-like structures at 7 days of aging which evolve into network-like structures at 14 days of aging similarly seen in the pure **ILVAGK** sample. This supports the theory that these fractal-like structures are indeed building blocks of the network-like structures. We also see these structures further evolve to give more densely interlinked networks at 21 days of aging before the final formation of a large amorphous structure. To further investigate the effect the addition of DNA-peptide conjugate has on **ILVAGK** self-assembly, the concentration of conjugate was increased to 0.5 equivalents.

By increasing the ratio between DNA-peptide conjugate and **ILVAGK** 0.1 to 0.5 equivalents, it is expected that there would be further deviation in the self-assembly of **ILVAGK** when compared to the pure sample. Figure 3.9 shows the morphologies obtained during the aging of this sample set. At 0 days of aging the appearance dot-like structures with a few small network-like structures were visible. The dot-like structures had an average height of 1.9 ± 1.5 nm, and a diameter of 87.6 ± 14.6 nm, the network-like structures had a height of 4.1 ± 3.1 nm. This is the first time during this experiment where both dot-like structures and network-like structures are seen side by side, the mixed morphologies observed so far had been small flakes and network-like structures. At 7 days of aging, we see the formation of small flakes accompanied by network-like structures, which may suggest that what was observed at 0 days of aging was an accelerated form of self-assembly driven by the further addition of DNA-peptide conjugate, particularly as network-like structures were not previously observed prior to 14 days of aging. The height (2.0 ± 2.2 nm) and diameter (296.8 ± 96.9 nm) of the small flakes were larger in height and diameter when compared to previous observations of small flakes in samples 0.01 eqv and, **ILVAGK**. The network-like structures had an average height of 15.5 ± 9.2 nm which when compared with **ILVAGK** and, 0.1 eqv was much taller than those

previously observed. At 14 days of aging a deviation in the observed structures occurs, unlike seen previously in the DNA-peptide doped samples, where the large structures generally evolve into larger more complex structures, the devolution to smaller structures like that observed at 28 days of aging of **ILVAGK** occurs. The formation of small flakes was observed, intertwined with fibre-like structures, these structures also cover the entirety of the surface. These structures had an average height of 3.6 ± 1.6 nm, and a height and diameter for the small flakes of 1.4 ± 0.6 nm and 48.5 ± 27.2 nm.

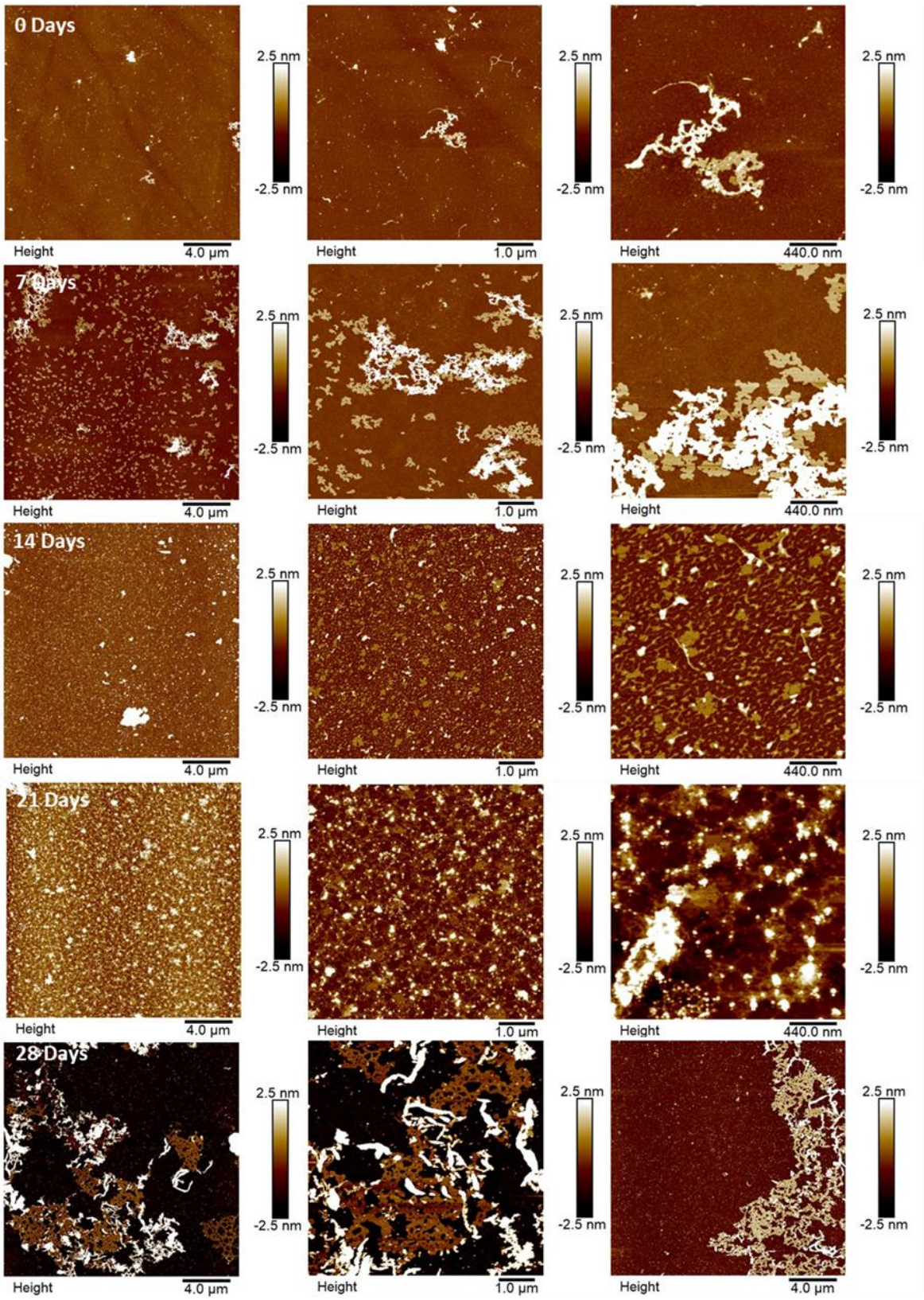

Figure 3.9: AFM images of **N_3-ILVAGK-NH_2** doped with 0.5 equivalents of **A'-ILVAGK** in tris magnesium acetate buffer over 28 days of aging, images from left to right show increased magnification of the same area.

At 21 days of aging, the structures observed at 14 days of aging, further grow, into a more densely packed network, indicative of those observed in sol-gel self-assemblies.[128] With areas of more

densely packed nodes, and areas of space around these, with a 3-dimenstional structure. This 3-D structure is well depicted in the right-hand image of Figure 3.9: 21 days. Due to the density of the structures on the surface, it was difficult to obtain accurate height and diameter data, the average height of the deposit was calculated as 8.4 ± 8.3 nm, and the average diameter of the nodes was 307.1 ± 95.1 nm. At 28 days the appearance of a highly interlinked network-like structure is observed, like that seen at 28 days of aging in the 0.1 eqv DNA-peptide conjugate doped sample. This structure covers a large portion of the surface, with areas of greater height than that of the bulk structure (12.8 ± 10.4 nm and 2.4 ± 2.0 nm) This differs from the structure in Figure 3.8: 21 days where the structure appears to be of uniform height (4.0 ± 1.8 nm) What is interesting is that again a change in the timeline upon which self-assemblies appeared, this may be due to the DNA-peptide conjugate having an increasing influence on the peptide driven self-assembly. DNA is more hydrophilic than **ILVAGK**, it is possible this change in hydrophilicity of the overall system is likely due to the DNA portion of the added conjugates. As these DNA-conjugates assemble with **ILVAGK**, these assemblies are made more hydrophilic moving the system towards hydrophilicity giving rise to more kinetically ordered structures.

Finally, the effect of a 1:1 ratio of DNA-peptide conjugate to **ILVAGK** was investigated, Figure 3.10 shows the AFM images collected from the final experiment in this chapter. At 0 days of aging dot-like and fibre-like structures were observed, comparable those seen at 14 days of aging in the 0.5 eqv sample, however the presence of small flakes was absent. The dot-like structures had an average height and diameter of 1.5 ± 1.0 nm and 35.7 ± 18.0 nm respectively. The fibre-like structures had a height between of 0.5-3 nm. At 7 days of aging, these structures develop into amorphous assemblies with a height of 4.9 ± 3.8 nm, some of these assemblies when examined more closely resemble fibrous clusters. However, at 14 days of aging, these structures devolve back to a mixture of small flakes and fibre-like structures, this may suggest that the amorphous structures observed at 7 days of aging were not kinetically stable and the product of disordered self-assembly. The height of the small flakes was 2.1 ± 1.5 nm, the diameter 104.6 ± 28.1 nm, and

the height of the fibres was 0.5 and 2 nm. At 21 days of aging, two assemblies were observed, the network-like structure was observed, but appeared to feed into a very large structure. This large structure appeared to be made up of striated sheets, like those seen in β-sheet forming peptides. The height of the large structure was between 1 and 6 nm across its surface. At 28 days of aging, the large structure seen at 21 days of aging was not observed. Given the size of the structure it is possible that the self-assembly of such size would not be viable to image by AFM, without causing damage to the cantilever.

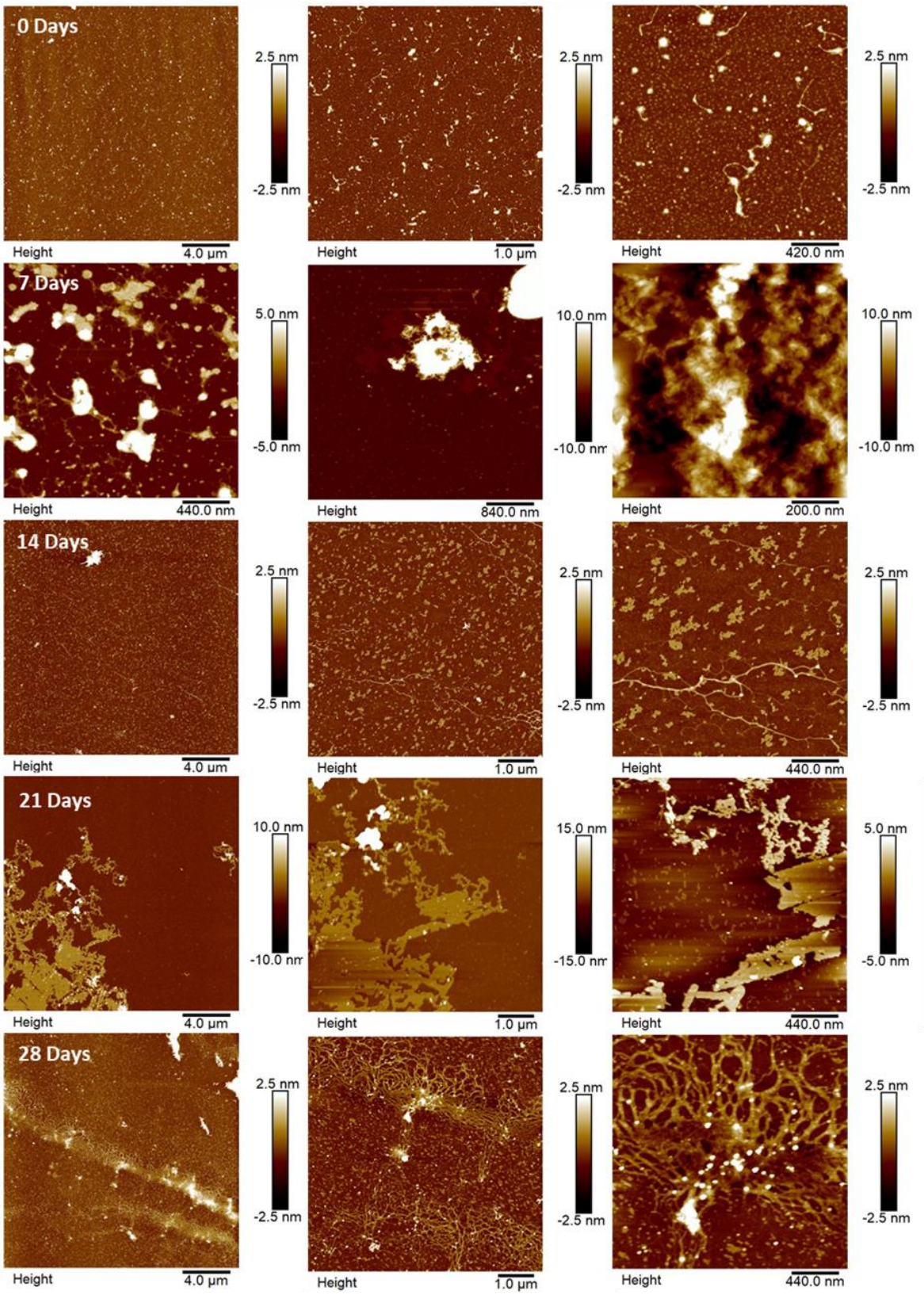

Figure 3.10: AFM images of **N_3-ILVAGK-NH_2** doped with 1 equivalent of **A'-ILVAGK** in tris magnesium acetate buffer over 28 days of aging, images from left to right show increased magnification of the same area.

Interlinked fibre-like network structures were seen at 28 days of aging, this may support that there were larger assemblies on the surface which could not be imaged. The height of these fibre-like networks was 3.1 ± 2.5 nm.

Several controls were also analysed as part of this experiment, TAMg buffer, **A** and **A'** were all analysed by AFM, Figure 3.11 shows these images. These controls were not analysed over the 28-day period for AFM because it was not expected that there would be any change in self-assembly, due to DNA requiring its complement to be able to form a double helix, this is supported by the lack of change over 28 days as observed in the CD data (Fig. 3.4). From Figure 3.11a there was very little on the surface, and the structures that were visible are likely salt residues from the washing process.

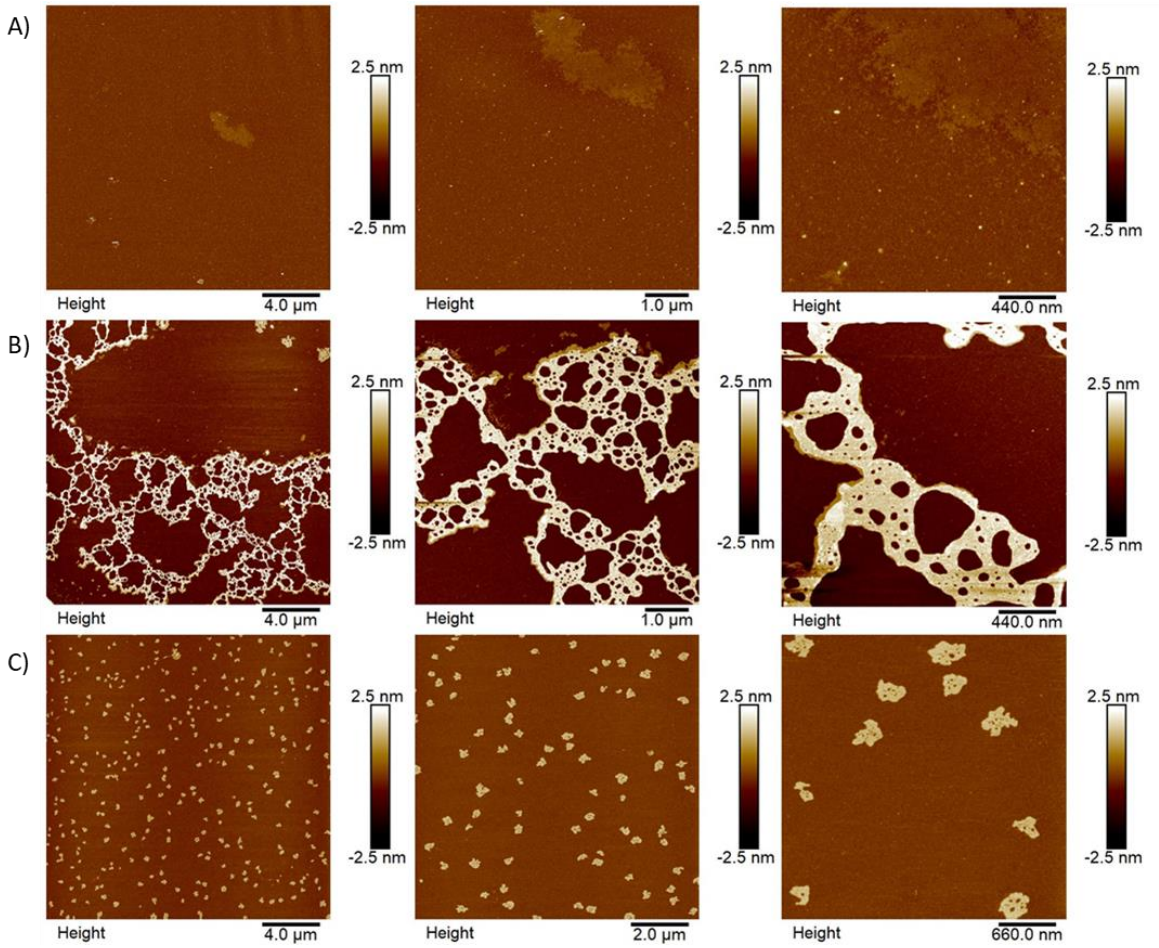

Figure 3.11: AFM images of controls; A: 1x TAMg, B: **A**, C: **A'**, in tris magnesium acetate buffer, images from left to right show increased magnification of the same area.

Figure 3.11 b shows DNA sequence **A**, network-like structures are observed, but this may be due to a drying artifact, as DNA is hydrophilic and mica, the surface used to hold samples is hydrophobic. This may suggest that the DNA aggregates at the boundary edge of the evaporating buffer. However, the height of these structures was 3.7 ± 1.0 nm. Interestingly, Figure 3.11 c shows the images collected for DNA sequence **A'**, here small flakes are observed, this differs from **A** (Fig. 3.11 b) possibly due to the difference in sequence or a variation in the solvent removal from the surface. The height and diameter of these structures was 1.7 ± 0.1 nm and 260.7 ± 44.3 nm respectively.

3.3: Conclusions and Further Work

Throughout this chapter the influence of the addition of DNA-peptide conjugate on the self-assembly of **ILVAGK** was explored. It was found that the self-assembly in **ILVAGK** was changed with addition of DNA-peptide conjugate and continued to change with increasing amounts of **DNA-ILVAGK**. **ILVAGK** (Fig. 3.6) showed a progressive change from dot-like structures at 7 days of aging, to network-like (14 days), large flakes (21 days), and finally back to dot-like structures which may suggest that dot-like structures were the most thermodynamically stable for **ILVAGK** without heating. **ILVAGK** when heated can form gelating aggregates, which can produce hydrogels which can be used to in the topical application and delivery of medicines.[131,142,143] With the addition of DNA-peptide conjugate, the formation of larger more ordered structures was generally observed; this was especially true for the 0.5 and 1 equivalent samples. At the lower ratios of DNA-peptide conjugate to peptide, the self-assembly seemed to initially speed-up with the formation of small flakes at 0 days of aging or disordered structures, unlike what was seen in **ILVAGK** at this point. The self-assembly visualised then seemed to slow down, leading into fractal-like self-assembly (Fig. 3.7, 21 and 28 days). This structure appeared to be an intermediate between small flakes and the formation of the network-like structure (Fig. 3.8, 7 and 14 days). Upon further increasing the proportion of DNA-peptide present, the emergence of fibre-like structures appeared. These then began to form more densely packed and interlinked networks, with areas of greater density, similar

to nodes where fibres come together and interlink. These fibrous networks then lead to much larger network-like structures than previously observed in the experiment. The formation of the very large self-assembly with a height of 1-6 nm across the surface (Fig. 3.10: 21 days) is suggestive that this self-assembly could be the final stage in the evolution of self-assemblies that have been observed throughout this experiment. To confirm this, longer experiments would be required to establish if these assemblies were thermodynamic products. Using heat to induce thermodynamically stable assemblies, was not an option in this experiment, as **ILVAGK** is known to gel with heating, especially in the presence of salt ions such as magnesium. The aim of this study was to explore the effect the addition of DNA-peptide conjugates had on the self-assembly of **ILVAGK**. The role DNA-peptide conjugates have on this system may be due to the size (DNA: 20 nucleotides, ILVAGK: 6 amino acids) and charge (DNA: - 20 and ILVAGK: + 1) of the DNA portion of the conjugates. The DNA portion likely interferes with the ability of **ILVAGK** monomers to come close to each other and interact; this would disrupt the general disordered kinetically trapped structures found in **ILVAGK** assembly from forming, promoting more thermodynamically stable structures, which is indicative of the size of the structures formed, increasing with the increasing concentration of **DNA-ILVAGK**. In the literature, the pre-assembly of the peptide or DNA portion of DNA-peptide based systems is generally chosen as the preferable method of analysing these systems, as it removes the external influence that one could have on the other.[124,125] This will generally give well defined individual structures, which are then combined, but miss out on the information which can be gained by studying them together, as has been done in this chapter.

To further explore the effect of DNA-peptide conjugates on the assembly of **ILVAGK**, the introduction of other external stimuli could have been employed if there were more time. Stimuli such as temperature, pH, and salt, as well as component concentrations could have been introduced. **ILVAGK** is temperature and salt sensitive, these would have been the first conditions to manipulate to explore their effects on the system discussed in this chapter. Temperature may increase the speed at which the system reaches a thermodynamic equilibrium, allowing the

observation of larger and more defined structures. Salt may well have had an additional effect, in this sense, as well as reducing the charge repulsion between DNA strands (Fig.3.12).

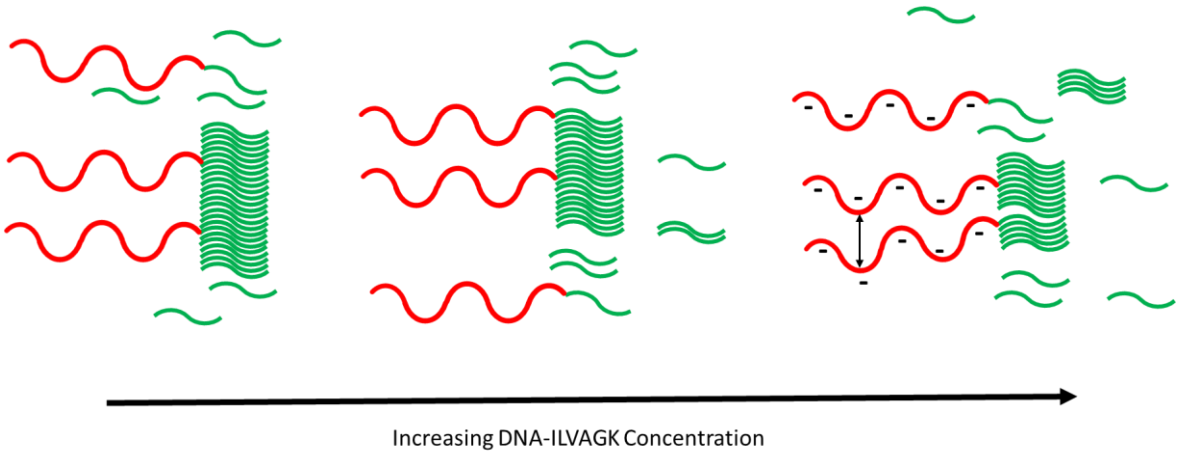

Figure 3.12: Cartoon depicting how an increase in DNA-**ILVAGK** concentration could affect the self-assembly of **ILVAGK** within this chapter.

The introduction of a DNA complement to the study may have reduced the DNA interference with the assembly of **ILVAGK**, by increasing its rigidity.[144] The pre-assembly of **ILVAGK** could have been studied with the addition of DNA-peptide conjugates of different concentrations, similarly, to as outlined in this chapter, allowing a better understanding of the stability of **ILVAGK** self-assembly, and whether it can be modified with DNA-peptide conjugates.

In conclusion, this chapter showed that the self-assembly of **ILVAGK** was disrupted by the addition of **DNA-ILVAGK**, and that by increasing the concentration of **DNA-ILVAGK** present in the sample, larger and more complex structures were obtained, similarly as seen when studying amyloid forming peptides and proteins.[145,146] To further investigate the role DNA plays within this system, Chapter 4 will discuss the addition of DNA directed self-assembly into the peptide directed system.

Chapter 4: Peptide and DNA Directed Self-assembly of DNA ILVAGK Conjugates

4.1: Introduction

In Chapter 3 the self-assembly of **ILVAGK** was explored as well as the effect that the addition of **DNA-ILVAGK** had on its assembly. It was discovered that the addition of **DNA-ILVAGK** did in fact alter the system and gave rise to large fractal-like assemblies as well as altering the timeline in which these assemblies occurred. In Chapter 4 this effect will be further explored by introducing DNA directed self-assembly through the addition of the DNA double helix. Double stranded DNA is more rigid than that of single stranded DNA.[135,144,147] This as well as the increase in charge density was predicted to give rise to different self-assemblies to those observed in Chapter 3.

Generally, when studying DNA-peptide conjugate self-assembly, either the DNA or the peptide portion of the conjugate is pre-assembled. An example of this is the work by Jin *et al.*, where they preassemble DNA-origami building blocks with peptide tails.[124] These blocks are then brought together by the introduction of complementary DNA-peptide conjugates.[124] Another example is the work by Daly *et al.*, where they pre-assembled their diphenylalanine fibres, and then brought them together via DNA hybridisation.[99] Daly *et al.*, also showed that the addition of DNA hybridisation to their system changed the assembly of their diphenylalanine fibres into bundles.[99] They were also able to demonstrate controlled helicity within their structures based on the amount of DNA hybridisation in the system.[99] In this chapter **A-ILVAGK** was hybridised with complementary DNA sequences of different lengths **A'** (single complement length), **2A'** (double complement length), and **3A'** (triple complement length). This meant that each double helix was decorated with either, 1, 2 or 3, peptides. The hybridised DNA-peptide conjugates were then left to assembly through the **ILVAGK** peptide over 28-days of aging, in the presence of tris magnesium acetate buffer (composition, section 7.1). This chapter explores the effect of DNA hybridisation on the self-assembly of DNA-peptide conjugates.

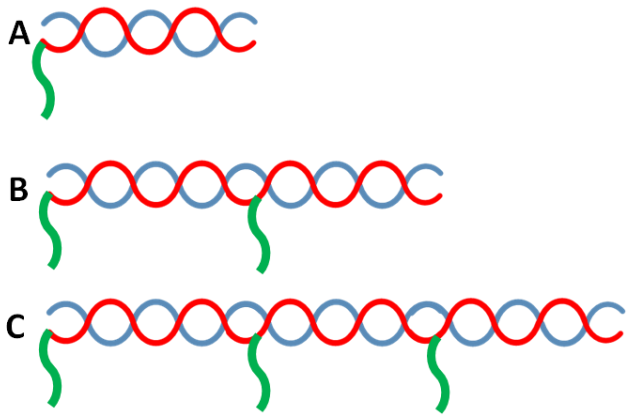

Figure 4.1: Cartoon figure depicting the single, double, and triple length complementary DNA-peptide structures in this chapter.

The arrangement of the peptide on the conjugate was determined on the surface by the pitch of the DNA helix, at 10.5 bases per 360 ˚ turn, this would result in all of the peptides being on the same side of the helix. It was thought that these units may crosslink or deform the peptide self-assemblies, giving rise to different structures. It was thought that the addition of double stranded DNA may give rise to hierarchical behaviour within this system because of the addition of a second type of self-assembly. Hierarchy is of special interest in the field of nanoscale control, as it most closely resembles the complexity that is found in biological systems,[97,148] as well as the generation of interesting properties which are not achieved by the individual parts.

4.2: Results and Discussion

A-ILVAGK was hybridised with complementary strands of **A'** (one), **2A'** (two) and **3A'** (three). Hybridisation was carried out in 1x TAMg buffer, using heat-cooling. **A-ILVAGK** was hybridised with 1 eqv **A'**, 0.5 eqv **2A'**, and 0.333 eqv **3A'**, the samples were then heated to 55 ˚C for 10 minutes, cooled to 35 ˚C for 20 minutes, and finally cooled to 4 ˚C. The melting temperature of **A** and **A'** (**2A'** and **3A',** as outlined by IDT) was 42 ˚C, so by taking the samples to 55 ˚C above the melting temperature it can be assured that the strands are fully separated. Cooling to 35 ˚C which is below the melting temperature promotes hybridisation as the strands cool, so the hydrogen bonds can form between complementary strands, by carrying this process out over 20 minutes it gives the

strands time to come together correctly. Cooling 4 ˚C stops any further changing of structure within the sample and helps to prevent DNA degredation. The control samples for DLS were discussed in Chapter 3, but further DLS samples were not carried out for **2A'** and **3A'** due to the fact they are extended forms of **A'**, and therefore there should be little relative difference between **A'**, **2A'** and **3A'**. In Figure 4.2 the DLS size distribution for **A-ILVAGK + A'** (a), **A-ILVAGK + 2A'** (b), and **A-ILVAGK + 3A'** (c) are shown. In general, there was an overall increase in hydrodynamic diameter for **A-ILVAGK + A'** and **A-ILVAGK + 2A'** over time, however this is not seen in **A-ILVAGK + 3A'**. Starting with **A-ILVAGK + A'** (Fig. 4.2a), at 0 days of aging two peaks are observed one smaller peak around 100 nm and a much larger peak around 900 nm. At 7 days of aging the apparent hydrodynamic diameter sat around the 5 nm mark, suggesting a change in the scattering particles, this may be due to a change in the structures formed, and a reduction in scattering intensity.

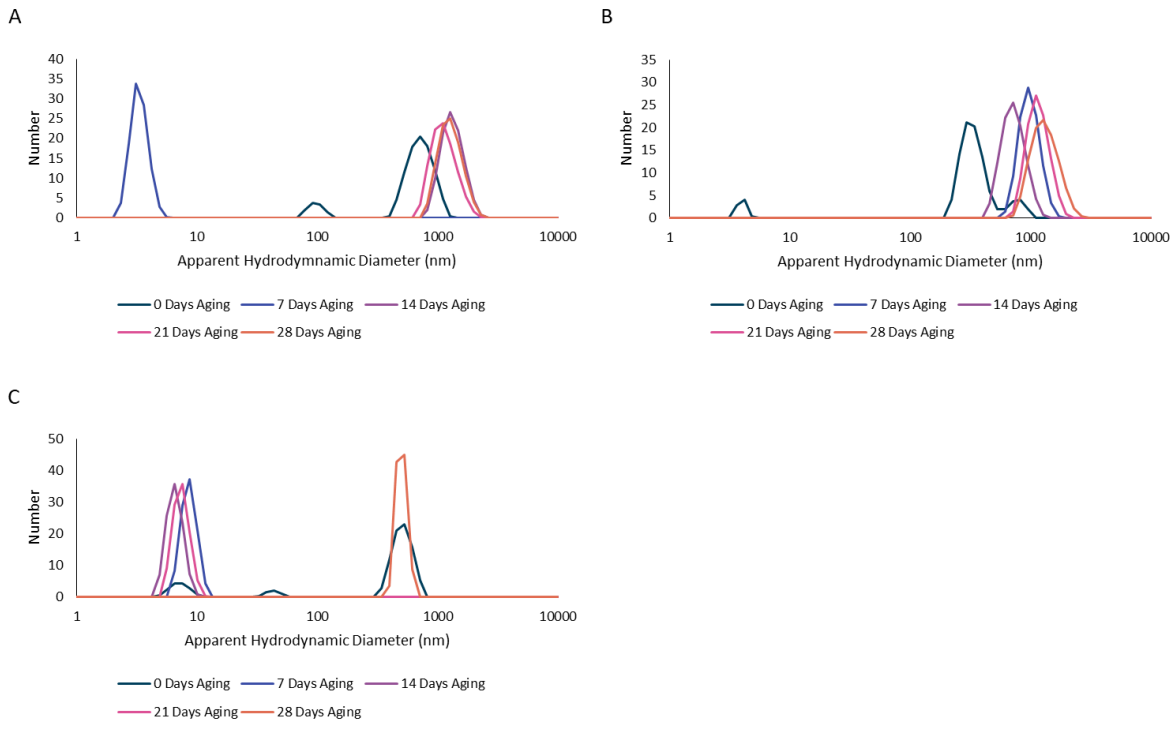

Figure 4.2: DLS graphs, A) **A-ILVAGK** hybridised with **A'** (1:1), B) **A-ILVAGK** hybridised with **2A'** (2:1), and C) **A-ILVAGK** hybridised with **3A'** (3:1). All samples measured in tris magnesium acetate buffer (pH 8.0), at 25 ˚C, with a final DNA/peptide concentration of 10 µM. Measurements taken at 0, 7, and 14,21, and 28 days of aging.

DLS relies on light scattered by particles in the solution reaching the detector, this scattering is affected by the size and type of structures within the solution. The diameter was observed to increase to around the 1000 nm for the remainder of the experiment, and stayed consistent in spectra height and shape, this may suggest similar particles being present in this sample at each of these time points. Figure 4.2b (**A-ILVAGK + 2A'**) 0 days, shows a multi-peak spectra - this was likely due to low scattering intensity, however the peaks sat around 6 nm, 400 nm, and 900 nm respectively from left to right. At all other time-points the peaks sat around the 1000 nm point, with a lower diameter of 900 nm, and an upper of 1100 nm. This could be interpreted as similar assembly structures being present in each sample, however further investigation was required. For **A-ILVAGK + 3A'** (Fig. 4.2c) at 0 days of aging, another multi-peak spectrum is observed, suggesting a low scattering intensity, the peaks for this had values of; 8 nm, 75 nm, and 800 nm respectively. At 7, 14 and 21 days of aging, the peaks were around 8 nm in their spectra. Again, it is possible that there are similar structures in the sample at each of these time-points, but confirmation was required by AFM, which will be discussed later in this chapter. At 28 days of aging, the hydrodynamic diameter increased to around 800 nm, suggesting a structural change in the sample. Due to the inability of DLS to give structural information on the self-assembly occurring, CD was used to investigate the type of self-assembly occurring.

Figure 4.3 Shows the CD spectrum obtained for, **A-ILVAGK + A'** (a), **A-ILVAGK + 2A'** (b), and **A-ILVAGK + 3A'** (c). From Figure 4.3, you can see an overall increase in signal as the length of the DNA double helix increases, this confirmed the successful hybridisation of **A-ILVAGK** with **A'**, **2A'**, and **3A'** with the addition of polyacrylamide gel electrophoresis (Fig. 4.5). Figure 4.3 a Shows the spectrum for the double helix with 1 decorated peptide, the maxima around 203 nm was indicative of the presence of the peptide, a stronger maximum and minimum of 2 and -2 mdeg at 275 and 220 nm respectively was seen when compared with the single stranded DNA in Chapter 3. The spectrum shape changed less across the time of measurement. Figure 4.3b and c show even greater definition of the spectra, with strong maxima and minima of 5, - 5 mdeg, 6, and – 6 mdeg for the

double helix of b and c respectively. This increase in spectrum signal, is due to the increase in length of the DNA double helix, which in turn increased the chirality of the system giving an increase in signal.

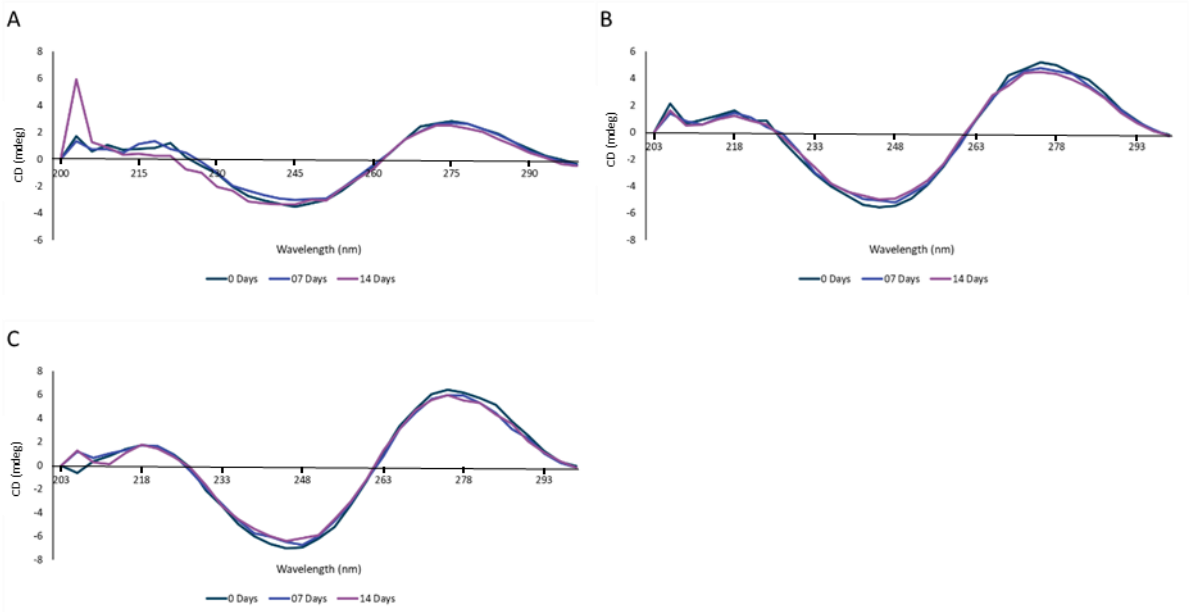

Figure 4.3: CD spectra of 0-14 days of aging, days 21 and 28 were missing due to Covid-19 isolation. A: **A-ILVAGK** hybridised with **A'** (1:1), B: **A-ILVAGK** hybridised with **2A'** (2:1), and C: **A-ILVAGK** hybridised with **3A'** (3:1). All samples measured in tris magnesium acetate buffer (pH 8.0), at 25 ˚C, with a final DNA/peptide concentration of 10 µM. Measurements taken at 0, 7, and 14 days of aging.

Both Figure 4.3 b and c also show the peak maxima around 203 nm for the peptide portion, with little change over the aging period. All samples in Figure 4.3 showed little change over the full aging period. This lack of change would suggest the DNA double helix was stable throughout the aging process. To further support the analysis above, **A + A'**, **2A'**, and **3A'** were analysed by CD as controls, Figure 4.4 shows the CD spectra for **A + A'** (a), **2A'** (single stranded) (b), and **3A'** (single stranded) (c). From Figure 4.4a the shape and signal of the spectrum collected changed little over the time-period, with the classic synodal shape, and maxima around 275 nm and minima around 220 nm. However, Figure 4.4b and c showed a slightly lower signal of around 3, and -3 mdeg for both samples despite their increase in length, this is due to these samples being single stranded without rigid structure, when compared with the single length DNA double helix in Figure 4.4a, and Figure 4.3.

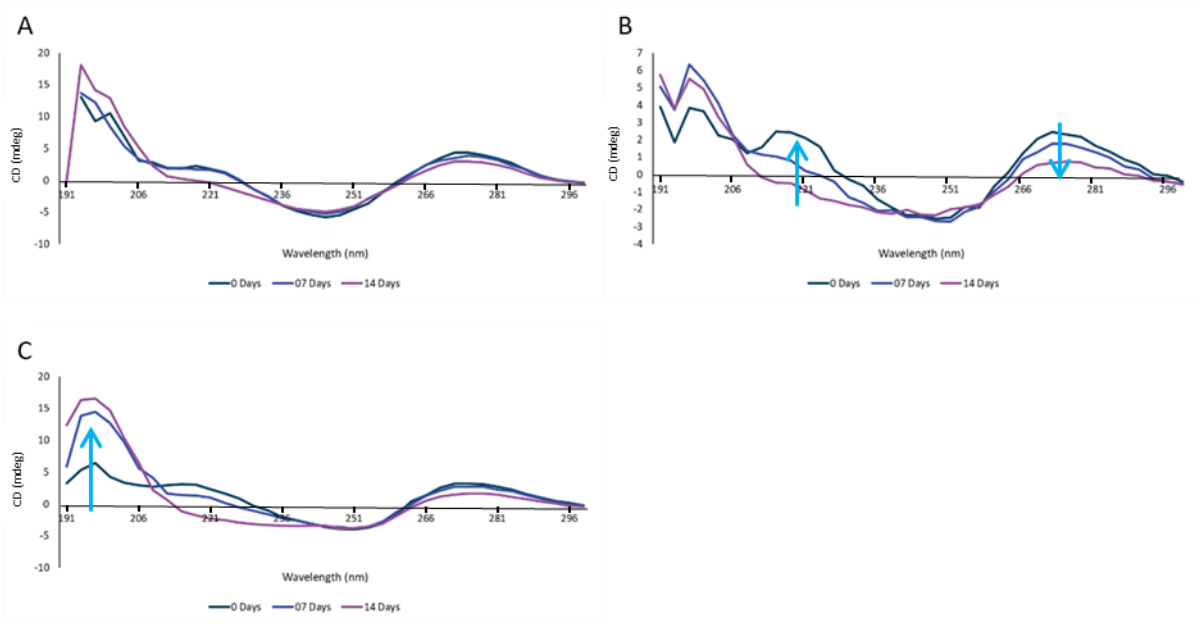

Figure 4.4: CD spectra of 0-14 days of aging, days 21 and 28 were missing due to Covid-19 related isolation. A: **A** hybridised with **A'** (1:1), B: **2A'**, and C: **3A'**. All samples measured in tris magnesium acetate buffer (pH 8.0), at 25 ˚C, with a final DNA/peptide concentration of 10 µM. Measurements taken at 0, 7, and 14 days of aging. Blue arrows highlight direction of movement in the spectra over 28-days of aging.

The formation of the double helix was also confirmed by polyacrylamide gel electrophoresis. A native PAGE of 8 % was used to analyse the successful hybridisation. An 8 % gel was selected due to the irregular shape of the DNA-peptide DNA double helices, it was thought that the peptide sections may self-assemble and prevent even migration of each sample, especially as the length of each samples DNA helix increased. However, with the presence of heat-cooling to achieve hybridisation, it would be possible that self-assembly would accelerate and structures with high negative charge or compact structure may migrate quicker than the DNA ladder reference. Lane 1 in Figure 4.5 shows **A,** the single stranded DNA control in this experiment. According to the DNA ladder, its relative length is 15 bp, which for the single stranded version without the poly-T spacer and amine linker was correct, the single stranded DNA with these additions, sat around 20 bp. Lane 2 shows the control **A-ILVAGK**, with an increased mass due to the addition of the peptide, it was believed the extra bands were due to self-assembly of the peptide portion of the DNA-peptide conjugate. Lanes 5 and 6 show the **2A'**, and **3A'** single stranded sequences, as reference for the hybridisation of these strands. Lanes, 4, 6, and 8 shows the hybridised samples; **A-ILVAGK + A'**, **A-ILVAGK + 2A'**, and **A-ILVAGK + 3A'**, respectively. When compared to their controls, a band of higher

molecular weight was seen, bands with a higher molecular weight generally move slower during electrophoresis, due to their size and mass to charge ratio. The smearing seen in lanes 6 and 7 was indicative of several different sized structures migrating through the gel, this would suggest the formation of new structures outside of the single hybridised structures. Given the presence of these new bands and the CD data, it was confirmed the successful hybridisation of the DNA double helix in these samples.

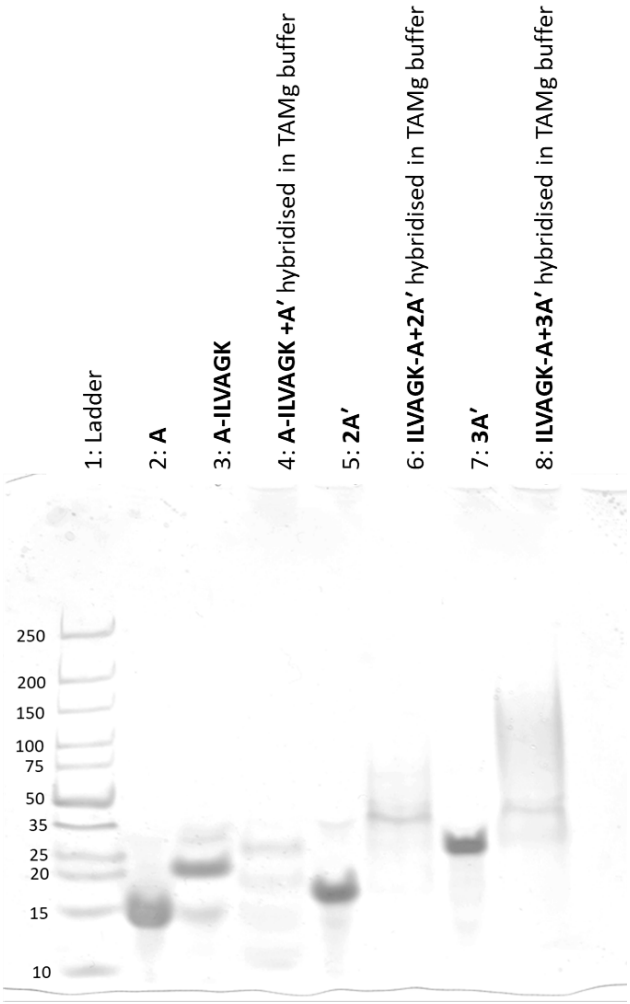

Figure 4.5: 8 % native polyacrylamide gel in TAMg buffer, stained in stains-all gel stain. 1: Ultra-low range DNA Ladder, 2: **A**, 3: **A-ILVAGK**, 4: **A-ILVAGK + A'**, 5: **2A'**, 6: **A-ILVAGK + 2A'**, 7: **3A'**, and 8: **A-ILVAGK + 3A'**.

To explore the types of structures formed through DNA and peptide directed self-assembly, the samples were deposited onto mica, and AFM carried out. Figure 4.6 Shows the AFM images collected for **A-ILVAGK + A'**, over the 28-day aging period. At 0 days of aging, fractal-like structures

were observed, with varying size and a height of 2.5 - 5 nm. At 7 days of aging these structures became larger and more frequent across the surface, with a height of 4.5 ± 3.5 nm.

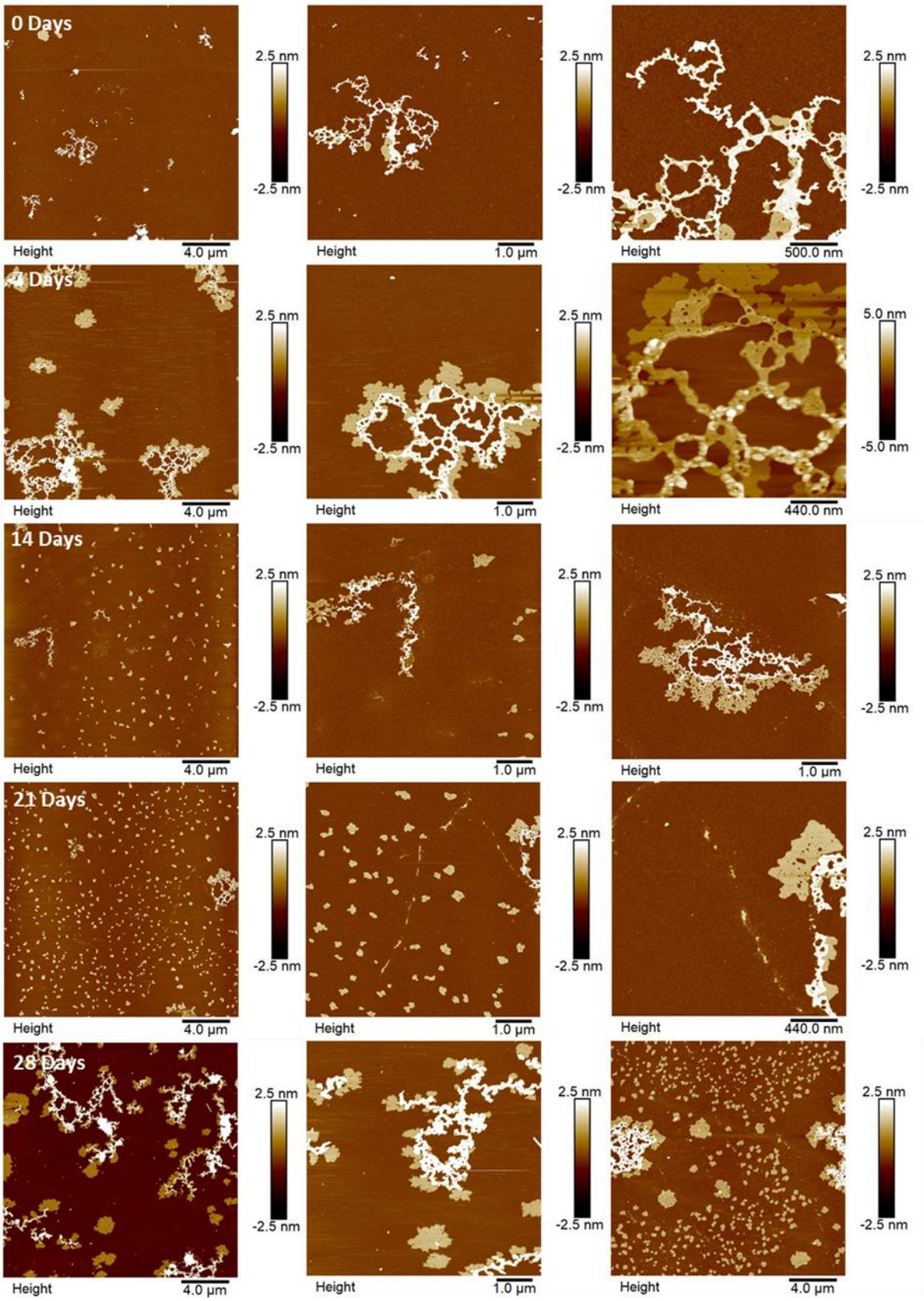

Figure 4.6: AFM images of **A-ILVAGK** hybridised with **A'** (1:1) in TAMg buffer over 28 days of aging, images from left to right show increased magnification of the same area.

The appearance of fractal-like structures was not observed at such an early stage in the peptide driven assembly (Chapter 3) (Fig. 3.7 21 days and Fig. 3.8 14 days), they were also only observed in the low 0.01 and 0.1 equivalents doping samples not the 1:1 eqv sample, suggesting that the addition of the DNA double helix may be shifting the timeline of assembly again, like that seen in Chapter 3. At 14 days of aging the self-assembly tended towards small flakes with the appearance of fewer fractal-like structures, suggesting that they were breaking down into smaller structures. These flakes had a height and diameter of 2.9 ± 5.6 nm and 306 ± 75 nm respectively. At 21 days of aging, more small flakes were observed with the presence of a few fractal-like structures. These flakes had a height of 1.9 ± 0.4 nm, and a diameter of 379.3 ± 113.4 nm, showing an increase in diameter and reduction in height when compared to 14 days of aging suggesting that these flakes were changing with aging. At 28 days a mixture of self-assemblies could be observed, small flakes (H: 2.0 ± 1.5 nm, D: 353.9 ± 154.0 nm), large flakes (H: 2.7 ± 1.1 nm , D: 810.3 ± 176.2 nm), and fractal-like structures (H: 20.8 ± 13.7 nm), this would suggest that several different stages of self-assembly within the timeline was being observed. This change in self-assembly which is similar in appearance to **ILVAGK** was due to the rigidity of the DNA double helix, that by forming this double helix, the DNA interference was minimised between **ILVAGK** monomers. However, the growth and change from fractal-like, to flakes and fractal-like structures, may also suggest that the addition of the DNA double helix also tends towards smaller flakes as the most stable form of assembly, this may be due to the negative charge density of the DNA portion of the monomers.

By doubling the length of the monomer unit and increasing the number of peptides that decorate the DNA helix to two, the complexity of this system increased, giving rise to a change in the assemblies observed. Figure 4.7 shows the images collected for **A-ILVAGK + 2A'** over the 28 days of aging. At 0 days of aging, small flakes could be observed in one area, these flakes had a height of 4.3 ± 4.7 nm and a diameter of 226.9 ± 4.8 nm, however in others, dot-like structures could be

observed near to a very large fractal-like structure. The height and diameter of these dot-like structures were 3.9 ± 1.0 nm and 219.6 ± 76.5 nm respectively. The dot-like structures could be aggregates, due to their consistency across the surface it was not likely to be a drying artifact. At 7 days of aging, large flakes were observed with a height of 2.6 ± 1.6 nm and a diameter of 65.0 ±74.2 nm, this was not surprising given that small flakes were observed at 7 days alongside the dot-like structures. These structures evolved into network-like structures at 14 days of aging, with a height of 1.5-3 nm. At 21 days of aging, the network-like structures breakdown into fractal-like structures, with a height between 0.5-1.5 nm at the edges and 2.5-4 nm at the centre. These structures further devolve into large flakes at 28 days of aging with a height of 10.7 ± 3.9 nm and diameter of 2.5 ± 2.2 nm. Like seen in Figure 4.6, an evolution of similar self-assembly structures was observed at multiple stages during the aging process, supporting the importance of dynamism in DNA-peptide self-assembly. It is challenging to compare this work directly with any other in the literature due to the type of peptide and the system used to assess their self-assembly. However, there are some papers which show the evolution of complex systems which move towards hierarchy and emergence. A good example of this is the work by Kye *et al*., where they achieve the synthesis of a deoxyribonucleoprotein, using DNA-β-sheet conjugates.[98] Kye *et al*. synthesised their DNA-β-sheet conjugates through solid phase fragment condensation, to overcome the difficulties of combining two biological materials which are synthesised with different chemistries. Once the conjugate was obtained, DNA-hybridisation was carried out followed by peptide assembly. By using a β-sheet forming peptide fragment, instead a β-turn peptide like **ILVAGK**, the type of assembly possible is limited to β-sheets. However, ILVAGK can show different types of assembly, including α-helices, and β-turns, which means directing control over the self-assembly is more difficult.[129] External stimuli is required to help the self-assembly move forward, such as temperature, and ions contained within the buffer used, like the methods used within this thesis.[98,114,149,150]

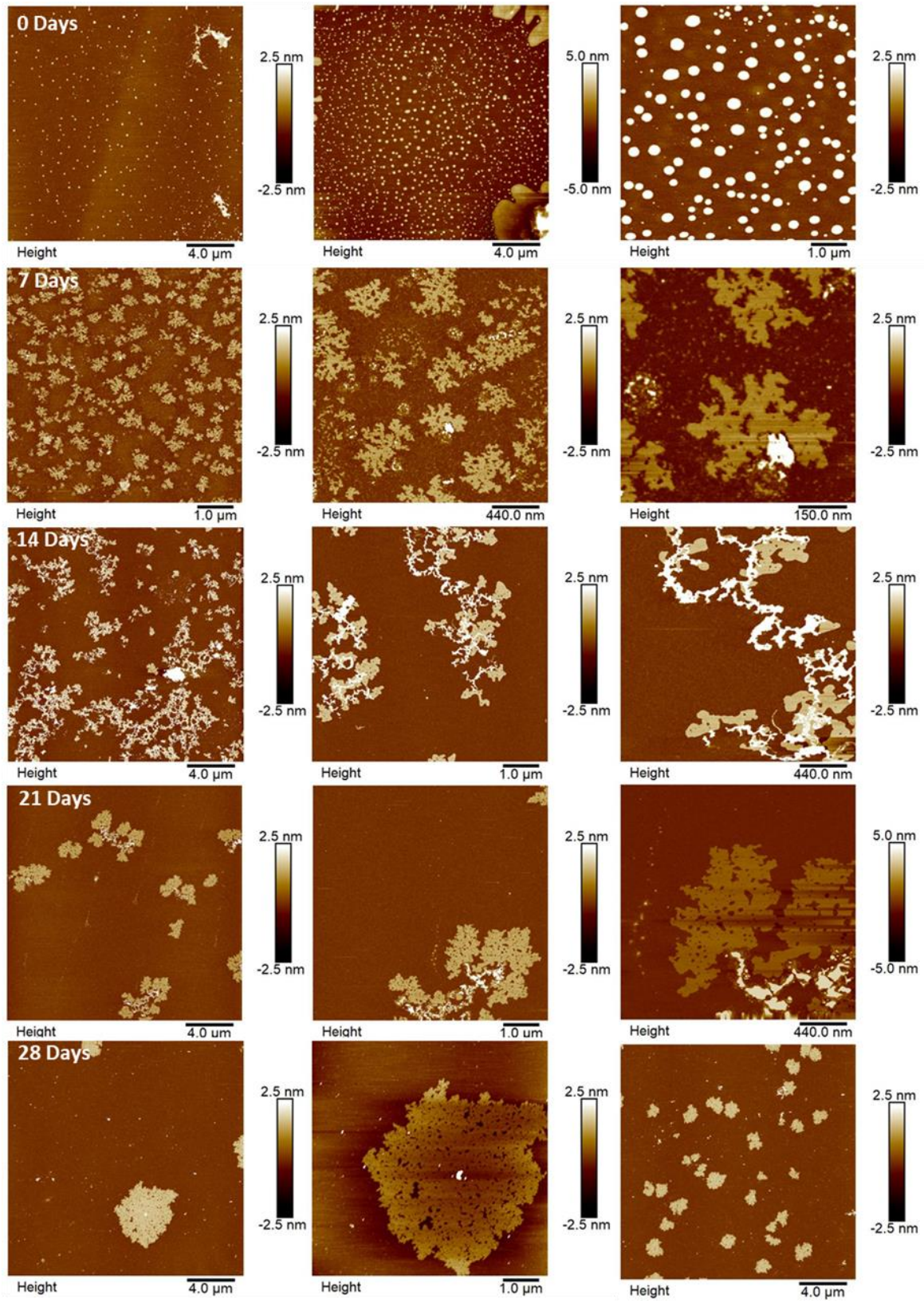

Figure 4.7: AFM images of **A-ILVAGK** hybridised with **2A'** (2:1) in TAMg buffer over 28 days of aging, images from left to right show increased magnification of the same area.

The difference in observed structures between Figure 4.6 and 4.7 may be due to the increased potential of crosslinking due to the second peptide residue, this may also be the reason for the appearance of larger overall structures.

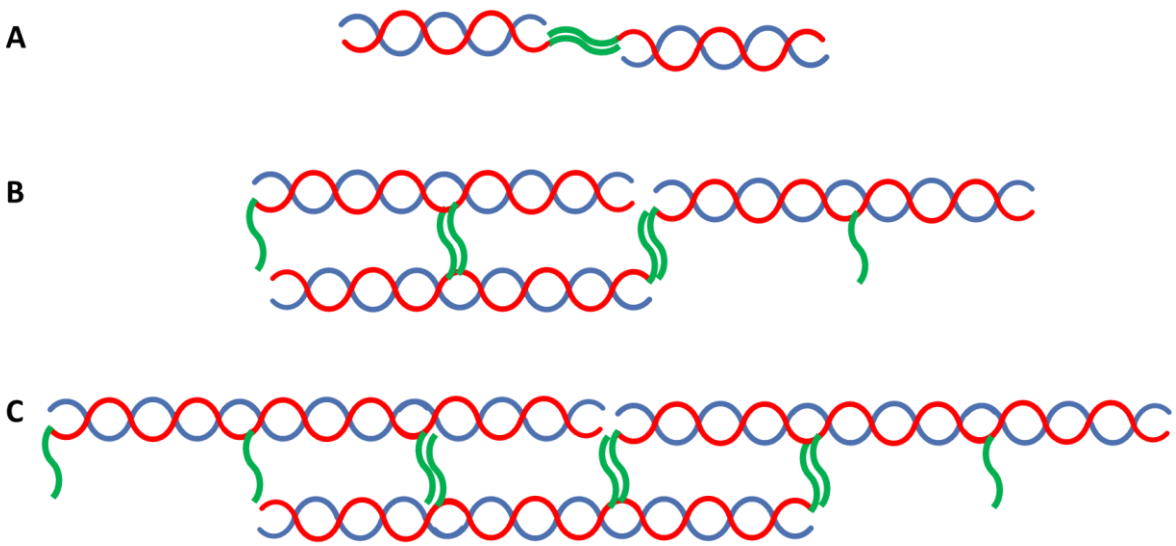

Figure 4.8: Cartoon illustrating the proposed increase in crosslinking between hybridised DNA-peptide conjugates as a function on length. A: one peptide on the double helix, B: two peptides on the double helix, and C: three peptides on the double helix.

The assembly observed in **A-ILVAGK + 3A'** at 0 days of aging, was not yet observed in either Chapter 3 or this chapter. The emergence of fibre-like structures which densely covered the surface were observed, with a height of between 0.5 and 1 nm. Unlike the previous samples, **A-ILVAGK + A'** and **A-ILVAGK + 2A'**, a devolution into smaller dot-like structures was noted at 7 days of aging, with a height of 6.4 ± 3.6 nm. These dot-like structures were stable and seen at 14 days of aging with a height of between 3-4 nm. However, in contrast, at 21 days of aging the emergence of small flakes, and fractal-like structures were found. The flakes had a height and diameter of 1.7 ± 0.4 nm and 284.5 ± 52.0 nm respectively, the fractal-like structures had a height of between 1 and 2.5 nm. At 28 days of aging a large flake (H: 1.8 ± 0.1 nm) was seen in the left-hand image, as well as the appearance of what appeared to be bundled aggregates of fibre-like structures (H: 5.5 ± 7.6 nm), supported by the middle image. However, the right-hand image showed a densely coated surface

with dot-like structures interlinked with fibre-like structures (H: 2.3 ± 2.3 nm). It would not be impossible to suggest that these structures were all along the same trajectory of self-assembly. The structures observed at 21 days of aging in Figure 4.9 were not unlike those observed in Figure 4.6 at the same time point. The only difference between these two samples being the addition of two phosphodiester linkages. It is possible self-assemblies that could accommodate this addition would have similar structures, although the routes at which these similarities occurred were different as well as the final path they were heading towards fibre-like (Fig. 4.9 28 days) or fractal-like (Fig. 4.6 28 days). The change in self-assembly over the 28-days of aging is indicative of a dynamic system highlighting the importance of this in DNA-peptide self-assembly. For comparison Stephanopoulos *et al*. showed the importance of DNA structural morphology and peptide expression on the surface of these DNA-peptide conjugates.[104] The structural morphology had an increased effect on the neural differentiation of the conjugates.[104] To validate the independence of the self-assembly motifs explored in this chapter **A** and **ILVAGK** were heat-cooled together, without hybridisation or a biorthogonal conjugation. To explore whether the structures observed throughout this chapter were truly through two independent forms of self-assembly, and not the peptide and DNA directly interacting with each other.

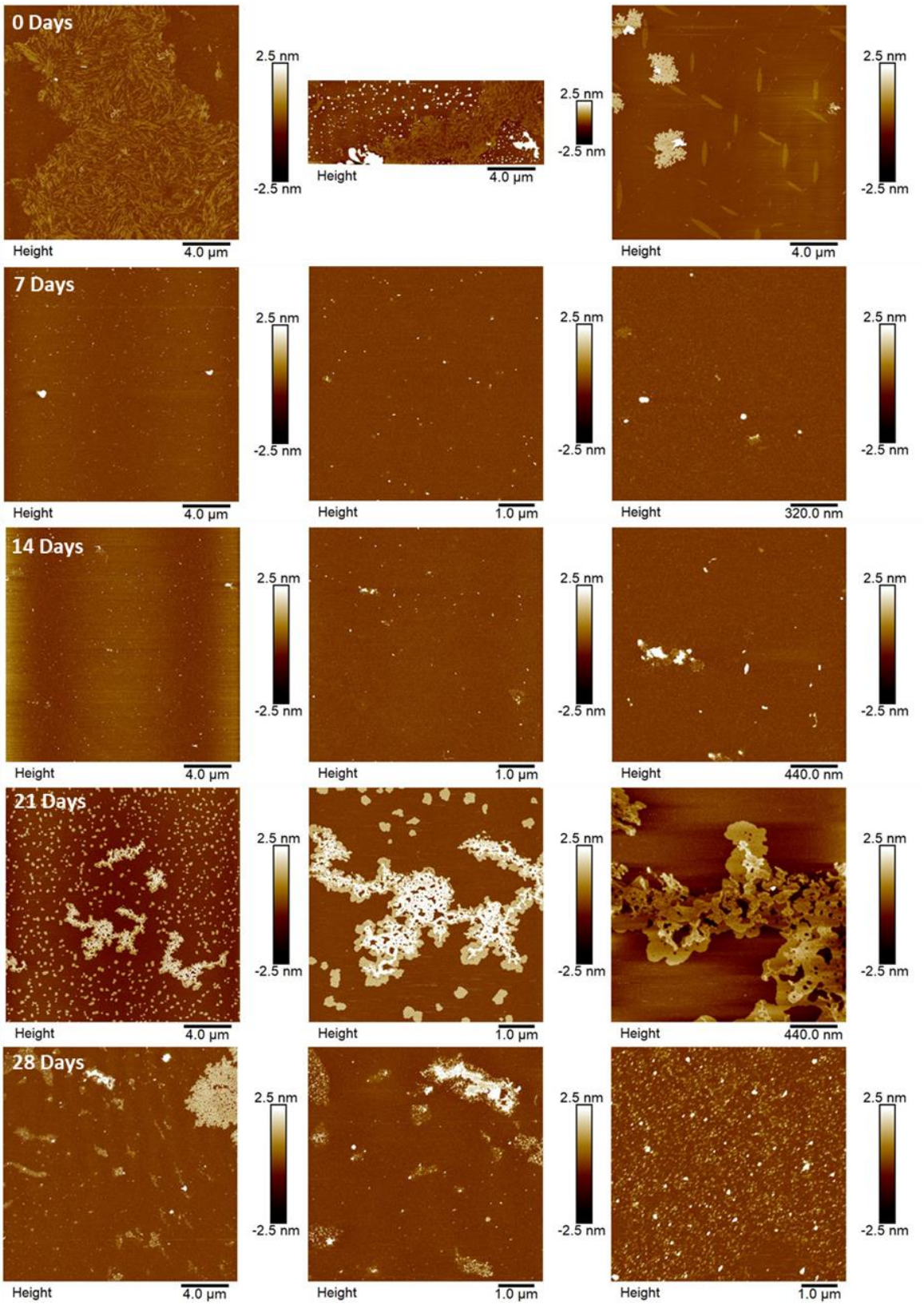

Figure 4.9: AFM images of **A-ILVAGK** hybridised with **3A'** (3:1) in tris magnesium acetate buffer over 28 days of aging, images from left to right show increased magnification of the same area.

Figure 4.10 shows the AFM images collected for **A + ILVAGK** over the 28-day aging period. At 0 days of aging network-like (H: 3.6 ± 0.2 nm) and fractal-like structures (H: 6.9 ± 6.6 nm) were observed,

however at 7 days of aging the appearance of small flakes was seen, with a height of 1.7 ± 0.1 nm and a diameter of 41.5 ± 10.0 nm. Long fibres were also observed with a height of 6.4 ± 2.6 nm.

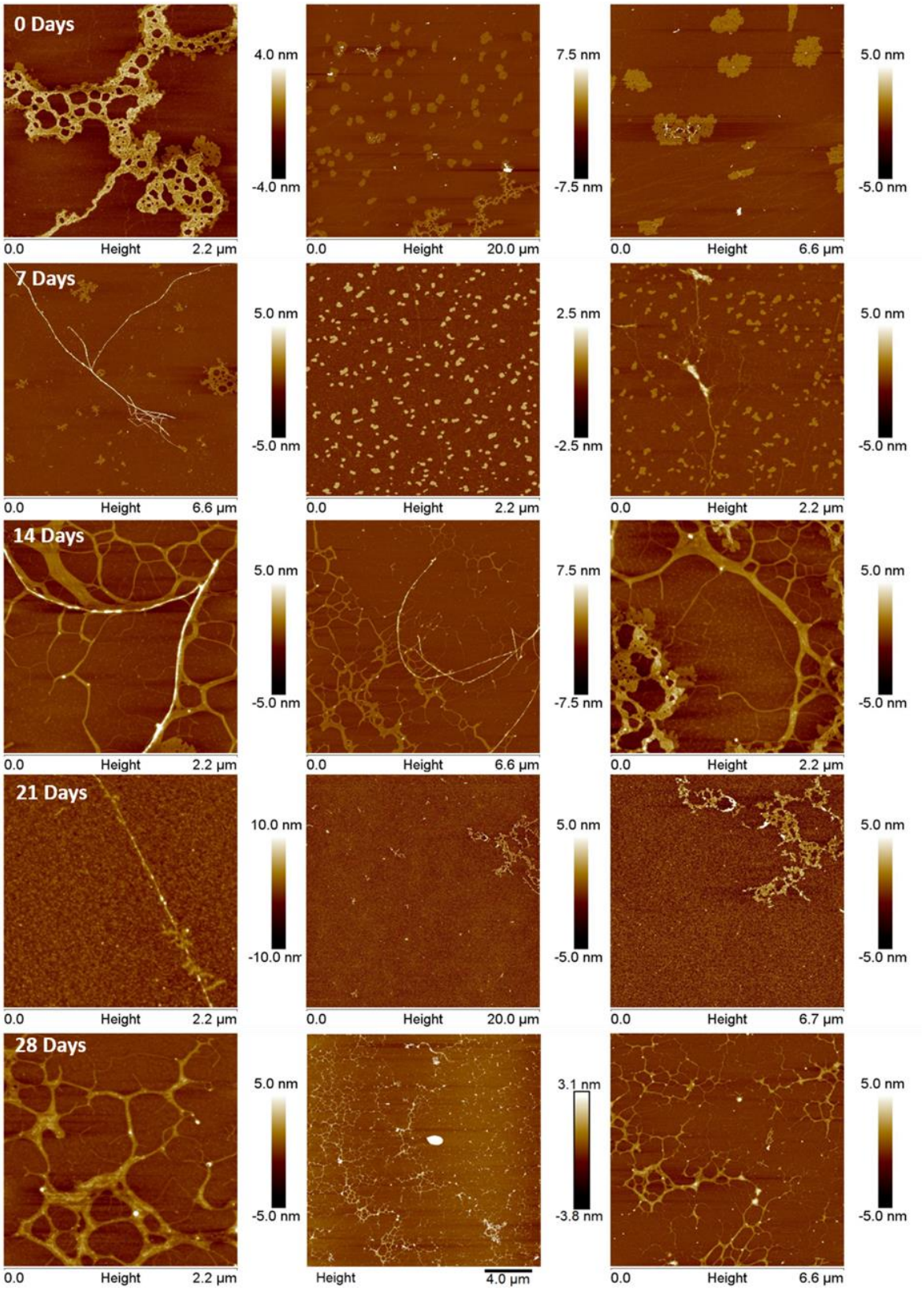

Figure 4.10: AFM images of **A** and **ILVAGK** (1:1) in TAMg buffer over 28 days of aging after thermocycling.

These long fibres were further observed at 14 (H: 2.4 ± 0.9 nm), 21 (H: 7.3 ± 2.5 nm), and 28 days (H: 3.2 ± 1.5 nm) of aging. These long fibres are suggestive of the parent peptide assembly and not unlike those seen in the doping studies in Chapter 3, the small flakes were also indicative of the DNA on its own, as seen in Chapter 3. This would suggest that the DNA and peptide assemble independently of each other and supports the validity of the results discussed within this chapter.

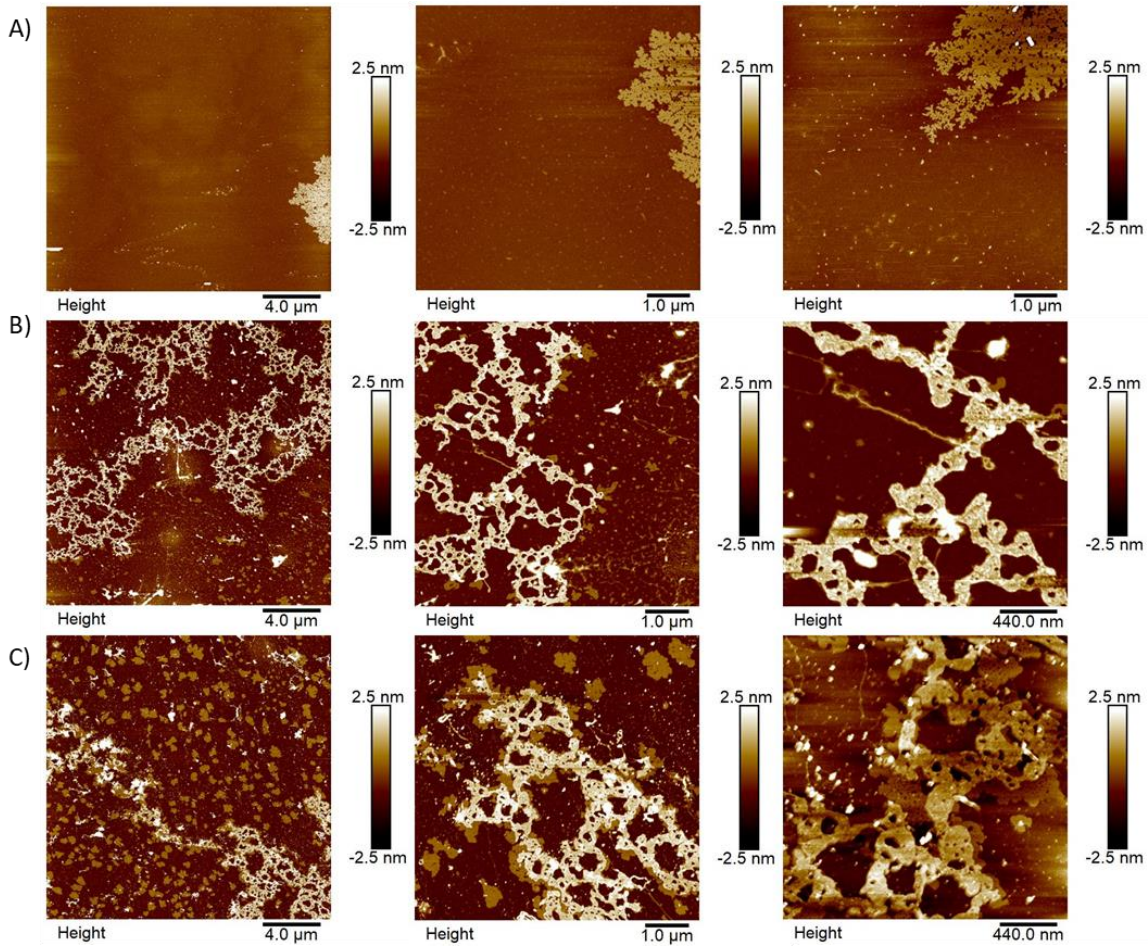

Figure 4.11: AFM images of A: **A+A'** hybridised, B: **2A'**, and C: **3A'** in tris magnesium acetate buffer over 28 days of aging.

Figure 4.11 shows the AFM images collected for **A + A'** hybridised, **2A'** and **3A'** due to the lack of peptide in these samples they were not analysed over 28 days of aging, because the assembly observed was not expected to change. Large flakes (H: 1.6 ± 0.1 nm) were observed for the **A+A'** sample (Fig. 4.11 a), the lack of large flakes seen in **A-ILVAGK + A'**, suggested that the self-assembly observed was the product of the peptide and DNA driven self-assembly. For **2A'** network-like (H: 5.1 ± 2.5 nm) structures were observed (Fig. 4.11 b), these again differed to the structures

observed in **A-ILVAGK + 2A'**, further suggesting that the assembly seen was due to both the peptide and DNA driven assembly. These network-like structures (H: 5.7 ± 3.4 nm) were also observed for **3A'** with the presence of some small flakes (H: 5.0 ± 4.2 nm, D: 462.9 ± 205.4 nm), this is unsurprising given the difference between **2A'** and **3A'** is a single phosphodiester linkage. However, this structure was observed at 21 days of aging for **A-ILVAGK + 3A'**, this may suggest that at this time-point the DNA driven self-assembly was more prominent, possibly due to interference due to the positioning of the third peptide on the double helix. However, the overall difference in the structures observed in the **A'**, **2A'**, and **3A'** hybridised samples, versus their controls would suggest the presence of emergence and hierarchical assembly within this system.

4.3: Conclusions

In this chapter the addition of DNA driven self-assembly as well as peptide driven assembly was investigated over 28 days of aging. This gave rise to a different timeline of structure formation over that observed in Chapter 3 with the doped parent peptide. The hybridisation of the samples examined in this chapter was confirmed by CD spectroscopy and PAGE. The CD showed an increase in signal which was due to an increase in chirality of each sample as the length of the DNA double helix increased (Fig. 4.3). The shape of the spectrum improved when compared to the single stranded controls, **2A'**, **3A'** (Fig. 4.4). The polyacrylamide gel showed the increase in mass, due to hybridisation when compared to the single stranded controls, as well as alluding to self-assembly occurring due to the smearing seen at higher molecular weights (Fig. 4.5). The DLS tended more towards larger diameters over the aging period for **A-ILVAGK + A'** and **A-ILVAGK + 2A'** but not for **A-ILVAGK + 3A'**. The DLS showed a higher hydrodynamic diameter at 0 and 28 days of aging of around 800 nm mark, and 8 nm for 7, 14, and 21 days of aging. This is the reverse to what was observed in the AFM, a change from small well-defined structures at 0 days of aging to larger structures at 21 days, with a return to smaller structures at 28 days. Although the DLS and AFM disagreed, it is known that DLS is a technique developed for the analysis of predominantly spherical

particles in solution, whereas AFM looks at collapsed dried samples, which may account for the difference in interpretation between the data sets. When the density of the small structures observed at 0 and 28 days of aging are considered, it was possible that these particles were forming aggregates in solution during the DLS, giving an inaccurate reading. It was seen at 0 days of aging **A-ILVAGK + A'** (Fig. 4.6) the formation of fractal-like structures (H: 2.5 - 5 nm) which were not previously seen until 14 days of aging in chapter 3, and only occurred in the low DNA concentration samples. However, as the aging progressed these fractal-like structures increased in size at 7 days of aging, before breaking down primarily into small flakes at 14 (H: 2.9 ± 5.6 nm, D: 306 ± 75 nm) and 21 (H: 1.9 ± 0.4 nm, D: 379.3 ± 113.4 nm) days of aging. At 28 days these small flakes came back together to form fractal-like structures (H:) again, this change in self-assembly between two main types may be due in large to the presence of the rigid DNA double helix.[144] This rigidity, causing the DNA to move less during self-assembly allowing the peptides to come closer together unlike in Chapter 3. By increasing the length of the DNA double helix, and adding an extra peptide, it was possible that the self-assembly may change, the diversity of structures observed did increase. At 0 days of aging (Fig. 4.7), small flakes with a height of 4.3 ± 4.7 nm and diameter of 226.9 ± 4.8 nm, were observed as well as dot-like structures (H: 3.9 ± 1.0 nm, D: 219.6 ± 76.5 nm). At 7 days of aging the surface was covered in small flakes (H: 2.6 ± 1.6 nm, D: 65.0 ±74.2 nm), which evolved into network-like structures (H: 1.5-3 nm) at 14 days of aging. The network-like structures then changed into fractal-like structures (H: 0.5-1.5 nm at the edges and 2.5-4 nm at the centre) at 21 days of aging before evolving into very large flakes (H: 10.7 ± 3.9 nm, D: 2.5 ± 2.2 nm) at 28 days. This change observed in **A-ILVAGK + 2A'**, is further proof of the importance of dynamism within DNA-peptide self-assembly and mechanisms at which different structures are formed.[31] It is possible that the inclusion of a second peptide link on the DNA double helix increased crosslinking across the self-assemblies, leading to the formation of larger structures when compared with **A-ILVAGK + A'**. **A-ILVAGK + 3A'** at 0 days of aging saw the appearance of well-defined fibre-like structures (H: 0.5-1 nm), which densely covered the mica surface. However, unlike the **A'** and **2A'** samples, at 7 days

of aging these structures broke down into small dot-like structures (H: 6.4 ± 3.6 nm), which remained stable and were observed at 14 days of aging (H: 3-4 nm). At 21 days of aging, the appearance of small flakes (H: 1.7 ± 0.4 nm, D: 284.5 ± 52.0 nm) and fractal-like structures (H: 1-2.5 nm) were observed. At 28 days of aging a mixture of, large flakes (H: 1.8 ± 0.1 nm), bundled fibres (H: 5.5 ± 7.6 nm), and dot-like structures were observed. These structures were all observed at earlier stages of aging for **A-ILVAGK + 3A'**, it is possible that the different structures present are structures at different stages of their self-assembly. The similarity of structures observed in the **A'** and **3A'** samples at 21 days of aging was not unsurprising, given the only chemical difference between the two samples was the addition of two phosphodiester linkages. The generally smaller structures observed in **A-ILVAGK + 3A'**, may be due to the addition of the third peptide, increasing the ability for the peptide portion to form more well-defined structures. The independence of the self-assembly observed in this chapter was assessed by analysing the self-assembly seen when **A** and **ILVAGK** were mixed and heated without the addition of biorthogonal conjugation. It was seen that the structures tended towards fibre-like structures for the peptide, and small flakes for the DNA, like the controls analysed in Chapter 3. It was also seen, that in general the hybridised **A'**, **2A'**, and **3A'** samples were different to their individual self-assembly as highlighted within in the control samples. This behaviour is indicative of the presence of hierarchical self-assembly and possible emergence within this system.[97,99,151]

Further work into understanding the self-assembly of this system could be achieved through further experiments. Strand switching experiments could give more information on the effect of DNA hybridisation on the ILVAGK self-assembly. Extending the length of the DNA complement to the DNA-peptide conjugate, could increase the size of the assemblies observed. Which may lead to more complex, better-defined structures. If the structure is well-defined, it is easier to consider their wider applications, in fields such as medicine, and nanotechnology. This could also be achieved by adding further stimuli into the system, like temperature. By annealing the hybridised DNA-peptide conjugate structures, **ILVAGK** self-assembly would be promoted. Ageing these structures

over 28-days was a time consuming and sensitive process, especially due to the world climate at the time. This meant there were several occasions when experiments, were missed due to factors outside of my control. Designing experiments at their proposed equilibrium would allow them to be studied in a shorter amount of time, reducing the risk of external factors. The best piece of advice I can give is to own your own measurement cells, so that you can clean them and ensure their suitability for your experiments. Contamination of measurement equipment can cause damage to your experiments, and in the worst case, cause them to have to be abandoned and restarted. The same can be said for having all instrument methods in a separate fil, to prevent them being modified or overwritten by another user, this is especially important on shared analytical equipment.

To further explore the presence of hierarchy and emergence, the peptide self-assembly was 'switched off' with sodium dodecyl sulphate solution, and then self-assembled over 28-days of aging. The results of which will be discussed in Chapter 5.

Chapter 5: DNA Directed Self-assembly of DNA-ILVAGK Conjugates, Leading to Orthogonal Self-assembly.

5.1: Introduction

Orthogonality within non-natural systems, is of keen interest to the chemical community, due to the ability to more closely mimic and interact with biology.[73,152] If the assembly observed in Chapter 4 was a product of orthogonality, then this would open numerable avenues of nanoscale controllability and complexity, previously only seen in biological systems.[22,153] In Chapter 4 the roles of peptide and DNA directed self-assembly were explored in **DNA-ILVAGK** conjugates. In this chapter the peptide directed assembly was stopped by the addition of a denaturant. If there was orthogonality present within this system, the assemblies seen previously should not change over the time-period.

5.2: Results and Discussion

To maintain the DNA double helix hybridisation, but switch off the peptide assembly, a new buffer system was selected. A solution of 1 % sodium dodecyl sulphate (SDS) was chosen; SDS is a known denaturant and surfactant used in biology to breakdown folded proteins, whereas TAMg is a buffer which does not contain a denaturant, and should not break down peptide self-assembly.[154,155] SDS also contains free sodium ions, these ions are sufficient in a 1 % solution to overcome the charge repulsion of the DNA backbone to form the DNA double helix.[154,156] Figure 5.1a shows the CD spectra of hybridised single DNA double helix in both TAMg and 1 % SDS buffer at 7 days of aging. The shape of both spectra is very similar, supporting the formation of the double helix with a maximum of around 275 nm and a minimum of around 245 nm. Figure 5.1b shows the spectra of **ILVAGK** in TAMg and 1 % SDS buffer at 7 days of aging. In TAMg buffer the spectrum showed that **ILVAGK** was in the β-turn formation, with a maximum around 198 nm. However, in 1 % SDS **ILVAGK** exhibits the random coil formation, indicated by the minimum around 200 nm. The similarity

between the spectra suggest the formation of the double helix, whereas the dissimilarity between the spectra for **ILVAGK**, would suggest that the 1 % SDS is sufficient in preventing further self-assembly of **ILVAGK**. These spectra remained stable over the full 28-days of aging (Fig. 5.4 and 5.5).

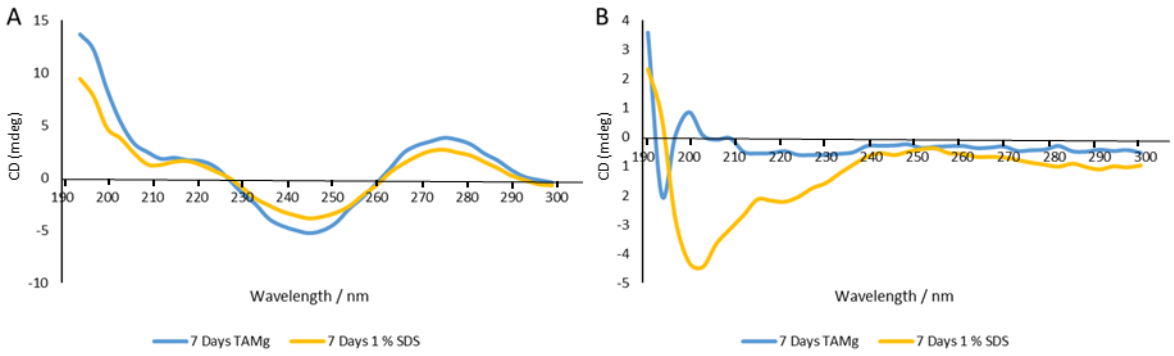

Figure 5.1: CD spectra for A) **A + A'** and B: **ILVAGK**. In tris magnesium acetate buffer and in 1 % sodium dodecyl sulfate buffer. All samples measured at 25 ˚C, with a final DNA/peptide concentration of 10 µM.

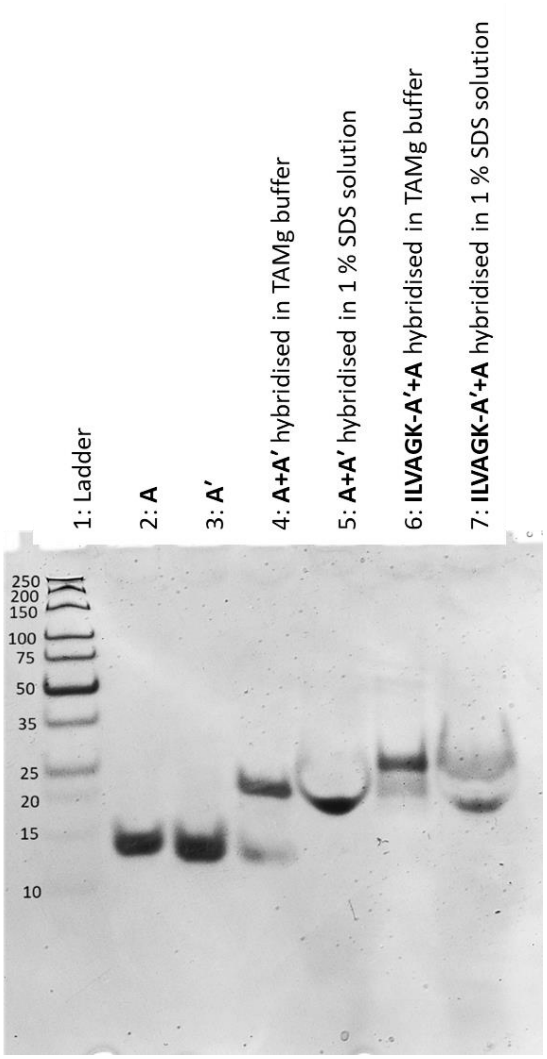

Figure 5.2: 12 % native PAGE (TAMg buffer). 1: Ladder, 2: **A,** 3: **A',** 4: **A+A'** hybridised in TAMg, 5: **A+A'** hybridised in 1 % SDS, 6: **A'-ILVAGK+A** hybridised in TAMg, 7: **A'-ILVAGK+A** hybridised in 1% SDS.

The successful hybridisation of the double helix was also confirmed by gel electrophoresis (Fig. 5.2). Lanes 2 and 3 were the single stranded DNA **A** and **A'**, with lane 4 being the **A + A'** hybridised TAMg, and lane 5 the **A + A'** hybridised in 1 % SDS. There is an increase in mass for lane 4 and 5 when compared with lanes 1 and 2, which confirmed the successful hybridisation of the DNA helix. Lanes 6 and 7 show the increase in mass for the hybridised **A'-ILVAGK + A** in TAMg (lane 6) and 1 % SDS (lane 7). The lack of smearing above these samples would suggest there is little formation of higher molecular weight structures which may have self-assembled, adding further support to the use of 1 % SDS as the buffer system for this experiment.

The data sets within this chapter are incomplete because of isolation related to Covid-19, and there was not enough time to repeat the experiments. DLS analysis was carried out for **A**, **A'** and **A + A'** in 1 % SDS buffer to assess any changes in hydrodynamic radius over the aging period (Fig. 5.3). All three samples showed consistent peaks centred around 2 nm. This is likely due to the presence of SDS preventing aggregation of individual molecules, meaning the radius did not change over the time-period. Little change is seen in the hybridised sample, when compared with the single stranded DNA, this is because although the double helix has formed there is little interaction between helices.

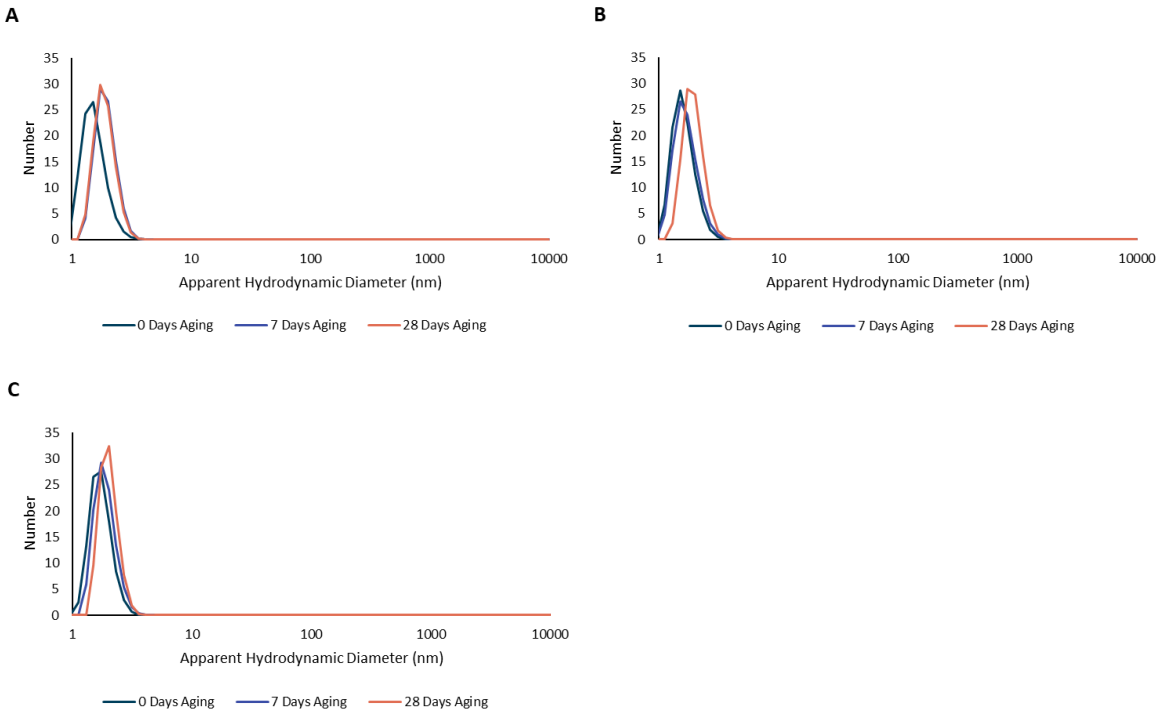

Figure 5.3: DLS graphs. A: **A**, B: **A'**, C: **A + A'** hybridised over 28 days of aging. All samples measured in 1 % sodium docecyl sulphate solution, at 25 ˚C, with a final DNA/peptide concentration of 10 µM. Measurements taken at 0, 7, and 28 days of aging, 14 and 21 days of aging missing due to Covid-19 isolation.

Figure 5.4 shows the graphs obtained for **A'-ILVAGK + A** (Fig. 5.4 a) and **ILVAGK** (Fig. 5.4 b) in 1 % SDS over 28 days of aging. **A'-ILVAGK + A** showed little change over the 28-days of aging in hydrodynamic diameter, with the peak centred around 7 nm. This would suggest there was little change in the size of the structures during this period, and that the 1 % SDS buffer was achieving the goal of preventing further peptide assembly. **ILVAGK**, however showed a disordered multi-peak spectrum at 7 days of aging but reverted to a single peak centred around 3 nm at 28 days of aging. This would suggest that the peptide portion already had some form of self-assembly prior to treatment with the 1 % SDS solution but the SDS may have broken down these structures, yielding smaller hydrodynamic diameters as a result at 28 days of aging. Further analysis by CD and AFM was required to support this hypothesis.

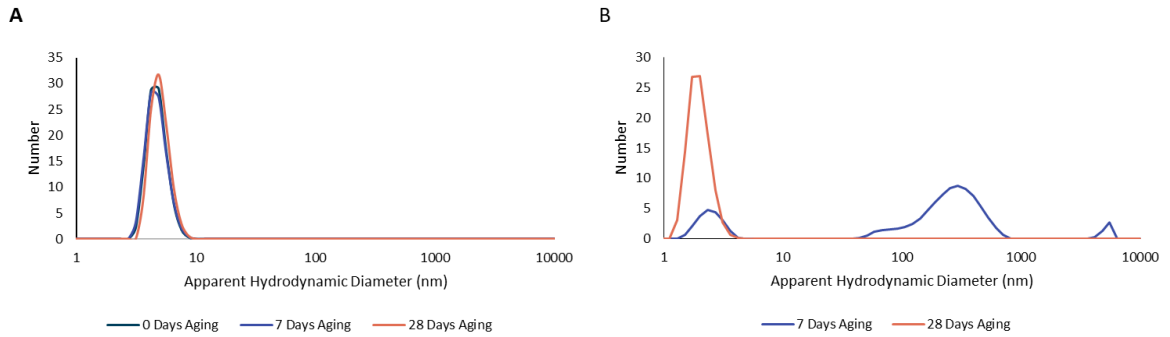

Figure 5.4: DLS graphs. A: **A'-ILVAGK + A**, B: **ILVAGK** over 28 days of aging. All samples measured in 1 % sodium docecyl sulphate solution, at 25 ˚C, with a final DNA/peptide concentration of 10 µM. Measurements taken at 0, 7, and 28 days of aging, 14 and 21 days of aging missing due to Covid-19 isolation.

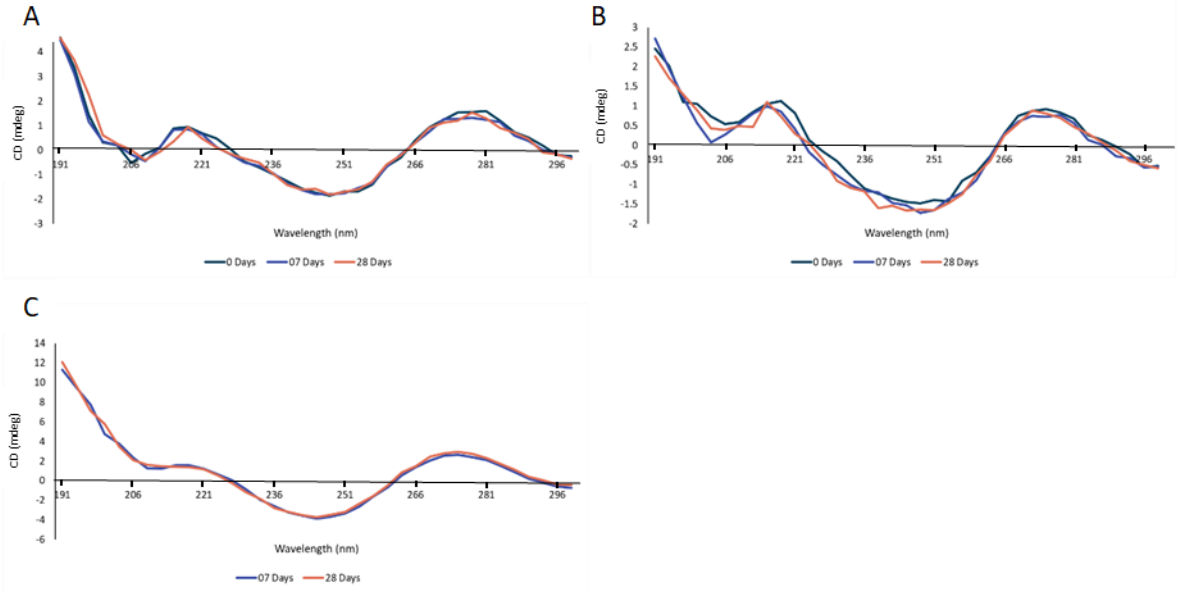

Figure 5.5: CD spectra for, A: **A**, B: **A'**, and C: **A + A'** hybridised, over 28 days of aging. All samples measured in 1 % sodium dodecyl sulfate buffer (pH 8.0), at 25 ˚C, with a final DNA/peptide concentration of 10 µM. Measurements taken at 0, 7, and 28 days of aging, 14 and 21 days of aging missing due to Covid-19 isolation.

.

The CD spectra for **A**, **A'**, and **A + A'** in 1 % SDS are show in Figure 5.5, all three spectra are stable over the 28 days of aging. Both **A** (Fig. 5.5 a) and **A'** (Fig. 5.5 b) showed the consistent single DNA shape, with a maximum around 275 nm and a minimum around 245 nm. **A + A'**, shows the same shape spectra with a stronger intensity of around 4 mdeg for the maxima and – 4 mdeg for the minima, when compared to Figure 5.5 a and b (2, -2 and 1, -1.5). **A'-ILVAGK + A** (Fig. 5.6 a) maintained a consistent spectrum over the aging period, with a maximum of around 275 nm and minimum of around 245 nm for the DNA double helix portion of the conjugate. **ILVAGK** (Fig. 5.6b) showed again consistent spectra over the aging period, with a distinct minimum of around 200 nm.

The lack of change in the peptide CD spectra would suggest there is little change occurring in the conformation of **ILVAGK** within this system. Both the CD and DLS spectra seem to suggest that there was limited change in the structures formed during the 28-days of aging, AFM was employed to confirm this and get a visual understanding of what kind of structures were observed.

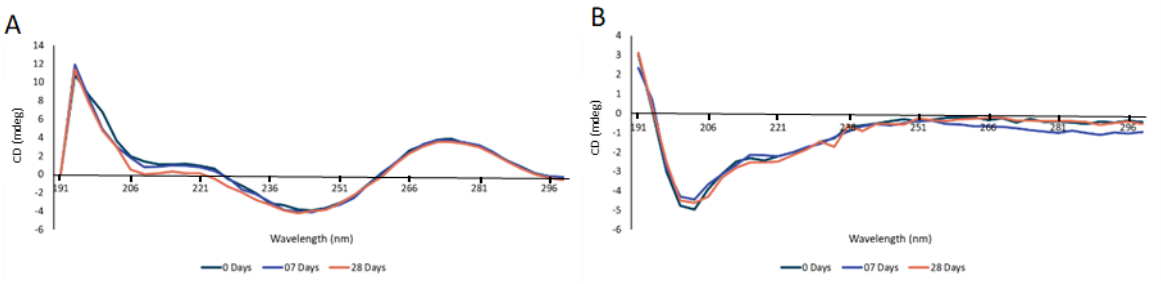

Figure 5.6: CD spectra for, A: **A'-ILVAGK + A**, B: **ILVAGK**, over 28 days of aging. All samples measured in 1 % sodium dodecyl sulfate buffer (pH 8.0), at 25 ˚C, with a final DNA/peptide concentration of 10 µM. Measurements taken at 0, 7, and 28 days of aging, 14 and 21 days of aging missing due to Covid-19 isolation.

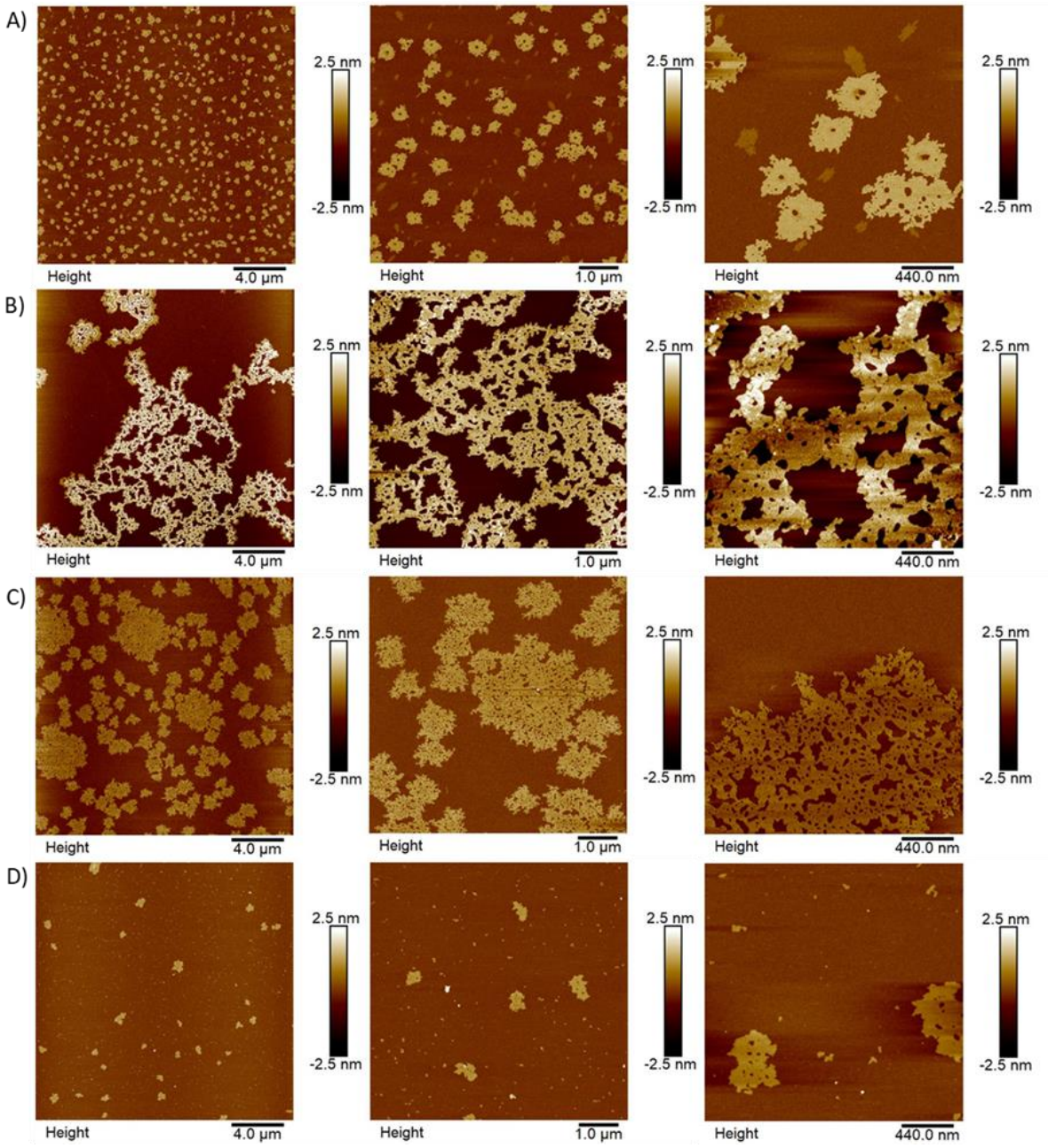

Figure 5.7: AFM images of, A: 1 % SDS, B: **A**, C: **A'**, D: **A+A'**, over 28 days of aging. At a concentration of 10 µM and in 1 % SDS buffer.

A, **A'**, **A + A'**, and 1 % SDS were analysed by AFM to assess their structures, and the effect the addition of SDS had on their observed structure. Figure 5.7 a showed the 1 % SDS deposits on the mica surface exhibited small flakes with a height of 1.6 ± 0.05 nm and a diameter of 348.7 ± 97.9 nm. These structures were consistent across the surface. **A** showed a network-like structure comparable to that seen in TAMg in Chapter 3 (Fig. 3.11 b), with a height around 3.8 ± 1.8 nm. Suggesting that the presence of 1 % SDS buffer had little effect on the aggregation of single stranded

DNA when compared to those seen in TAMg buffer. This was similar for **A'**, which showed large flakes in 1 % SDS buffer with a height of 1.2 ± 0.4 nm and a diameter of 622.9 ± 505.9 nm. **A'** exhibited small flakes in TAMg buffer with a height of 1.7 ± 0.1 nm and 260.7 ± 44.3 nm in Chapter 3 (Fig. 3.11 c). Although the size of structures observed were different the morphology was not. For **A + A'** in 1 % SDS, small flakes were observed with a height and diameter of 3.5 ± 4.6 nm and 214.5 ± 115.7 nm respectively. Again, this was not dissimilar to the structures observed for **A + A'** in TAMg buffer (Chapter 4, Fig. 4.8 a), which produced large flakes with a height of 1.6 ± 0.1 nm. This is not unexpected given the fact that this buffer was selected to not interfere with the self-assembly of the DNA double helix.

ILVAGK and **A'-ILVAGK + A** were aged over 28 days, to assess their self-assembly in 1 % SDS, Figure 5.8 shows the images collected for **ILVAGK**. At 0 days of aging I**LVAGK** exhibited a network-like structure with a height between 1-2 nm, like those seen in Chapter 3 (Fig. 3.6, 14 days, H: 2.3 ± 2.2 nm). It was thought that the network-like structure observed, was likely due to pre-assembled **ILVAGK**. This was because the samples were not immediate treated with 1 % SDS and some self-assembly may have occurred. The percentage of SDS was low and would not be able to break down larger structures immediately. It was seen from Figure 5.8 that the structures observed over the aging period generally tended towards small flakes suggesting the breakdown of the network-like structure due to the SDS. At 7 days of aging small flakes were observed with a height of 3.1 ± 7.2 nm and a diameter of 296.9 ± 54.9 nm, again like those seen in Chapter 3. At 21 days of aging, the surface was covered with dot-like structures (H: 17.9 ± 13.6 nm) and streaks. It is possible that the structures observed were a form of self-assembly, but given the height of these structures, it is more likely due to poor sample preparation. However, at 28 days of aging, small flakes were observed once again. These flakes had a height and diameter of 1.8 ± 0.6 nm and 363.9 ± 100.8 nm respectively. This would suggest a break down in nanostructure, with a stable structure achieved after 7 days of aging, if 21 days of aging is discounted.

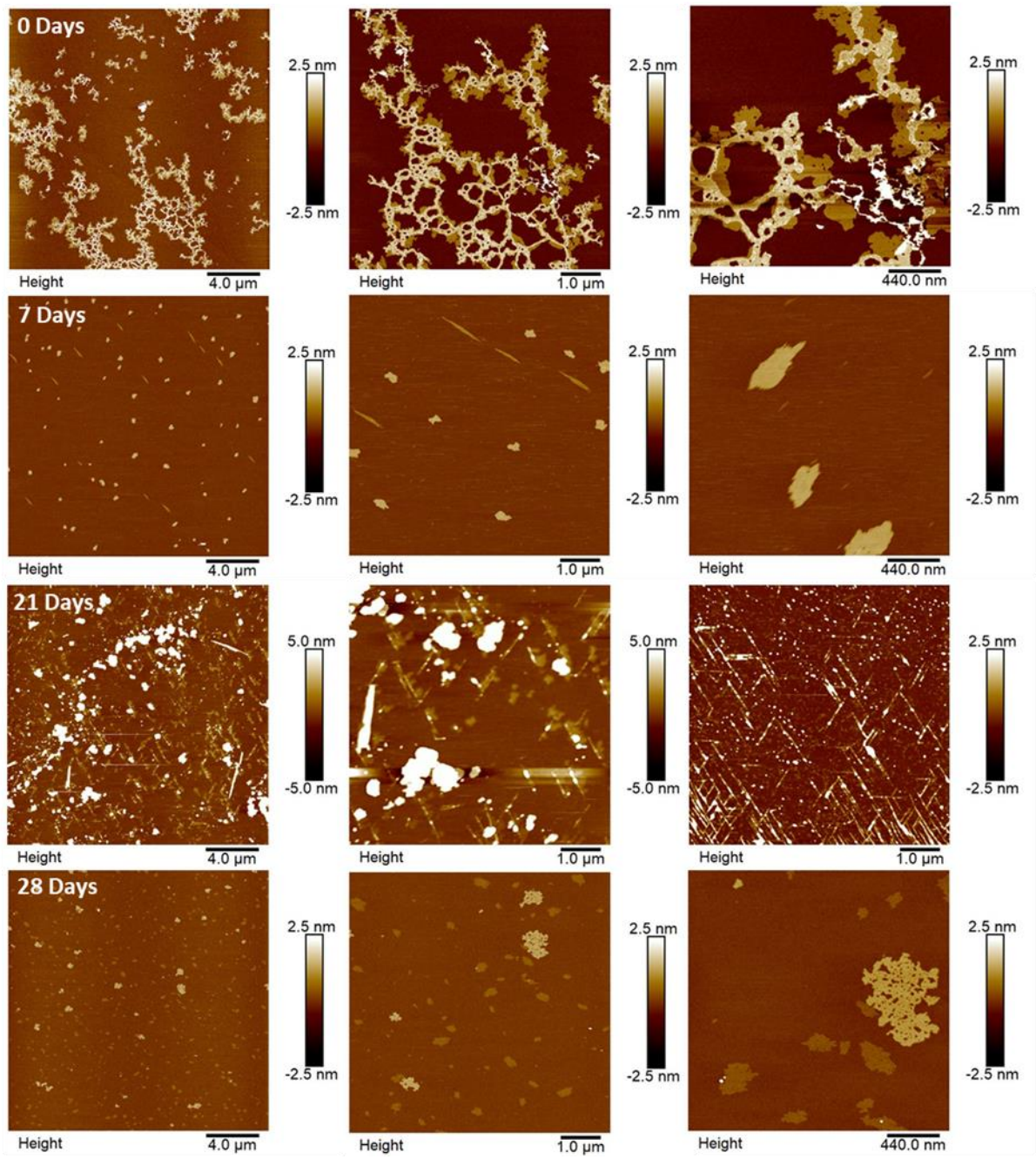

Figure 5.8: AFM images of **ILVAGK** over 28 days of aging, in 1 % SDS buffer and at a concentration of 10 µM.

Figure 5.9 Shows the AFM images collected for **A'-IVAGK + A** over 28 days of aging. At 0 days of aging, large flakes were observed with a height 1.5 ± 0.1 nm and a diameter of 1.0 ± 0.1 µm. At 7 days of aging small, layered flakes were observed. The flatter flakes shrank in height to an average of 1 nm, the layered flakes had a diameter of 505.2 ± 234.4 nm and an average height of 18.1 ± 12.4 nm. At 21 days of aging the entire surface was covered in a flake-like film with a height of 409.4 ± 565.3 pm, and a few dot-like structures (H: 5.8 ± 3.4 nm, D: 90.7 ± 17.9 nm). At 28 days of aging

small flakes was the predominant structure observed, with a few small network-like structures (H: 16.0 ± 12.9 nm). The flakes had a height of 1.8 ± 1.8 nm, and a diameter of 282.5 ± 120.6 nm. The structures observed in Figure 5.9, changed in size over 28 days of aging, however the morphology was generally alike, and the lack of diversity seen within these assemblies would confirm the 'switching off' of **ILVAGK** by tailoring the buffer conditions.

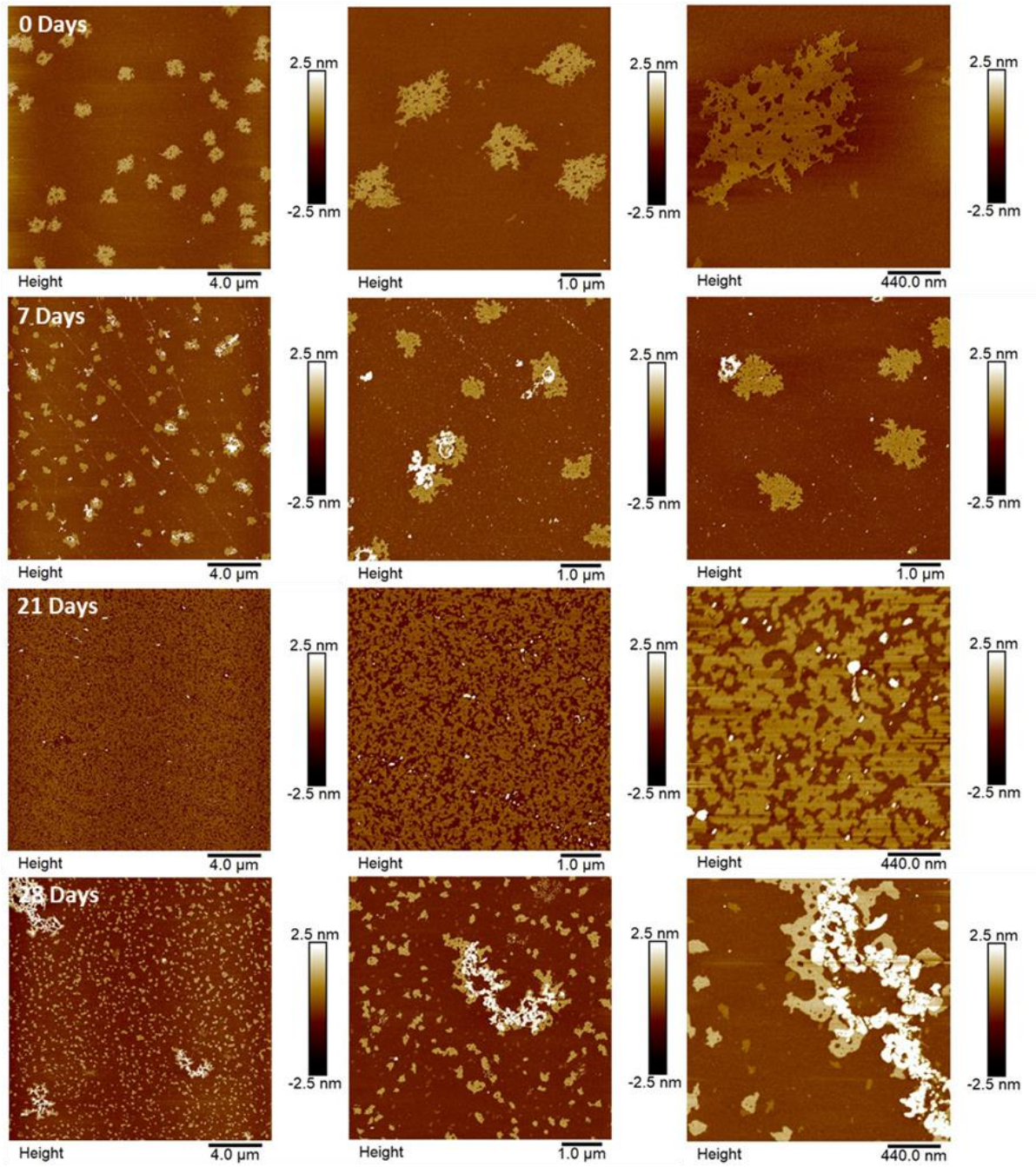

Figure 5.9: AFM images of **A'-ILVAGK + A** over 28 days of aging, in 1 % SDS buffer and at a concentration of 10 µM.

ILVAGK is known to self-assemble to give hydrogels, this assembly takes the form of a network.[85,157] The introduction of a surfactant like SDS breaks down the self-assembly of ILVAGK. In this chapter it is observed that the initial structures observed were network or fractal-like structures, these are like what might be observed from a collapsed hydrogel network. As the structures are observed through 28-days of aging, the morphology changed away from fractal-like and network-like structures towards flakes, and dot-like structures. This confirms the breakdown in self-assembly of the ILVAGK portion of the conjugate.[158] This is like the work shown by Daly *et al*. where their bundles of fibres return to individual fibres when the DNA self-assembly was switched off.[99] Buchberger *et al*. also showed tuneable self-assembly of their triangular nanostructures, through peptide control.[159] Buchberger et al. also demonstrates this control in their work around the DNA origami blocks, with coiled peptide handles.[97] All of these systems require both types of self-assembly, to yield structures with more complex architecture, as seen in this chapter.

5.3: Conclusions

In this chapter 1 % SDS was used to 'switch off' the self-assembly of **ILVAGK** in this DNA-peptide conjugate system, by turning off peptide assembly it was hoped to confirm the orthogonal or emergent assembly thought to have occurred in Chapter 4. If the presence of hierarchical behaviour was confirmed, this would open a wide range of avenues for nanoscale control like that observed in nature. The integrity of the DNA double helix was maintained by using 1 % SDS as confirmed by CD (Fig. 5.1) and PAGE (Fig. 5.2). Figure 5.1 showed the difference in CD spectra between **ILVAGK** and **A + A'** in TAMg and 1 % SDS buffer. **A + A'** (Fig. 5.1 a) showed a consistent spectra and shape despite being in different buffers, confirming the formation of the double helix. **ILVAGK**, however showed a distinctive negative intensity around 200 nm indicative of the random coil formation. In TAMg **ILVAGK** showed a maximum around 198 nm, indicative of the β-turn conformation (Chapter 3). This would suggest success in preventing further self-assembly of **ILVAGK** using 1 % SDS. The DLS (Fig. 5.3 and 5.4) showed little change over the time-period, for all samples accept **ILVAGK**.

ILVAGK, showed a change from a multi-peak spectrum at 0 days of aging to a single smooth peak centred around 3 nm. This would suggest a change from multiple forms of assembly to a breakdown to a single form of assembly for **ILVAGK** due to 1 % SDS.

Atomic force microscopy was used to assess if there were any changes in self-assembly when the peptide assembly was disrupted by the addition of 1 % SDS. To be able to fully understand the structures that may be encountered in this chapter **A**, **A** and **A + A'** were analysed in 1 % SDS. **A** (Fig. 5.7 b) and **A'** (Fig. 5.7 c), showed network-like structures and large flakes respectively, which were very similar to those observed in TAMg in Chapter 3 for **A** and **A'**. The only difference being in the size of the flakes observed for **A'**, small flakes in TAMg and large flakes in 1 % SDS. **A + A'**, showed similar morphology to that observed in TAMg, yielding small flakes in 1 % SDS (H: 3.5 ± 4.6 nm) and large flakes in TAMg (H: 1.6 ± 0.1 nm). This lack of change was unsurprising given that the 1 % SDS buffer system was chosen to aid DNA assembly, like TAMg. **ILVAGK** (Fig. 5.8) gave network-like structures (H: 1-2 nm) at 0 days of aging. These structures were thought to be due to preassembled peptide, as the sample was prepared from a stock solution and any pre-assembly could not be prevented. The percentage of SDS was also low enough to not cause instantaneous disassembly of these structures. The network-like structures devolved into small flakes at 7 days of aging, with a height of 3.1 ± 7.2 nm and a diameter of 296.9 ± 54.9 nm. Suggesting that the SDS was breaking down these structures. This was further supported by the presence of small flakes at 28 days of aging with a height and diameter of 1.8 ± 0.6 nm and 363.9 ± 100.8, respectively. The stability of the structure type seen and the size becoming smaller would confirm that peptide driven self-assembly was successfully 'switched off'. How this effected the structures observed in **A'-ILVAGK + A**, was seen in Figure 5.9. At 0 days of aging large flakes were observed with a height of 1.5 ± 0.1 nm and a diameter of 1.0 ± 0.1 µm. This morphology was maintained throughout the 28 days of aging, bar a densely covered surface at 21 days of aging. A few small network-like structures (H: 16.0 ± 12.9 nm) alongside small flakes (H: 1.8 ± 1.8 nm, D: 282.5 ± 120.6 nm), were seen at 28 days of aging. Although the size of the structures observed did change over the aging period their

morphology was alike throughout. This would suggest that there was limited self-assembly due to the DNA helix and peptide assembly being 'switched off'. The breadth and diversity of structures observed in previous chapters, especially Chapter 4 would confirm the presence of hierarchy within this **DNA-ILVAGK** conjugate system. This is because when each individual assembly motif was observed the structures were not as diverse or as dynamic as those seen in Chapter 4, confirming that both assembly motifs were required to yield these structures. This is the definition of orthogonality, that the system yields greater and more diverse properties than those of the individual parts.[97,99,151]

Chapter 6: Overall Conclusions and Future Work.

6.1: Conclusions

This thesis discusses the synthesis of two types of bi-functional crosslinkers to DNA, maleimide NHS and cyclooctyne NHS. These linkers were selected due to their biocompatibility and well-established chemistries. Maleimide-thiol conjugation experiments were conducted with **HYFNIF**, **POG_6**, and **KLVFFA** peptides. Numerous conditions were assessed and analysed by polyacrylamide gel electrophoresis. The final conditions which were selected was, a pH of 8.0, in potassium phosphate buffer, at a reaction temperature of 50 ˚C. These peptides were then taken on for further analysis by another PhD student within the group. Cyclooctyne modified DNA was reacted with azide modified **ILVAGK**, which was provided by the University of Vienna. Although azide terminated **POG_6** was available for use, it had a crude yield of 50 % and due to time constraints **ILVAGK** was progressed with as the peptide for the bulk of this work. Due to **ILVAGK** being water soluble conjugation reactions could take place in water, removing the need for organic solvents. The optimum reactions conditions were found to be 1 hour at 37 ˚C, followed by purification with anion exchange resin, and size exclusion chromatography.

Chapter 3 explored the peptide driven self-assembly the **ILVAGK** system. Pure **ILVAGK** was doped with increasing amounts of **ILVAGK-A**, 0.01, 0.1, 0.5 and 1 eqv of **ILVAGK-A** to **ILVAGK**. The assembly observed over the 28-day aging period, changed significantly, as well as the time at which different types of assembly was observed, such as fractal-like networks. The addition of DNA to the peptide did change the assembly observed. This was further explored in Chapter 4, by the introduction of DNA hybridisation. The addition of the DNA helix into the assembly profile, was thought to change the structures seen. What was mainly seen was an increase in the speed of which certain structures were seen, and the size of them. With large network-like structures being observed with increasing length of the DNA helix. However, by increasing the helix length to 3 conjugate units a shift in the observed assembly was seen, with move towards smaller structures. This may suggest that by increasing the length of the DNA helix, and therefore crosslinking between peptide residues this

may push the system towards more thermodynamically stable structures. Finally, Chapter 5 explored the possibility of hierarchy within this system. It was thought the dynamic nature and varying structures observed was due to both types of assembly being present. SDS was added to hybridised **ILVAGK-A',** because the sodium ion concentration was strong enough to assist in the formation of the double helix, but to also act as a denaturant and prevent the further assembly of the peptide portion of the conjugate. It was found that little varying architectures were observed over the 28-day period, flakes of varying sizes were observed. There were no network-like of fractal-like structures seen, suggesting that the presence of both the DNA and peptide self-assembly was required to form the complex structures observed in Chapter 4. This may suggest that there is hierarchy present within the system, bringing this work in line with the literature in an attempt to truly mimic the complexities of nature. This work discusses the self-assembly of **DNA-ILVAGK**, a β-turn DNA-peptide conjugate, the first of its kind in the literature.[160] **ILVAGK** has previously been shown to assemble into hydrogels, with temperature and salt sensitivity, this work has shown the ability to 'switch on' and 'switch off' DNA and peptide self-assembly through DNA hybridisation and buffer selection respectively. This work forms the foundation of better understanding and achieving emergence in synthetic systems, similarly to the work by Kye *et al*. and Daly *et al*. [98,99] Further work is required to investigate the full potential of these materials and the applications they may benefit. The gelling properties of **ILVAGK**, opens the possibility of programmable and tuneable drug delivery systems. Whereas the DNA portion of **DNA-ILVAGK** may be able to open exploration into nanotechnology, cellular mimics, and medicine.[31,56,104,161]

6.2: Future Work

Moving forward a focus on achieving more well-defined structures would be beneficial to the identifying the most appropriate area of application for these conjugates. This could be achieved through experimental design, for example applying different forms of external stimuli would help the system achieve thermodynamic equilibrium more quickly.[126] Another example would be to

change the buffer that the experiments were conducted in, this would be useful for modifying salt concentration which may reduce electrostatic repulsion between the DNA and **ILVAGK**.[126] After further exploring external stimulation of the system, the system can be modified to explore the role of DNA hybridisation in the system. The length of the DNA complement can be extended to explore how this effects the system. In principle introducing a longer DNA complement, would also change the orientation of ILVAGK on the double helix. This in turn would also increase the three dimensionality of the system which may demonstrate more as yet unseen structures. Strand displacement reactions could be employed to assess the intrinsic importance of DNA hybridisation to this system. Strand displacement and switching could also be used to further explore emergence within the system, by assessing how one half of the assembly being modified effects the overall system. Further control over the system could be employed by using larger peptides with a strong self-assembly character such as alpha coils, collagen mimetic peptides, or β-sheet peptides. The assembly of these types of peptides is well understood and have had wide use in the literature with DNA-peptide conjugates.[89,159,162] This work has shown the ability to form collagen mimetic peptide DNA conjugates, it would not be unreasonable to study these materials in the same process as discussed within this thesis. I hope that whoever takes this work on moving forwards, is able to continue to develop these systems to their full potential.

7.0: Experimental

This chapter outlines the experimental methods discussed throughout this thesis. The methods are split into their respective chapters, any methods which were used repeatedly are detailed in the first section they were used, with any changes to sample preparation stated within the subsection.

7.1: Materials

Dry acetonitrile, urea, EDTA, triethanolamine, triethylamine, and 6-maleimidohexanoic acid were purchased from Acros. acrylamide/bisacrylamide 37.5:1 solution; dichloromethane, formamide, dimethylformamide, glycerol, potassium carbonate anhydrous, hydrochloric acid, sodium chloride, tris base, boric acid, magnesium acetate tetrahydrate, magnesium acetate hexahydrate, acetic acid, sodium dodecyl sulfate, magnesium sulfate anhydrous, sodium borate, and *N*-hydroxy succinimde were purchased from Fisher Scientific. dA-CE, dC-CE, dG-CE, and dT-CE phosphoramidites were purchased from Link Technologies and diluted in autoclaved, deionised water, as recommended. Deblock, cap A, cap B, oxidiser and ETT activator reagents were purchased from Link Technologies. Ammonium phosphate, *N*, *N, N'*, *N'*-tetramethylethylenediamine (TEMED) and (1R,8S,9s)-bicyclo[6.1.0]non-4-yn-9-ylmethyl *N*-succinimidyl were purchased from Sigma Aldrich. *N*-(3-Dimethylaminopropyl)-*N* -ethylcarbodiimide hydrochloride (EDC.HCl) and *N*, *N*-diisopropylethylamine were purchased from Fluorochem. Zetadex-25 medium was purchased from EMP Biotech. Oligomers: T5-A, T5-A , H_2N-A and H_2N-A were purchased from IDT. Q Sepharose fast flow, 25 mL was purchased from GE healthcare. Stains-All, sodium dihydrogen phosphate dihydrate and sodium hydrogen phosphate were purchased from Alfa Aesar. Deuterated dimethyl sulfoxide and chloroform were purchased from Goss Scientific. All materials were used as provided, without further purification, and had a minimum purity of 98 %.

Table 7.1: DNA sequences used in this thesis, Tm taken from technical datasheet as provided by IDT.

Name	Sequence	Length	T_m (°C)
A	CTG TAT GGT CAA CTG	15*mer*	42
A-T5	TT TTT CTG TAT GGT CAA CTG	20*mer*	42
A-NH_2	NH_2 - TT TTT CTG TAT GGT CAA CTG	20*mer* + C_6 - NH_2	42
A'	CAG TTG ACC ATA CAG	15*mer*	42
A'-T5	TT TTT CAG TTG ACC ATA CAG	20*mer*	42
A'-NH_2	NH_2 - TT TTT CAG TTG ACC ATA CAG	20*mer* + C_6 - NH_2	42
2A'	CAG TTG ACC ATA CAG CAG TTG ACC ATA CAG	30*mer*	42
3A'	CAG TTG ACC ATA CAG CAG TTG ACC ATA CAG CAG TTG ACC ATA CAG	45*mer*	42

7.1.1: Buffer Compositions

Tris Magnesium Acetate (TAMg) Buffer:

Composed of 45 mM Tris base and 12.5 mM $Mg(OAc)_2 \cdot 6H_2O$ in autoclaved deionised water. The pH was adjusted to 8.0 using glacial acetic acid.

Tris Borate EDTA (TBE) Buffer:

TBE buffer contains 90 mM Tris, 90 mM boric acid and 1.1 mM EDTA with a pH of 8.0.

Sodium Phosphate Buffer:

0.2 M Na_2HPO_4 (35.61 g/L) and 0.2 M NaH_2PO_4 (71.64 g/L) combined in the following volumes, 47.35 mL and 2.65 mL respectively. Diluted to 100 mL with autoclaved deionised water for a pH 8.0.

Triethanolamine/ EDTA (TEA) Buffer:

Triethanolamine (821.7 µL) diluted to 50 mL with autoclaved deionised water (49.1793 mL) for a 100 mM solution. 0.5 M EDTA solution, 18.612 mg EDTA dissolved in 100 mL autoclave deionised water and 2 mM sodium hydroxide solution. Buffer solution, 8 mL TEA 100 mM combined with 2 mL 0.5 M EDTA solution dissolved up to 200 mL with 1x PBS.

1% SDS Solution:

Sodium dodecyl sulphate (10 g) dissolved in autoclaved deionised water up to 100 mL. Dilute 10x with autoclaved DI water for a 1x solution.

TEAA) Buffer:

Dilute 5.71 mL of 100 mM acetic acid solution and 13.9 mL of 100 mM triethylamine to 1 L using autoclaved deionised water other solvent system (HPLC (MeCN:H_2O 80:20)) for 100 mM TEAA buffer solution.

7.2: Chapter 2 Experimental Methods

All polyacrylamide gel plates were prepared as follows: Glass plates for a mini gel cassette were cleaned with ethanol to remove any residual acrylamide from previous uses. The cassette was assembled and placed into a loading dock. All gels were stained with Stains All stain, unless stated otherwise in the relevant method. All gels were analysed as follows: The gel was imaged on a document scanner. Images were enhanced using GIMP 2.10.8 imaging software, to enhance contrast, colour, rotation and to crop the background.

7.2.1: Synthesis of Compound **1** (**1**), Maleimide Aminoethoxyacetyl

Maleic anhydride (3.59 g, 36.6 mmol) and 2-(2-aminoethoxy)ethanol (3.01 g, 28.6 mmol) were dissolved in 200 mL acetic acid. The mixture was heated to reflux at 170°C. The crude material was dried in vacuo giving a yellow oil which was dissolved in 20 mL DCM and purified by aqueous washing with concentrated HCl (3 x 20 mL), K_2CO_3 (3 x 20 mL) and brine (3 x 20 mL). The organic phase was dried over magnesium sulfate and filtered before solvent removal by rotary evaporation. The purified product was a clear yellow oil (3.78 g, 16.6 mmol, 58 % yield). Purified compound **1** was confirmed by 1-dimesional proton and carbon NMR (Fig.7.1-7.2). Purified compound **1**: ^{1}H 1D NMR (400 MHz, $CDCl_3$) δ H_a 6.64 (2H, s) H_b 4.11-4.08 (2H, t) H_c 3.68-3.65 (2H, t) $H_{d,e}$ 3.60-3.56 (4H, dt) H_f 1.99 (3H, s). ^{13}C NMR (100 MHz, $CDCl_3$, ^{1}H decoupled) δ C_a CH 134.17, C_b CO 170.60, C_c CH_2 37.02, C_d CH_2 63.42, C_e CH_2 68.45, C_f CH_2 67.74, C_g CO 170.96, C_h CH_3 20.82.

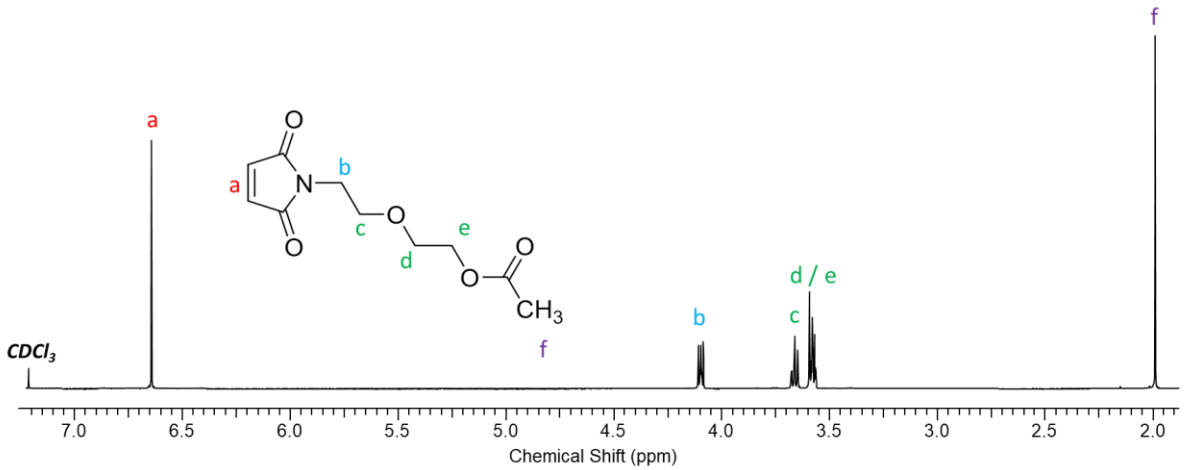

Figure 7.1: ^{1}H 1D NMR spectrum of compound **1** in deuterated chloroform. : ^{1}H 1D NMR (400 MHz, $CDCl_3$) δ H_a 6.64 (2H, s) H_b 4.11-4.08 (2H, t) H_c 3.68-3.65 (2H, t) $H_{d,e}$ 3.60-3.56 (4H, dt) H_f 1.99 (3H, s).

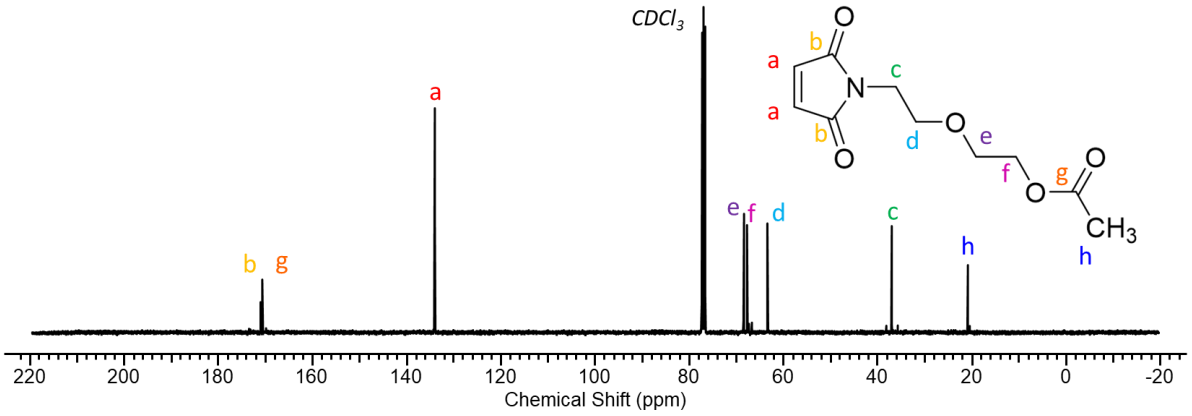

Figure 7.2: Decoupled carbon NMR spectrum of compound 1 in deuterated chloroform. ^{13}C NMR (100 MHz, $CDCl_3$, ^{1}H decoupled) δ C_a CH 134.17, C_b CO 170.60, C_c CH_2 37.02, C_d CH_2 63.42, C_e CH_2 68.45, C_f CH_2 67.74, C_g CO 170.96, C_h CH_3 20.82.

7.2.2: Synthesis of Compound **2** (2), Furan Protected Maleimide Aminoethoxyethanol

Compound **1** (3.78 g, 16.6 mmol) was dissolved in 30 mL of acetonitrile, to this 9.5 mL (8.47 g, 88.1 mmol) of 2,5–dimethyl furan was added.[19] The mixture was heated to 65 °C under nitrogen and left to stir overnight. The crude mixture was dried in vacuo and analysed by proton and carbon NMR. Compound **2** (2.61 g, 9.3 mmol, 55.9 % yield) was then stirred directly with concentrated ammonia hydroxide (30 mL) overnight to fully degrade the *endo* form to the preferable *exo* form. This was confirmed by NMR after aqueous washing with concentrated HCl and brine. The organic

phase (DCM) was dried with magnesium sulfate and filtered before solvent removal in vacuo, the resultant oil was yellow-brown in colour. ^{1}H 1D NMR (400 MHz, $CDCl_3$) δ H_a 6.24 (2H, s) H_d 3.68-3.65 (3H, t), $H_{e,f}$ 3.60-3.55 (6H, dt), H_g 3.49-3.46 (3H, t), H_c 2.78 (2H, s), H_b 1.85 (6H, s) (Fig.7.3). ^{13}C 1D NMR (100 MHz, $CDCl_3$, decoupling) δ C_a (CH) 87.83, C_b (CO) 72.53, C_c (CH_3) 16.40, C_d (CH) 140.80, C_e (CO) 174.93, C_f (CH_2)38.40, C_g (CH_2) 61.55, C_h (CH_2) 61.55, C_i (CH_2) 67.04 (Fig. 7.4).

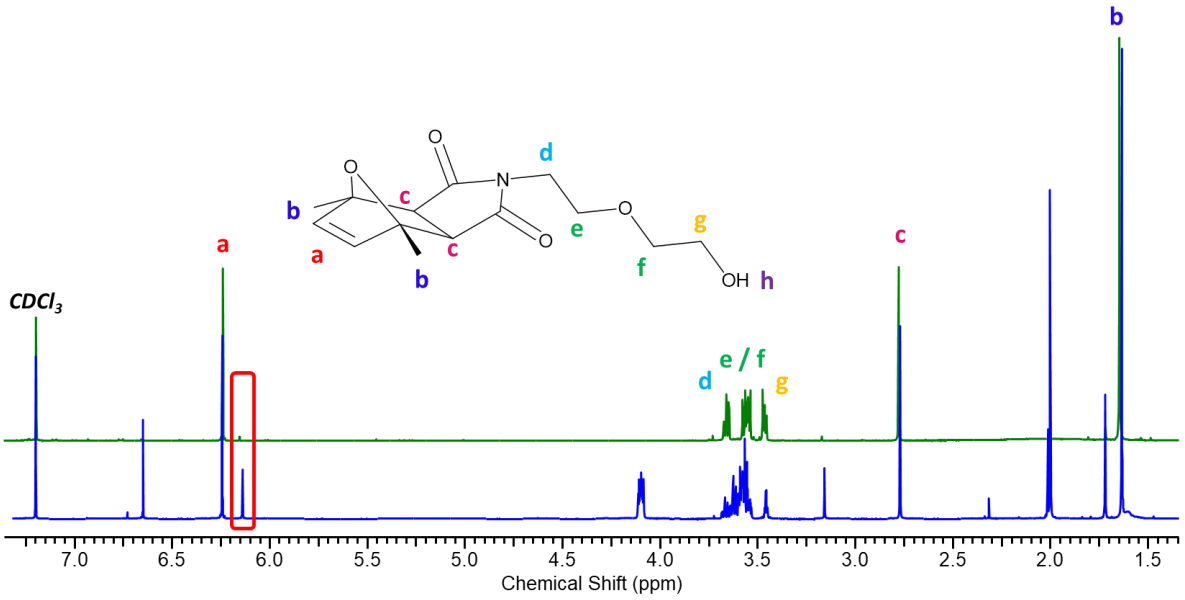

Figure 7.3: Overlaid ^{1}H 1D NMR spectra of compound **2** (*endo*) and (*exo*), crude spectrum is shown in blue. Unreacted compound **1**, can be seen by the triplet at 4.1 ppm, representing the protons situated next to the amine in the maleimide ring. The endo form of compound **2** is shown by the peak at 6.16 ppm. Purified spectrum of compound **2** is shown in green, after treatment with concentrated aqueous ammonia to remove the *endo* form. Carried out in deuterated chloroform. Note the disappearance of the highlighted peak at approximately 6.16 ppm which represents the *endo* form of compound **2**. The peak at 4.11 ppm in the blue spectrum is a peak relating to the H_d proton of the endo form of compound **2**. ^{1}H NMR (400 MHz, $CDCl_3$) δ H_a 6.24 (2H, s) H_d 3.68-3.65 (3H, t), $H_{e,f}$ 3.60-3.55 (6H, dt) H_g 3.49-3.46 (3H, t) H_c 2.78 (2H, s) H_b 1.85 (6H, s).

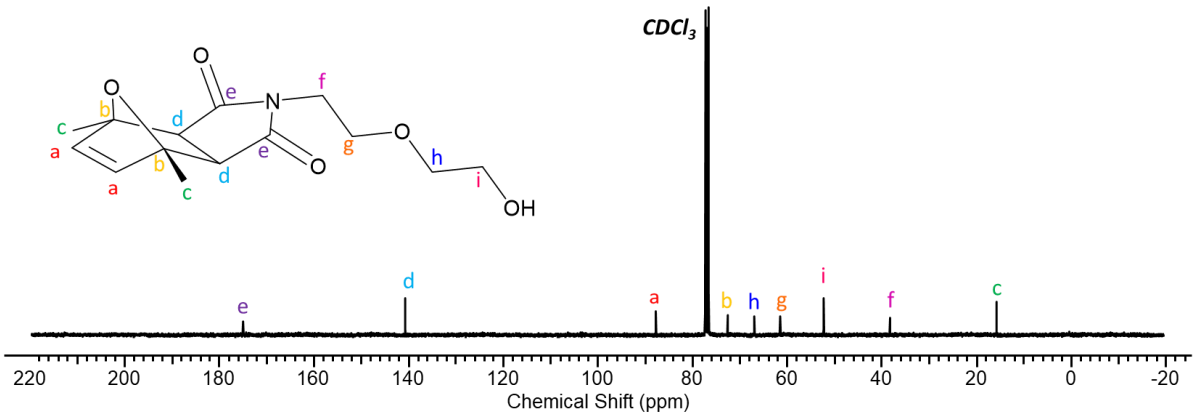

Figure 7.4: Decoupled carbon spectrum of compound **2** after treatment with concentrated aqueous ammonia solution in deuterated chloroform. ^{13}C NMR (100 MHz, $CDCl_3$, decoupling) δ C_a (CH) 87.83, C_b (CO)

72.53, C_c (CH_3) 16.40, C_d (CH) 140.80, C_e (CO) 174.93, C_f (CH_2)38.40, C_g (CH_2) 61.55, C_h (CH_2) 61.55, C_i (CH_2) 67.04.

7.2.3: Synthesis of Compound 3 (3), Furan Protected Maleimide Aminoethoxy Phosphoramidite

Phosphoramidite preparation of compound **2** was adapted from literature.[20] Compound **2** (56 mg, 0.2 mmol) and a catalytic amount of DMAP were dissolved in 2 mL of dry DCM, dried in vacuo. Under nitrogen, 5 mL of DCM containing 2-cyanoethyl phosphoramidite chloride (133 µL, 0.6 mmol) and DIPEA (166 µL, 1 mmol) were added and left to stir for 2 hours. Aqueous solvents, concentrated sodium bicarbonate and brine were degassed before washing crude compound 3. Compound **3** was washed with K_2CO_3 (2 x 3 mL) and brine (2 x 3 mL). Compound **3** was further purified by silica gel chromatography in 95 ; 5, DCM : triethylamine (TEA). Fractions were monitored by thin layer chromatography (TLC) with a product with retention factor (R_f) of 0.46. Oxidised phosphoramidite remained on the baseline of silica gel columns. The fractions were dried in vacuo and analysed by proton and phosphorous NMR. Compound **3** was dissolved in 2 mL of dry acetonitrile and placed onto the DNA synthesiser for addition to pre-synthesised DNA strands. The resultant oil was orange in colour, resultant mass and yield were not measured, in favour of limiting potential oxidation of the phosphoramidite. ^{1}H 1D NMR (400 MHz, DCM, DMSO capillary) δ H_c 7.66 (2H, s) H_a 6.06 (2H, s), H_d 4.24 (4H, m), H_e 4.04 (8H, m), H_f 3.44 (2H, sep), H_b 2.89 (6H, t), H_g 1.19 (12H, dt). ^{31}P NMR (161 MHz, DCM, DMSO capillary) 11.29 (phosphorous 5), 15.22 (phosphorus 5), 147.72 (phosphorous **3** *exo*). A ^{13}C NMR was not obtained to prevent oxidation of compound **3** before further use.

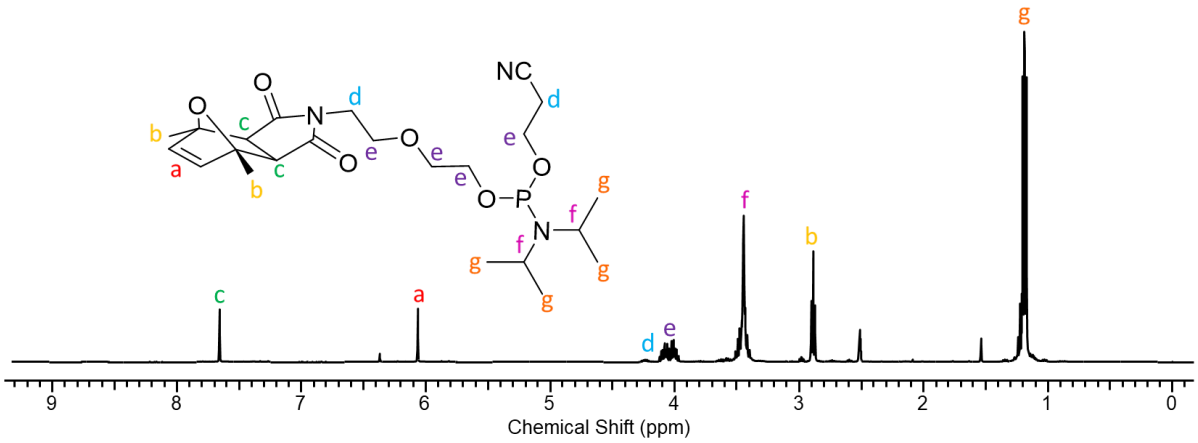

Figure 7.5: ^{1}H 1D NMR of compound **3** in dichloromethane with a deuterated DMSO capillary (a thin, sealed glass tube containing deuterated DMSO, allowing for analysis in solvents which are typically not deuterated such as dichloromethane). ^{1}H NMR (400 MHz, DCM, DMSO capillary) δ H_c 7.66 (2H, s) H_a 6.06 (2H, s), H_d 4.24 (4H, m), H_e 4.04 (8H, m), H_f 3.44 (2H, sep), H_b 2.89 (6H, t), H_g 1.19 (12H, dt).

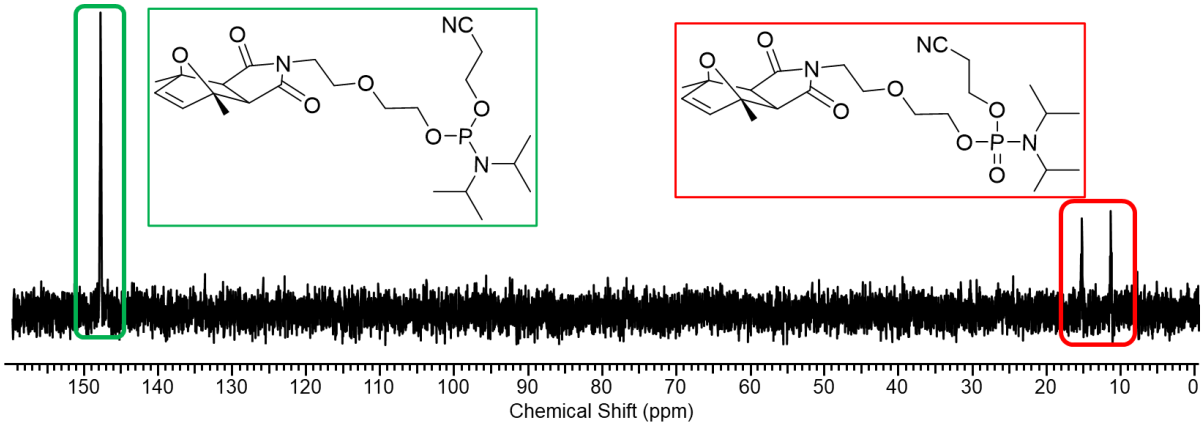

Figure 7.6: Phosphorous NMR of compound **3** in dichloromethane with a deuterated DMSO capillary. ^{31}P NMR (161 MHz, DCM, DMSO capillary) 11.29 (phosphorous 5), 15.22 (phosphorus 5), 147.72 (phosphorous **3** *exo*).

7.2.4: Synthesis of Compound **4** (**4**), Maleimidohexanoic Activated NHS Ester

Compound **4** was synthesised from 6-maleimidohexanoic acid (422 mg, 2.00 mmol), *N*-hydroxy succinimide (691 mg, 6.00 mmol) and EDC.HCl (1829 mg, 9.54 mmol) were dissolved in 100 mL anhydrous dichloromethane. The solution was sealed and reacted under nitrogen at room temperature with stirring overnight. The reaction was monitored by thin layer chromatography

(TLC) in 95:5 dichloromethane (DCM) : methanol (MeOH). The product had (R_f) 0.78. The reaction mixture was washed with 1M hydrochloric acid (2 x 50 mL), saturated potassium carbonate (2 x 50 mL) and brine (2 x 50 mL). The organic layer was dried with anhydrous magnesium sulfate and filtered before being dried under reduced pressure in a rotary evaporator. The resultant product was a pale-yellow oil (520 mg, 1.69 mmol, 84 % yield). The product was analysed by 1D proton and carbon NMR and electrospray ionisation mass spectrometry (ESMS). M/Z = 309.2 $[M+H]^{+1}$. NMR: ^{1}H 1D NMR (400 MHz, $CDCl_3$) δ H_a 6.62 (2H, s), H_b 3.47 (2H, t), H_f 2.77 (2H, s), H_e 2.54 (2H, t) 1.71 (2H, q), H_g 1.57 (2H, q), H_c 1.34 (2H, q). ^{13}C 1D NMR (100 MHz, $CDCl_3$, decoupled) δ C_b 170.89, C_i 169.16, C_h 168.36, C_a 134.08, C_c 37.49, C_g 30.82, C_d 28.02, C_e 25.89, C_j 25.62, C_f 24.02.

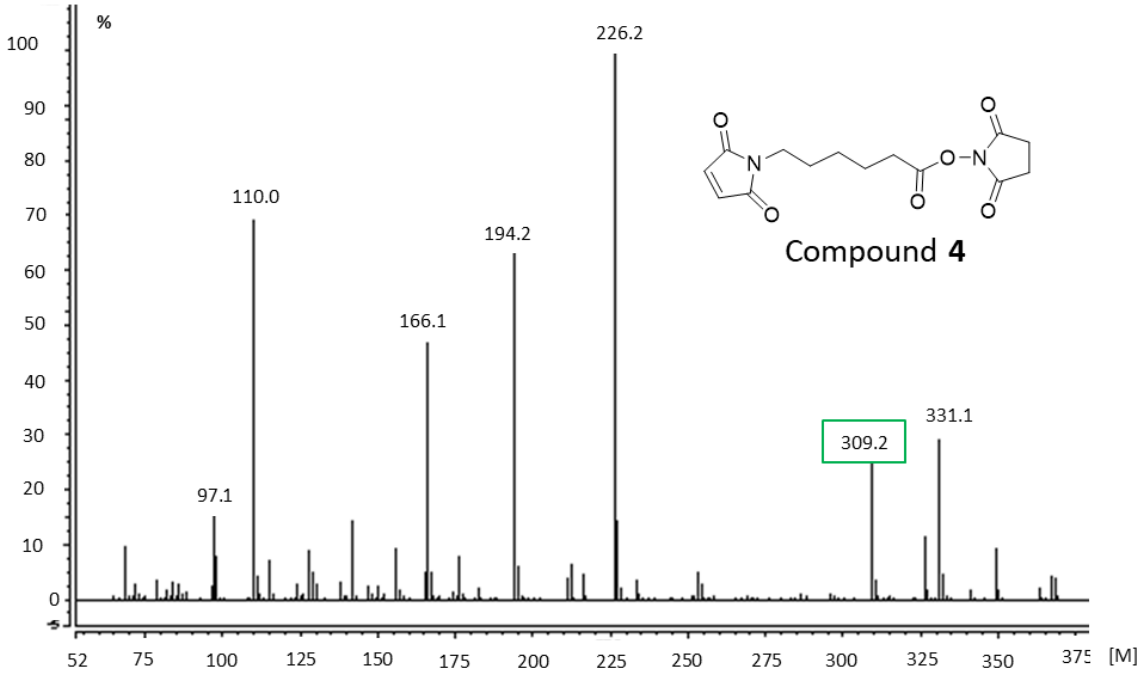

Figure 7.7: Mass spectrometry of 6-maleimidohexanoic acid activated ester. ESI -: Expected M = 308.9, observed M = 309.2 [M+H].

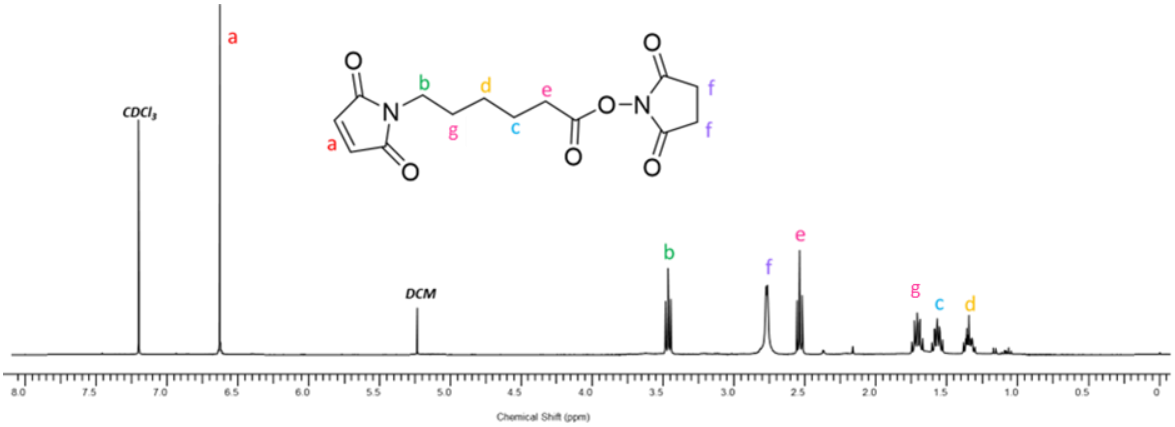

Figure 7.8: ^{1}H 1D NMR of 6-maleimidohexanoic activated NHS ester in $CDCl_3$. ^{1}H 1D NMR (400 MHz, $CDCl_3$) δ H_a 6.62 (2H, s), H_b 3.47 (2H, t), H_f 2.77 (2H, s), H_e 2.54 (2H, t) 1.71 (2H, q), H_g 1.57 (2H, q), H_c 1.34 (2H, q).

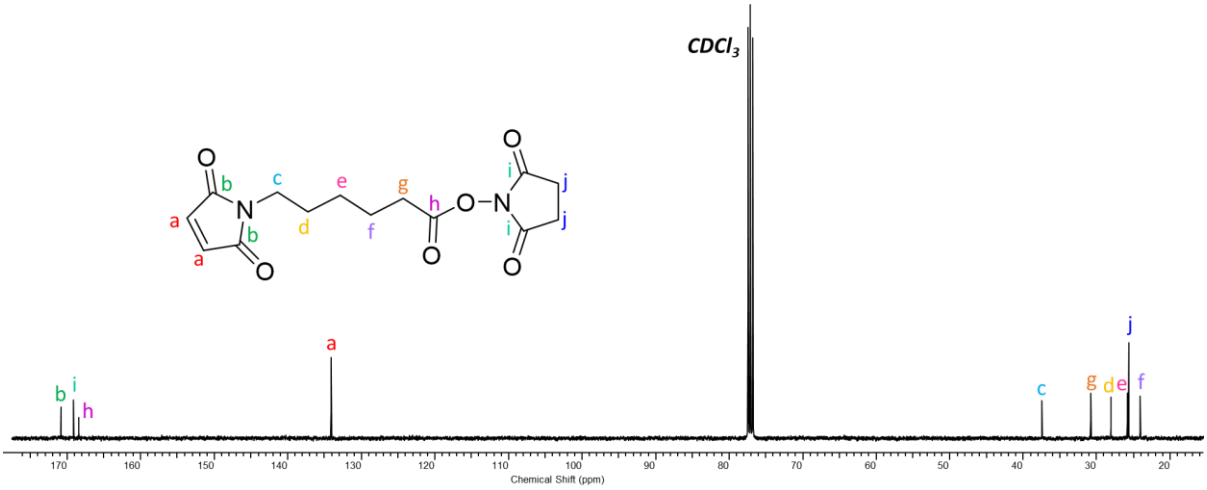

Figure 7.9: Carbon NMR of 6-maleimidohexanoic activated NHS ester in $CDCl_3$.

7.2.5: Synthesis of Compound 5 (5) Fluorescein Isothiocyanate Thiol

Fluorescein isothiocyanate (FITC) (13 mg, 0.0257 mmol) was dissolved in 4 mL DMF, to this a solution of L-cystine in 3 mL DMSO was added (3.18 mg, 0.0141 mmol). 8 µL (0.1089 mmol) of triethylamine was added and reacted overnight at room temperature with stirring. Production of the FITC-cysteine tag was monitored by TLC in DCM : MeOH : AcOH (89.5 : 9.5 : 1). The resultant material was dried by dried in vacuo, and then stirred with ethanol overnight at room temperature to remove excess starting material (the product does not dissolve in ethanol). Ethanol was removed by filtration and the remaining solid dried in vacuo. Fluorescein isothiocyanate has two isomeric

forms which it can switch between, the open (isomer II) and ring closed (isomer I) forms with a mass difference of 1 proton. M/Z = 466.07 $[M+H]^{+1}$ (monomer), M/Z = 930.12 $[M+H]^{+1}$ (dimer).

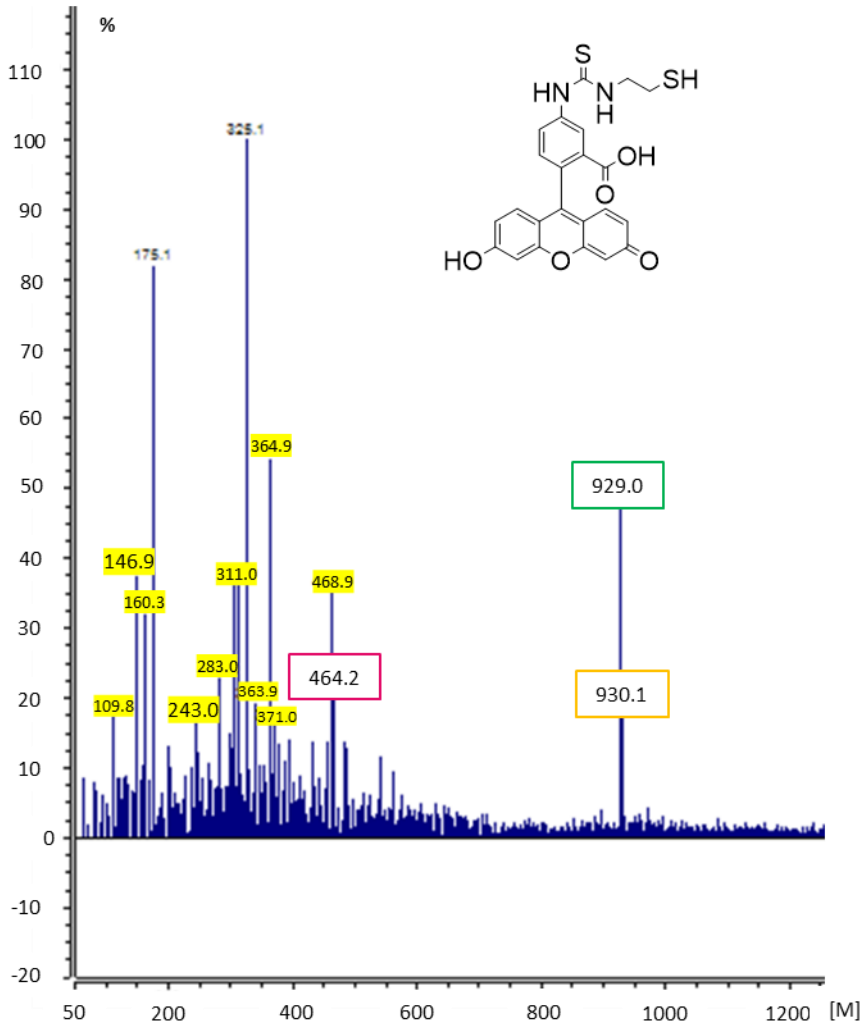

Figure 7.10: Mass spectrometry of fluorescein isothiocyanate thiol. ESI (-): Expected M (monomer) = 466.07, (dimer) 930.12, observed M = 929.0 [M-H] (dimer), M = 930.1 [M] and 464.2 [M – 2H] (monomer, ring closed isomer).

7.2.6: Synthesis, Cleavage and Deprotection of Complementary DNA Maleimide Oligomers

Two complimentary oligomers were synthesised using solid phase phosphoramidite chemistry as previously used within the group and literature.[19]

Oligonucleotides were synthesised with compound **3** attached at the 5 terminus on control pore glass beads (CPG). The modified DNA strands were synthesised on an Expedite 8909 system produced by ABI. Phosphoramidites were dissolved in dry acetonitrile to the concentrations as

suggested by the supplier, solvents were used as provided. Oligomers were synthesised on a 1 µM scale. The following oligomers: **A**, **A'**, **T5-A** and **T5-A'** were purchased from Link Technologies and prepared as directed to a concentration of 1 mM.

Table 7.2: Table of DNA sequences synthesised by solid phase phosphoramidite chemistry from 5 – 3 or purchased commercially from IDT. Melting temperature was taken from data sheets obtained from IDT. All synthesised oligonucleotides were synthesised on a 10 µM scale. Purchased oligomers were diluted to a concentration of 1mM.

Name	Sequence	Length	T_m (°C)
A	CTG TAT GGT CAA CTG	15*mer*	42
T5 - A	TT TTT CTG TAT GGT CAA CTG	20*mer*	42
NH_2 - A	NH_2 - TT TTT CTG TAT GGT CAA CTG	20*mer* + C_6 - NH_2	42
A'	CAG TTG ACC ATA CAG	15*mer*	42
T5 - A'	TT TTT CAG TTG ACC ATA CAG	20*mer*	42
NH_2 - A'	NH_2 - TT TTT CAG TTG ACC ATA CAG	20*mer* + C_6 - NH_2	42

Oligomers were cleaved and deprotected in one step from the solid support by incubating the beads in 1.5 mL concentrated aqueous ammonia solution at 55 °C overnight. The solution was centrifuged at 1000 x g for 10 minutes, the supernatant was removed and collected. The aqueous ammonia solution was removed by centrifugal vacuum concentration at 65 ˚C for 4 hours. Oligomers were re-suspended in 1 mL of autoclaved deionised (DI) water. Oligomers synthesised with compound **3** were abbreviated to **3-A** and **3-A'**. These oligomers contain the T5 nonbinding region. Oligomer purity was assessed by denaturing polyacrylamide gel electrophoresis and mass spectrometry. The yield of full-length DNA sequences were low, and so, gave a DNA synthesis with un-extended sequences.

7.2.7: Hand Coupling of Phosphoramidite Components

DNA sequences **A** and **A'** with a poly T spacer were synthesised using solid phase synthesis by the method outlined in section 7.2.6. In some circumstance compound **3** was attached to synthesised oligomers by hand to prevent loss of product. Dried columns were placed solvated using automated flushing of acetonitrile, the column was detritylated on the expedite system and incubated in dichloroacetic acid for 5 minutes. The column was flushed with acetonitrile to remove detritylation products and removed from the synthesiser. 0.5 mL of activator solution was combined with 0.5

mL (56 mg) of compound **3** in dry acetonitrile. A 1 mL syringe was inserted into the column, another was used to collect compound **3** and placed into the top of the column. The solution was passed through the column between the syringes ten times, most of the solution was pushed into the column and the system left to incubate at room temperature for 1 hour. Excess compound **3** was removed from the column and the column placed back onto the expedite system. The column was flushed with acetonitrile before being incubated with capping reagent for 5 minutes. The column was flushed with acetonitrile and incubated with oxidiser for a further 5 minutes before a final flushing with acetonitrile and nitrogen to dry the column. This same procedure was used to attach a six-carbon amine linker to sequences **A** and **A'**.

7.2.8: Conjugation of Maleimidohexanoic Activated NHS Ester (**4**) to Amine Terminated DNA

A 1 mL 100 µM solution of **H_2N–A** was prepared from a 562.9 µM stock by diluting it (177.7 µL) with phosphate buffer (pH 8.0) (822.3 µL). A 1 mL 100 µM solution of **H_2N–A'** was prepared from a 585.3 µM stock by diluting **H_2N–A'** (170.9 µL) with phosphate buffer (pH 8) (829.1 µL). 6-maleimidohexanoic activated NHS ester (3.08 mg, 0.01 mmol, 100 eqv) was dissolved in DMF (200 µL). The DMF solution was added to **H_2N–A** 100 µM DNA solution. This was repeated for **H_2N–A'**. The solution became cloudy. A further 200 µL of DMF was added to each sample to fully dissolve 6-maleimidohexanoic activated NHS ester, this yielded solutions with a total volume of 1.4 mL. The reaction mixtures were split into aliquots of 200 µL and incubated at 37 °C for 120 minutes in a thermocycler. Maleimide ester modified DNA was abbreviated to **4-A** and **4-A'**.

7.2.9: Conjugation of Cyclooctyne Activated NHS Ester (CO) to Amine Terminated DNA

A 1 mL 100 µM solution of **H_2N-A** was prepared from a 562.9 µM stock by diluting **H_2N-A** (177.7 µL) with phosphate buffer (pH 8.0) (822.3 µL). A 1 mL 100 µM solution of **H_2N-A'** was prepared from a 585.3 µM by diluting **H_2N-A'** (171 µL) with phosphate buffer (pH 8) (829 µL). Cyclooctyne NHS ester (2.91 mg, 0.01 mmol, 100 eqv) was dissolved in DMF (200 µL). The DMF solution was added to **H_2N-**

A 100 µM solution. This was repeated for **H_2N-A'**. The solution became cloudy. A further 200 µL of DMF was added to each sample to fully dissolve the cyclooctyne NHS ester, this yielded solutions with a total volume of 1.4 mL. The mixtures were split into aliquots of 200 µL and incubated at 37 °C for 120 minutes in a thermocycler. Cyclooctyne modified DNA were abbreviated to **CO–A** and **CO-A'**.

7.2.10: Purification of Modified Oligonucleotides by Size Exclusion Gel Chromatography

Purification of modified DNA was carried out by size exclusion gel chromatography using Zetadex resin. A 20 mL column was prepared as follows; 1 mL of cotton wool was placed into the bottom of a 20 mL column. A slurry of zetadex resin and autoclaved DI water was prepared the column was then filled to the 20 mL line. 1 mL of modified DNA was loaded onto the column and collected as fraction 1. 1 mL of deionised water was loaded onto the column, this was collected as fraction 2. This was repeated a total of twenty times yielding twenty fractions. This was repeated with a fresh column for each sample. The fractions were analysed for DNA content by UV-Visible spectrometry (section 7.2.8). The DNA containing fractions were dried by centrifugal vacuum concentration at 65 °C for five hours. The fractions were re-suspended in autoclaved DI water. The samples were stored in the freezer.

7.2.11: Purification of Modified Oligonucleotides by Aqueous Extraction

500 µL of **4-A** or **4-A'** in water was placed into a microcentrifuge tube. To this 500 µL of ethyl acetate was added. The solution was agitated using an automatic pipette for 30 seconds and left to separate. The organic layer was removed with an automatic pipette, and the process repeated twice more. The aqueous layer was dried by centrifugal vacuum concentration and resuspended in 500 µL autoclaved DI water. This was carried out to extract excess compound **4** that was not removed by size exclusion gel chromatography in section 7.2.10.

7.2.12: Analysis of Oligonucleotide Concentration

DNA concentration was analysed by UV-Visible spectrometry. Samples were analysed on a Nanodrop spectrometer. 2 µL of deionised water was deposited onto the pedestal and a blank was ran, the pedestal was cleaned with deionised water and a Kimtech wipe. A sample of 2 µL was then deposited onto the pedestal and a spectrum was ran between the regions of 200-400 nm. Each sample was repeated until a minimum of three consecutive results were obtained. Using the calculated A260 from IDT (**A**, 5.5 and **A'**, 5.2) and the measured A260 from the data, a concentration was calculated by multiplying them together.

7.2.13: Mass Spectrometry of Modified Oligonucleotides

Solutions of modified **A** and **A'** (30 µL, 10 µM) were prepared from 100 µM stocks (3 µL) and autoclaved DI water (27 µL). The samples were vortexed to ensure homogeneity and centrifuged in a mini centrifuge for 20 seconds to collect the solution into the bottom of the tube. These samples were then analysed using mass spectrometry by Kevin Howland (Biosciences, University of Kent). Electrospray LC-MS of Oligonucleotides. Electrospray mass spectra were recorded on a Bruker micrOTOF-Q II mass spectrometer. Samples were introduced into the mass spectrometer by on-line reverse-phase HPLC on a Phenomenex Nucleosil C18 column (3 µm, 120Å, 2.0 mm x 150 mm) running on an Agilent 1100 HPLC system at a flow rate of 0.2 ml/min using a short gradient from 10% B to 100% B (A: 15 mM TEA, 400 mM HFIP in water; B: 15 mM TEA, 400 mM HFIP in methanol). The eluent was monitored at 200-800 nm and then directed into the electrospray source, operating in negative ion mode, at 3.5 kV and mass spectra recorded from 400-3000 m/z. Data was analysed and deconvoluted to give uncharged oligonucleotide masses with Bruker's Compass Data Analysis software.

7.2.14: Oligonucleotide-Peptide Conjugation: Michael Addition

A 100 µL 50 µM **4-A** solution was prepared by diluting 100 µM **4-A** (50 µL) with phosphate buffer (pH 6.8) (50 µL). A 100 µL 50 µM **4-A'** solution was prepared by diluting 100 µM **4-A'** (50 µL) with

phosphate buffer (pH 6.8) (50 µL). The solutions were degassed with nitrogen for 10 minutes. A 2.5 mM solution of peptide was prepared by dissolving 1 mg of peptide in phosphate buffer (**Ac-CGSGHYFNIF-NH_2** 337 µL, **Ac-CGSGKLVFFA-NH_2** 334 µL and **Ac-CGSG$(POG)_6$-NH_2** 227 µL). The peptide solution was then degassed with nitrogen for 10 minutes. 100 µL of 2.5 mM peptide solution was added to each DNA solution. The solutions were spun down mini centrifuge for 5 seconds, to ensure homogeneity of the solution and collect the total volume into the bottom of the tube. The oligonucleotide-peptide solutions were incubated at room temperature overnight, before being analysed by denaturing polyacrylamide gel electrophoresis (PAGE).

7.2.15: Oligonucleotide-Peptide Conjugation: Strain Promoted Alkyne Azide Click Chemistry (SPAAC)

A 100 µL each was taken from a 20 µM stock of **CO-A** and **CO-A'** respectively. To each 0.27 mg of azide peptide (**N_3-ILVAGK-COOH**, 0.0004 mmol) was added and directly dissolved. The solutions were spun down in a mini centrifuge for 5 seconds, to ensure homogeneity of the solution and collect the total volume into the bottom of the tube. The oligonucleotide – peptide solutions were incubated at 37 °C for 120 minutes in a thermocycler, before being analysed by denaturing PAGE.

7.2.16: Amine Oligonucleotide Activity Studies

Amine terminated oligonucleotide A was reacted with 5 k polyethylene glycol NHS ester (PEG NHS) and Traut's reagent to assess amine accessibility to modification. Five solutions of **A** were prepared from a 100 µM (0.0001 mmol) stock solution. Five (40 µL, 100 µM) were diluted to 50 µM with either pH 8 or 9 phosphate buffer and 100, 250 and 500 mM NaCl aqueous solution (40 µL). 5k PEG NHS (25 mg, 0.005 mmol 50 eqv) was directly dissolved in each solution. Mixtures were heated at 37 ˚C for 2 hours in a thermocycler before being cooled to RT and stored at 4 ˚C until analysis by denaturing PAGE. Two solutions of **A** were prepared from a 100 µM (0.0001 mmol) stock solution. **A** (40 µL, 100 µM) was diluted with water (40 µL) to a concentration of 50 µM. Traut's reagent of 10 (0.137 mg, 0.001 mmol) and 20 (0.275 mg, 0.002 mmol) equivalents were dissolved directly into

solutions of **A**. Mixtures were reacted at 37 ˚C for 2 hours in a thermocycler before being stored at 4 ˚C until treatment with 5k PEG maleimide (5 µL, 2 mM, overnight at RT) before analysis by denaturing PAGE.

7.2.17: Kaiser Test, Confirmation of the Presence of Primary Amines

Reagent A (1 mL (16.5 mg KCN in 25 mL H2O) in 49 mL pyridine). Reagent B (1.0 g ninhydrin in 20 mL butanol) and reagent C (40.0 g phenol in 20 mL butanol). 10 µL of 20 µM modified DNA solution was added to a vial and 2 drops of each reagent was also added. The vial was heated to 110 ˚C for 5 minutes. A colour change to dark blueish purple would indicate the presence of primary amines, confirming no modification of oligonucleotide with a linker, no colour change would indicate the successful conjugation of a linker to the oligonucleotide.

7.2.18: Oligonucleotide-4-FITC Thiol Time Course Studies

A solution of **A** (10 µM, 80 µL) and **A'** (10 µM, 80 µL) were added to PCR tubes. To these 80 µL of 10 x solution of FITC-SH (16 µL) in 8 M urea (64 µL) was added. These samples were heated at 37 ˚C in a thermocycler over 4 hours. Aliquots (20 µL) were removed and quenched with 100 mM iodoacetamide at the following time points: 5, 10, 20, 30, 60, 120, 180 and 240 minutes. Samples were stored at 4 ˚C before analysis by denaturing PAGE.

7.2.19: Maleimide Thiol Reactivity Studies

Proton NMR studies were conducted to assess the reactivity of maleimide compound with a thiol. Two concentrations of maleimide (6-maleimidohexanoic acid) were investigated (0.5 and 1 mol eqv) with a thiol (β–mercaptoethanol, BME) and a base (diisopropylethyl amine, DIPEA). Monitoring the disappearance of the peak at 6.7 ppm which represents the protons in the double bond of the maleimide ring; if a successful Michael addition occurs with a thiol this peak disappears. Maleimide acid (26.5 mg) and BME (17.6 µL) were premixed in a vial in a 0.5 : 1 mole ratio. DIPEA (21 µL, 0.5 mole) was added with 300 µL of deuterated chloroform then transferred into an NMR tube. ^{1}H 1D NMR spectra were taken at 0 and 48 hours.

7.2.20: Denaturing Polyacrylamide Gel Electrophoresis (PAGE)

A 5 mL 20 % denaturing polyacrylamide gel was prepared from a 20 % acrylamide / bis-acrylamide denaturing gel stock solution. Different concentrations can be prepared by diluting the stock with the relevant amount of buffer. To this 5 µL of TEMED and 10 µL of 40 % APS stock solution was added and mixed well. The gel was added to the cassette and a 10-well comb inserted; the gel was left to polymerise. Samples were prepared from cleaved oligomers in water (10 µL, 20 µM) and 8 M aqueous urea (10 µL). Samples were mixed well and centrifuged to ensure the sample was in the bottom of the tube. Once polymerised the well comb was removed from the cassette and the samples loaded (10 µL per well). The gel was placed into the inner chamber and placed within the gel tank. 1 x TBE buffer was added to the inner and outer chamber. The gel ran for 60 minutes at maximum volts and 15 mAmps. The gel was removed from the cassette and stained in Stains All (Fig. 7.13) gel stain (0.05 mg / mL in 50 : 50, formamide : 1 x TBE buffer) for a minimum of 1 hour. Stains All is a carbocyanine dye which interacts with biomolecules through electrostatic interactions and can intercalate with double stranded DNA.[163]

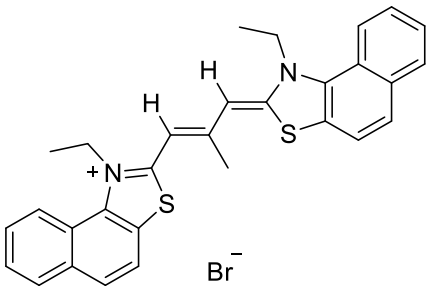

Figure 7.13: Structural illustration of the cationic carbocyanine dye Stains All, stabilised with the bromine anion.

7.2.21: Non-denaturing Native Tris Magnesium Acetate Polyacrylamide Gel Electrophoresis (TAMg-PAGE)

A 5 mL 12 % non-denaturing polyacrylamide gel was prepared from a 12 % acrylamide / bis-acrylamide gel stock solution (5 mL). Different concentrations can be prepared by diluting the stock with the relevant amount of buffer. To this 5 µL of TEMED and 10 µL of 40 % APS stock solution was

added and mixed well. The gel was added to the cassette and a 10 well comb inserted, the gel was left to polymerise. 10 µL of sample (10 µM) was mixed with its complement (10 µM) and 5 µL of glycerol. This was repeated for each sample. Controls were prepared from stocks of the individual oligomers (10 µL, 20 µM) without their complements, and glycerol (10 µL). All samples were thermocycled using a thermocycler using the following programme: Heated to 55 °C for 5 minutes then cooled to 35 °C for 30 minutes, and finally cooled to 4 °C and held there for 1 hour. 10 µL of each sample was loaded onto the gel. The gel ran at maximum volts (300 V), constant mAmps (15 mAmps per gel) for 90 minutes in 1 x TAMg buffer. The gel was removed from the cassette and stained in Stains-All gel stain (0.05 mg / mL in 50 : 50, formamide : 1 x TAMg buffer) for a minimum of 1 hour.

7.2.22: Fluorescein Isothiocyanate Polyacrylamide Gel Electrophoresis (FITC-PAGE)

The gel was prepared as above in 7.2.20. FITC-PAGE samples were prepared by diluting 10 µL of **4/CO-A** and **4/CO-A'** (20 µM) with 10 µL of 8 M urea (without FITC azide/SH) and mixed well. 10 µL of **4/CO-A** and **4/CO-A'** (20 µM) with 8 µL of 8 M urea solution and 2 µL of 10 µM FITC azide or FITC-SH solution and mixed well. FITC-SH samples were incubated at 37 ˚C overnight before analysis by gel. FITC-azide samples were incubated at room temperature overnight before analysis by gel. A control of **H_2N–A** / **A'** was prepared by diluting a 20 µM stock (10 µL) with 8 M urea solution (10 µL) and mixed well. A second control of 10 µM FITC azide solution was prepared by diluting a stock (100 µM, 2 µL) with 8M urea (8 µL). The polymerised gel was removed from the loading dock, wells labelled and placed into the running tank in 1 x TBE buffer (pH 8). The well comb was removed and 10 µL of each sample was loaded onto the gel. The gel ran for 60 minutes at constant mAmps (15 mAmps per gel) and maximum volts (300 V). The gel was imaged on a transilluminator then stained in stains all stain for a minimum of 1 hour.

7.2.23: Sodium Dodecyl Sulfate Polyacrylamide Gel Electrophoresis (SDS-PAGE)

An 8 mL 10 % polyacrylamide gel was prepared from a 40 % acrylamide / bis-acrylamide gel stock solution (2 mL), 1.5 M Tris HCl buffer (Lower Tris) (2 mL) and deionised water (3.8 mL). To this 8 µL of TEMED and 10 µL of 40 % APS stock solution was added and mixed well. The gel was pipetted into the cassette and a 10 well comb was inserted, the gel was left to polymerise. SDS-PAGE samples were prepared by diluting 10 µL of sample (20 µM) with 10 µL of SDS containing sample buffer and mixed well. This was repeated for each sample, the samples were heated at 90 °C for half an hour in a thermocycler. A control of **H_2N–A/A'** was prepared by diluting a 20 µM stock (10 µL) with SDS sample buffer (10 µL). The polymerised gel was removed from the loading dock, wells labelled and placed into the running tank in 1 x tris glycine running buffer (pH 8). The well comb was removed and 10 µL of DNA control was loaded onto the gel; followed by the samples. The gel ran for thirty minutes at constant volts (180 V) and 25 mAmps per gel. The gel was soaked in water for twenty minutes then stained in methylene blue stain for a minimum of thirty minutes.

7.2.24: Non-denaturing Native Sodium Tris Borate Polyacrylamide Gel Electrophoresis (NaB-PAGE)

A 5 mL 12 % PAGE was prepared from a 12 % stock solution of sodium borate PAGE stock. Different concentrations can be prepared by diluting the stock with the relevant amount of buffer. To this 5 µL of TEMED and 10 µL of 40 % APS stock solution was added and mixed well. The gel was added to the cassette and a 10 well comb inserted, the gel was left to polymerise. 10 µL of sample (10 µM) was mixed with its complement (10 µM) and 5 µL of glycerol. This was repeated for each sample. Controls were prepared from stocks of the individual oligomers (10 µL, 20 µM) without their complements and glycerol (10 µL). All samples were annealed using a thermocycler using the following programme: Heated to 55 °C for 5 minutes then cooled to 35 °C for 30 minutes, and finally cooled to 4 °C and held there for 1 hour. 10 µL of each sample was loaded onto the gel. The gel ran at maximum volts (300 V), constant mAmps (15 mAmps per gel) for 60 minutes in 1 x Na borate

buffer (50 mM NaCl). The gel was removed from the cassette and stained in Stains All gel stain (0.05 mg / mL in 50 : 50, formamide : 1 x Na Borate buffer) for a minimum of 1 hour.

7.2.25: Anion Exchange Resin Purification of DNA-peptide Conjugates

Anion exchange resin in 20 % EtOH (750 µL) was added to a centrifuge tube. The resin was span at 14.8 RPM for 1 minute to collect the resin into the bottom. The supernatant was removed and discarded. To this 750 µL of autoclaved DI water was added to the resin, mixed and span at 14.8 RPM for 1 minute. The supernatant was then removed and discarded this was repeated three more times. To the clean resin 750 µL of **ILVAGK-DNA** was added and mixed. The resin was incubated at RT for two hours. The resin was centrifuged at 14800 RPM for 1 minute and the supernatant collected into fraction 1. The resin was washed with 8M Urea (zero salt) for two hours and then centrifuged at 14800 RPM for 1 minute. The supernatant was collected as fraction 2, this was repeated once more and collected as fraction 3. Autoclaved DI water (1000 µL) was added to the resin, mixed and centrifuged at 14.8 RPM for 1 minute. The supernatant was collected and labelled as fraction 4. This was repeated once more, and these fractions analysed by UV-Vis for presence of peptide. NaCl (0.6 M, 750 µL) in autoclaved DI water was added to the resin and incubated overnight at 4°C. The resin was brought to room temperature. The resin was then centrifuged at 14800 RPM for 1 minute, the supernatant was collected and labelled fraction 6. The above was repeated 4 times and collected as fractions 7 to 10.

7.3: Experimental Methods and Instrumentation for Chapters 3, 4, and 5

7.3.1: Chapter 3 Sample Preparation

A sample of 20 µM **ILVAGK** in 500 µL of filtered TAMg was prepared by diluting a 1 mM (10 µL) stock of **ILVAGK** with 490 µL of filtered TAMg buffer. A 20 µM solution of **A-ILVAGK** was prepared from a stock (42.5 µM, 235.3 µL) diluted to 500 µL with filtered TAMg buffer. The two were combined to give the 100 % (1:1) 10 µM solution. This method was repeated to yield 50 % (1:0.5, 117.7 µL **A-ILVAGK** stock), 10 % (1:0.1, 23.5 µL **A-ILVAGK** stock) and 1 % (1:0.01, 2.4 µL **A-ILVAGK** stock).

Samples were stored at room temperature; in the dark and in 200 µL aliquots. Aliquots were extracted at 0, 7, 14, 21 and 28 days of aging for AFM, aliquots were further analysed by DLS and CD. CD data is missing for 21 and 28 days of aging due to university enforced Covid-19 lab shutdown.

7.3.2: Chapter 4 Sample Preparation

Three 500 µL samples of; 20 µM (143.8 µL), 40 µM (287.8 µL) and 60 µM (431.6 µL) were prepared from a 69.5 µM stock of **A-ILVAGK** in filtered TAMg buffer. A 500 µL, 20 µM sample of **A'** was prepared from a 1 mM (10 µL) stock in filtered TAMg buffer and added to the 20 µM sample of **A-ILVAGK**. A 500 µL, 20 µM sample of **2A'** was prepared from a 666.7 µM (15 µL) stock in filtered TAMg buffer and added to the 40 µM sample of **A-ILVAGK**. A 500 µL, 20 µM sample of **3A'** was prepared from a 625 µM (16 µL) stock in filtered TAMg buffer and added to the 60 µM sample of **A-ILVAGK**. The samples were annealed in a thermocycler by the following program: 55 °C for 10 mins, 35 °C for 20 mins, cool to 4 °C. Samples were analysed by native PAGE (TAMg buffer, section 7.2.21) to assess successful hybridisation of the DNA double helix. Samples were stored at room temperature; in the dark and in 200 µL aliquots. Aliquots were extracted at 0, 7, 14, 21 and 28 days of aging for AFM, aliquots were further analysed by DLS and CD. CD data is missing for 21 and 28 days of aging due to university enforced Covid-19 lab shutdown.

7.3.3: Chapter 5 Sample Preparation

A 10 % w/v solution of sodium dodecyl sulphate (SDS) was prepared in filtered autoclaved DI water. A 1 % solution of SDS was prepared by diluting 5 mL of 10 % solution with 45 mL of filtered autoclaved DI water. The 1 % solution was then filtered to remove particulates.

A 500 µL, 20 µM solution of **A'-ILVAGK** was prepared from a 42.5 µM stock by diluting 235.3 µL of **A'-ILVAGK** with 264.7 µL of 1 % SDS in filtered autoclaved DI water. A 500 µL, 20 µM sample of **A** was prepared from a 100 µM (100 µL) stock in 1 % SDS buffer and added to the 20 µM sample of **A'-ILVAGK**. The sample was annealed in a thermocycler by the following program: 55 °C for 10 mins, 35 °C for 20 mins, cool to 4 °C. A sample of 10 µM **ILVAGK** in 1000 µL of filtered 1 % SDS buffer was

prepared by diluting a 1 mM (10 µL) stock of **ILVAGK** with 990 µL of filtered 1 % SDS buffer. As samples were prepared from stocks in 1 % SDS solution final SDS concentration varies between 0.95 and 0.64 %. Samples were analysed by TAMg PAGE to assess successful hybridisation of the DNA double helix (Fig. 5.2). Samples were stored at room temperature; in the dark and in 200 µL aliquots. Aliquots were extracted at 0, 7, 14, 21 and 28 days of aging for AFM, aliquots were further analysed by DLS and CD. DLS and CD data is missing for 14 and 21 days of aging due to university enforced Covid-19 lab shutdown.

7.3.4: Chapter 3 and 4 Control Sample Preparation

A 500 µL 20 µM solution of **A-T5** was prepared from a 100 µM stock by diluting 100 µL of **A-T5** with 400 µL of TAMg buffer. A 500 µL 20 µM solution of **A'-T5** was prepared from a 100 µM stock by diluting 100 µL of **A'-T5** with 400 µL of filtered TAMg buffer solution. The two were combined and annealed in a thermocycler by the following program: 55 °C for 10 mins, 35 °C for 20 mins, cool to 4 °C. Two 1000 µL, 10 µM samples were prepared from 100 µM stocks of **A-T5** and **A'-T5** by diluting 50 µL with 950 µL of TAMg buffer. A 10 µM sample of **ILVAGK** was prepared from a 1 mM stock by diluting 10 µL with 990 µL of filtered TAMg buffer. Samples were stored at room temperature; in the dark and in 200 µL aliquots. Aliquots were extracted at 0, 7, 14, 21 and 28 days of aging for AFM, aliquots were further analysed by DLS and CD. CD data is missing for 21 and 28 days of aging due to university enforced Covid-19 lab shutdown.

7.3.5: Chapter 5 Control Sample Preparation

A 500 µL 20 µM solution of **A-T5** was prepared from a 100 µM stock by diluting 100 µL of **A-T5** with 400 µL of 1 % SDS buffer. A 500 µL 20 µM solution of **A'-T5** was prepared from a 100 µM stock by diluting 100 µL of **A'-T5** with 400 µL of 1 % SDS solution. The two were combined and annealed in a thermocycler by the following program: 55 °C for 10 mins, 35 °C for 20 mins, cool to 4 °C. Two 1000 µL, 10 µM samples were prepared from 100 µM stocks by diluting 50 µL with 950 µL of 1 % SDS buffer. Samples were stored at room temperature; in the dark and in 200 µL aliquots. Aliquots

were extracted at 0, 7, 14, 21 and 28 days of aging for AFM, aliquots were further analysed by DLS and CD. DLS and CD data is missing for 14 and 21 days of aging due to Covid-19 related isolation.

7.3.6: Dynamic Light Scattering (DLS)

A 200 µL aliquot was extracted from each sample as prepared in sections 7.1.1-7.1.4 at 0, 7, 14, 21 and 28 days of aging then measured by the following method. Analysis was carried out on a Malvern Zetasizer Nano ZS, using a small volume quartz cuvette (200 µL). The sample was equilibrated to 25 °C before 3 runs of 11 consecutive scans which were averaged by the software. All samples were prepared with filtered buffer solutions, but not further filtered after self-assembly studies begun.

7.3.7: Circular Dichroism (CD)

A 200 µL aliquot was extracted from each sample as prepared in sections 7.1.1-7.1.4 at 0, 7, 14, 21 and 28 days of aging then measured by the following method. Circular dichroism measurements were recorded using a Jasco J-715 spectropolarimeter, with temperature control provided by a NesLab RTE-111 circulating chiller operating at 20 ± 0.05 °C. Spectra were recorded in a 0.2 cm pathlength quartz cell, maintaining consistent cell orientation. Specific parameters; sensitivity: standard [100 mdeg], scan range: 300-190 nm, data pitch: 1 nm, scan mode: continuous, scan speed: 100nm/min, response: 0.5 sec, band width: 2.0 nm, and accumulation: 4. Spectra were averaged over 20 readings, and subsequently smoothed using 3-point median smoothing in excel.

7.3.8: Atomic Force Microscopy (AFM)

A 200 µL aliquot was extracted from each sample as prepared in sections 7.1.1-7.1.4 at 0, 7, 14, 21 and 28 days of aging then prepared and measured by the following method. Mica was cleaved with tape until a smooth surface was achieved (no loose leaves of mica, or inconsistent reflection on the surface.. Sample was deposited onto freshly cleaved mica (20 µL of 10 µM). The samples were incubated for 30 minutes at room temperature, then wicked off using filter paper. The surfaces were then washed with 750 µL filtered autoclaved DI water (not in direct deposition on surface) at an angle, excess water was removed using filter paper and samples dried under nitrogen for 2

minutes. Samples were stored in a petri dish with lid at room temperature. Measurements were conducted on a Bruker Multi-Mode microscope with a Quadrexed Nanoscope III controller using Bruker ScanAsyst-Air silicon tip on nitride lever, with frequency of 70 Hz. Data was analysed using Nanoscope Analysis 1.5 software (Bruker, CA, US). Mica discs, 10 mm were purchased from Agar Scientific.

7.3.9: Non-denaturing Native Tris Magnesium Acetate Polyacrylamide Gel Electrophoresis (TAMg-PAGE)

A 5 mL 12 % non-denaturing polyacrylamide gel was prepared from a 12 % acrylamide / Bis-acrylamide gel stock solution (5 mL). Different concentrations can be prepared by diluting the stock with the relevant amount of buffer. To this 5 µL of TEMED and 10 µL of 40 % APS stock solution was added and mixed well. The gel was added to the cassette and a 10 well comb inserted, the gel was left to polymerise. 10 µL of sample (20 µM) was mixed with its complement (20 µM) and 5 µL of glycerol. This was repeated for each sample. Controls were prepared from stocks of the individual oligomers (10 µL, 20 µM) without their complements and glycerol (10 µL). All samples were heat cooled using a thermocycler using the following programme: Heated to 55 °C for 5 minutes then cooled to 35 °C for 30 minutes, and finally cooled to 4 °C and held there for 1 hour. 10 µL of each sample was loaded onto the gel. The gel ran at maximum volts (300 V), constant mAmps (15 mAmps per gel) for 90 minutes in TAMg buffer. The gel was removed from the cassette and stained in Stains All gel stain (0.05 mg / mL in 50 : 50, formamide : TAMg buffer) for a minimum of 1 hour. The gel was imaged on a document scanner. Images were enhanced using GIMP 2.10.8 imaging software, only to enhance contrast and colour.

8.0: References

1 L. P. Datta, S. Manchineella and T. Govindaraju, Biomolecules-derived Biomaterials, *Biomaterials*, 2020, 230, 119633.

2 K. N. Ganesh and Y. Krishnan, Nucleic Acids – Chemistry and Applications, *Journal of Organic Chemistry*, 2013, 78, 12283–12287.

3 S. Minchin and J. Lodge, Understanding biochemistry: Structure and Function of Nucleic Acids, *Essays in Biochemistry*, 2019, 63, 433–456.

4 Y. Suzuki, M. Endo and H. Sugiyama, Mimicking Membrane-Related Biological Events by DNA Origami Nanotechnology, *ACS Nano*, 2015, 9, 3418–3420.

5 C. Lou, M. C. Martos-Maldonado, C. S. Madsen, R. P. Thomsen, S. R. Midtgaard, N. J. Christensen, J. Kjems, P. W. Thulstrup, J. Wengel and K. J. Jensen, Peptide-oligonucleotide Conjugates as Nanoscale Building Blocks for Assembly of an Artificial Three-helix Protein Mimic, *Nature Communications*, 2016, 7, 12294.

6 P. O'Donoghue, J. Ling and D. Söll, Transfer RNA Function and Evolution, *RNA Biology*, 2018, 15, 423–426.

7 Jan. Barciszewski and B. F. C. Clark, *RNA Biochemistry and Biotechnology*, Springer Netherlands, 2012.

8 M. Asif, M. Akram, H. M. Asif, M. Uzair, N. Akhtar, A. Madni and S. M. A. Shah, Amino Acids: A review article, *Journal of medicinal plants research*, 2011, 5, 3997–4000.

9 C. J. C. Edwards-Gayle and I. W. Hamley, Self-assembly of Bioactive Peptides, Peptide Conjugates, and Peptide Mimetic Materials, *Organic and Biomolecular Chemistry*, 2017, 15, 5867–5876.

10 N. Stephanopoulos, Peptide−Oligonucleotide Hybrid Molecules for Bioactive Nanomaterials, *Bioconjugate Chemistry*, 2019, 1915–1922.

11 K. Lu, Q. P. Duan, L. Ma and D. X. Zhao, Chemical Strategies for the Synthesis of Peptide-Oligonucleotide Conjugates, *Bioconjugate Chemistry*, 2010, 21, 187–202.

12 T. Macculloch, A. Buchberger and N. Stephanopoulos, Emerging Applications of Peptide–oligonucleotide Conjugates: Bioactive Scaffolds, Self-assembling Systems, and Hybrid Nanomaterials, *Organic and Biomolecular Chemistry*, 2019, 17, 1668–1682.

13 M. Akbarian, A. Khani, S. Eghbalpour and V. N. Uversky, Bioactive Peptides: Synthesis, Sources, Applications, and Proposed Mechanisms of Action, *International Journal of Molecular Sciences*, 2022, 23, 1445.

14 R. Perlikowska, J. Silva, C. Alves, P. Susano and R. Pedrosa, The Therapeutic Potential of Naturally Occurring Peptides in Counteracting SH-SY5Y Cells Injury, *International Journal of Molecular Sciences*, 2022, 23, 11778.

15 M. Varga, Fabrication and Self-Assembly of Nanobiomaterials: Applications of Nanobiomaterials, Volume 1, Chapter 3, Self-assembly of Nanobiomaterials, William Andrew Publishing, 2016, 57–90.

16 G. M. Whitesides and M. Boncheva, *Beyond Molecules: Self-assembly of Mesoscopic and Macroscopic Components*, *Proceedings of the National Academy of Sciences*, 2002, 99, 4769-4774.

17 W. George and G. Bartosz, Self-Assembly at All Scales, *Science*, 2002, 295, 2418–2421.

18 L. Wang, C. Gong, X. Yuan and G. Wei, Controlling the Self-assembly of Biomolecules into Functional Nanomaterials Through Internal Interactions and External Stimulations: A Review, *Nanomaterials*, 2019, 9, 285.

19 A. Scacchi, S. J. Nikkhah, M. Sammalkorpi and T. Ala-Nissila, Self-assembly in soft matter with multiple length scales, *Physical Review Research*, 2021, 3.

20 P. Ball, *Synthetic Biology-Engineering Nature to make materials*, 2018, *Materials Research Society Bulletin*, 43, 477-484.

21 A. Jain, S. Dhiman, A. Dhayani, P. K. Vemula and S. J. George, Chemical Fuel-driven Living and Transient Supramolecular Polymerization, *Nature Communications*, 10, 450, 2019.

22 C. Guindani, L. C. da Silva, S. Cao, T. Ivanov and K. Landfester, Synthetic Cells: From Simple Bio-Inspired Modules to Sophisticated Integrated Systems, *Angewandte Chemie - International Edition*, 2022, 61, 16.

23 S. I. Stupp and L. C. Palmer, Supramolecular Chemistry and Self-Assembly in Organic Materials Design, *Chemistry of Materials*, 2014, 26, 1, 507-518.

24 D. Lombardo, P. Calandra, L. Pasqua and S. Magazù, Self-assembly of Organic Nanomaterials and Biomaterials: The Bottom-Up Approach for Functional Nanostructures Formation and Advanced Applications., *Materials (Basel)*, 2020, 13, 5, 1048.

25 S. I. Stupp, R. H. Zha, L. C. Palmer, H. Cui and R. Bitton, *Self-Assembly of Biomolecular Soft Matter*, *Farady Discussions*, 2013, 166, 9, 30.

26 J. L. England, Dissipative adaptation in Driven Self-assembly, *Nature Nanotechnology*, 2015, 10, 919-923.

27 Y.-D. Yang, X.-L. Chen, J. L. Sessler and H.-Y. Gong, Emergent Self-Assembly of a Multicomponent Capsule via Iodine Capture, *Journal of the American Chemical Society*, 2021, 143, 5, 2315-2324.

28 D. Mandal, A. Nasrolahi Shirazi and K. Parang, Self-assembly of Peptides to Nanostructures, *Organic and Biomolecular Chemistry*, 2014, 12, 3544–3561.

29 Q. Li, Y. Jia, L. Dai, Y. Yang and J. Li, Controlled Rod Nanostructured Assembly of Diphenylalanine and Their Optical Waveguide Properties, *American Chemical Society Nano*, 2015, 9, 3, 2689–2695.

30 P. Li, X. Chen and W. Yang, Graphene-induced Self-assembly of Peptides into Macroscopic-Scale Organized Nanowire Arrays for Electrochemical NADH sensing, *Langmuir*, 2013, 29, 8629–8635.

31 M. Deluca, Z. Shi, C. E. Castro and G. Arya, Dynamic DNA Nanotechnology: Toward Functional Nanoscale Devices, *Nanoscale Horizons*, 2020, 5, 182–201.

32 A. P. de Alba Ortíz, J. Vreede and B. Ensing, Sequence Dependence of Transient Hoogsteen Base Pairing in DNA, *Public Library of Science Computational Biology*, 2022, 18.

33 D. Mariottini, A. Idili, A. Valleé-Beíisle, K. W. Plaxco and F. Ricci, A DNA Nanodevice That Loads and Releases a Cargo with Hemoglobin-Like Allosteric Control and Cooperativity, American Chemical Society Nano Letters, 2017, 17, 5, 3225-3230.

34 D. Ghosh, L. P. Datta and T. Govindaraju, Molecular architectonics of DNA for functional nanoarchitectures, *Beilstein Journal of Nanotechnology*, 2020, 9, 11, 124–140.

35 J. Spiegel, S. Adhikari and S. Balasubramanian, The Structure and Function of DNA G-Quadruplexes, *Trends in Chemistry*, 2020, 2, 123–136.

36 P. L. Scognamiglio, C. Vicidomini and G. N. Roviello, Dancing with Nucleobases: Unveiling the Self-Assembly Properties of DNA and RNA Base-Containing Molecules for Gel Formation, *Gels*, 2023, 10, 16.

37 E. Winfree, F. Liu, L. A. Wenzler and N. C. Seeman, Design and Self-assembly of Two-dimensional DNA Crystals, *Nature*, 1998, 394, 539–544.

38 P. W. K. Rothemund, Folding DNA to Create Nanoscale Shapes and Patterns, *Nature*, 2006, 440, 297–302.

39 H. Ijäs, S. Nummelin, B. Shen, M. A. Kostiainen and V. Linko, Dynamic DNA Origami Devices: from Strand-Displacement Reactions to External-Stimuli Responsive Systems, *International Journal of Molecular Sciences*, 2018, 19, 7, 2114.

40 A. Alisha Arora, C. de Silva and A. Seifalian, Beyond the Smiley Face: Applications of Structural DNA Nanotechnology, *Nanotechnology Reviews*, 2018, 9, 1, 1430976.

41 D. Han, S. Pal, J. Nangreave, Z. Deng, Y. Liu and H. Yan, DNA Origami with Complex Curvatures in Three-dimensional Space, *Science (1979)*, 2011, 332, 342–346.

42 S. M. Douglas, H. Dietz, T. Liedl, B. Hogberg, F. Graf and W. M. Shih, Self-assembly of DNA into Nanoscale Three-dimensional Shapes, *Nature*, 2009, 459, 414–418.

43 L. Liu, Z. Li, Y. Li and C. Mao, Rational Design and Self-Assembly of Two-Dimensional, Dodecagonal DNA Quasicrystals, *Journal of the American Chemical Society*, 2019, 141, 4248–4251.

44 B. Wei, M. Dai and P. Yin, Complex Shapes Self-assembled from Single-stranded DNA Tiles, *Nature*, 2012, 485, 623–626.

45 Y. Ke, L. L. Ong, W. M. Shih and P. Yin, Three-dimensional Structures Self-assembled From DNA Bricks, *Science*, 2012, 338, 1177–83.

46 B. Ji, J. Song, D. Wang, A. Kenaan, Q. Zhu, J. Wang, S. M. Sønderskov and M. Dong, Room Temperature Study of Seeding Growth on Two-Dimensional DNA Nanostructure, *Langmuir*, 2019, 35, 4140–4145.

47 S. M. Douglas, I. Bachelet and G. M. Church, A Logic-Gated Nanorobot for Targeted Transport of Molecular Payloads, *Science (1979)*, 2012, 335, 831–834.

48 Y. Xing, B. Liu, J. Chao and L. Wang, DNA-based Nanoscale Walking Devices and Their Applications, *Royal Society of Chemistry Advances*, 2017, 7, 47425–47434.

49 O. Birkholz, J. R. Burns, C. P. Richter, O. E. Psathaki, S. Howorka and J. Piehler, Multi-functional DNA Nanostructures that Puncture and Remodel Lipid Membranes into Hybrid Materials, *Nature Communications*, 2018, 9, 1521.

50 D. Y. Tam, X. Zhuang, S. W. Wong and P. K. Lo, Photoresponsive Self-Assembled DNA Nanomaterials: Design, Working Principles, and Applications, *Small*, 2019, 115, 26, 18054811.

51 H. Yang, K. L. Metera and H. F. Sleiman, DNA Modified with Metal Complexes: Applications in the Construction of Higher Order Metal–DNA Nanostructures, *Coordination Chemistry Review*, 2010, 254, 2403–2415.

52 S. P. W. Wijnands, E. W. Meijer and M. Merkx, DNA-Functionalized Supramolecular Polymers: Dynamic Multicomponent Assemblies with Emergent Properties, *Bioconjugate Chemistry*, 2019, 30, 1905–1914.

53 A. M. Peterson and J. M. Heemstra, Controlling self-assembly of DNA-polymer Conjugates for Applications in Imaging and Drug Delivery, *Wiley Interdisciplinary Reviews. Nanomedicine and Nanobiotechnology*, 2015, 7, 3, 282–297.

54 Y. Guo, J. Zhang, F. Ding, G. Pan, J. Li, J. Feng, X. Zhu and C. Zhang, Stressing the Role of DNA as a Drug Carrier: Synthesis of DNA–Drug Conjugates through Grafting Chemotherapeutics onto Phosphorothioate Oligonucleotides, *Advanced Materials*, 2019, 31, 16, 1807533.

55 N. Avakyan, A. A. Greschner, F. Aldaye, C. J. Serpell, V. Toader, A. Petitjean and H. F. Sleiman, Reprogramming the Assembly of Unmodified DNA with a Small Molecule, *Nature Chemistry*, 2016, 8, 368–376.

56 L. Zhang, R. Abdullah, X. Hu, H. Bai, H. Fan, L. He, H. Liang, J. Zou, Y. Liu, Y. Sun, X. Zhang and W. Tan, Engineering of Bioinspired, Size-Controllable, Self-Degradable Cancer-Targeting DNA Nanoflowers via the Incorporation of an Artificial Sandwich Base, *Journal of the American Chemical Society*, 2019, 141, 4282–4290.

57 N. Gour, J. N. Abraham, M. Chami, A. Castillo, S. Verma and C. Vebert-Nardin, Label-free, Optical Sensing of the Supramolecular Assembly into Fibrils of a Ditryptophan-DNA Hybrid, *Chemical Communications*, 2014, 50, 6863–6865.

58 I. M. A. del Mundo, K. M. Vasquez and G. Wang, Modulation of DNA Structure Formation using Small Molecules, *Biochimica et Biophysica Acta (BBA) - Molecular Cell Research*, 2019, 1866, 118539.

59 H. Cheng, C. Qin, B. Yang, X. Hu, M. Gatheru Waigi, G. K. Vasilyeva and Y. Gao, Non-covalent binding interaction between phthalic acid esters and DNA, *Environment International*, 2022, 161, 107095.

60 S. Dasari and P. Bernard Tchounwou, Cisplatin in Cancer Therapy: Molecular Mechanisms of Action, *European Journal of Pharmacology*, 2014, 740, 364–378.

61 B. J. Pages, D. L. Ang, E. P. Wright and J. R. Aldrich-Wright, Metal Complex Interactions with DNA, *Dalton Transactions*, 2015, 44, 3505-3526.

62 K. Suntharalingam, O. Mendoza, A. A. Duarte, D. J. Mann and R. Vilar, A Platinum Complex that Binds Non-covalently to DNA and Induces Cell Death via a Different Mechanism than Cisplatin, *Metallomics*, 2013, 5, 514-523.

63 Lu DF, Wang YS, Li C, Wei GJ, Chen R, Dong DM, Yao M. Actinomycin D Inhibits Cell Proliferations and Promotes Apoptosis in Osteosarcoma Cells, *International Journal of Clinical and Experimental Medicine,* 2015, 8, 1904–1911.

64 A. A. Almaqwashi, T. Paramanathan, I. Rouzina and M. C. Williams, Mechanisms of Small Molecule–DNA Interactions Probed by Single-molecule Force Spectroscopy, *Nucleic Acids Research*, 2016, 44, 3971–3988.

65 H. M. Sobell, Actinomycin and DNA transcription, *Proceedings of the National Academy of Sciences USA*, 1985, 82, 5328–5331.

66 B. J. Pages, K. B. Garbutcheon-Singh and J. R. Aldrich-Wright, Platinum Intercalators of DNA as Anticancer Agents, *European Journal of Inorganic Chemistry*, 2017, 12, 1613–1624.

67 N. Kosiol, S. Juranek, P. Brossart, A. Heine and K. Paeschke, G-quadruplexes: A Promising Target for Cancer Therapy, *Molecular Cancer 2021 20, 1*, 2021, 20, 1–18.

68 J. Mitteaux, P. Lejault, F. Wojciechowski, A. Joubert, J. Boudon, N. Desbois, C. P. Gros, R. H. E. Hudson, J. B. Boulé, A. Granzhan and D. Monchaud, Identifying G-Quadruplex-DNA-Disrupting Small Molecules, *Journal of the American Chemical Society*, 2021, 143, 12567–12577.

69 F. Jia, H. Li, R. Chen and K. Zhang, Self-Assembly of DNA-Containing Copolymers, *Bioconjugate Chemistry*, 2019, 30, 7, 1880-1888.

70 B. de Lambert, C. Chaix, M.-T. Charreyre, A. Laurent, A. Aigoui, A. Perrin-Rubens and C. Pichot, Polymer-Oligonucleotide Conjugate Synthesis from an Amphiphilic Block Copolymer. Applications to DNA Detection on Microarray, *Bioconjugate Chemistry*, 16, 2, 265-274.

71 C. J. Whitfield, M. Zhang, P. Winterwerber, Y. Wu, D. Y. W. Ng and T. Weil, Functional DNA−Polymer Conjugates, *Chemical Reviews*, 2021, 121, 18, 11030-11084.

72 K. Liu, G. Du, M. Zhao, L. Ye, H. Shen, L. Jiang, K. Liu, G. Du, M. Zhao, L. Ye, H. Shen and L. Jiang, A Polymer-based Probe for Specific Discrimination of Cysteine, *Organic Biomolecular Chem*istry, 2016, 14, 1–372.

73 P. Wei, X. Yan and F. Huang, Supramolecular Polymers Constructed by Orthogonal Self-assembly Based on Host–guest and Metal–ligand Interactions, *Chemical Society Reviews*, 2015, 44, 815–832.

74 P. De, M. Li, S. R. Gondi and B. S. Sumerlin, Temperature-regulated Activity of Responsive Polymer-protein Conjugates Prepared by Grafting-from via RAFT Polymerization, *Journal of the American Chemical Society*, 2008, 130, 11288–11289.

75 L. A. Arkinstall, J. T. Husband, T. R. Wilks, J. C. Foster and R. K. O'reilly, DNA-polymer Conjugates via the Graft-through Polymerisation of Native DNA in Water, *Chemical Communications*, 2021, 57, 5466-5469.

76 T. Lückerath, T. Strauch, K. Koynov, C. Barney-Kowollik, D. Y. W. Ng and T. Weil, DNA-Polymer Conjugates by Photoinduced RAFT Polymerization, *Biomacromolecules*, 2019, 20, 212–221.

77 Y. Vyborna, M. Vybornyi and R. Häner, Functional DNA-grafted Supramolecular Polymers – Chirality, Cargo Binding and Hierarchical Organization, *Chemical Communications*, 2017, 53, 5179–5181.

78 F. Jia, X. Lu, X. Tan and K. Zhang, Facile Synthesis of Nucleic Acid–polymer Amphiphiles and their Self-assembly, *Chemical Communications*, 2015, 51, 7843–7846.

79 X. Zhu, H. Ye, J.-W. Liu, R.-Q. Yu and J.-H. Jiang, Multivalent Self-Assembled DNA Polymer for Tumor-Targeted Delivery and Live Cell Imaging of Telomerase Activity, *Analytical Chemistry*, 2018, 90, 22, 13188-13192.

80 X. Xu, P. Winterwerber, · David Ng and · Yuzhou Wu, DNA-Programmed Chemical Synthesis of Polymers and Inorganic Nanomaterials, *Topics in Current Chemistry*, 2020, 378, 31.

81 N. Alleva, P. Winterwerber, C. J. Whitfield, D. Ng and T. Weil, *ChemRxiv*, 2022. This content is a preprint and has not been peer-reviewed, DOI:10.26434/CHEMRXIV-2022-6LVGB. Accessed 11/01/2024 at https://chemrxiv.org/engage/chemrxiv/article-details/6250071985d81407b401b1e1

82 Y. Loo, A. Lakshmanan, M. Ni, L. L. Toh, S. Wang and C. A. E. Hauser, Peptide Bioink: Self-Assembling Nanofibrous Scaffolds for Three-Dimensional Organotypic Cultures, *Nanotechnology Letters*, 2015**,** 15, 6919–6925.

83 A. A. Vinogradov, Y. Yin and H. Suga, Macrocyclic Peptides as Drug Candidates: Recent Progress and Remaining Challenges, *Journal of the American Chemical Society*, 2019, 141, 10, 4167–4181.

84 M. Rivas, L. J. del Valle, C. Alemán and J. Puiggalí, Peptide self-assembly into Hydrogels for Biomedical Applications Related to Hydroxyapatite, *Gels*, 2019, 5, 1–29.

85 N. Yadav, M. K. Chauhan and V. S. Chauhan, Short to Ultrashort Peptide-based Hydrogels as a Platform for Biomedical Applications, *Biomaterials Science*, 2019, 8, 84.

86 K. Kulkarni, N. Habila, M. P. del Borgo and M. I. Aguilar, Novel materials from the Supramolecular Self-assembly of Short Helical β3-peptide Foldamers, *Frontiers of Chemical Science and Engineering*, 2019, 7, 1–12.

87 J. Chen and X. Zou, Self-assemble Peptide Biomaterials and their Biomedical Applications, *Bioactive Materials*, 2019, 4, 120–131.

88 Q. Shao, K. M. Wong, D. T. Seroski, Y. Wang, R. Liu, A. K. Paravastu, G. A. Hudalla and C. K. Hall, Anatomy of a Selectively Coassembled β-sheet Peptide Nanofiber, *Proceedings of the National Academy of Sciences*, 2020, 117, 4710–4717.

89 F. Thomas, N. C. Burgess, A. R. Thomson and D. N. Woolfson, Controlling the Assembly of Coiled-coil Peptide Nanotubes, *Angewandte Chemie - International Edition*, 2016, 55, 987–991.

90 Y. Xu and M. Kirchner, Collagen Mimetic Peptides, *Bioengineering*, 2021, 8, 1–24.

91 J. Qin, T. Luo and K. L. Kiick, Self-Assembly of Stable Nanoscale Platelets from Designed Elastin-like Peptide-Collagen-like Peptide Bioconjugates, *Biomacromolecules*, 2019, 20, 1514–1521.

92 L. Wang, N. Wang, W. Zhang, X. Cheng, Z. Yan, G. Shao, X. Wang, R. Wang and C. Fu, Therapeutic Peptides: Current Applications and Future Directions, *Signal Transduction and Targeted Therapy*, 2022, 48, 7.

93 K. Fosgerau and T. Hoffmann, Peptide Therapeutics: Current Status and Future Directions, *Drug Discovery Today*, 2015, 20, 122-128.

94 R. He, B. Finan, J. P. Mayer, R. D. Dimarchi, H. Mosberg, T. Sawyer and C. Haskell-Luevano, Peptide Conjugates with Small Molecules Designed to Enhance Efficacy and Safety, *Molecule*s, 2019, 24, 10, 1855.

95 T. Fan, X. Yu, B. Shen and L. Sun, Peptide Self-Assembled Nanostructures for Drug Delivery Applications, Journal of Nanomaterials, 2017.

96 N. Stephanopoulos, Peptide-oligonucleotide Hybrid Molecules for Bioactive Nanomaterials, *Bioconjugate Chemistry*, 2019, 30, 1915–1922.

97 A. Buchberger, C. R. Simmons, N. E. Fahmi, R. Freeman and N. Stephanopoulos, Hierarchical Assembly of Nucleic Acid/Coiled-Coil Peptide Nanostructures, *Journal of the American Chemical Society*, 2020, 142, 1406–1416.

98 M. Kye and Y. B. Lim, Reciprocal Self-Assembly of Peptide–DNA Conjugates into a Programmable Sub-10-nm Supramolecular Deoxyribonucleoprotein, *Angewandte Chemie - International Edition*, 2016, 55, 12003–12007.

99 M. L. Daly, Y. Gao and R. Freeman, Encoding Reversible Hierarchical Structures with Supramolecular Peptide-DNA Materials, *Bioconjugate Chemistry*, 2019, 30, 1864–1869.

100 T. Jiang, T. A. Meyer, C. Modlin, X. Zuo, V. P. Conticello and Y. Ke, Structurally Ordered Nanowire Formation from Co-Assembly of DNA Origami and Collagen-Mimetic Peptides, *Journal of the American Chemical Society*, 2017, 139, 14025–14028.

101 D. Datta, O. Tiwari and M. K. Gupta, Self-Assembly of Diphenylalanine-Peptide Nucleic Acid Conjugates, *American Chemical Society Omega*, 2019, 4, 10715–10728.

102 A. D. Merg, R. V Thaner, S. Mokashi-Punekar, S. T. Nguyen and N. L. Rosi, Triblock Peptide-oligonucleotide Chimeras (POCs): Programmable Biomolecules for the Assembly of Morphologically Tunable and Responsive Hybrid Materials, *Chemical Communications*, 2017, 53, 12221–12224.

103 S. Biswas, W. Song, C. Borges, S. Lindsay and P. Zhang, Click Addition of a DNA Thread to the N-Termini of Peptides for Their Translocation Through Solid-State Nanopores, *American Chemical Society Nano*, 2015, 9, 9652–9664.

104 N. Stephanopoulos, R. Freeman, H. A. North, S. Sur, S. J. Jeong, F. Tantakitti, J. A. Kessler and S. I. Stupp, Bioactive DNA-Peptide Nanotubes Enhance the Differentiation of Neural Stem Cells into Neurons, Journal of the American Chemical Society Nanotechnology Letters, 2015, 15, 1, 603-609.

105 F. Zhang, J. Nangreave, Y. Liu and H. Yan, Structural DNA Nanotechnology: State of the Art and Future Perspective, *Journal of the American Chemical Society*, 2014, 136, 11198–11211.

106 N. C. Seeman, An Overview of Structural DNA Nanotechnology, *Molecular Biotechnology*, 2007, 37, 246–257.

107 J. Zheng, J. J. Birktoft, Y. Chen, T. Wang, R. Sha, P. E. Constantinou, S. L. Ginell, C. Mao and N. C. Seeman, From Molecular to Macroscopic via the Rational Design of a Self-assembled 3D DNA Crystal, *Nature*, 2009, 461, 74–77.

108 Y. Ke, J. Sharma, M. Liu, K. Jahn, Y. Liu and H. Yan, Scaffolded DNA Origami of a DNA Tetrahedron Molecular Container, *Nanotechnology Letters*, 2009, 9, 2445–2447.

109 H. Zhang, J. Chao, D. Pan, H. Liu, Q. Huang and C. Fan, Folding super-sized DNA Origami with Scaffold Strands from Long-range PCR, *Chemical Communications*, 2012, 48, 6405.

110 C. M. Niemeyer, DNA as a Material for Nanotechnology, *Angewandte Chemie International Edition in English*, 1997, 36, 585–587.

111 Y. Li and D. Sen, A Catalytic DNA for Porphyrin Metallation, *Nature Structural Biology*, 1996, 3, 743.

112 O. Birkholz, J. R. Burns, C. P. Richter, O. E. Psathaki, S. Howorka and J. Piehler, Multi-functional DNA Nanostructures that Puncture and Remodel Lipid Membranes into Hybrid Materials, *Nature Communications*, 2018, 9, 1521.

113 Y. Suzuki, M. Endo and H. Sugiyama, Mimicking Membrane-Related Biological Events by DNA Origami Nanotechnology, *American Chemical Society Nano*, 2015, 9, 3418–3420.

114 H. Ijäs, S. Nummelin, B. Shen, M. A. Kostiainen and V. Linko, Dynamic DNA Origami Devices: From Strand-displacement Reactions to External-stimuli Responsive Systems, *International Journal of Molecular Science*, 2018, 19, 7, 2114.

115 T. Jiang, T. A. Meyer, C. Modlin, X. Zuo, V. P. Conticello and Y. Ke, Structurally Ordered Nanowire Formation from Co-Assembly of DNA Origami and Collagen-Mimetic Peptides, *Journal of the American Chemical Society*, 2017, 139, 14025–14028.

116 Y. Xu, S. Jiang, C. R. Simmons, R. P. Narayanan, F. Zhang, A. M. Aziz, H. Yan and N. Stephanopoulos, Tunable Nanoscale Cages from Self-Assembling DNA and Protein Building Blocks, *American Chemical Society Nano*, 2019, 13, 3545–3554.

117 C. J. Serpell, M. Barłóg, K. Basu, J. F. Fakhoury, H. S. Bazzi and H. F. Sleiman, Nucleobase Peptide Amphiphiles, *Materials Horizons*, 2014, 1, 348–354.

118 N. Venkatesan and B. H. Kim, Peptide Conjugates of Oligonucleotides: Synthesis and Applications, *Chemical Reviews*, 2006, 106, 9, 3712–3761.

119 A. Sánchez, E. Pedroso and A. Grandas, Maleimide-dimethylfuran Exo Adducts: Effective Maleimide Protection in the Synthesis of Oligonucleotide Conjugates, *Organic Chemistry Letters*, 2011, 13, 4364–4367.

120 C. Paris, O. Brun, E. Pedroso and A. Grandas, Exploiting Protected Maleimides to Modify Oligonucleotides, Peptides and Peptide Nucleic Acids, *Molecules*, 2015, 20, 6389–6408.

121 C. Y. Lim, N. A. Owens, R. D. Wampler, Y. Ying, J. H. Granger, M. D. Porter, M. Takahashi and K. Shimazu, Succinimidyl Ester Surface Chemistry: Implications of the Competition Between Aminolysis and Hydrolysis on Covalent Protein Immobilization, *Langmuir*, 2014, 30, 12868–12878.

122 G. T. Hermanson, *Bioconjugate Techniques: Third Edition*, Academic Press, 2013.

123 G. T. Hermanson and G. T. Hermanson, *Bioconjugate Techniques*, 2008, pp. 1003–1039.

124 J. Jin, E. G. Baker, C. W. Wood, J. Bath, D. N. Woolfson and A. J. Turberfield, Peptide Assembly Directed and Quantified Using Megadalton DNA Nanostructures, American Chemical Society Nano, 2019, 13, 9, 9927-9935.

125 M. B. Danielsen, H. Mao and C. Lou, Peptide-DNA conjugates as building blocks for de novo design of hybrid nanostructures, *Cell Reports Physicals Science*, 2023, 4, 101620.

126 Y. Gao, L. Wang, X. Zhang, Z. Zhou, X. Shen, H. Hu, R. Sun and J. Tang, Recent Progress in Extracellular Vesicle-Based Carriers for Targeted Drug Delivery in Cancer Therapy, *Pharmaceutics*, 2023, 15, 7, 1902.

127 Y. Dong, Y. Guo, W. Song, G. Nie and F. Li, Functional Integration of DNA and Peptide-Based Supramolecular Nanoassemblies for Cancer Therapy, *Accounts of Material Research*, 2023, 410, 892-905.

128 W. Y. Seow and C. A. E. Hauser, Short to Ultrashort Peptide Hydrogels for Biomedical Uses, *Materials Today*, 2014, 17, 381–388.

129 E. Rosa, C. Diaferia, L. De Mello, J. Seitsonen, I. W. Hamley and A. Accardo, Self-assembled Aggregates Based on Cationic Amphiphilic Peptides: Structural Insight, *Soft Matter*, 2023, 19, 4686–4696.

130 N. Yadav, M. K. Chauhan and V. S. Chauhan, Short to Ultrashort Peptide-based Hydrogels as a Platform for Biomedical Applications, *Biomaterials Science*, 2020, 8, 84–100.

131 M. R. Reithofer, K. H. Chan, A. Lakshmanan, D. H. Lam, A. Mishra, B. Gopalan, M. Joshi, S. Wang and C. A. E. Hauser, Ligation of Anti-cancer Drugs to Self-assembling Ultrashort Peptides by Click Chemistry for Localized Therapy, *Chemical Science*, 2014, 5, 625–630.

132 K. M. Rodrigue, K. M. Kennedy and D. C. Park, Beta-Amyloid Deposition and the Aging Brain, *Neuropsychology Rev*, 2009, 19, 4, 436–450.

133 E. Y. Hayden and D. B. Teplow, Amyloid β-protein oligomers and Alzheimer's disease, *Alzheimer's Research and Therapy,* 2013, 5, 1–11.

134 E. Stroo, M. Koopman, E. A. A. Nollen and A. Mata-Cabana, Cellular Regulation of Amyloid Formation in Aging and Disease, *Frontiers Neuroscience*, 2017, 11, 64.

135 M. Zacharias, Base-pairing and Base-stacking Contributions to Double-stranded DNA Formation, *Journal of Physical Chemistry B*, 2020, 124, 10345–10352.

136 G. Zhang, X. Zhai, Z. Ma, L. Jin, P. Zheng, W. Wang, S. Z. D. Cheng and B. Lotz, Morphology Diagram of Single-Layer Crystal Patterns in Supercooled Poly(ethylene oxide) Ultrathin Films: Understanding Macromolecular Effect of Crystal Pattern Formation and Selection, American Chemical Society Macro Letters, 2012, 1, 217-221.

137 E. R. Taylor, S. Cavuoto, D. M. Beal, S. Caujolle, A. Podoleanu and C. J. Serpell, Development of Gold-PAGE: Towards the Electrophoretic Analysis of Sulphurous Biopolymers, *Journal of Materials Chemistry B*, 2019, 7, 5156–5160.

138 B. Ranjbar and P. Gill, Circular Dichroism Techniques: Biomolecular and Nanostructural Analyses- A review, *Chemical Biology and Drug Design*, 2009, 74, 101–120.

139 M. Migliore, A. Bonvicini, V. Tognetti, L. Guilhaudis, M. Baaden, H. Oulyadi, L. Joubert and I. Sé Galas-Milazzo, Characterization of b-turns by Electronic Circular Dichroism Spectroscopy: A Coupled Molecular Dynamics and Time-dependent Density Functional Theory Computational Study, *Physical Chemistry Chemical Physics*, 2020, 22, 1611.

140 C. A. Bush, S. K. Sarkar and K. D. Kopple, Circular Dichroism of Beta Turns in Peptides and Proteins, 1978, 17, 23, 4951-4954.

141 M. R. Reithofer, A. Lakshmanan, A. T. K. Ping, J. M. Chin and C. A. E. Hauser, In situ Synthesis ofSize-controlled, Stable Silver Sanoparticles Within Ultrashort Peptide Hydrogels and Their Anti-bacterial Properties, *Biomaterials*, 2014, 35, 7535–7542.

142 Y. Loo, Y. C. Wong, E. Z. Cai, C. H. Ang, A. Raju, A. Lakshmanan, A. G. Koh, H. J. Zhou, T. C. Lim, S. M. Moochhala and C. A. E. Hauser, Ultrashort Peptide Nanofibrous Hydrogels for the Acceleration of Healing of Burn Wounds, *Biomaterials*, 2014, 35, 4805–4814.

143 S. Gupta, I. Singh, A. K. Sharma and P. Kumar, Ultrashort Peptide Self-Assembly: Front-Runners to Transport Drug and Gene Cargos, *Frontiers in Bioengineering and Biotechnology*, 2020, 8.

144 Y. Wang, Y. He, Z. Yu, J. Gao, S. ten Brinck, C. Slebodnick, G. B. Fahs, C. J. Zanelotti, M. Hegde, R. B. Moore, B. Ensing, T. J. Dingemans, R. Qiao and L. A. Madsen, Double Helical Conformation and Extreme Rigidity in a Rodlike Polyelectrolyte, *Nature Communications*, 2019, 10, 801.

145 J. N. Abraham, N. Gour, S. Bolisetty, R. Mezzenga and C. Nardin, Controlled Aggregation of Peptide-DNA Hybrids into Amyloid-like Fibrils, *European Polymer Journal*, 2015, 65, 268–275.

146 D. Kedracki, S. K. Filippov, N. Gour, H. Schlaad and C. Nardin, Formation of DNA-copolymer Fibrils Through an Amyloid-like Nucleation Polymerization Mechanism, *Macromolecular Rapid Communications*, 2015, 36, 768–773.

147 H. G. Hansma, I. Revenko, K. Kim and D. E. Laney, Atomic Force Microscopy of Long and Short Double-stranded, Single-stranded and Triple-stranded Nucleic Acids, *Nucleic Acids Research*, 1996, 24, 713–720.

148 K. Ariga, X. Jia, J. Song, J. P. Hill, D. T. Leong, Y. Jia and J. Li, Nanoarchitectonics Beyond Self-Assembly: Challenges to Create Bio-Like Hierarchic Organization, *Angewandte Chemie International Edition*, 2020, 59, 36, 15424-15446.

149 B. A. Badeau and C. A. Deforest, Programming Stimuli-Responsive Behaviour into Biomaterials, *Annual Review of Biomedical Engineering*, 3029, 4, 21, 241-265.

150 Y. Yu, B. Jin, Y. Li and Z. Deng, Stimuli-Responsive DNA Self-Assembly: From Principles to Applications, *Chemistry - A European Journal*, 2019, 42, 25, 9785–9798.

151 C. Gong, S. Sun, Y. Zhang, L. Sun, Z. Su, A. Wu and G. Wei, Hierarchical Nanomaterials via Biomolecular Self-assembly and Bioinspiration for Energy and Environmental Applications, *Nanoscale*, 2019, 11, 4147–4182.

152 L. Jiang, D. Xu, K. E. Namitz, M. S. Cosgrove, R. Lund and H. Dong, Protein-like Nanoparticles Based on Orthogonal Self-Assembly of Chimeric Peptides, *Small*, 2016, 12, 5126–5131.

153 P. Ball, *Synthetic Biology-Engineering Nature to Make Materials*, Materials Research Society Bulletin, 2018, 43, 477-484.

154 K. Rose, J. O. Mason and R. Lathe, Hybridization Parameters Revisited: Solutions Containing SDS, *Biotechniques*, 2002, 33, 54–58.

155 Nowakowski AB, Wobig WJ, Petering DH, Native SDS-PAGE: High Resolution Electrophoretic Separation of Proteins With Retention of Native Properties Including Bound Metal Ions, 2014, 6, 1068-1078.

156 M. Jafari, F. Mehrnejad, F. Rahimi and S. M. Asghari, The Molecular Basis of the Sodium Dodecyl Sulfate Effect on Human Ubiquitin Structure: A Molecular Dynamics Simulation Study, *Scientific Reports*, 2018, 8, 1–15.

157 J. Hoque, N. Sangaj and S. Varghese, Stimuli-Responsive Supramolecular Hydrogels and Their Applications in Regenerative Medicine, *Macromolecular Bioscience*, 2019, 19, 1800259.

158 Y. Gao, L. Wang, X. Zhang, Z. Zhou, X. Shen, H. Hu, R. Sun and J. Tang, Recent Progress in Extracellular Vesicle-Based Carriers for Targeted Drug Delivery in Cancer Therapy, *Pharmaceutics*, 2023, 15, 7, 1902.

159 A. Buchberger, M. Al-Amin, C. R. Simmons and N. Stephanopoulos, Self-Assembly of Hybrid Peptide−DNA Nanostructures using Homotrimeric Coiled-Coil/Nucleic Acid Building Blocks, *ChemBioChem*, 2023, 24, 17.

160 E. R. Taylor, A. Sato, I. Jones, P. G. Gudeangadi, D. M. Beal, J. A. Hopper, W. F. Xue, M. R. Reithofer and C. J. Serpell, Tuning dynamic DNA- and Peptide-driven Self-assembly in DNA-Peptide Conjugates, *Chemical Science*, 2022, 14, 196–202.

161 F. Xu, Q. Xia and P. Wang, Rationally Designed DNA Nanostructures for Drug Delivery, *Frontiers in Chemistry*, 2020, 8, 751.

162 P. J. S. King, M. G. Lizio, A. Booth, R. F. Collins, J. E. Gough, A. F. Miller and S. J. Webb, A Modular Self-assembly Approach to Functionalised b-sheet Peptide Hydrogel Biomaterials, *Soft Matter*, 2016, 12, 1915–1923.

163 W. T. Cong, W. J. Ye, M. Chen, T. Zhao, Z. X. Zhu, C. Niu, D. dan Ruan, M. W. Ni, X. Zhou and L. T. Jin, Improved Staining of Phosphoproteins with High Sensitivity in Polyacrylamide Gels using Stains-All, *Electrophoresis*, 2013, 34, 3277–3286.